Second Generation Electric Vehicle Development at the University of Kansas

By

Patrick Gordon Collins

Submitted to the graduate degree program in the Department of Mechanical Engineering and the Graduate Faculty of the University of Kansas in partial fulfillment of the requirements for the degree of Master of Science.

_____

Chair: Dr. Christopher Depcik

_____

Dr. Bedru Yimer

_____

Dr. Huazhen Fang

Defended: April 24th, 2015

The Thesis Committee for Patrick Collins certifies that this is the approved version of the following thesis:

Second Generation Electric Vehicle Development at the University of Kansas

By

Patrick Gordon Collins

_____

Chair: Dr. Christopher Depcik

Accepted: _____, 2015

Abstract

Due to more stringent emissions and fuel economy standards, many automotive manufacturers are implementing more electric and hybrid vehicles into their model fleets. Hybrid and purely electric powertrains offer more sustainable transportation methods; however, larger sport utility vehicles and trucks occupy a significant majority of the vehicles on the road in the United States. To this end, this work covers the development of a second generation electric sport utility vehicle at the University of Kansas.

Chapter 2 of this thesis outlines the use of CAN bus in the automotive industry throughout the evolution of the Electronic Control Module. Chapter 2 also showcases the different types of control modules installed in vehicles. CAN bus theory of operation, message formats, error handling, wiring techniques, and additional vehicle networking methods are also discussed. Lastly, electric vehicle case studies at the University of Kansas are presented to illustrate the importance and benefits of implementing CAN bus.

Chapter 3 focuses on the development of the JimmE-V. The JimmE-V serves as a research vehicle that has features similar to EVs available to consumers. In order for the vehicle to generate research quality data, vehicle operation and systems integration are discussed. CAN bus communication allows components to be controlled, calibrated, and monitored in real-time allowing the JimmE-V to be adjusted for a variety of research studies. Safety information is also provided due to the high voltage potential when working with EVs. The different causes for vehicle failure are additionally included in this chapter.

Chapter 4 examines the complete energy and emissions produced by the JimmE-V. This chapter highlights the energy used in the vehicle manufacturing process in addition to examining the benefit of reusing vehicle components. Furthermore, a Life-Cycle Analysis (LCA) was generated using Argonne National Laboratory's Greenhouse Gasses, Regulated Emissions, and Energy Use in Transportation (GREET) model. The LCA provides estimations for the JimmE-V's energy use and emissions produced throughout the vehicle's lifetime use. Accompanying this information is information regarding the

production and recycling of $LiFePO_4$ batteries. This work's LCA efforts for the JimmE-V are compared to the previous LCA efforts for the VW Beetle. Drive cycle data was collected to examine the efficiency of the JimmE-V, and to compare the results to the VW Beetle. Lastly, the solar generation capabilities of the newly built (2013) Hill Engineering Research and Development Center are presented.

Lastly, Chapter 5 focuses on the conclusions of the JimmE-V project mainly highlighting the author's main contributions to EV projects at the University of Kansas. The author's main contributions were centered on the powertrain of the JimmE-V including the motor, controller, ECM, and battery pack. This chapter additionally focuses on the vehicle's future impact as a research platform.

Acknowledgements

The efforts presented in this thesis could not have been accomplished without the assistance of multiple individuals and entities. During their time at the University of Kansas, the Transportation Research Institute provided financial support to the KU EcoHawks sustainable transportation endeavors. The KU Mechanical Engineering Department provided additional project funding, and their machine shop staff members Charles Gabel and Ash Shadrick. The KU EcoHawks JimmE-V teams from 2010 until 2014 were a vital component to the JimmE-V project; specifically, Josh Petty, Nathaniel Mayhew, Dustin Bergstrom, and Kevin Helton. In addition to the undergraduate students involved with this project, there were also graduate students involved. Dr. Michael Mangus offered his knowledge and support, and the occasional tow during the initial testing of the JimmE-V. Additionally, Chenaniah Langness provided advice for electrical troubleshooting, and additional feedback during the early stages of vehicle calibration. Jonathan Mattson provided assistance during drive cycle testing by monitoring the vehicle's data acquisition systems. Similarly, Brian Gessler and Matthew Cole aided in drive cycle testing. Lastly, EcoHawks Alumni Matthew Choate assisted in collecting drive cycle data. Former graduate student Bryan Strecker is recognized for his previous LCA efforts on the VW Beetle, and providing feedback on the JimmE-V model assumptions made in this thesis. Former graduate student Austin Hausmann is additionally recognized for his efforts involved with the JimmE-V project and helping get the 2011-2012 JimmE-V team educated on electric vehicle architecture. Dr. Christopher Depcik provided the opportunity to study electric vehicle powertrains, and was an excellent advisor offering additional resources, knowledge, and advice. In addition to colleagues, this work could not have been completed without the family support behind the scenes. Specifically, my mother, Charlene Frye, provided her love, support, and encouragement throughout my education process. Additionally, my father, John Collins, offered an infinite source of automotive knowledge in addition to his love, support, and encouragement. My step-father William Frye offered similar support, and accompanied me on many trips to the salvage yard to help locate missing pieces for the JimmE-V. Finally, none of this work could have been accomplished without the love and support of my patient wife Charlotte.

Table of Contents

Nomenclature…… xxii

1.1 Introduction……... 1

1.2 Past Efforts in Electrified Vehicles at the University of Kansas……...3

1.3 Thesis Focus……...4

Chapter 2: Vehicle Communication Networks Focusing on the Development of a Controller Area Network for a Full-Scale Electric Vehicle Conversion**.**……**.....** 6

2.1 Abstract……... 6

2.2 Introduction…… 7

2.2.1 Electronic Control Unit Construction…… 8

2.2.2 Electronic Control Unit Applications…….. 8

2.2.3 CAN Bus Theory of Operation……... 11

2.2.3.2 CAN Message Frame and Error Reporting.…… 13

2.2.4 CAN Bus Wiring and Setup…… 15

2.2.5 Additional Vehicle Networking Techniques……...17

2.3 On Board Diagnostics…… 19

2.3.2 OBD-I……...19

2.3.3 OBD-II…… 20

2.4 University of Kansas EcoHawks Case Studies……... 22

2.4.1 EcoHawks GEM Short-Range Electric Vehicle Swappable Battery Pack…….. 26

2.4.2 EcoHawks 1997 GMC Jimmy KU EV 2.0…….. 39

2.5 Conclusions…….. 56

Chapter 3: JimmE-V Operation and Overview…… 57

3.1 Abstract……... 57

3.2 Introduction…… 57

3.3 Vehicle Overview…… 60

3.4 Vehicle Chassis…… 62

3.5.1 Three-phase AC Induction Motor…… 70

3.5.2 JimmE-V Motor Controller & Inverter…… 75

3.5.3 JimmE-V Electronic Control Module…… 93

3.6.1 Vehicle Traction Battery Pack…… 109

3.6.2 JimmE-V Battery Management System…… 118

3.6.3 Manzanita Micro PFC Battery Charger…… 142

3.7 JimmE-V 12 VDC System…… 152

3.8 DC-DC Converters…… 162

3.9 Electric Power Steering System…… 166

3.10 Vehicle Air Conditioning System…… 171

3.11 Causes for Vehicle Failure…… 179

3.12 **Conclusion**…… 181

Chapter 4: Well-to-Wheels energy and emissions analysis of a recycled 1997 GMC Jimmy converted into a battery electric vehicle…… 182

4.1 Abstract…… 182

4.2 Introduction…… 183

4.3 Previous Efforts for the 1974 VW Super Beetle…… 186

4.4 Reuse of Vehicle Components…… 191

4.5.1 Lithium Battery Production…… 195

4.5.2 Lithium Battery Recycling…… 198

4.6 Outcomes of this Study…… 202

4.7 GREET Recycling and Reuse Energy and Emissions Analysis..... 204

4.8 GREET Electricity Energy and Emissions Analysis..... 207

4.9 Drive Cycle Results.....213

4.10 Hill Center Solar Array..... 217

4.11 Conclusion.....218

Chapter 5: Conclusions and Future Work..... 220

Appendix..... 229

Table of Figures

Introduction

Figure 1: Automotive industry vehicle production share [4]..... 1

Figure 2: Tesla charging stations in the United States [5]..... 2

Chapter 2: Vehicle Communication Networks Focusing on the Development of a Controller Area Network for a Full-Scale Electric Vehicle Conversion.

Figure 3: Image showing the electrical components assembled to construct an ECU [10].....8

Figure 4: Orion BMS system overview showing the different components that communicate with the BMS [11].....10

Figure 5: CAN Layer Architecture for the first two layers [8].....12

Figure 6: Diagram of a two node CAN bus with either node close to the termination point [11].....16

Figure 7: Diagram of a nodal CAN bus of length n [11].....16

Figure 8: Schematic showing how LIN is used to control secondary vehicle components that do not require the complexities of CAN [7]..... 18

Figure 9: An example of an OBD-II scan tool with the standardized Data Link Connector [14].....21

Figure 10: OBD-II pinout illustrating the different message lines [15].....21

Figure 11: KU EcoHawks 1974 VW Super Beetle.....23

Figure 12: KU EcoHawks 1997 JimmE-V..... 24

Figure 13: GEM Neighborhood EV..... 25

Figure 14: GEM Powertrain Layout..... 27

Figure 15: GEM Motor Layout [18]..... 27

Figure 16: CANadapter wiring diagram for the Orion BMS [11].....28

Figure 17: GEM potentiometer accelerator pedal schematic [18]..... 30

Figure 18: Digi-Key Reed Relay #725-1033-ND [20]..... 31

Figure 19: GEM Revised Accelerator Pedal Schematic with the BMS current liming by toggling a relay on/off [18]..... 32
Figure 20: Updated Orion BMS Software GUI showing the discharge relay tripping at 10% above the specified limit and the minimum reset time..... 34
Figure 21: Initial BMS Voltage Drift settings provided by the Orion BMS software utility..... 36
Figure 22: Reprogrammed Voltage Drift using the provided battery profile provided by the Orion BMS software utility..... 36
Figure 23: Drive Cycle Route shown on Google Maps..... 37
Figure 24: GEM Drive Cycle Elevation Profile. Elevation was calculated using http://www.doogal.co.uk/RouteElevation.php..... 38
Figure 25: JimmE-V powertrain layout..... 40
Figure 26: Azure DMOC445 and AC55 system schematic [24]..... 42
Figure 27: DMOC445 connection terminals. The 8-pin teminal for vehicle communication is on the left, the 35-pin interface terminal is in the middle, and the 14-pin terminal for motor data is on the left [24]..... 43
Figure 28: High voltage connections for the DMOC445 [24]..... 43
Figure 29: The New Eagle ECM system schematic showing the larger components..... 46
Figure 30: An enlarged view of how the accelerator pedal, brake light, ignition switch, and the five-way (position) switch are integrated into the New Eagle ECM system..... 47
Figure 31: New Eagle ECM pin diagram showing the A, B, and C terminals. The image to the right shows a close up of terminal B, pin C1 [25]..... 48
Figure 32: The New Eagle dual potentiometer pedal..... 48
Figure 33: The New Eagle five-position switch schematic showing the different drive positions..... 49
Figure 34: A typical Wheatstone Bridge voltage divider [26]..... 49
Figure 35: AnyVolt Micro Voltage Regulator and breakout board. Voltage adjustments are made via a potentiometer screw on the regulator [27]..... 50

Figure 36: The voltage regulator is located under the hood of the JimmE-V on top of the driver side wheel well..... 51

Figure 37: The four, five-terminal relays plugged into the relay plugs. The relays are installed under the hood of the JimmE-V located next to the ECU and motor controller..... 52

Figure 38: In-line fuse holder and 30 AMP fuse to prevent excessive current from the 12 VDC battery.. 52

Figure 39: The Smartcraft connector has six terminals that display the same data on each pin..... 54

Figure 40: The Smartcraft connector has ten pins labeled A-K (omitting I). Pin A shows the same data on each terminal..... 54

Chapter 3: JimmE-V Operation and Overview

Figure 41: JimmE-V full-scale electric vehicle conversion..... 58

Figure 42: Electrical hook, isolating gloves, facemask, and other proper safety tools for working on Hybrid and Electric Vehicles..... 59

Figure 43: Air suspension adjustment valve location. The valve is located above the rear differential towards the left wheel..... 63

Figure 44: Completed JimmE-V chassis [22]..... 63

Figure 45: JimmE-V master cylinder and brake booster..... 64

Figure 46: JimmE-V electric vacuum pump..... 65

Figure 47: Vacuum brake assist system schematic..... 66

Figure 48: JimmE-V pedal layout including the braking system..... 67

Figure 49: The Bosch four-channel ABS module is installed forward of the master cylinder and brake booster. Even though the system does not function, brake fluid passes through the controller to the brake calipers..... 67

Figure 50: The tire size is indicated on the sidewall of the tire. Tire width, aspect ratio, and wheel diameter must all be considered when replacing the tires..... 69

Figure 51: The JimmE-V rear differential. The motor directly drives the wheels through the rear differential. This allows the rear wheels to rotate at different speeds while turning. 70
Figure 52: AC55 motor installation location between the frame rails. 72
Figure 53: Motor wiring schematic for the Azure Dynamics AC55 motor. 72
Figure 54: DMOC445 three-phase AC connections. 73
Figure 55: The shielding is grounded through the controller chassis by fastening the large nut on the cord grip. 73
Figure 56: Motor encoder harness connected to the 14-pin connector on the DMOC445. 74
Figure 57: The AC55 encoder is located on the front of the motor. 75
Figure 58: Exposed AC55 encoder. 75
Figure 59: The Azure Dynamics DMOC445 AC motor controller and inverter under the hood of the JimmE-V. 76
Figure 60: The DMOC has four vibration isolating mounts located at each corner of the controller. 77
Figure 61: The ATEN USB to RS-232 adapter is located in the glove box of the JimmE-V. 80
Figure 62: Connect the DMOC USB cord to COM 6 on the vehicle's laptop. COM 8 is used for the Elithion BMS. 80
Figure 63: ccShell can be opened from the desktop shortcut or taskbar icons. 81
Figure 64: The current COM port selection is displayed in the bottom left of the ccShell window. 81
Figure 65: The configuration menu is used to alter the current COM port settings. 81
Figure 66: COM Port configuration window [31]. 82
Figure 67: Once the .ccs file has been successfully opened there will be four options available to select in the ccShell window [31]. 82
Figure 68: The connection time is displayed at the top right corner of the ccShell window [31]. 83
Figure 69: Selecting the "Viewer" option allows the user to view parameters in real-time and log controller data [31]. 84

Figure 70: The Scope tool can be used to view what is happening with variables at a faster rate than the Viewer tool [31]..... 86

Figure 71: The ccShell parameters edit tool with and Rxd error. In this instance, the .ccs file can be closed and reopened, or the display can be refreshed [31]..... 87

Figure 72: To change a variable type in the new desired value and hit enter. After reviewing the proposed change, select accept change to approve the new value, or select discard change to cancel the variable change [31]..... 88

Figure 73: Variable changes can be stored to the DMOC's internal memory by selecting the "Save to EEPROM" option in ccShell [31]..... 89

Figure 74: The ignition switch in the off position (left), and in the on position (right)..... 91

Figure 75: The contactor control button is in the 'OFF' position on the left, and in the 'ON' position on the right..... 91

Figure 76: DC-DC converter enable switch box located behind the passenger seat..... 93

Figure 77: The JimmE-V ECU..... 94

Figure 78: The Mototune software license information is contained on the Crypto-Box USB drive..... 94

Figure 79: The Kvaser Leaf Lite CAN to USB connection..... 95

Figure 80: The Kvaser CAN adapter is connected to the laptop using the USB port next to the Crypto-Box USB drive..... 95

Figure 81: The green LED indicates that the adapter is powered; while the amber LED indicates the CAN bus connection has been established..... 96

Figure 82: Mototune can be accessed by selecting the icon or shortcut on the desktop screen..... 96

Figure 83: Initial display window when Mototune is opened..... 97

Figure 84: ECU calibration files are in the Cals folder..... 98

Figure 85: To view current ECU calibration parameters and alter parameters, the most recent calibration file should be opened..... 99

Figure 86: Once a calibration file is opened, the calibration explorer window is populated with parameter folders. Additionally, recently saved paramterers will be displayed in the main window. 99
Figure 87: The JimmE-V accelerator pedal torque map. 100
Figure 88: The ECU motor rated torque parameter. 101
Figure 89: The ECU motor acceleration and regenerative power limits. 101
Figure 90: The final drive ratio parameter used to determine the vehicle speed. 101
Figure 91: In order to view and open display files, the file type needs to be changed to .dis. 102
Figure 92: The display window allows users to view ECU parameters during vehicle operation. 103
Figure 93: The MotoServer icon is located on the far right end of the taskbar. To view the connection settings, select the ports option. 104
Figure 94: MotoServer port configuration window. 104
Figure 95: Electronic shift knob in the 2015 Chrysler 200 [32]. 105
Figure 96: The JimmE-V shift knob is located on the vehicle's dash board. 105
Figure 97: The different JimmE-V shifter positions to operate the vehicle. 106
Figure 98: The Miniview display shows the operator accelerator pedal position and the current torque command from the ECU. 107
Figure 99: The regenerative braking toggle switch is located below the toggle switch for the vehicle's lights. 108
Figure 100: The ECU relays are located under the hood of the JimmE-V next to the ECU. 108
Figure 101: The fault light is located on the dashboard above the 12 VDC gauge. 109
Figure 102: The JimmE-V battery packs in the rear passenger compartment (far) and rear cargo section (near). 111
Figure 103: CAD drawing illustrating how the locking bars function [34]. 112
Figure 104: The locking bars can be accessed from the sides of the battery boxes. They safely secure the batteries to the boxes. 112

Figure 105: High voltage schematic illustrating all the components on the isolated high voltage circuit. …… ……113
Figure 106: The HV fuses are located inside the driver's side passenger door.…..114
Figure 107: HV junction box illustrating the two contactors (top) and two junction blocks (bottom)…..115
Figure 108: HV isolating gloves, and the rubber dipped tool for working on the JimmE-V battery pack. ……..…… 116
Figure 109: The JimmE-V battery pack consists of cells connected in series with bus bars, bolts, washers, and lock washers…..... 117
Figure 110: The BMS cell boards are installed between the positive (right) and negative terminal (left) of each cell.…..119
Figure 111: Schematic showing the BMS location, and the cell and bank numbering used for the BMS in relation to other components in the JimmE-V.…..... 120
Figure 112: The BMS Hall effect sensor is installed in-between cells one and two.…..... 121
Figure 113: The cell boards in each bank are connected using the molex connectors.…..122
Figure 114: BMS controller wiring connections [36]..... 123
Figure 115: The control pin wiring for the JimmE-V BMS.…..124
Figure 116: DMOC445 schematic showing how the BMS interfaces with the motor controller to control the high and low limits [38]..... 125
Figure 117: The SOC gauge displays the current SOC along with displaying additional faults and warnings when present. The source power light indicates when the vehicle is plugged into an electrical outlet..... 127
Figure 118: The ATEN RS-232 to USB connection on the BMS controller.…..127
Figure 119: JimmE-V laptop with the BMS plugged into COM port 8.…..128
Figure 120: JimmE-V laptop desktop screen showing the Elithion BMS utility shortcuts.…..... 129
Figure 121: The main screen of the BMS GUI. In this screenshot, load power is present along with a warning and a fault.…..... 130

Figure 122: The BMS GUI status tab without errors present. The status tab can be used to see battery pack information in greater detail than the meters tab. 130
Figure 123: The BMS GUI graph tab can be used for data logging desired battery pack parameters. 131
Figure 124: The configuration tab is used to program the BMS with the cell specifications. 133
Figure 125: BMS configuration options available for the user to select. 133
Figure 126: The Cell-V tab is used to program the cell voltage parameters in the BMS. 134
Figure 127: The BMS test tab allows the current profile configuration to be tested to ensure it responds correctly. 135
Figure 128: The BMS GUI with a fault condition present. 136
Figure 129: While viewing the meters tab, a fault is indicated by a red exclamation mark. The orange exclamation mark indicates a warning is present. 136
Figure 130: When a fault is present, the fault output changes from opened (green) to closed (red). 137
Figure 131: When the mouse is placed above the effected bank, the GUI shows additional information to assist the user in correcting the fault condition. 138
Figure 132: The multimeter fuse can be checked using the resistance or continuity options. 139
Figure 133: To measure current, ensure the probes are inserted into the current input terminal before rotating the dial to the indicated position. 140
Figure 134: Elithion BMS cell board polarity. 141
Figure 135: The completed cell board testing circuit. 141
Figure 136: Manzanita Micro PFC-20 charger operating panel 143
Figure 137: Charger controls layout. 144
Figure 138: Magnified image of the timer adjustment and dip switches on the battery charger. 145
Figure 139: Fluke multimeter for measuring high current. 147
Figure 140: The ice cube relay provides the BMS with 12 VDC power when an AC power source is present. This ensures that the BMS can actively balance cells as needed. 148

Figure 141: The SAE J1772 charging plug on the JimmE-V. The plug is located where the gas tank filling cap was previously located. 149
Figure 142: AVC2 Board for controlling the J1772 pilot signal. 150
Figure 143: 12 VDC automotive relay for the BMS to control the battery charger through the Reg Bus connection. 150
Figure 144: The 240 VAC charging plug can be switched with the J1772 plug by safely disconnecting the gray Anderson Connectors and re-connecting the desired charging plug. 151
Figure 145: Schematic showing how the battery charger interfaces with the charging plug, AVC2 board, battery pack, BMS, DC-DC converter, and the 12 VDC system. 152
Figure 146: The 12 VDC circuit is grounded through the body of the vehicle. 153
Figure 147: The main 12 VDC fuse block is installed in the dashboard to the left of the steering column. 154
Figure 148: JimmE-V light switch location and operating positions. 158
Figure 149: Turn indicator location and operating instructions. 158
Figure 150: The wiper speed is controlled by rotating the end of the turn indicator switch. 159
Figure 151: The hazard light switch is on top of the steering column. 160
Figure 152: The JimmE-V solar panels on top of the roof. 161
Figure 153: HQPR solar controller and system relay. 161
Figure 154: Propeller microprocessor and analog to digital converter. 162
Figure 155: DC-DC converter wiring specifications [43]. 164
Figure 156: The 12 VDC gauge indicating a low battery (left) and a charging battery (right). 165
Figure 157: Verification that the DC-DC converter is functioning correctly. The voltage measured at the battery should approximately equal the output voltage of the DC-DC converter. 166
Figure 158: Toyota MR2 electric power steering unit. 167
Figure 159: The electric power steering pump was installed on a steel plate in the front of the vehicle to locate the pump close to the steering gearbox. 168

Figure 160: Electric power steering system schematic. 169
Figure 161: Toyota electric power steering pump pinout diagram [44]. 170
Figure 162: The power steering circuit components. 171
Figure 163: An automotive AC system schematic [38]. 172
Figure 164: The electric AC compressor (left) and electric power steering pump (right). 173
Figure 165: The AC compressor inlet, accumulator, and outlet. 173
Figure 166: Schematic showing how the AC system is integrated into the HV system [45]. 174
Figure 167: Schematic showing how the compressor is wired to the AC controller [45]. 175
Figure 168: The AC condenser and fans are installed in the front of the JimmE-V. They are located behind the front grille to provide sufficient airflow. 175
Figure 169: The condenser fan relays are installed on the sub-frame by the AC compressor. 176
Figure 170: Blower motor schematic showing the components and their respective locations under the hood of the JimmE-V. 176
Figure 171: AC system components under the hood of the JimmE-V. 177
Figure 172: AC system operation panel inside the JimmE-V. 178

Chapter 4: Well-to-Wheels energy and emissions analysis of a recycled 1997 GMC Jimmy converted into a battery electric vehicle

Figure 173: KU EcoHawks 1974 VW Super Beetle 184
Figure 174: KU EcoHawks 1997 JimmE-V. 185
Figure 175: The original 1997 GMC Jimmy prior to the EV conversion. The front end of the vehicle had been damaged in an accident prior to donation of the vehicle. 193
Figure 176: The original body shell installed on the recycled frame. 193
Figure 177: The final body assembly with the new panels on the front of the vehicle. 194
Figure 178: The completed JimmE-V full-scale EV conversion. 195
Figure 179: Overall snapshot of a typical LiFePO4 battery [59]. 196

Figure 180: GREET hydrothermal production path for LiFePO4 batteries [62]..... 197
Figure 181: GREET solid-state production path for LiFePO4 batteries [62]..... 197
Figure 182: GREET model total energy cycle for transportation technologies [67]..... 203
Figure 183: GR1 map for regional electricity generation mixes [70]..... 208
Figure 184: Drive cycle route map (left) along with elevation profile (right) for Lawrence, Kansas..... 214
Figure 185: The Hill Engineering Research and Development Center solar arrays. The roof panels (left) provide 11.7 kW, and the front awning (right) provides 3.1 kW..... 217

Appendix

Figure 186: DMOC445 ccShell .par file parameters..... 230
Figure 187: DMOC445 ccShell .par file parameters..... 230
Figure 188: DMOC445 ccShell .par file parameters..... 231
Figure 189: DMOC445 ccShell .par file parameters..... 231
Figure 190: DMOC445 ccShell .par file parameters..... 232
Figure 191: DMOC445 ccShell .par file parameters..... 232
Figure 192: Elithion BMS schematic for Azure DMOC w/CAN..... 233
Figure 193: BMS GUI Basic tab configuration settings..... 234
Figure 194: BMS GUI Cell-V tab configuration settings..... 234
Figure 195: BMS GUI Cell-R tab configuration settings..... 235
Figure 196: BMS GUI Battery tab configuration settings..... 235
Figure 197: BMS GUI Measure tab configuration settings..... 236
Figure 198: BMS GUI Protect tab configuration settings..... 236
Figure 199: BMS GUI Balance tab configuration settings..... 237
Figure 200: BMS GUI Evaluate tab configuration settings..... 237

Table of Tables

Chapter 2: Vehicle Communication Networks Focusing on the Development of a Controller Area Network for a Full-Scale Electric Vehicle Conversion.

Table 1: CAN Bit Segment Timing Options for 500 kbits/second [24]..... 44

Chapter 3: JimmE-V Operation and Overview

Table 2: Azure Dynamics AC55 motor and DMOc445 controller specifications [24]..... 71

Table 3: DMOC445 8-pin connections used on the JimmE-V [24]..... 77

Table 4: DMOC445 35-pin connections used on the JimmE-V [24]..... 78

Table 5: CALB LiFePO4 cell specifications [33]..... 110

Table 6: BMS Control Pins [37]..... 124

Table 7: Manzanita Micro PFC 20 Charger specifications [39]..... 142

Table 8: Optima D75/25 deep cycle battery specifications..... 155

Table 9: MES-DEA 1000 W Specifications [43]..... 163

Chapter 4: Well-to-Wheels energy and emissions analysis of a recycled 1997 GMC Jimmy converted into a battery electric vehicle

Table 10: 1974 VW Super Beetle series hybrid specifications [48]..... 186

Table 11: 1974 VW Super Beetle route statistics [48]..... 187

Table 12: Calculated emissions and energy use avoided in the reuse of Beetle stock components [48].. 188

Table 13: Emissions factors developed in GREET 1 2011 [48]..... 189

Table 14: Emissions results for US 2010 electricity consumption mix and the solar/coal mix [48]..... 190

Table 15: 1974 VW Beetle EV mode Well-to-Wheel energy usage [48]..... 191

Table 16: GREET total energy consumed for LiFePO4 cathode material [62]..... 198

Table 17: GR2 calculated emissions and energy use avoided in the reuse of Jimmy stock components. 205

Table 18: Energy and emissions associated with battery assembly per vehicle lifetime for HT and SS lithium cathode production techniques..... 207

Table 19: GR1 WtW electricity production emissions results..... 209

Table 20: GR1 WtW electricity production energy results..... 210

Table 21: GR1 U.S. and SPP generation mix distribution from the Annual Energy Outlook 2013..... 211

Table 22: GR2 TEC energy results..... 212

Table 23: GR2 TEC solar energy results..... 212

Table 24: GR2 TEC emissions results..... 213

Table 25: 1997 JimmE-V specifications..... 215

Table 26: JimmE-V drive cycle route statistics from three driving tests..... 216

Table 27: Drive cycle test weather conditions [70]..... 216

Nomenclature

A - Amps

ABS – Anti-lock Brake System

AC – Air Conditioning

AC – Alternating Current

ACK – Acknowledgment

ACU – Airbag Control Unit

ADR – Assembly, Disposal, and Recycling

AGM – Absorbed Glass Mat

Ah – Amp hour

ANL – Argonne National Laboratory

ANSI – American National Standards Institute

APP – Accelerator Pedal Position

BAJ – Battery Association of Japan

BCM – Brake Control Module

BCU – Body Control Unit

BEV - Battery Electric Vehicle

BMS – Battery Management System

BSCM – Brake System Control Module

CA – Cranking Amps

CAFÉ – Corporate Average Fuel Economy

CAN – Controller Area Network

CANH – CAN High

CANL – CAN Low

CARB – California Air Resources Board

CCA – Cold Cranking Amps

CD – Collision Detection

CH_4 – Methane

CO - Carbon Monoxide

Co – Cobalt

CO_2 - Carbon Dioxide

CRC – Check and Redundancy Checksum

CSMA – Carrier Sense Multiple Access

CSV – Comma-Separated Value

DC – Direct Current

DLC – Data Link Connector

DMOC – Azure Dynamics DMOC445 motor controller

DOE – Department of Energy

DOT – Department of Transportation

ECM – Electronic Control Module

ECU – Electronic Control Unit

EEPROM – Electronically Erasable Programmable Read Only Memory

EGR – Exhaust Gas Recirculation

EMF – Electromotive Force

EOL – End of Life

EPA - Environmental Protection Agency

ESS - Energy Storage System

EV- Electric Vehicle

FSM – Finite State Machines

FWD – Front Wheel Drive

GEM – Global Electric Motorcar

GHG - greenhouse gasses

Gnd – Ground

GR1 – GREET1_2014

GR2 - GREET2_2014

GREET – Greenhouse Gases, Regulated Emissions, and Energy Use in Transportation

GUI – Graphic User Interface

GVW – Gross Vehicle Weight

HT – Hydrothermal

HV – High Voltage

IC – Internal Combustion

ICE – Internal Combustion Engine

ICEV – Internal Combustion Engine Vehicle

IGBT – Insulated Gate Bipolar Transistor

ISO – International Organization for Standardization

JimmE-V – 1997 GMC Jimmy (aka Chevy Blazer) EV conversion

KU – University of Kansas

kW – Kilowatt

kWh – Kilowatt hour

LCA – Life Cycle Analysis

LFP – Lithium Iron Phosphate

$LiFePO_4$ – Lithium Iron Phosphate

Li-ion – Lithium Ion

LIN – Local Interconnect Network

LLC – Logical Link Control

LMO – Lithium Manganese Dioxide

m – meter

MAC – Medium Access Control

MDI - Medium-Dependent Interface

mi - mile

MIL – Malfunction Indication Light

mpg_e – miles per gallon equivalent

mph – miles per hour

NEMA – National Electrical Manufacturers Association

NI – National Instruments

Ni – Nickel

NO_x – Oxides of nitrogen

OBD – On Board Diagnostics

OH – Hydroxide

Pb – Lead

PCM – Powertrain Control Module

PHEV – Plug-in hybrid electric vehicle

PLS – Physical Signaling

PM_{10} - Particulate matter smaller than 10 microns

$PM_{2.5}$ - Particulate matter smaller than 2.5 microns

PMA – Physical Medium Attachment

Pot – Potentiometer

PtW – Pump-to-Wheels

PV – Photovoltaic

PVC – Polyvinyl Chloride

RC – Reserve Capacity

RTR – Remote Transmit Request

RWD – Rear Wheel Drive

SAE – Society of Automotive Engineers

SOC – State of Charge

SOH – State of Health

SO_x – Oxides of sulfur

SPP – Southwest Power Pool

SS – Solid State

SUV – Sport Utility Vehicle

TCU – Traction Control Unit

TEC – Total Energy Consumption

USCAR - United States Council for the 1998 Automotive Research

V2G – Vehicle to Grid

VAC – Volts Alternating Current

VCM – Vehicle Control Module

VDC – Volts Direct Current

VOC - Volatile Organic Compounds

VW – Volkswagen

WtP – Well-to-Pump

WtW – Well-to-Wheels

Ω – Ohm

1.1 Introduction

The Environmental Protection Agency (EPA) was established in 1970 with the objective to protect human health and the environment [1]. Consequently the EPA is largely involved in the regulation of vehicle exhaust emissions. While currently under the EPA's Tier 2 emissions standards, their Tire 3 standards take hold in 2017 [2]. As these regulations continue becoming more stringent, automotive manufactures will need to further develop internal combustion (IC) engine technology and implement hybrid and electric powertrains into more production vehicles. To this end, Ford predicts that 1%-2% of vehicle sales will be purely electric, while 10%-25% of sales will be vehicles with hybrid powertrains [3]. Currently, trucks and sport utility vehicles (SUVs) hold the majority production share in the United States (Figure 1).

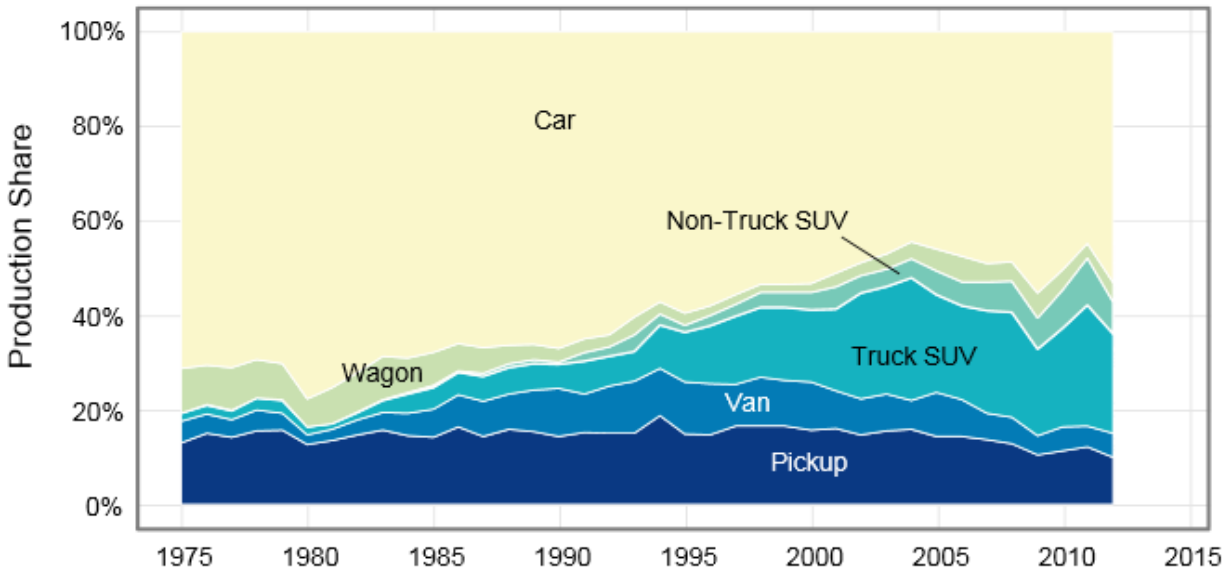

Figure 1: Automotive industry vehicle production share [4].

Hybrid vehicles offer a viable solution to the EPA's regulations by offering a more efficient and environmentally friendly option as opposed to a purely combustion powered vehicle. Since hybrid vehicles require battery packs, the incurred costs can be more than a traditional combustion vehicle. However, over the vehicle's lifetime these higher initial costs can be recouped through the higher fuel economy offered by hybrid powertrains. Hybrid powertrains also alleviate consumer range anxiety since

they can use the combustion engine and not rely on pure electric power from a battery pack. Furthermore, hybrid vehicles do not require as large of a battery pack compared to pure EVs [4].

Despite the larger battery pack EVs offer additional benefits not offered by hybrid vehicles. EVs offer a simple drivetrain system that is more efficient and requires less maintenance. EV drivetrains consist of an electric motor powered directly from an energy storage source (ESS). Currently, the majority of ESSs in EVs are lithium-ion battery packs. Additionally, since EVs do not contain a combustion engine components, they further reduce the oil dependence in the transportation industry. From an efficiency standpoint EVs are sensible because they convert more power to actual work compared to IC engine powered vehicles. Through their simpler drivetrains EVs transfer around 75% of power compared to an IC engine's 30-40% [4]. From the EPA's emissions regulations EVs are beneficial because they produce zero tailpipe emissions. However, the main consumer concern when it comes to purchasing an EV is their range limitations. Companies such as Tesla Motors offer strategically placed charging stations to alleviate consumer range anxiety, and additionally provide owners the opportunity to charge their Tesla vehicles for free within Tesla's charging network (Figure 2).

Figure 2: Tesla charging stations in the United States [5].

1.2 Past Efforts in Electrified Vehicles at the University of Kansas

Mechanical Engineering Associate Professor Dr. Christopher Depcik established the University of Kansas (KU) EcoHawks in 2008 with the goal to provide engineering students with sustainable design projects that focus on transportation and its associated energy infrastructure. These projects focus on the following five metrics: Education, Energy, Environment, Economics, and Ethics. Since the EcoHawks establishment in 2008, a variety of sustainable projects have been completed. Of note, two of the major EcoHawks projects have involved converting internal combustion (IC) engine vehicles into full-scale EVs.

The first of the two unique vehicles was a 1974 Volkswagen (VW) Super Beetle that was converted into a plug-in hybrid electric vehicle (PHEV). This project began in 2008, and the vehicle has been operational and providing a medium for ongoing research since 2010. Students further increased the Beetle's sustainability by including a biodiesel generator, and the fabrication of a solar photovoltaic charging station at a previous program facility. The VW Beetle has also served as a research platform for graduate work on developing electrified vehicle dynamics modeling techniques. To examine the overall sustainability of the conversion process additional graduate work was conducted on the Beetle to complete a Well-to-Wheels (WtW) analysis to examine the emissions and energy impact of the vehicle. This research then led to additional smart grid research focusing on smart grid technology, system sensing and control, and the implementation of vehicle to grid (V2G) architecture.

The second unique vehicle produced by the KU EcoHawks was a 1997 GMC Jimmy that was converted into a battery electric vehicle (BEV) also known as the JimmE-V. The JimmE-V project began in 2010, and was completed in 2013. The goal of the JimmE-V project was to take the knowledge gained from the Beetle project to fabricate a consumer representative BEV. Road legal since 2015, the JimmE-V features many amenities found on consumer vehicles including power steering, air conditioning, and heating. The JimmE-V additionally implements Controller Area Network (CAN) controlled components which is a standard technique in the automotive industry. Since its completion in 2013, the JimmE-V has served as a research vehicle focusing on the calibration of the CAN bus and three-phase alternating

current (AC) motor. While the Beetle utilizes a lead acid battery pack, the JimmE-V uses an advanced composition lithium iron phosphate ($LiFePO_4$) battery pack that is monitored by a Battery Management System (BMS). Together both of these vehicles provide platforms for sustainable automotive research.

1.3 Thesis Focus

Chapter 2 of this thesis outlines the use of CAN bus in the automotive industry throughout the evolution of the Electronic Control Module. This provides context on the role that CAN plays for the controlling of alternative energy powertrain systems. Due to the increasing technology demand in consumer vehicles, Chapter 2 also showcases the different types of control modules installed in vehicles. In order to understand how CAN functions on the micro level, the theory of operation, message formats, and error handling are also discussed. In order to understand how these networks are setup in vehicles the wiring techniques are explained accompanied with additional vehicle networking methods. Lastly, to examine how CAN has been implemented by the KU EcoHawks different vehicle case studies are presented to illustrate the importance and benefits of implementing CAN bus technology in electric vehicle (EV) applications.

Chapter 3 focuses on the development of the second generation EV, the JimmE-V. The JimmE-V serves as a research vehicle that has features similar to EVs available to consumers. In order for the vehicle to generate research quality data, it is important to understand how the vehicle operates and how the different systems are integrated into the JimmE-V. Through the vehicle's CAN bus components can be controlled, calibrated, and monitored in real-time. As a result, the JimmE-V can be adjusted for a variety of studies. Safety information is also provided due to the high voltage potential when working with EVs.

Chapter 4 examines the complete energy and emissions produced by the JimmE-V. This chapter highlights the energy used in the vehicle manufacturing process in addition to examining the benefit of reusing vehicle components. Furthermore, a Life-Cycle Analysis (LCA) was generated using Argonne National Laboratory's Greenhouse Gasses, Regulated Emissions, ,and Energy Use in Transportation

(GREET) model. The LCA provides estimations for the JimmE-V's energy use and emissions produced throughout the vehicle's lifetime use. Accompanying this information is information regarding the production and recycling of $LiFePO_4$ batteries. Additionally, the LCA efforts for the JimmE-V are compared to the previous LCA efforts for the VW Beetle. While the GREET model was used to calculate the vehicle LCA, vehicle efficiencies were obtained through drive cycle testing. Drive cycle data was logged through the vehicle's CAN bus to provide route statics that were then compared to the Beetle's statistics generated by an identical drive cycle route. Lastly, this chapter examines the solar generation capabilities of the newly built (2013) Hill Engineering Research and Development Center.

Finally, Chapter 5….

Chapter 2: Vehicle Communication Networks Focusing on the Development of a Controller Area Network for a Full-Scale Electric Vehicle Conversion.

2.1 Abstract

In-vehicle networking has rapidly evolved since the introduction of the Controller Area Network (CAN). CAN plays a crucial role in vehicle safety and operation. As the automotive market begins to further explore electric and hybrid vehicles, a CAN will provide reliable control for these alternative energy powertrain systems. To this end, this chapter introduces CAN systems. It is meant to provide an outline of the development and history of CAN, and its use in Electronic Control Units (ECUs). Due to the large number of ECUs in use by automotive manufacturers, different types of ECUs will be examined. Moreover, in order to understand how CAN functions on the micro level, the theory of operation, message formats, and error handling will also be discussed. Additionally, the wiring and initial network setup will be discussed before examining other vehicle networking techniques that have arisen due to the increased demand for more technology on-board vehicles. To accompany the discussions on the background and theory of CAN buses, the use of CAN bus with on-board vehicle diagnostics is examined to illustrate the important role vehicle networking has played in the automotive industry. Lastly, case studies involving the author's work with the University of Kansas EcoHawks Electric Vehicle (EV) projects will be examined to illustrate the importance and benefits of utilizing CAN bus technology in EV applications.

2.2 Introduction

Vehicles in use during the early 21st century are composed of networks of complex control modules as consumer demand for technology in vehicles continues to increase. From safety features, including air bags and anti-lock brakes, to engine and transmission control units, these elements are designed to communicate seamlessly with other control modules and components throughout the vehicle. Some of the key control modules found in vehicles include the Airbag Control Unit (ACU), Body Control Unit (BCU), Engine Control Module (ECM), Powertrain Control Module (PCM), Transmission Control Unit (TCU), Brake Control Module (BCM), and in hybrid and electric vehicles, the Battery Management System (BMS) [6]. In order for a vehicle to operate efficiently and safely, all of these modules demand reliable, repeatable, and high-speed communication. This is achieved through a Controller Area Network (CAN) bus.

CAN is a serial communications protocol originally conceived by Robert Bosch. The International Organization for Standardization (ISO) published the first CAN specifications in 1986, with development beginning in 1983 [7]. Bosch published the current CAN specification, CAN 2.0, in 1991 [8]. CAN 2.0 provides efficient and reliable serial communication that allows electronic control modules to communicate at speeds up to one Mbit/second while minimizing vehicle cost and weight by reducing the amount of wiring needed [8]. Utilizing a CAN bus reduces wiring because there are only three lines needed for the entire vehicle network: CAN high, CAN low, and ground. The CAN high line typically exhibits data transfer rates up to one Mbit/second, and is reserved for priority commands, such as throttle position, motor condition, motor speed, and other commands that are vital for the vehicle to operate safely [9]. The CAN low line normally has data transfer rates up to 125 Kbit/second and is used for less vital commands that govern interior lights, stereo commands, and other interior functions [9]. The main advantage for using a CAN bus is that multiple CAN controllers can be linked together so that devices may communicate with each other. This multi-device communication allows the logging of information, such as vehicle statistics, service reports, and time per job. CAN also significantly reduces the number of mechanical components and, as a result, largely minimizes failures. Another advantage with CAN is that

it offers high reliability with no need for special technology, while performing consistent precise work. In order to understand how CAN interacts with the function of electronic control modules, the basic construction of this piece of equipment is discussed next.

2.2.1 Electronic Control Unit Construction

National Instruments (NI) defines an electronic control unit (ECU) as an embedded electronic device that reads incoming signals coming from sensors located in various parts and components of the car, and depending on the control unit's function, the read information can control various outputs [6]. ECU hardware consists of the physical electronic components soldered to a circuit board. The internal components along with the input and output terminals for the microprocessor is displayed in Figure 3. The primary hardware element for any ECU is the microcontroller chip with Electronically Erasable Programmable Read Only Memory (EEPROM). EEPROM is also referred to as Flash memory, or non-volatile storage. The software component in an ECU is the installed code that runs in the microcontroller. Internally, the majority of ECUs are similar; however, when applied to different areas in a vehicle, software differences arise. The next section examines the most common ECUs and their primary functions.

Figure 3: Image showing the electrical components assembled to construct an ECU [10].

2.2.2 Electronic Control Unit Applications

Despite having similar hardware, there are a variety of ECUs in use within the automobile industry. Common control modules can be differentiated by their name and function. In order to understand which ECU is responsible for vehicle operations, their different functions will be examined in

this section. Internal combustion engine vehicles use the Engine Control Module (ECM) to control engine functions, such as monitoring and controlling fuel injection, ignition timing (spark ignition engines), and idle speed. These parameters are regulated by monitoring variables like coolant temperature, air flow, throttle position, crank shaft position, cam shaft position, and other data measured by various sensors. Another widely used control module is the Powertrain Control Module. The PCM and ECM share similar responsibilities with the objective being to transfer the generated engine power to the wheels. The PCM communicates with the ECM to examine throttle position, crankshaft speed, and output speed of the drive shaft. Additionally, this control module receives data from speed sensors, the brake light switch, and cruise control. By monitoring all the mentioned variables, the PCM governs the torque converter clutch, transmission shifting, and provides feedback to the driver [6]. Together these are the main control modules governing the vehicle powertrain. Vehicle safety and comfort are governed by a different set of control modules.

Vehicle safety is one of the different functions of the Vehicle Control Module. In addition to vehicle safety, the VCM monitors electric power steering, cruise control, airbag control, and electronic stability control systems [6]. The Body Control Module is another module added to vehicles for controlling windshield wipers, window defrosters, power windows, power door locks, convertible tops, electronic seats, seat heaters, and other amenities found in vehicles. The Braking System Control Module (BSCM), also referred to as the Anti-lock Brake System (ABS) module, primarily reads speed sensors on the wheels and the brake switch to determine if the system needs to be activated. All together, the previously discussed control modules communicate with each other and with sensors installed throughout the vehicle. Many of these control modules transfer over to alternative powertrain vehicles, such as parallel or series hybrid vehicles, or electric vehicles.

While vehicle electrification may remove control modules related to engine control, they require an additional set of control modules responsible for supervising vehicle charging and discharging, and regulating motor power. The Battery Management System (BMS) examines battery cell voltage, total pack voltage, battery pack current, and battery temperature. The BMS communicates this information to

external devices, such as loads, sources, and battery chargers. Figure 4 provides a system overview diagram for an Orion BMS and the connections needed so the BMS can interact with the battery pack, charger, load, and source. This information helps to protect, manage, monitor, and maintain the battery pack [11].

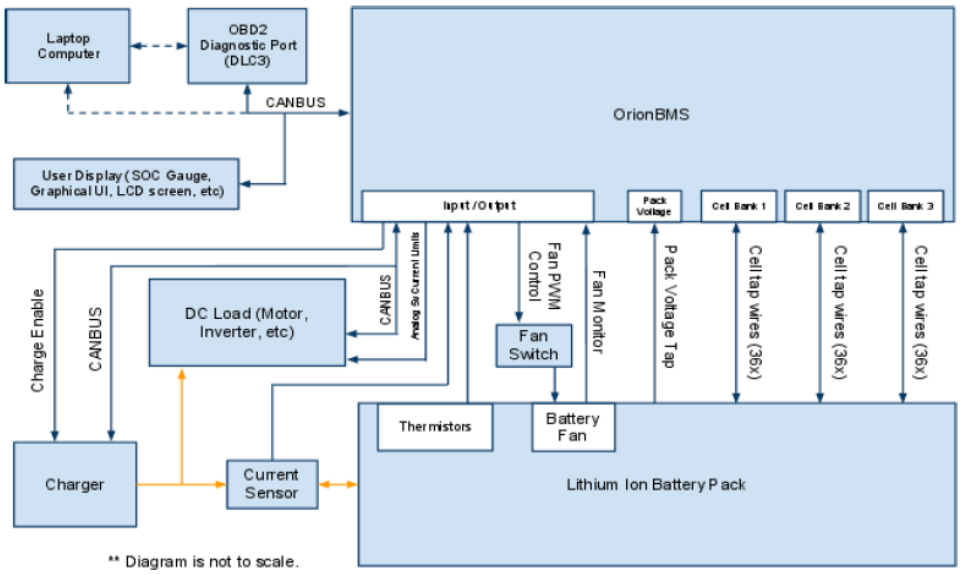

Figure 4: Orion BMS system overview showing the different components that communicate with the BMS [11].

In addition to a BMS, electric and hybrid vehicles require a motor controller to govern the power output from the electric motor. Motor controllers are paired with their own ECU that monitors the accelerator pedal position and sends commands to the motor controller. In conjunction with the BMS, these components regulate the power from the battery pack and safely apply this energy to the wheels of the vehicle, as discussed in detail later in this document. Regardless of the vehicle powertrain (internal combustion engine, hybrid, or full electric), vehicle control module communication remains constant during its operation. *The vehicle CAN bus is the link that integrates all of the vehicle systems together*. Along with learning how vehicle components interact on a CAN bus, additional understanding is needed to gain perspective on how messages are generated, transmitted, and received on the bus.

2.2.3 CAN Bus Theory of Operation

In order to understand how components function on a CAN bus, the theory of CAN operation must be examined. The programming aspect of CAN is beyond this scope of work; however, a basic summary of key aspects of CAN are presented in this section to broaden the comprehension of how vehicle control modules operate on a CAN bus.

The CAN ISO standard contains seven layers, but the CAN protocol is only contained in layers one and two. The remaining layers in the CAN protocol are left to the development of the component software engineers for the particular product [12]. Since the bottom two layers are the primary CAN layers, the remaining top five layers will not be discussed.

Layer one is referred to as the Physical Layer. Within the Physical Layer, there are three additional embedded layers: Physical Signaling (PLS), Physical Medium Attachment (PMA), and Medium-Dependent Interface (MDI). The Physical Layer determines the specific process in which the signal is transmitted. This layer is directly responsible for transferring bits between nodes. Since this layer transmits bits throughout the entire network, the Physical Layer must be the same for each node in a given network. Bit representation (coding, timing, etc.), bit synchronization, electrical signal definitions, and transmission medium definitions are all responsibilities carried out by the Physical Layer [7].

The second layer in the CAN ISO standard is the Data Link Layer. Similar to layer one, the Data Link Layer contains additional embedded layers. In specific, the Medium Access Control sublayer (MAC) is the core of CAN protocol. It presents messages received from the Logical Link Control (LLC) sublayer. The MAC sublayer is additionally responsible for message framing, arbitration, acknowledgement, error detection, and signaling. The LLC sublayer filters messages, provides network overload notifications, and contains the error recovery procedure [7]. Figure 5 shows the network architecture for layers one and two of the CAN protocol along with the additional sublayers that are embedded within the main layers. Within these layers associated with the CAN protocol, there are additional protocol fundamentals of these complex systems.

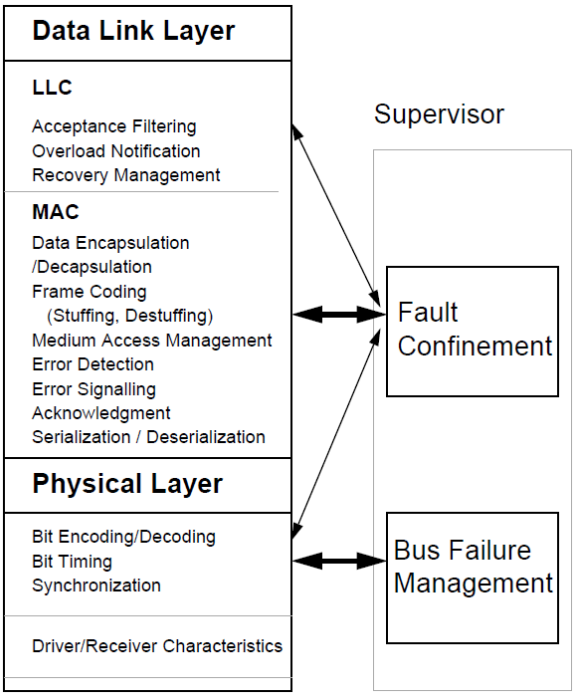

Figure 5: CAN Layer Architecture for the first two layers [8].

The CAN protocol is a message based protocol, not an address based protocol. An example of an address based protocol would be the internet. Whereas, CAN is a message based protocol that sends messages between networked components. Thus, messages are not transmitted node to node by address. Instead, each CAN message is embedded with the priority and the contents of the transmitted data. All network nodes receive the same transmitted message and acknowledge if the message was properly heard. Once a message has been received, it is each node's responsibility to determine if the message needs to be kept and processed. Messages that do not need to be processed are discarded. Since every node receives the same message, this allows multiple components at different nodes to employ the same message [12].

The CAN protocol is a Carrier Sense Multiple Access (CSMA)/Collision Detection (CD) protocol. CSMA indicates that each node monitors the network for a period of inactivity before the node can send a message. During the period of inactivity, every node has an equal chance to transmit a message. The CD part of the protocol prevents two nodes from transmitting a message on the bus simultaneously [7]. Network nodes can request additional information from other nodes. This process is called a Remote Transmit Request (RTR). Since components communicating on a CAN bus utilize the

same standardized protocol, additional nodes can be added to the system without the need to reprogram the existing nodes in the system. This encourages flexibility, adaptability, and ready expansion of a CAN bus to account for new technologies to be implemented in a vehicle.

With a basic understanding of how communication works on a CAN bus, further detail should be examined to grasp the CAN message format, and how the system processes errors. The following section goes further into the CAN protocol examining the different message frames and modes for reporting and processing errors.

2.2.3.2 CAN Message Frame and Error Reporting

The CAN protocol defines four different types of messages, also called Frames. The first and most common is the Data Frame. Data Frames are used when a node transmits information to any or all other system nodes. Additionally, Data Frames contain Arbitration Fields, Control Fields, Data Fields, CRC Fields, a two-bit Acknowledge Field, and an End of Frame. The Arbitration Field is used to determine message priority. In the CAN protocol, a logical 0 represents the dominant state. The lower the number in the Arbitration Field, the higher the priority the message has on the bus. The arbitration field can have a Standard or Extended Frame. Standard Frame messages consist of 11-bit identifiers; whereas, Extended Frames use 29-bit identifiers. The Acknowledge Field indicates if the message was received correctly by putting a dominant bit on the bus in the ACK position [12].

The second type of message is the Remote Frame. The Remote Frame is essentially a Data Frame with the RTR bit set to signify if it is a Remote Transmit Request. A node uses an RTR bit when the sending node requires additional information from other nodes on the bus. There is a bit in the arbitration field that is used to determine if the message is a Remote Frame or a Data Frame. A recessive bit indicates a Remote Frame, and a dominate bit indicates a Data Frame message [12].

The remaining two Frames are for handling errors. The first error handling Frame is the Error Frame, and the second is the Overload Frame. Nodes that detect any protocol errors as defined by the CAN generated error messages. Overload errors are generated when a node requires more time to process

previously received messages. A node sending an Overload Frame is not ready to receive additional messages at that moment in time [12].

Another vital part of communication through CAN is the ability to indicate when a particular device is registering an error. There are five portions to error checking in CAN: bit monitoring, bit stuffing, frame check, acknowledgment (ACK) check, and cyclic redundancy checksum (CRC). Each device performs bit monitoring and it is simply comparing the transmitted signal to the bus level. When a bit does not match up it will register a Bit Error. The bit monitoring only begins after arbitration. Bit Stuffing Error occurs when a node transmits five identical bits in succession; it will always follow with the opposite bit. The following bit is ignored by the receivers and is used for error checking. The frame check is the concept of each node verifying that the message has the correct amount of bits per section, and if a frame is incorrectly formatted, a Form Error is generated. With an error detected, it triggers an immediate, automatic retransmission of the original incorrect message after a predefined time interval. The ACK frame is when all receivers acknowledge that they are on the network and send a dominant (0) level while the transmitting node sends a recessive (1). If the transmitter does not detect the dominant level, the ACK check mechanism signals an Acknowledge Error. Each receiver calculates a checksum of the message and compares it to the CRC field of the transmission. If the CRC values do not match, a CRC error is generated since at least one node did not receive the message. Similar to a Form Error, when a CRC error occurs the original message is resent after a defined time interval [12].

When an error frame is generated by any of the previously discussed methods, that error becomes visible to all other nodes on the bus through Error Frames or Error Flags. The error producing message is often aborted and then resent when the message has priority on the bus. During this time, each node is in one of three error states: Error-Active, Error-Passive, or Bus-Off. When a node is in an Error-Active status, the node can be active in bus communication, and is the normal operation mode. A node will remain Error-Active while the Transmit Error Counter and the Receive Error Counter remain below a value of 128. As long as the node remains in the Error-Active mode, it can transmit Active Error Flags. A node becomes Error-Passive when the Transmit Error Counter or Receive Error Counter equals or

exceeds 128. In Error-Passive mode, nodes are not allowed to transmit Active Error Flags, but instead transmit Passive-Error Flags. Passive-Error Flags have no effect on the bus since the error flag is recessive. When an Error-Passive node transmits a Passive-Error Flag and detects a dominant bit, the sending node is required to see the bus as inactive for eight additional bit times. Once the node recognizes the bus as available, message transmission is reattempted. The final node error state is the Bus-Off mode. This mode is enabled when the Transmit Error Counter exceeds 255. In this condition, Receive Errors Counters do not cause the node to go into Bus-Off mode. The Bus-Off mode prohibits a node from sending or receiving messages of any kind. This feature allows the CAN bus to go into Fault Confinement. From this point, there is a bus recovery sequence defined by the CAN protocol that allows a Bus-Off node to recover and then return to an Error-Active state. Once the node has successfully recovered, message transmission resumes [12]. The nature of the response allows CAN to have a short error recovery time, as well as high data integrity. The system as a whole is required to work with the automated error handling and needs monitoring to ensure the two are working together. In order to ensure that a CAN network is functioning properly, the bus has to be properly wired and set up. The next section further examines how to properly wire and setup a CAN bus.

2.2.4 CAN Bus Wiring and Setup

With a basic understanding of the theory behind CAN bus operation, the next step is to construct the communication network. An improperly assembled network may appear to function, but will not work reliably. CAN buses are differential mode buses that use two wires twisted together, referred to as a twisted pair wire, to communicate. In addition to the twisted pair wire, shielding is commonly used to protect the system against electrical noise. It is important that bus shielding is connected to a common ground in one location to prevent ground loops. Additionally, differences in ground potentials can damage CAN transceivers and other devices on the network. In some cases where the same ground connection cannot be made, an external CAN isolation device needs to be utilized. Depending on the application, specific shield grounding instructions may vary in order to divert noise properly. At connection points,

the wires are not covered in shielding, and exposed distances should be kept as short as possible **[11]**. When wiring a CAN bus, the network also needs to be terminated correctly.

To terminate a CAN bus, two 120 Ohm (Ω) resistors are needed on either end of the physical bus. As previously mentioned, CAN buses can be composed of multiple components. These components are connected to the network at nodes in-between the bus termination points. There can be several nodes on a network, but if there are only two nodes, the nodes should be at the ends of the bus as close to the termination resistor as possible. Figure 6 shows the correct wiring for a two node CAN bus.

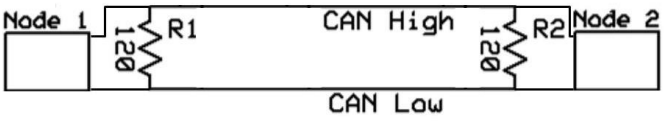

Figure 6: Diagram of a two node CAN bus with either node close to the termination point [11].

When designing a network with more than two nodes they should "T" off the main network wires in-between the two termination points. A multi-node diagram is shown in Figure 7. Due to the popularity and reliability of CAN, termination resistors are often incorporated into components. Depending on the component location on the bus, the built in termination resistor can be bypassed. The physical network length can vary based on the desired baud rate.

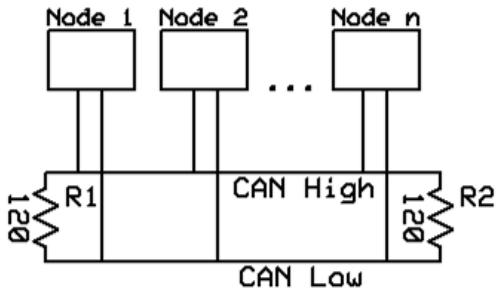

Figure 7: Diagram of a nodal CAN bus of length n [11].

The network baud rate refers to the data transmission rate speed in bits per second. For speeds of 1 Mbit/second, the bus should be approximately 30 meters in length. Lengths around 100 meters support data transmission of 500 kbit/second, and a 500-meter long bus can accommodate slower baud rates of 125 kbit/second [11]. Once the CAN bus has been properly terminated and all the controllers are

connected to the network, proper network termination can be verified by using an ohmmeter to check the resistance value between the CAN High and Can Low wires. This resistance value should be checked with all the devices on the network powered off. A properly terminated and setup network will read a total resistance of 60 Ohms reflecting that there are two 120 Ω resistors in parallel. From this discussion, it is observed that the wiring of a CAN bus is relatively simple as opposed to how nodes communicate on the bus. Since the establishment of CAN, other vehicle networking techniques have been developed to accompany and further enhance the benefits of utilizing a CAN bus. The next section discusses two of the main vehicle networking techniques developed and implemented to work with CAN.

2.2.5 Additional Vehicle Networking Techniques

As consumer demand for more vehicle amenities increase, the number of network components subsequently has grown. With more network traffic, less bandwidth is available for components that are crucial for vehicle operation. In order to increase network availability, other vehicle networking methods were developed. These techniques were not meant to replace CAN, but to compliment and work alongside CAN. Local Interconnect Network (LIN) and FlexRay are two specific networking strategies utilized in the automotive industry.

Local Interconnect Network (LIN) was developed by Motorola to primarily support mechatronic control elements for motor vehicle applications. LIN uses slower data transmission speeds with a maximum transmission speed of 20 kbits/second. It was designed to be simpler than CAN, and to provide a sub-bus for CAN to lower costs for controlling simpler automotive components. LIN can be used where the desired network bandwidth is lower, and the reliability and robustness offered with CAN are not required. Components found in automobiles that operate using LIN are all seat adjustments and functions, steering wheel mounted controls, doors, windows, side mirrors, wiper control, and interior lighting [7]. A simple multi-network vehicle schematic is shown in Figure 8. Along with having networks with slower transmission rates, other companies began seeing the need for vehicle networks with faster bandwidths

than CAN. As a result, the FlexRay protocol was designed to meet the growing demands of faster vehicle data transmission.

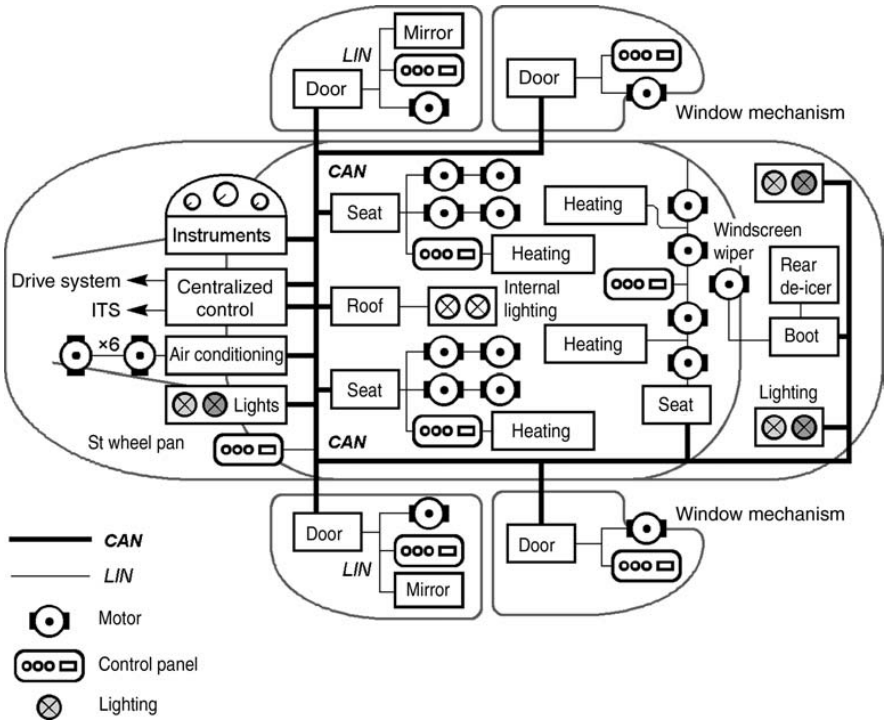

Figure 8: Schematic showing how LIN is used to control secondary vehicle components that do not require the complexities of CAN [7].

A number of companies conducted meticulous testing on existing network protocols (i.e., CAN and others) to determine if they were able to meet all the technical requirements for intended applications [7]. It was concluded that CAN was not fast enough for newer applications and its operation is difficult to make transmissions deterministic and redundant. From their results, FlexRay was developed to work alongside CAN. The primary objective of FlexRay is to communicate with higher bit rates to enhance, complement, and supplement CAN limited applications. FlexRay is also designed to be capable of serving all future electronic functions in automobiles with bandwidths up to 10 Mbit/s [7]. Combined, all of these techniques reduce the amount of bus traffic while accommodating consumer demand for new vehicle technologies, such as on board vehicle diagnostics. The next section highlights this relatively new feature in automobiles, and how CAN contributed to its evolution.

2.3 On Board Diagnostics

Automotive control methods prior to the 1980's were rudimentary. Manufacturers utilized mechanical and vacuum actuated controls. With the introduction of ECU's in the early 1980's, vehicle diagnostics became complex with the need to comprehensively diagnose a system with hundreds of failures. Early ECU's controlled engine, fuel, and emission control systems (i.e., coolant temperature, manifold pressure, crank position to control spark timing, fuel delivery, and sometimes Exhaust Gas Recirculation). These systems were simple at first with minimal use of sensors and electronically controlled components. However, issues with components would create relatively high vehicle emissions without adversely affecting vehicle performance or drivability. As a result, customers were failing vehicle inspections with what they perceived to be a well running vehicle. Technicians were then faced with the challenge to identify one or all faulty components in the system and often resulted in a high repair bill [13].

Manufacturers began to address the added complexities by modifying their ECU to have some On Board Diagnostics (OBD). Diagnostic tests were initiated by grounding an ECU pin, and would provide the technician with flashes of lights to indicate a specific fault or code number (i.e., three flashes indicates a Code 3). This code was used to better pinpoint the vehicle issue by referencing a sensor or service procedure outlined in a service manual. However, the codes, tests, and procedures were not standardized among manufacturers. The California Air Resources Board (CARB) became aware of these rudimentary on-board diagnostics capabilities of ECU's, and believed that ECU's could help identify vehicles with emission-related faults, as well as aiding technicians in being able to repair the issues easily [13]. OBD-I was the first iteration of OBD technology and is discussed in the following section.

2.3.2 OBD-I

OBD-I was proposed and then adopted in April 1985 with the objective to improve emissions compliance by continuously monitoring the emission control system. In particular, the system would alert driver of the need for repairs. OBD-I systems were required to run on-board tests to identify component

malfunctions and have a Malfunction Indicator Light (MIL) on the dashboard to notify the driver of an emissions related problem. The MIL was an amber light with either “Check Engine” or “Service Engine Soon” that would illuminate when a component failed. The mentioned MIL phrases were chosen assuming that the driver would see them and take their car in for immediate service, resulting in lowering the drive time with malfunctioning emission components. OBD-I requirements were simple and applied to light-duty vehicles from 1988 through some 1996 models. Emission related inputs monitored the system for open and short circuits. The components involved in the system were the ECU, fuel metering, ignition, and Exhaust Gas Recirculation (EGR) if applicable. In addition to illuminating the dashboard, OBD-I ECU’s were required to store fault codes. Fault codes were identified by grounding an ECU pin wire and then counting the pulses from the MIL. Some vehicles incorporated a serial data communication link with the data and fault codes obtained from the ECU using a scan tool. OBD-I represented a step forward in diagnosing vehicle emissions issues using ECU’s; however, OBD-I was limited because it did not monitor all emission control system components. Additionally, the OBD-I regulations did not contain standardizations, and as a result, different connectors had to be used with scan tools to view fault codes on different manufacturer’s vehicles [13].

2.3.3 OBD-II

Hence, CARB proposed revisions to on-board vehicle diagnostics in 1988 with the goal to monitor all emissions related components. OBD-II was adopted by CARB after working with the Environmental Protection Agency (EPA) and the Society of Automotive Engineers (SAE) in 1992 and applied to all 1994 and subsequent model year vehicles. This included gasoline, diesel, and alternative fuel passenger cars, light duty trucks, and medium duty vehicles up to 14,000 pounds Gross Vehicle Weight (GVW). Due to the extensive vehicle changes required by OBD-II, CARB could waive the new requirements if a vehicle manufacturer could demonstrate that they could not modify a current electronic control system in time to meet the new requirements for the 1994 model year, or if the changes did not coincide with the planned vehicle changeovers. As a result, very few manufacturers introduced OBD-II

compliant vehicles in 1994 and 1995. The majority of manufactured vehicles did not become OBD-II compliant until the 1996 model year. OBD-II regulations required that the following vehicle parameters be monitored: the catalyst system, engine misfire, evaporative emission controls, secondary air injection, fuel system, oxygen sensors, the EGR system, cold start emission reduction strategy, air conditioning system, variable valve timing system, direct ozone reduction system, and the diesel particulate trap. Additionally, OBD-II required the standardization of fault codes, scan tool test modes, and parametric data by all vehicle manufacturers [13].

Figure 9: An example of an OBD-II scan tool with the standardized Data Link Connector [14].

This ensured that that fault-codes and data could be extracted using a generic aftermarket scan tool similar to Figure 9. The connector, called a Data Link Connector (DLC), was also standardized to omit the need for plug adapters between vehicle manufacturers [13].

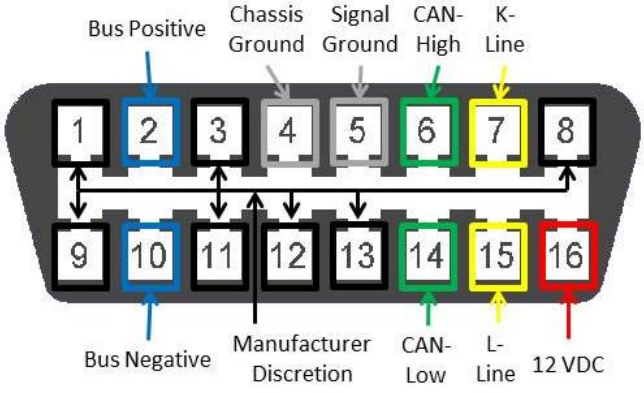

Figure 10: OBD-II pinout illustrating the different message lines [15].

OBD-II systems were additionally required to provide access to the Engine Control Module. This allowed scan tool access to additional engine performance data to aid in diagnosing vehicle emissions issues. Lastly, OBD-II required that vehicles store fault codes, and that fault codes could only be reset by disconnecting the battery, or by using a scan tool. With the added requirements and complexities of OBD-II, vehicle manufacturers, CARB, and the EPA needed a communication method that was standardized, fast, and reliable. Consequently, *they all agreed on the Controller Area Network protocol*.

The use of CAN for OBD-II addressed issues associated with the use of different protocols, and that all vehicles produced during and after 2008 were required to use CAN as the only protocol [13]. Currently, vehicle manufacturers are exploring the use of wireless telematics to conduct vehicle prognostics and remote diagnostics. Vehicle prognostics allow engineers predict the time when a system or component will fail and notify the consumer appropriately. Electric Vehicle (EV) manufacturer Tesla Motors is one such company that is currently implementing both prognostics and remote diagnostics to further their product development. Thus, vehicle diagnostics has developed and evolved at a rapid rate, and is continuing to develop to meet the demands of a rapidly evolving industry.

From the brief outline of OBD-II regulations, it is evident that OBD-II and the use of CAN have aided the transportation industry in automotive control standardization. By introducing students to the CAN protocol at the university level, students can begin to understand the complexities involved with vehicle control systems. Hence, the prior discussion of CAN and OBD-II was desired by the author's advisor in order to ensure proper context of the work contained within. The following sections outline specific case studies where CAN has been implemented in alternative energy vehicles at the University of Kansas by the author.

2.4 University of Kansas EcoHawks Case Studies

The Electric Vehicle (EV) case studies involving the use of a CAN bus are examined in detail in the following sections; however, first some context for these projects must be given. Dr. Christopher Depcik established the University of Kansas (KU) EcoHawks in 2008 with the goal to provide

engineering seniors with sustainable design projects. These projects primarily focused on transportation and its associated energy infrastructure while considering the five vectors of success: Education, Energy, Environment, Economics, and Ethics.

The first project involving the EcoHawks was a full-scale EV conversion of a 1974 Volkswagen (VW) Super Beetle. The intent of this project was to design and fabricate an electric vehicle using recycled parts and a simple vehicle architecture. The Beetle is equipped with a NetGain Warp 9, 120 VDC Brushed Series Wound motor that is matted to the original VW five speed manual transmission. The motor is powered by a 14.19 kWh lead acid battery pack. The total pack voltage is 120 VDC, and the Amp hour (Ah) capacity is 115 Ah. From a controls standpoint, the Beetle is relatively simple. The motor is controlled using a NetGain Controls Classic DC Speed Controller. The controller receives driver input via a potentiometer accelerator pedal. The motor and controller in this application do not provide any regenerative braking energy to the battery pack due to complexity issues with DC motors and regenerative braking. Overall, the Beetle achieves 106.1 miles per gallon equivalent (mpg_e) [16]. Along with providing a project for engineering seniors, the Beetle has additionally been used by previous graduate students for developing vehicle and battery models, and examining the well-to-wheels energy use of EVs. The lessons learned from developing the VW Beetle, as seen in Figure 11, were then applied to develop a next generation EV for KU.

Figure 11: KU EcoHawks 1974 VW Super Beetle

The second generation EV produced by the KU EcoHawks was a 1997 GMC Jimmy (aka Chevy Blazer) referred to as the JimmE-V (Figure 12). The JimmE-V was the focus of the author and will be covered in detail throughout the remaining sections of this chapter. This section is provided to serve as an introduction to the project that started in 2010 and was completed in 2013. The JimmE-V uses an Azure Dynamics AC 55 three-phase Alternating Current (AC) motor, coupled to an Azure Dynamics DMOC 445 motor controller and inverter. The DMOC 445 is CAN controlled and requires the use of an ECU to relay accelerator pedal input to the controller. The advanced composition battery pack consists of 104 CALB Lithium Iron Phosphate ($LiFePO_4$) batteries in series that provide 330 VDC to the controller. The battery pack has a capacity of 100 Ah. Each cell is 3.30 VDC and 100 Ah and is controlled by an Elithion Lithiumate Pro Battery Management System (BMS) to ensure that the batteries are properly charged, discharged, and maintained. The motor transfers power to the wheels of the vehicle by directly driving a drive-shaft through a differential to the rear wheels. In addition to a more advanced powertrain, the JimmE-V has additional amenities that make it comparable to a consumer available EV. The vehicle has electric air conditioning components, electric power steering, electric heating elements, two DC-DC converters to step down the high voltage source for automotive use (12 VDC), and solar panels on the roof to charge the 12 VDC batteries needed to run traditional automotive components.

Figure 12: KU EcoHawks 1997 JimmE-V

The author has worked with the JimmE-V as an undergraduate student from 2011 until 2012, and then as a graduate student from 2012 until 2015. During this time, the main concentration of the author

has been the powertrain system consisting of the motor, motor controller, the electronic control module, and the establishment of a vehicle CAN bus. This material is covered in detail later in this chapter.

Along with producing full-scale electric vehicles, the EcoHawks have also been involved in retrofitting existing EVs to improve their range and functionality. During the 2013-2014 academic year, a team of EcoHawks retrofitted a Global Electric Motorcar (GEM) with a swappable battery pack. The GEM can be seen in Figure 13.Figure 13: GEM Neighborhood EV. The original lead acid pack was removed and replaced with a detachable $LiFePO_4$ battery pack composed of twenty-four batteries in series with a 40 Ah capacity.

Figure 13: GEM Neighborhood EV.

As with any advanced composition battery pack, a new battery management system and battery charger had to be installed to properly maintain and regulate its charging and discharging. The selected BMS was the Orion BMS produced by Ewert Energy Systems. The accompanying charger was an Elcon charger. The advantage of selecting these two compatible components was that they communicate via a CAN bus. Since these two components communicate in this manner, the resulting setup and programming was simplified. However, the original motor controller in the GEM was not CAN capable; hence, additional relays were installed to allow the BMS to control how power was used in the vehicle. The author became involved with the GEM project during the summer of 2014 to trouble-shoot and diagnose BMS issues, and extend the vehicle range. More information on the GEM project and the work conducted on this vehicle are discussed in further detail in the following section.

2.4.1 EcoHawks GEM Short-Range Electric Vehicle Swappable Battery Pack

As previously mentioned, the GEM is a short range EV that was retrofitted with an advanced composition swappable battery pack. The goal of the GEM is to collect and deliver recycling to the university collection facility. In addition, the GEM will also be used to transport university staff to a variety of campus locations as needed. The GEM is a low speed vehicle that is restricted to a maximum vehicle speed of 25 miles per hour (mph), and can only transport up to two passengers. The key feature of this vehicle is the swappable battery pack. Utilizing modeling, the undergraduate students involved with this effort predicted that the GEM would require 63.76 Ah of charge capacity to complete the vehicle's pre-determined route while employing heavier lead-acid batteries (420 lbs). In order to minimize cost and vehicle weight, students selected 40 Ah $LiFePO_4$ batteries at a weight of 74 lbs that can be discharged to a lower state of charge. The battery pack can easily be swapped with a fully charged battery pack if it is found that 40 Ah is not sufficient [17]. The team additionally designed the battery storage drawer to accommodate 70 Ah and 100 Ah batteries. During the upgrading process, the team had to install a BMS and a new battery charger to maintain the $LiFePO_4$ batteries properly. Upon completion, the vehicle was struggling to achieve the desired range (student predicted at 15 miles) with the vehicle only able to travel four miles. Hence, the author was brought onto the project to troubleshoot and diagnose any issues with the BMS and CAN bus that could resolve the problem. The first step was to review and examine the powertrain layout.

The GEM powertrain is basic, consisting of a DC brushed motor that is transversely mounted to a transmission. The transmission provides a gear reduction to keep vehicle speed around 25 mph. There are three drive positions: drive high, drive low, and reverse. However, drive positions are electronically controlled through the motor controller, not through a traditional shift of transmission gears. The GEM is a Front Wheel Drive (FWD) vehicle with the battery containment drawer located forward and above the rear axle. Figure 14 shows an overall vehicle powertrain layout, and Figure 15 shows the motor layout. After examination of the vehicle powertrain it was determined that the motor likely need to be rebuilt. Klemp Electric Motor Company in Kansas City was selected to rebuild the motor. Klemp installed new

bearings and brushes in the motor, and the rebuild resulted in smoother motor operation. After examining the vehicle powertrain, the next step was to examine how the vehicle was controlling the power use through the BMS.

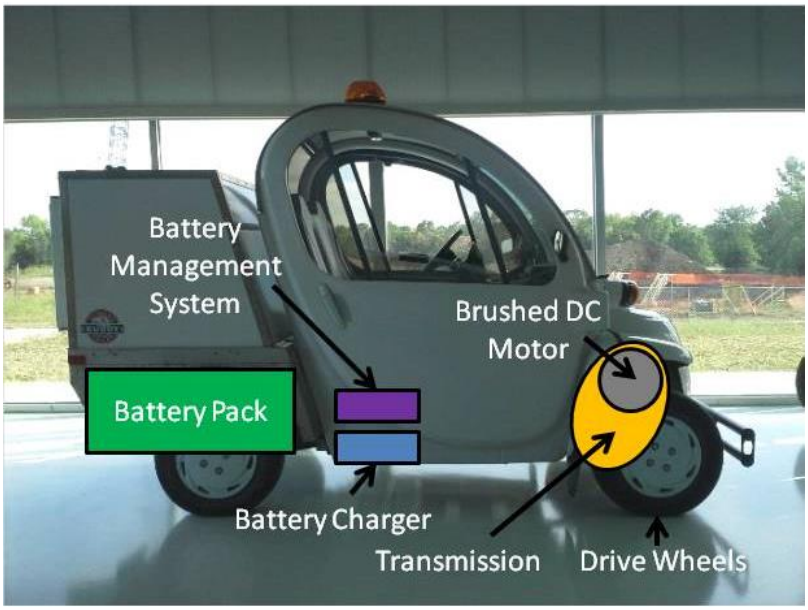

Figure 14: GEM Powertrain Layout

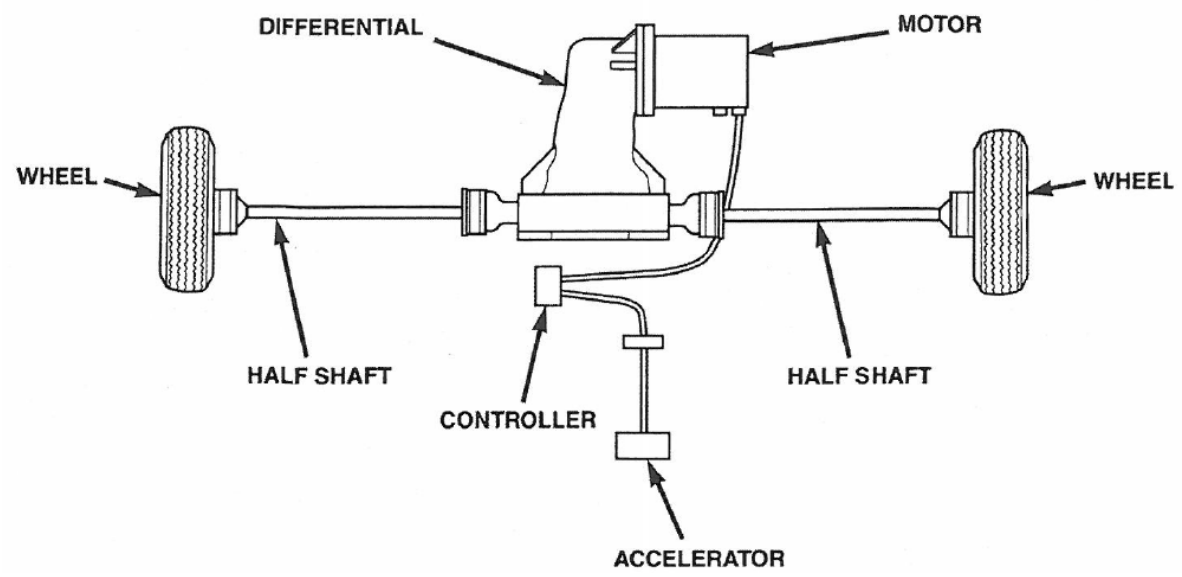

Figure 15: GEM Motor Layout [18].

The GEM BMS and battery charger communicate over a CAN bus, and from previous sections it is known that CAN is a digital protocol. Consequently, the BMS is calibrated using a computer through a

Universal Series Bus (USB) port and a CANadapter (Figure 16). The initial inspection of the CAN bus wiring showed that the team had correctly wired the Orion BMS to the Elcon charger and had the network properly terminated as described in section 2.2.4. However, it was observed that the CAN bus modulates the current discharge to the motor from the batteries within the BMS calibration utility tool. Since the CAN bus on the GEM is a simple two-node network, this was identified as an issue because there were no other components on the network to control current discharge. The Elcon battery charger only controls the charging current limits, and cannot control battery pack discharging. A quick solution would be to put the motor controller on the CAN bus; however, the controller was not capable of communicating via CAN. As a result, discharge current would have to be controlled using other methods.

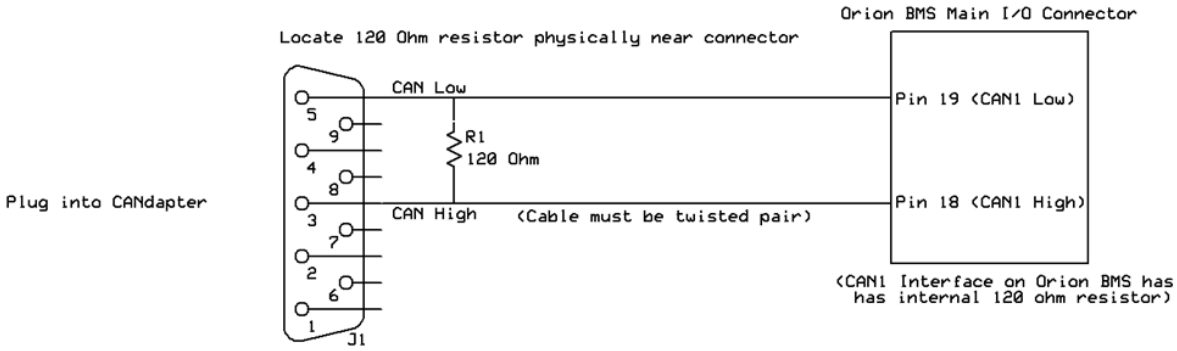

Figure 16: CANadapter wiring diagram for the Orion BMS [11].

In order to verify that the current discharge limit was not being enforced, the vehicle was driven while examining a real time plot of current draw from the battery pack using the BMS utility. It was observed that under heavy acceleration, the motor would draw over 100 Amps from the battery pack, subsequently reducing the capacity of the batteries due to excessive C-ratings [19]. This number varied based on the amount the accelerator pedal was depressed. This introduced another issue because the motor was only rated to handle 56 Amps. In order to ensure that discharge current would be regulated properly, the BMS manual was reviewed to determine if there were any other means to regulate current without significant vehicle control system modifications.

The goal of the Orion BMS system is to protect and monitor the battery pack through sensors. The BMS receives voltage information through cell voltage taps, a total voltage tap, a hall effect current

sensor, and thermostats to monitor cell temperature. The BMS uses pre-programmed settings to broadcast signals to control pack discharge current and pack charging current. Moreover, the BMS balances the cells using internal shunt resistors during the charging and resting processes. This ensures that all cells are balanced and at approximately the same voltage. The cell taps allow the BMS to monitor each cell voltage, ensuring that the voltages are not too high or too low according to the pre-programmed values. Using the measured cell voltages, pack current, and additional programmed values in the battery pack profile, the BMS calculates the individual cell's internal resistance, and open cell voltages. These calculations then allow the BMS to monitor the battery pack's State of Health (SOH) and State of Charge (SOC). The BMS additionally monitors battery pack safety issues, such as high voltage isolation, current sensor failure, and BMS internal failures. When a failure occurs, the BMS enters a safe mode and notifies the user by employing failure codes. Failure codes can be viewed using a computer and the BMS utility. This allows issues to be easily identified and repaired.

After reviewing the BMS manual, it was determined that the BMS can regulate current using three different methods: current limiting via CAN bus, current limiting via analog voltage outputs, and current limiting via on/off signals from the BMS. Current limiting using CAN bus is the simplest method due to the amount of chargers, controllers, and other EV equipment that employ a CAN bus interface. This allows components to broadcast desired limits and have the remaining components on the network monitor the broadcasted messages. Additionally, controlling current limits via CAN has proved to be just as fast and reliable in EV applications as CAN-based control in traditional combustion vehicles. An additional advantage of using CAN to control current and electrical power is that power can be gradually reduced when the battery pack capacity is nearing empty. Hence, the vehicle gradually slows down versus suddenly cutting out leaving the vehicle and passengers stranded. Unfortunately, the GEM motor controller is not CAN compatible, and as a result, this was not a viable method for limiting battery pack discharge current.

The second method limits current via analog voltage outputs that range from 0 to 5 VDC and provide an analog representation of the maximum current limits. For example, 0 VDC would represent

0%, and 5 VDC would be 100% with respect to the maximum current limit. This method is best applied in situations where a motor controller does not support CAN, but uses a 5 VDC potentiometer for the accelerator pedal. Upon further review of the vehicle wiring diagrams, it was determined that the GEM was indeed equipped with a 5 VDC potentiometer accelerator pedal. Figure 17 shows the accelerator pedal wiring diagram. Pin 8 on the motor controller provides the accelerator pedal voltage supply at 4.3 VDC to pin K of the accelerator pedal. Since the remaining method is a simple on/off function, this method appeared to be the better choice for current limiting the battery pack.

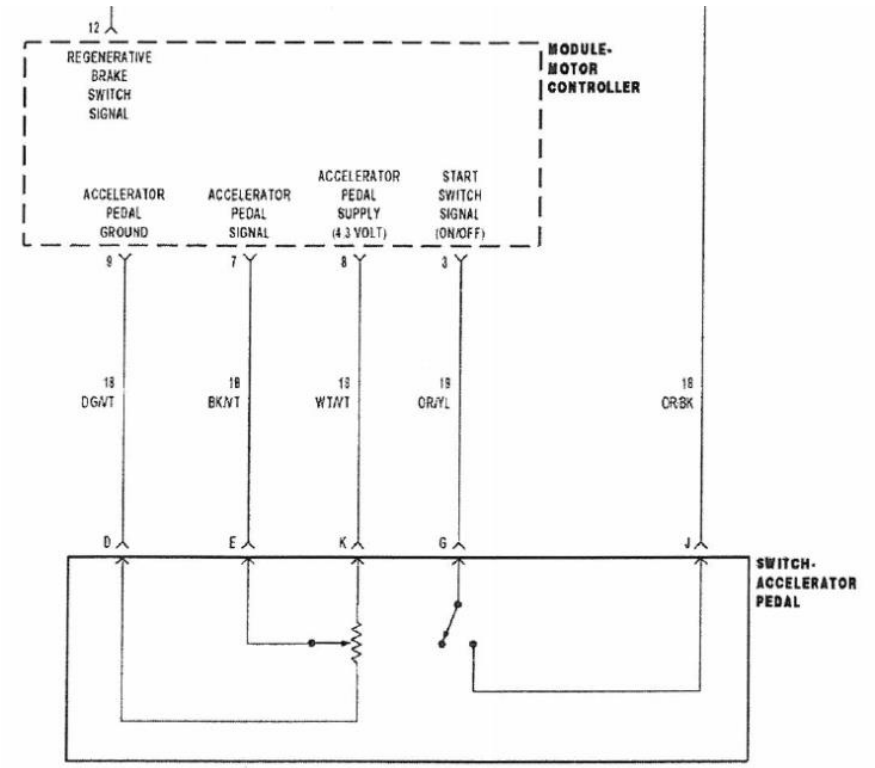

Figure 17: GEM potentiometer accelerator pedal schematic [18].

Upon attempting to substitute the BMS 5 VDC with the motor controller's 4.3 VDC signal, an error code was present on the GEM vehicle display, and the vehicle did not function. The code was investigated via the GEM repair manual, and it reflected a problem with the accelerator pedal wiring. It was concluded that since the BMS and the motor controller did not share a common ground, the BMS signal differed in voltage compared to the motor controller voltage signal. This issue could not be corrected because the motor controller was part of the isolated high voltage circuit and did not share a

common ground with the vehicle chassis. With the first two methods of current limiting unsuccessful, the only remaining method was to utilize an on/off signal from the BMS.

The final and simplest method for limiting battery pack discharge current through the BMS utilizes an on/off signal through the BMS outputs. In this case, the discharge enable output was utilized that toggles on or off depending on the driving conditions and the pre-programmed current discharge limits. This method could be implemented in multiple locations as well. The initial attempt of this method employed the GEM high voltage contactors. This added the BMS in series with the motor controller and main contactor while not requiring any additional components. However, when this was tested, another fault code related to the main contactor was displayed on the dash resulting in the vehicle ceasing to function. Further options for implementing the final current limiting method were to interrupt the accelerator pedal signals to the motor controller. Effectively, this would allow the BMS to disable the driver inputs to the controller preventing further current discharge from the battery pack.

To implement this method, an additional relay was needed. The selected relay was a reed relay sourced from Digi-Key, part number 725-1033-ND (Figure 18). The relay was initially installed in series with the accelerator pedal voltage supply, but another fault code was displayed identifying accelerator pedal wiring. In order to use this method successfully, a motor controller input wire would have to be interrupted without tripping a vehicle fault code.

Figure 18: Digi-Key Reed Relay #725-1033-ND [20].

Fortunately, the start switch signal that was wired to the accelerator pedal provided the desired results. From the wiring diagram presented in Figure 17, it was determined that this signal simply just toggled a switch in the accelerator pedal as a part of the vehicle start sequence. Since the relay would just act as an additional switch, it should not trip a fault code as in previous attempts. The relay coil was wired to a 12 VDC wire, and the other side was wired to the discharge enable pin on the BMS. When the current limit is reached, the BMS disconnects power to the relay coil causing the switching side of the relay to toggle to the open position. The switching side of the relay was wired into the start signal switch wire circuit. The revised pedal schematic is presented in Figure 19, On the coil side of the relay, it was important that current into the BMS did not exceed 175 mA. The selected relay's rated coil current was 126.3 mA, well below the current limit into the BMS.

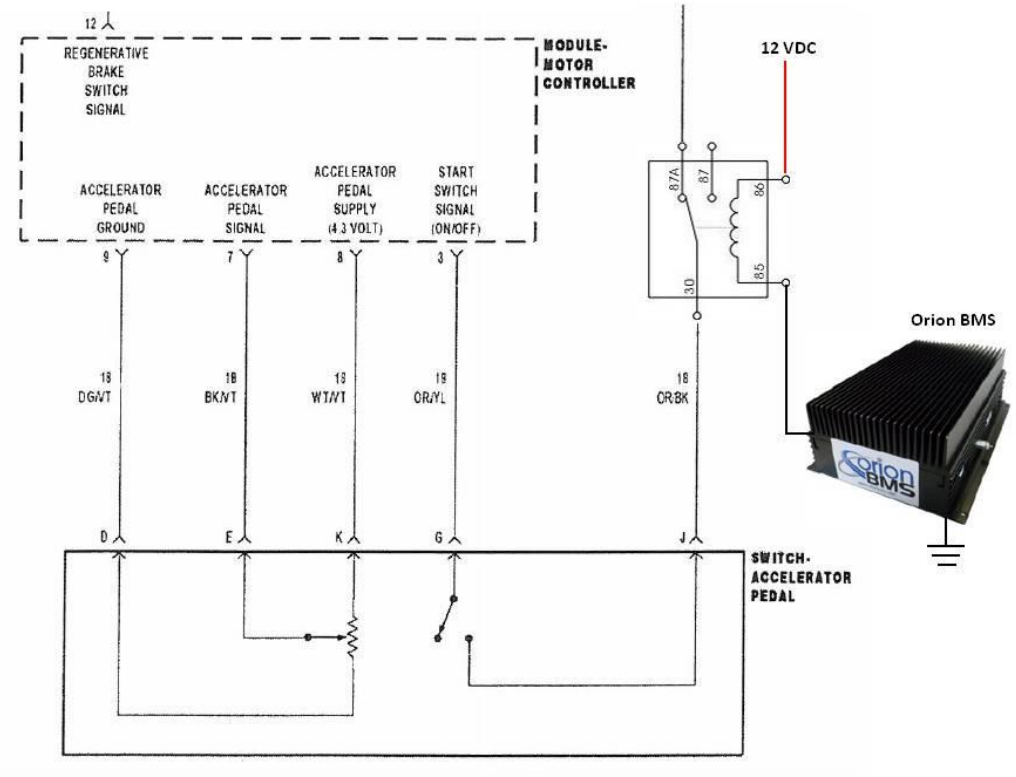

Figure 19: GEM Revised Accelerator Pedal Schematic with the BMS current liming by toggling a relay on/off [18].

Upon testing the relay, the system functioned as desired without tripping any vehicle fault codes. The goal of controlling the discharge current was to prevent drivers from rapid acceleration, subsequently depleting the battery pack. Hence, the current limit was set to 30 A in order to conduct additional vehicle range tests. During the first test, the relay functioned as designed, but it would not reengage once the current fell below the limit. After numerous emails with Ewert Energy regarding the issue, they stated that the BMS had not been programmed to be used that way, and that the only way to reset the relay was to cycle the BMS power through the key switch. This result was not desirable and would result in the user having drivability issues. Ewert Energy and the author then collaborated to develop and beta test updated BMS software (see Figure 20) that would allow the discharge enable relay to reset after a specified time amount. The minimum time of one second was programmed and resulted in a more desirable result. Further range tests were conducted with an improvement in range up to seven miles. However, the current limit of 30 A was not providing enough current to the motor to accelerate the vehicle up the steep elevation grades found on the University of Kansas campus. Moreover, during these range tests, another issue was discovered.

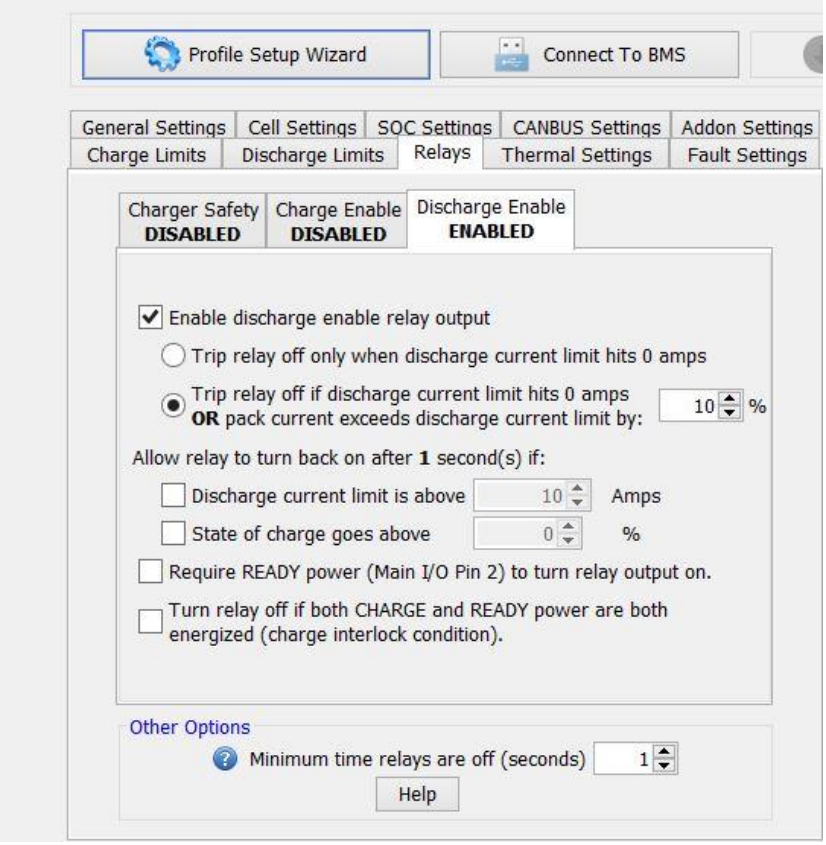

Figure 20: Updated Orion BMS Software GUI showing the discharge relay tripping at 10% above the specified limit and the minimum reset time.

After charging the battery pack to a perceived 100% SOC, the vehicle would drive around until the pack SOC was lowered to 20%. After a drive cycle, the vehicle was then plugged in and allowed time to charge. The battery pack capacity was 40 Ah, and the battery charger had a maximum charging amperage of 10 A. Hence, in order to go from a depleted battery pack to a fully charged battery pack, it should take approximately four hours based on the stated charging rate. During one of the vehicle's charging cycles, it was observed that the SOC went from 20% to 100% in under an hour. Upon this observation, it was concluded that there were further issues with the initial programming of the BMS unit.

When the BMS was first installed into the vehicle, the EcoHawks team had to program the BMS using basic guidelines provided by Orion online. During this effort they indicated there were areas of uncertainty with what they were accomplishing. During the process of assisting Ewert Energy with beta testing software updates, the BMS software was updated twice. One of the updates featured a battery

setup wizard that guided the user through the initial setup process using pre-programmed values for different battery types. Instead of filtering through the initially programmed BMS settings, the initial settings were saved and then the BMS was reset so that the new program could be compared to the initial program. Reprogramming the Orion BMS simply involved using the setup wizard tool to specify that twenty-four CALB 40 Ah batteries were being used in series, with a nominal cell voltage of 3.30 VDC. From those provided parameters, the BMS re-programmed itself using values from the selected battery profile. With the BMS reset, the new program could be compared with the original program to determine where the error had occurred.

The error occurred during the programming of the SOC settings. For lithium batteries, SOC is difficult to calculate due to a flat voltage discharge profile. As a result, the BMS has to monitor battery current and employ a method called Coulomb counting to estimate the battery pack SOC. Coulomb counting monitors battery current use over time and while this method is accurate the SOC needs frequent re-calibration. The Orion BMS uses battery profile settings to determine any discrepancies between the calculated SOC based on voltage versus the measured SOC based on Coulomb counting. When discrepancies are found, the BMS causes the calculated SOC to drift towards the correct SOC using specified voltage drift points. This drift allows the SOC to be adjusted over time that results in advanced system warnings and avoids system oscillations [21]. Figure 21 shows the original voltage drift settings, and Figure 22 shows the voltage drift settings after resetting the BMS.

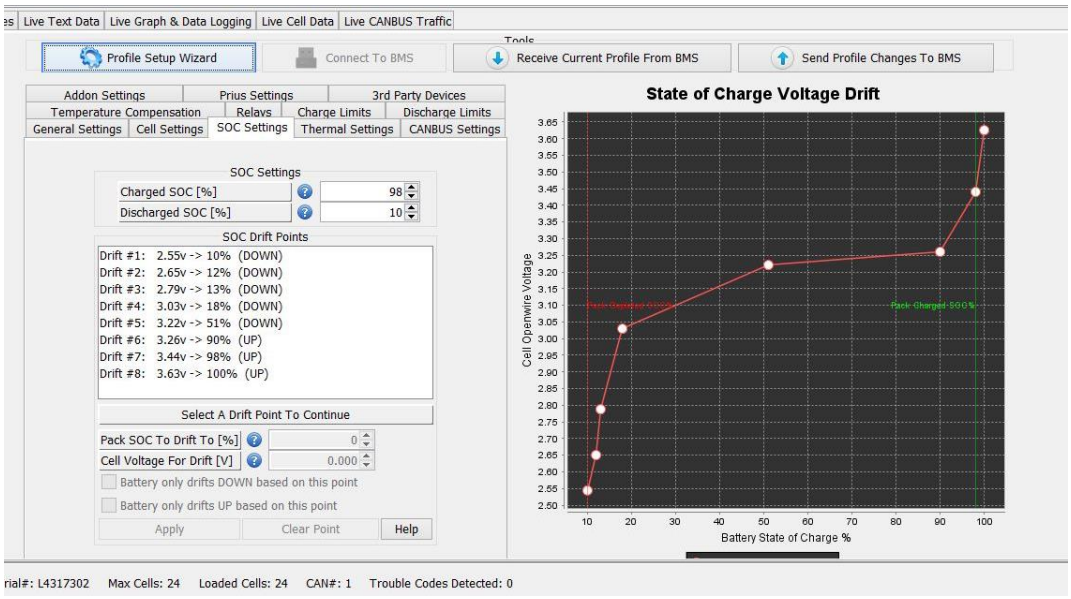

Figure 21: Initial BMS Voltage Drift settings provided by the Orion BMS software utility.

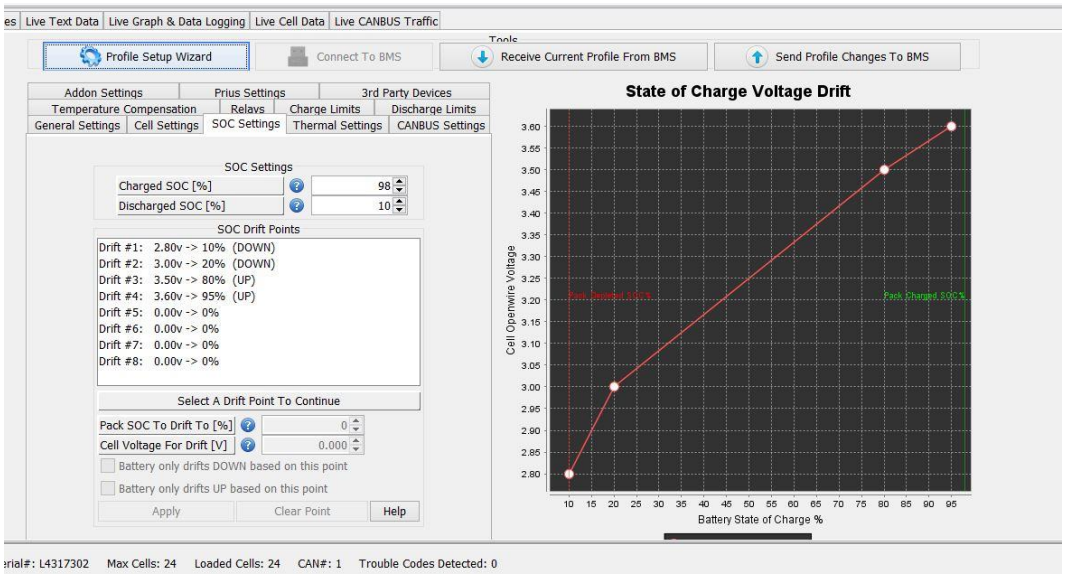

Figure 22: Reprogrammed Voltage Drift using the provided battery profile provided by the Orion BMS software utility.

After re-programming the BMS, the vehicle was tested again over the same route. However, as previously mentioned, 30 A was an insufficient current limit and it was preventing the GEM from climbing steep elevation grades. To allow the vehicle to climb steep hills, the current limit was set to the motor's current limit of 56 A. There is a 10% tolerance that allows the current to briefly exceed 56 A (61.6 A maximum) before tripping the discharge enable relay. The tested route was driven on the west side of KU's campus, as shown in Figure 23. The elevation profile was similar to the elevation profile

used in the undergraduate student's initial design calculations (Figure 24). From the route and elevation data presented, the test route was only 6.6 km, or 4.10 miles. Consequently, the route was repeated in circuit fashion until the SOC dropped to 10%. This resulted in a range of 16 miles and approximately 180 miles per gallon equivalent (mpge). These improved results align with the EcoHawks initial model predictions (i.e., 15 miles). Overall, having the ability to monitor battery pack data via CAN bus significantly aided the diagnostics process, subsequently improving vehicle range.

Figure 23: Drive Cycle Route shown on Google Maps.

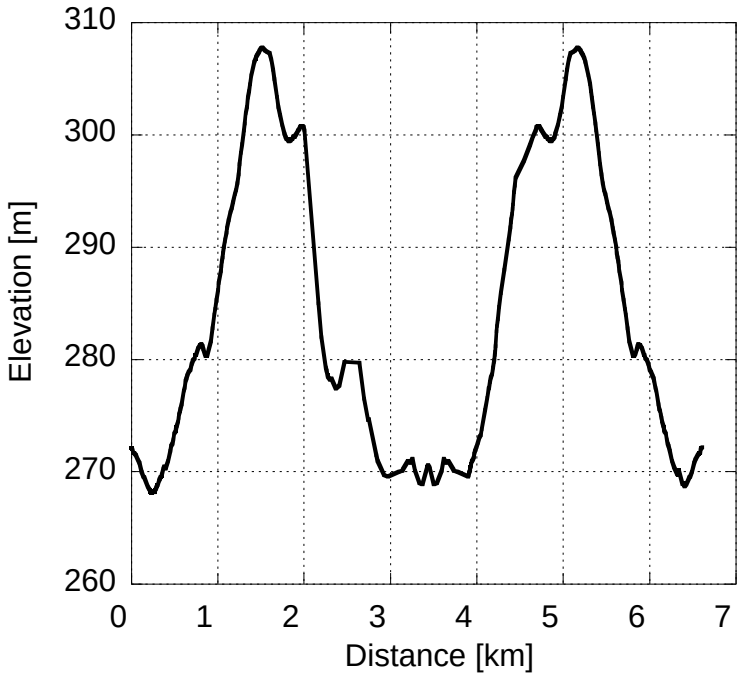

Figure 24: GEM Drive Cycle Elevation Profile. Elevation was calculated using http://www.doogal.co.uk/RouteElevation.php.

Being able to utilize a laptop connected to the BMS CAN bus significantly aided in vehicle diagnostics. Issues and faults were quickly identified through fault codes broadcasted by the BMS. Without the ability to view real time data transmitted over the CAN bus, the charging and discharging issues may have never been identified. The overall powertrain system was additionally protected with the installation of a relay to cycle driver input when battery current exceeded programmed limits. Through the combination of understanding how the vehicle systems work, the basics of CAN bus systems and its benefits, and system diagnostics skills, the overall range of the GEM short-range EV was increased resulting in a successful battery pack upgrade. Hence, the GEM vehicle proved to be a successful application of vehicle networking and diagnostic skills. The GEM proves to be a good example of simple and small vehicle networks; whereas, the JimmE-V introduces multi-node networks. The next section is dedicated to the design and installation of a multi-node CAN bus in a full-scale electric vehicle.

2.4.2 EcoHawks 1997 GMC Jimmy KU EV 2.0

The purpose of this project is to demonstrate the use of engineering principles in order to develop an innovative alternative energy vehicle as opposed to a vehicle that runs on non-renewable fossil fuels. By taking lessons learned from the VW Beetle EV conversion, the JimmE-V represents an EV that a consumer could purchase on today's automotive market. The vehicle chosen for the conversion was a 1997 GMC Jimmy with a 4.3 L six-cylinder engine. The engine was coupled to a five-speed automatic transmission with four-wheel drive. Due to the majority of sport utility vehicles on the roads in the United States, this vehicle was a perfect candidate for an EV conversion. Using current automotive technology, a CAN bus allows communication between vehicle components. Component communication over the same network offers improved efficiency and reliability and due to the potential high voltage hazards in electric vehicles, this is a desired feature. The JimmE-V's main features include an alternating current (AC) motor, a motor controller, a lithium iron phosphate ($LiFePO_4$) high voltage battery pack, an electric air conditioning compressor, an electric power steering pump, and a standard automotive 12 VDC system to run interior features. The focus of this section is the establishment of the vehicle CAN bus, covering why it was needed, the network architecture, the components on the bus, and the installation process. Since the vehicle powertrain is controlled via CAN, vehicle powertrain design and components will be covered to compliment the importance of the vehicle's CAN bus.

In comparison to the original GMC Jimmy, the JimmE-V powertrain is simpler and contains far less components. The AC motor, installed in the front of the vehicle, directly transfers power to a driveshaft that is coupled to the vehicle's rear differential, as seen in Figure 25. From the differential, there is a gear reduction through a final drive ratio of 3.08 before power finally reaches the wheels and pavement [22]. Since the motor directly drives the rear wheels, drivetrain losses are only present in the system's bearings and the differential. Whereas, the original Jimmy had drivetrain losses in the transmission, transfer case for four-wheel drive operation, and the rear differential. Each pair of gears used to transfer power are 95-97% efficient, with bearings and joints 98-99% efficient [23]. Further losses

can be found in the vehicle's torque converter or clutch depending on the transmission setup; however, the simplified EV powertrain does not contain those components.

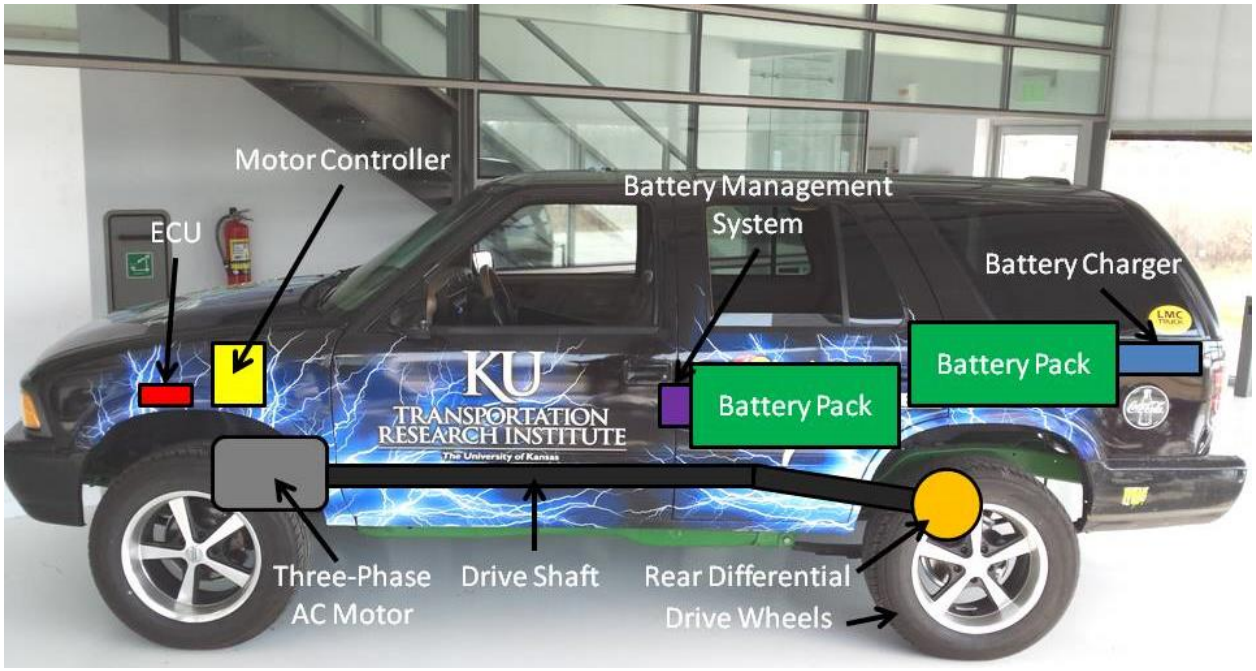

Figure 25: JimmE-V powertrain layout

Providing power to the motor is accomplished through 104 CALB $LiFePO_4$ batteries connected in series. Each cell in the battery pack is 3.30 VDC nominal and has a capacity of 100 Ah. Due to the size of the battery pack, the pack was split into two equal dimension battery boxes. To protect this energy source safely, the boxes were constructed from Polyvinyl Chloride (PVC), and are surrounded with recycled rubber mats to electrically isolate the pack. The boxes were placed in the vehicle as low as possible to lower the vehicle's center of mass and still provide easy access for service and data acquisition. Additional safety measures such as fuses and contactors were also installed, and will be covered in detail in Chapter 3 of this document.

From the battery pack, current flows through shielded high voltage cables to the motor controller that is located under the hood of the vehicle. The controller is an Azure Dynamics DMOC445 controller and inverter. The inverter is necessary to convert the DC power supply from the batteries into AC power for the three-phase motor. The DMOC445 is controlled via CAN bus, which requires the use of an ECU

to communicate driver input to the motor controller. Both the motor controller and ECU will be covered in more detail in this section, and operation and calibration will be covered in Chapter 3 of this thesis.

The JimmE-V also features an Elithion Lithiumate Pro BMS to maintain the lithium battery cells. As previously discussed, the BMS helps regulate battery pack charging and discharging based on pre-programmed limits. The BMS used in the JimmE-V is also capable of communicating via CAN bus; however, the selected Azure controller is not compatible with the Elithion BMS. The BMS can communicate battery SOC information via CAN bus to a display located next to the vehicle's emergency power disconnect contactors. Charging the battery pack is accomplished through a Manzanita Micro PFC 20 device. The charger is controlled via the BMS using AC and DC relays. Since this section is focused on how the vehicle powertrain and CAN bus functions, further BMS and battery charger information can be found Chapter 3. With an understanding on how the entire powertrain functions, the main CAN components will be examined.

The original JimmE-V design team selected the Azure motor and controller in 2010 due to an initially assumed simplicity. Both the motor and controller are air cooled negating the need for additional cooling and heat exchanging components. Additionally, the AC55 motor displayed a flatter efficiency curve over the motor's operating range. The AC55 motor was also designed and built for use in larger trucks and vans [22]. The motor was then paired with Azure's DMOC445 controller that is both a motor controller, as well as an inverter to transform the DC power into AC power. A system schematic is presented in Figure 26. The Energy Storage System (ESS) represents the high voltage battery pack. The ESS provides DC power to the DMOC and inverter, and from the inverter AC current powers the motor. Additionally, a 12 VDC auxiliary battery is required for the DMOC to operate. The ECU is not pictured in the figure, but is represented in the schematic from the arrow for application inputs and outputs.

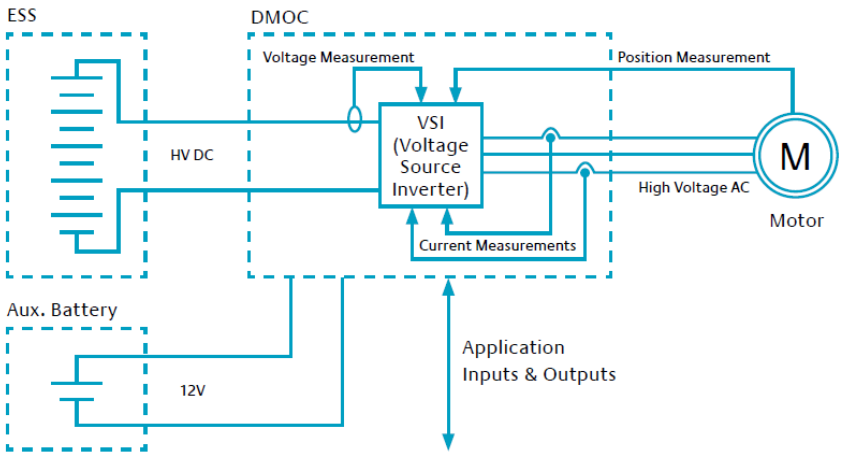

Figure 26: Azure DMOC445 and AC55 system schematic [24].

Since the DMOC is CAN controlled, an ECU is required to send command messages via CAN bus. To get the DMOC communicating on the CAN bus, the CAN bus needed to be wired, and then CAN parameters needed to be programmed in the controller using Azure's software utility ccShell. From section 2.2.4, it is evident that the wiring is relatively simple and will not be covered in depth. In order to plan the network properly, the network was set up as a multi-node network to allow the addition of other components in the future. The CAN bus was wired to the 8-pin terminal that plugs into the DMOC. That same connector also is connected to the RS232 communication to communicate with a laptop for programming and data logging. The middle terminal is the 35-pin connector that is used for interfacing with the vehicle to obtain 12 VDC power and drive enable inputs. The connector on the far right is the 14-pin connector that is connected from the controller to the motor. This connection monitors the speed, direction, and temperature of the AC55 motor [24]. The three different wiring terminals for the DMOC445 are shown in Figure 27.

Figure 27: DMOC445 connection terminals. The 8-pin teminal for vehicle communication is on the left, the 35-pin interface terminal is in the middle, and the 14-pin terminal for motor data is on the left [24].

In order for the DMOC to work, high voltage (330 VDC) and auxiliary voltage (12 VDC) need to be present. To ensure high voltage isolation, the DC high voltage cables are connected to terminals inside a moisture proof covered section of the motor controller case as seen in Figure 28. The 12 VDC connection is accomplished through the 35-pin connector terminal on pin 9. The 12 VDC power is controlled by the ECU that is discussed later in this section.

Figure 28: High voltage connections for the DMOC445 [24].

With both high and low voltage present, the internal contactors within the controller need to engage in order for the vehicle to operate, for the operator to change controller variables, or for the operator to view real-time data. The internal contactors will engage once the vehicle is shifted from the park position using the shift knob. Of note, the contactors can be engaged by shorting the drive enable pin

(pin 7) to a digital ground on 35-pin terminal on the controller (pin 35). The shift knob will be covered later during the discussion of the ECU.

The ECU is responsible for sending 12 VDC power to the DMOC along with torque command messages to accelerate the vehicle. However, before the DMOC can communicate with the ECU, the initial CAN parameters needed to be programmed.

Once initially programmed, the CAN parameters should not need to be changed. However, if any CAN bus systems change, the user can easily adjust the CAN variables if needed. In order for the ECU and DMOC to communicate, they first need to have the same baud rate. The programmed baud for the ECU and DMOC is 500 kbits/second. In ccShell (use discussed later), the variable EEXCANBitS specifies the current baud rate. With the baud rate adjusted to 500 kbits/second, the ECU and motor controller additionally need to have an equal status ID. EEXCANCommandID is the variable for programming the status ID, and the value is set to 562.0.

In order to ensure that the controller functions as designed, the bit segment timing needs to be properly programmed to avoid CAN errors. One requirement from Azure is that (TSeg1 + TSeg2 + 1) should be an even divisor of the internal clock frequency divided by the baud rate. The clock frequency for the DMOC is 40 MHz. Azure provided timing settings for frequently used baud rates, and the timing options for the designed 500 kbits/second baud rate are provided in Table 1. Either of the two-bit segment timing options are acceptable for the designed baud rate. Since these settings were initially established, there should be no need to modify or alter the CAN parameters. In the event it is desired to alter these parameters, please consult the DMOC CAN Controlled Application User Manual or the DMOC445 and DMOC645 User Manual to ensure that any proposed changes will not interfere with the operation of the motor or controller.

Table 1: CAN Bit Segment Timing Options for 500 kbits/second [24].

CAN Baud Rate EEXCANBitS	DMOC Clock ÷ Baud Rate	EEXCANTSeg1	EEXCANTSeg2
500	80	13	6
500	80	5	2

In addition to properly setting up the CAN parameters, the controller has built-in Finite State Machines (FSM) to control operation modes. These variables can be viewed in ccShell, and can be used to diagnose potential issues if the vehicle is not operating correctly. There are FSMs that exist at the core and application level for the DMOC445. The application specific FSM refers to the device connection state. If a device, such as an ECU, is not online, the controller will not allow operation. The remaining FSMs are present at the core level of the controller. These core level FSMs are the contactor and powerstage FSM. The contactor FSM handles the pre-charge of the DMOC and the closing of the internal contactor, and is the ISR2ContactorState variable. When engaged, the contactor operates rapidly to either display OPEN or CLOSED in ccShell. The powerstage FSM handles the enabling and disabling of the power switches. ISR2PowerStageState is the variable that reflects the status of the powerstage FSM. Once the vehicle has gone through the start-up sequence of checking the discussed parameters and requirements for operation, this variable will display READY in ccShell reflecting that the controller is waiting for a power request. These variables and the operation of ccShell will be discussed more in Chapter 3 but are presented here to provide background knowledge on the controller's start-up sequence. With an understanding on how the controller initializes its start-up sequence, the final component to examine is the ECU. The ECU acts as a gateway between the driver and the motor controller providing accelerator pedal input, and controlling 12 VDC power to the DMOC.

When initially installed, there were communication errors with the ECU and motor controller. However, before examining these issues and diagnostics performed, the purpose of the ECU needs to be examined. The main finding from the previous research was that the JimmE-V could not operate with just a potentiometer accelerator pedal (similar to the Beetle EV), as the 2010 – 2011 team had planned. The analog signal produced from the potentiometer would not work as an input for the motor controller because the controller requires a digital CAN input. The solution was to locate a pedal that could communicate via CAN. Extensive searching concluded that there are no pedals that communicate using CAN. However, a company called New Eagle offered a solution. New Eagle created and programmed an ECU specifically for the JimmE-V architecture. The ECU converts the analog signal from a dual

potentiometer pedal into a digital CAN signal that the Azure Dynamics motor controller can read as an input. The ECU installation was completed in the fall of 2012. To understand how the ECU system works, the system will be examined as a whole before breaking down the components individually.

New Eagle provided a system schematic that shows all the wiring connections to the ECU, Smartcraft connection junction, accelerator pedal, and the Azure DMOC445; as seen in Figure 29. An enlarged view of some of the smaller components can be seen in Figure 30.

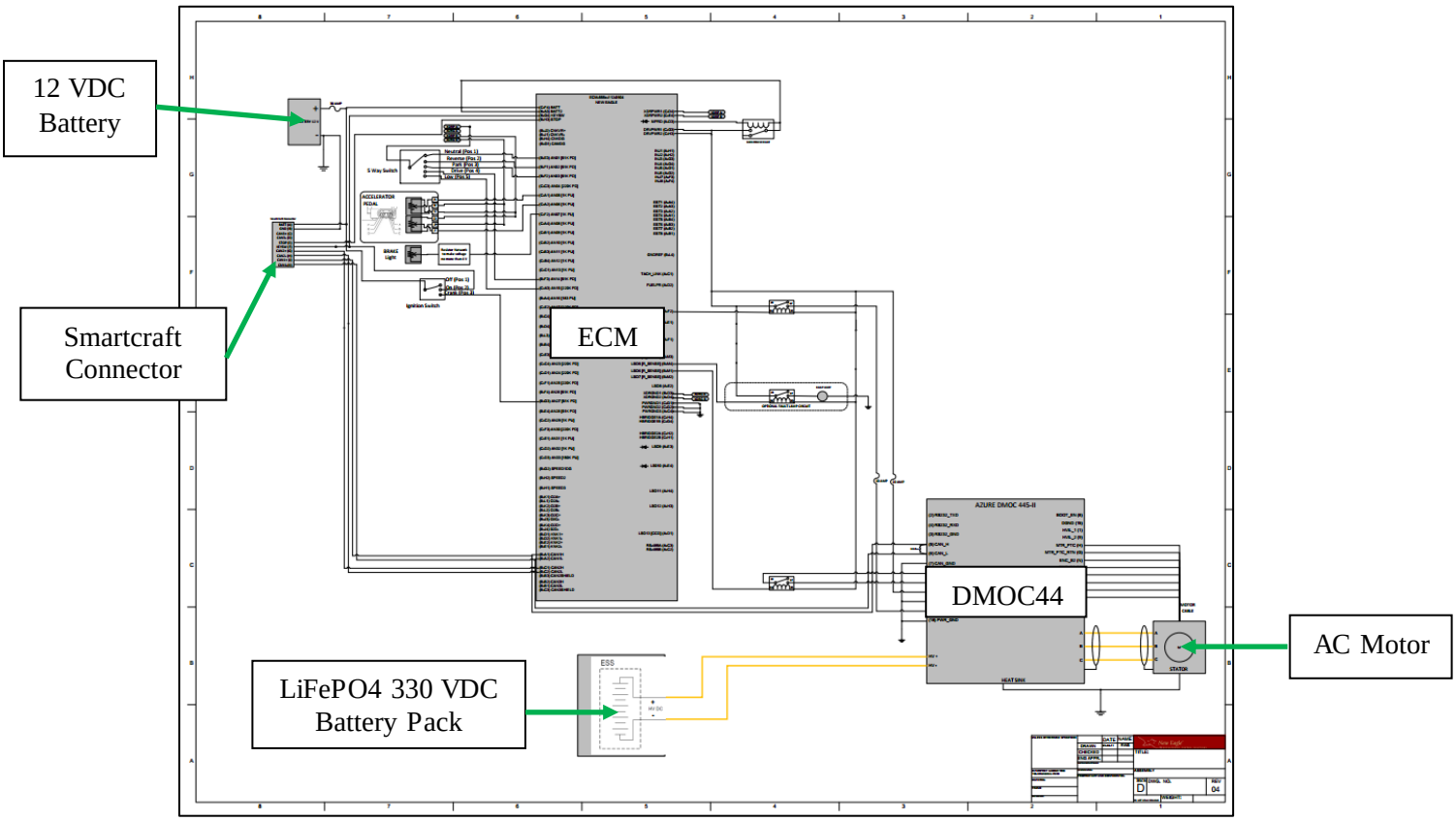

Figure 29: The New Eagle ECM system schematic showing the larger components.

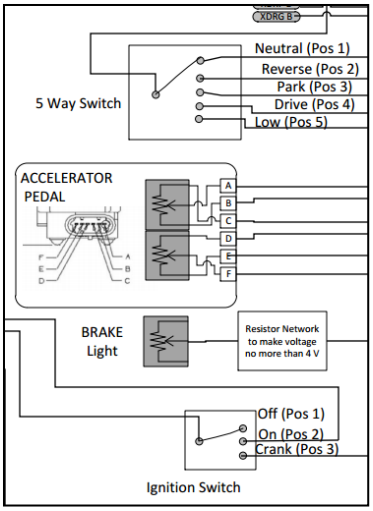

Figure 30: An enlarged view of how the accelerator pedal, brake light, ignition switch, and the five-way (position) switch are integrated into the New Eagle ECM system.

The New Eagle ECM operates on a 112-pin platform, and has three terminals labeled A, B, and C respectively, as indicated in Figure 31. The provided New Eagle wiring schematic has all the needed pins labeled, as seen in Figure 29. Initially, the connections in the wiring schematic for the ECM were difficult to interpret because the terminals lacked labeling. The A, B, and C terminals were determined by using a wiki page that New Eagle has setup for their product documents, as seen in Figure 31.

Here is how to interpret the ECM labeling: (B-C1) CAN1H represents one of the 112 pins on the ECM. The first B refers to the B terminal, and C1 refers to the grid set up within each terminal. The letters represent the column index, and the number represents the row index. CAN1H represents the function of the pin. This example represents one of three CAN high inputs. The ECM has two recommended gauges for wiring. The smaller pins on the ECM use 20-gauge wires and the larger pins use 18-gauge wire.

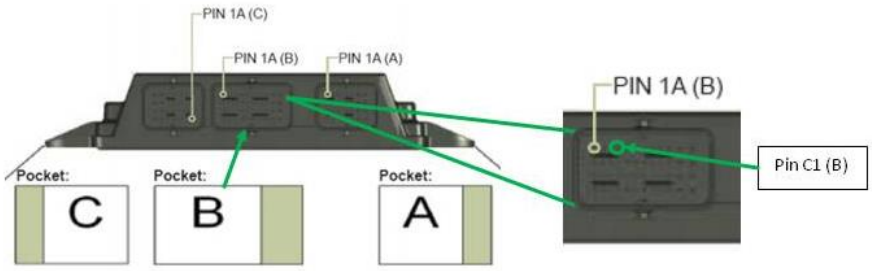

Figure 31: New Eagle ECM pin diagram showing the A, B, and C terminals. The image to the right shows a close up of terminal B, pin C1 [25].

The pedal that New Eagle selected and provided with their ECM system is a dual potentiometer pedal. When the pedal is pressed, the potentiometer changes the voltage sent to the ECM. The ECM takes the analog signal from the pedal and converts it into a digital CAN command message in the form of a torque request. The motor controller is then able to read the command message and operate the motor according to the message received. Figure 32 shows the accelerator pedal and the dual potentiometer pedal's position sensor. The 2012-2013 JimmE-V team leader, Kevin Helton, was responsible for designing and installing a bracket to accommodate the irregular dimensions of the accelerator pedal. The pedal bracket assembly uses the original Jimmy gas pedal mount on the firewall as a bolting location.

Figure 32: The New Eagle dual potentiometer pedal.

Another important part of the New Eagle ECM system is the five-position switch. This switch acts as the vehicle's "shifter." Each position on the switch represents a transmission function, similar to a standard automatic transmission (neutral, reverse, park, drive, and low). Despite having the standard drive functions on the shifter, the AC motor in the JimmE-V is a direct drive motor without a transmission.

Consequently, the JimmE-V only has three driving positions (forward, neutral, and reverse). Figure 33 shows the New Eagle schematic for the five-position switch. After initially testing the system, the switch position was changed by switching the neutral and park positions. Switching these positions resulted in a similar shifter present in a standard vehicle (park, reverse, neutral, drive, low).

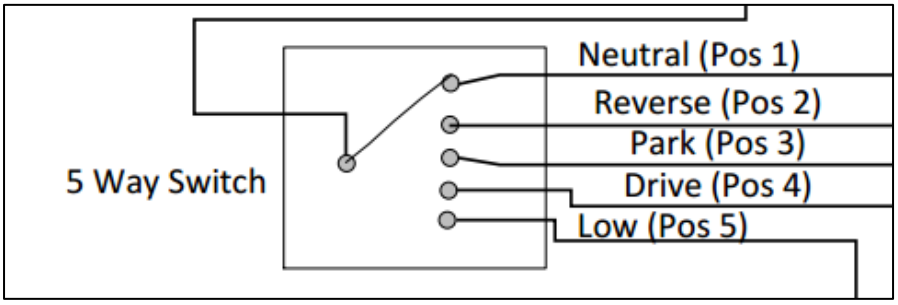

Figure 33: The New Eagle five-position switch schematic showing the different drive positions.

Initially there was a problem discovered while examining the New Eagle system schematic. In Figure 30 by the brake light symbol, New Eagle specified that a resistor network be implemented to limit the voltage going from the brake light (12 VDC when the brake pedal is depressed) to the ECU be no more than 4 VDC. They recommended the use of a voltage divider. A voltage divider is typically just resistors set up in series or parallel and provides an output voltage that is fractional to the input voltage. The most typical voltage divider is a Wheatstone Bridge, as seen in Figure 34.

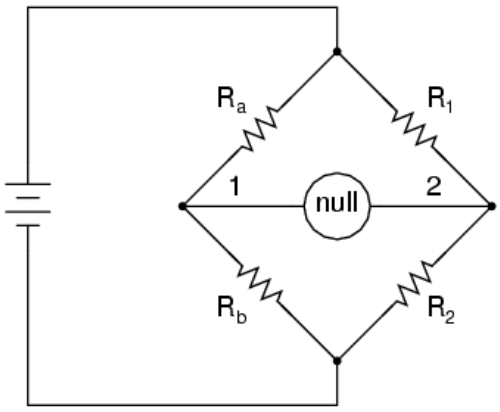

Figure 34: A typical Wheatstone Bridge voltage divider [26].

However, there is an issue with using a voltage divider. A 12 VDC battery is not a constant voltage source. As time increases under battery load, battery voltage decreases. Charging conditions produces the opposite effect. For the 12 VDC system, battery voltages could range from 14 VDC

(charging) to 10 VDC or lower (under load). Therefore, when the battery voltage drops to 10 VDC, the output voltage lowers by the fractional ratio created by the voltage divider. This is not a desired result because the brake light voltage signal to the ECU needs to remain a constant 4 VDC.

The solution to this problem is a voltage regulator. A voltage regulator maintains a constant output voltage, even if the input voltage is changing. There are set voltage regulators and there are adjustable voltage regulators. The voltage regulator used in the JimmE-V is AnyVolt Micro Voltage Regulator accompanied with a breakout board to simplify wiring. This voltage regulator is an adjustable voltage regulator, but after the initial installation and adjustment should not need further adjusting. The voltage regulator was installed under the hood of the JimmE-V located on the driver side wheel well. The wiring is part of the wire loom that runs from the ECU to the accelerator pedal. Figure 36 shows the location of the voltage regulator under the hood of the JimmE-V.

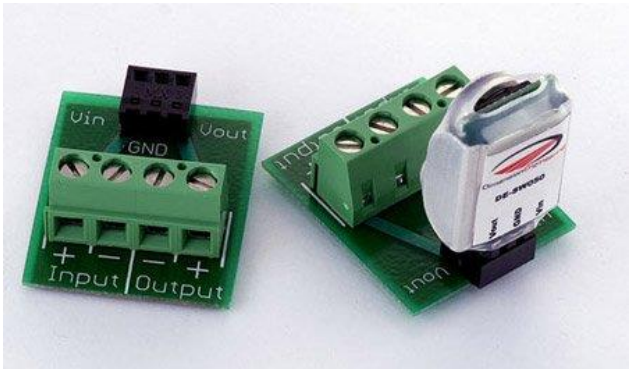

Figure 35: AnyVolt Micro Voltage Regulator and breakout board. Voltage adjustments are made via a potentiometer screw on the regulator [27].

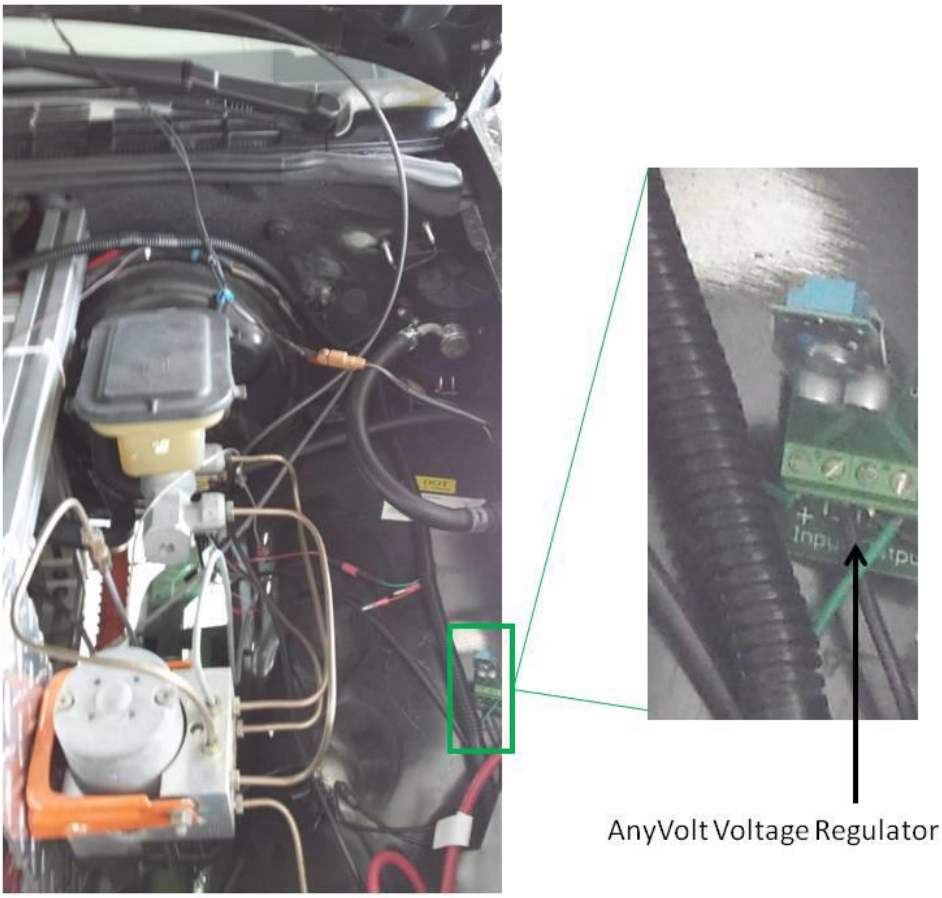

Figure 36: The voltage regulator is located under the hood of the JimmE-V on top of the driver side wheel well.

The relays and fuses in New Eagle ECU system may be the simplest, but they are the most important. The New Eagle system uses relays and fuses in order to provide overcurrent protection for the ECU and motor controller. A relay is an electrical switch. When supplied power, the relay electromagnetically switches to deliver power to the desired components. The relays in the New Eagle schematic switch power to the ECU and the Azure motor controller. The selected relays are five terminal relays rated at 40 A of current. The relays plug into terminals with wire leads (Figure 37) to allow easy replacement and troubleshooting.

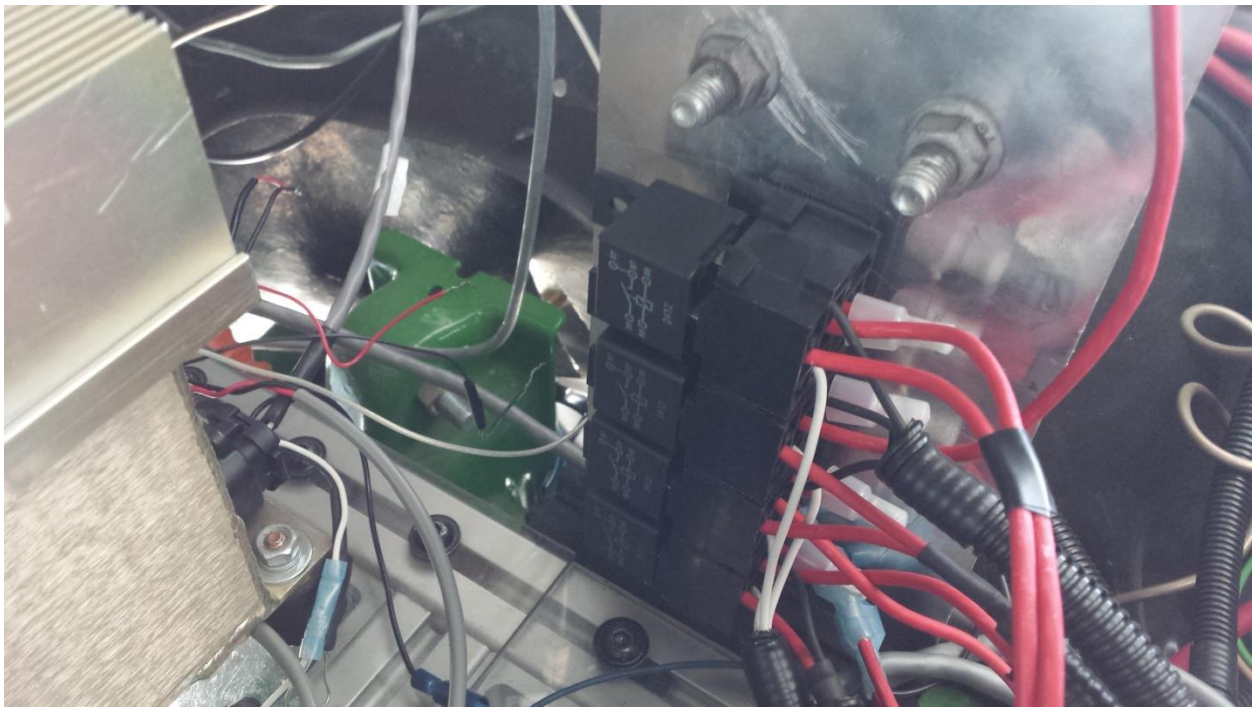

Figure 37: The four, five-terminal relays plugged into the relay plugs. The relays are installed under the hood of the JimmE-V located next to the ECU and motor controller.

To protect the ECU and motor controller from excessive current, fuses are used. The New Eagle schematic uses three main fuses. The main fuse is a 30 A fuse for the battery, as seen in Figure 38. There is also one smaller 10 A fuse to protect the motor controller. These relays and fuses are inexpensive safeguards that will protect expensive components from excess electrical current and damage. The final component in the New Eagle system is the Smartcraft connector. The Smartcraft connector allows the establishment of a vehicle CAN bus, allowing communication between the New Eagle ECU and Azure motor controller.

Figure 38: In-line fuse holder and 30 AMP fuse to prevent excessive current from the 12 VDC battery.

The Smartcraft connector plays a vital role in the establishment of the JimmE-V's CAN bus. It is through this bus that several critical components communicate: Azure Dynamics' motor controller, New Eagle ECU, and the laptop for monitoring and programming the ECU. The easiest way to visualize the JimmE-V's communication network is to compare it with a phone line. Components can send and receive messages over the bus (or phone line) as long as they are located anywhere in-between the two terminating resistors. The Smartcraft connector consists of multiple junctions on the bus, and the termination resistor occupies one of the terminals.

The Smartcraft connection junction allows multiple devices to connect at one central location. Originally, the Smartcraft connector was under the hood of the JimmE-V next to the ECM. However, a Minivew CAN gauge and computer can connect to this junction box. New Eagle programmed the Miniview gauge to display accelerator pedal position as a percent value including the torque request from the ECU. However, the gauge has a short cord to attach to the connection terminal. The Smartcraft connector also allows a computer to connect to the vehicle's network to obtain CAN data and monitor the ECU. The JimmE-V's glove box offered a central location to have accessibility to this network junction.

The Smartcraft connector has six terminal pockets, and each pocket has ten pins as seen in Figure 39. Even though the junction box has six terminals, the pins on each terminal are the same. The top left pin is Pin A, and the bottom right is Pin K, as seen in Figure 40. There is no Pin I because "I" is similar to a one, or the imaginary number symbol "i". Because each terminal has the same pin connections, the Smartcraft connector is an ideal junction to connect other components to the CAN bus. As previously mentioned, communication via CAN bus allows fast and reliable transmission of data. However, the first ECU installed in the JimmE-V did not allow the user to calibrate the ECU easily. In order to tailor the system for future research, another option was needed.

Figure 39: The Smartcraft connector has six terminals that display the same data on each pin.

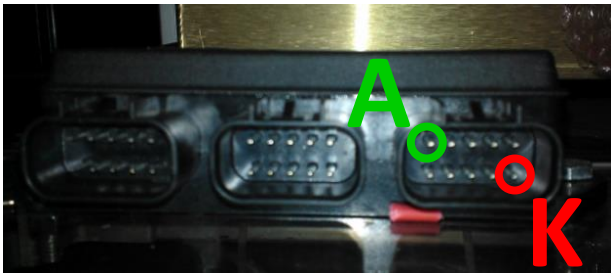

Figure 40: The Smartcraft connector has ten pins labeled A-K (omitting I). Pin A shows the same data on each terminal.

Initially, New Eagle supplied an ECU that was not capable of real-time calibrations. This was not desirable because anytime parameters needed to be changed, New Eagle had to change them and then send an updated version of the ECU code. Upon receiving the new version of the code, the ECU had to be re-programmed. To correct this, a different ECU was purchased through New Eagle in the spring of 2013 to allow real-time calibration, which is desirable from a research perspective. The two ECU's physically look the same, but there is internal hardware in the new ECU that allows the transmission of real-time data, and to instantly reprogram ECU parameters. Since the physical dimensions and wiring pockets were identical, the old ECU simply had to be disconnected from the wiring harness and unbolted. The new ECU was installed using the same bolt holes allowing the wire harnesses to plug back in without further

modification. The specific details pertaining to the ECU calibration and programming will be discussed in the user manual chapter of this document.

Overall, having the ability to connect a computer to the vehicle CAN bus and ECU to view real-time data and calibrate the system is a highly desirable feature. Without the foundation research on CAN bus features this system would not have been developed to its full potential. However, to get the ECU system operating correctly required additional system diagnostics and troubleshooting to get all the components communicating.

When the ECU wiring and installation was complete, the system did not function as designed. It was expected that upon completion of installation, the ECU and motor controller would communicate allowing operation of the motor. By using CAN diagnostic codes allocated by Azure, the issue was able to be resolved. The Azure DMOC445 has a variable that monitors the device connection state (ISR2DeviceConnectState). As mentioned, these variables can be viewed using Azure's ccShell software utility. Initially, ISR2DeviceConnectState was displaying a "1." After consulting the Azure CAN Controlled Application User Manual, it was identified that the motor controller was offline. With the controller offline, no CAN link was established. However, the controller was sending out a "ping" message that would be similar to a phone ringing waiting for answering. Once this ping message was answered, the controller could communicate through the CAN bus. After consulting New Eagle, it was established that the status IDs for the controller and ECU were not equal. As previously mentioned in this section, both components need to have an equal status ID in order to communicate. Once the EEXCANCommandID variable was changed to 562.0 in ccShell, the ISR2DeviceConnectState variable changed from displaying a "1" to a "2." When the variable ISR2DeiceConnectState displays a "2," the controller is indicating that contact has been established on the CAN bus, and that all messages are being sent. Once this occurred, the powerstage FSM mentioned earlier displayed "waiting on power request," and upon depressing the vehicle's accelerator pedal the motor rotated the wheels. Without the vehicle CAN bus and diagnostic abilities in the controller, getting the vehicle to move would have proved significantly more difficult.

Throughout both of the projects completed by the author and KU EcoHawks, CAN bus has played a vital role in the diagnostics and operation of the vehicles. With the network initially set up and programmed, real-time calibration delivers instant results that will aid in future vehicle research.

2.5 Conclusions

Vehicles in use during the early 21st century are composed of networks of complex control modules as consumer demand for technology in vehicles continues to increase. From safety features including air bags and anti-lock brakes to engine and transmission control units, these elements are designed to communicate seamlessly with other control modules and components throughout the vehicle. In order for a vehicle to operate efficiently and safely, all of these modules demand reliable, repeatable, and high-speed communication. This is achieved through a Controller Area Network (CAN) bus. Since the development on the CAN bus, the automotive industry has been able to successfully implement the technology to handle errors and faults in vehicle systems in addition to communicating data between different control modules onboard vehicles. Using CAN, automotive emission systems can be monitored and diagnosed. Because of the success of CAN in combustion-based vehicles, the protocol found an additional niche in electric and hybrid vehicles.

However, CAN is a difficult concept to initially understand. Through the implementation of CAN bus technology in small-scale networks, further insight can be gained. Both of the KU EcoHawks projects to implement a CAN bus demonstrated reliable and efficient operation. The GEM and JimmE-V additionally have served as excellent introductory work to a complicated subject. System issues can be diagnosed and addressed relatively quickly. Without the knowledge and background behind how CAN operates, these systems can be difficult to understand. Along with the knowledge gained through the development and installation of a CAN bus in electric vehicles, diagnostics skills were developed and honed throughout these project timeframes.

Chapter 3: JimmE-V Operation and Overview

3.1 Abstract

The JimmE-V was designed and constructed to serve as a research vehicle for the University of Kansas. The JimmE-V has amenities that make it similar to electric vehicles available to the consumer such as, electric power steering, heat, and air conditioning. Consequently, it is imperative to understand how the vehicle operates in order to generate research quality data. By implementing a CAN bus in the vehicle, the ECU and motor controller are able to reliably communicate offering repeatable results. Additionally, being able to view and calibrate powertrain control parameters in real-time allow the vehicle to be adjusted for multiple studies. In addition to operation and calibration, this chapter also highlights key safety points for maintaining and operating electric vehicles. The author's main area of work has been focused on the ECU and motor controller communication and calibration; however, since those systems interlink with additional vehicle systems, an entire knowledge of the vehicle is needed to ensure proper operation. The author additionally assisted with the high voltage battery system, battery management system operation, battery charging system, and with power steering and air conditioning system installation.

3.2 Introduction

The purpose of the JimmE-V is to demonstrate the use of engineering principles in the development of an innovative alternative energy vehicle. The JimmE-V (aka GMC Jimmy or Chevy Blazer) full scale Electric Vehicle conversion project was started by the KU EcoHawks in 2010 and was completed in 2013 (Figure 41). Further project background is provided in Chapter 2 of this thesis with this chapter providing an operation and overview in order to prolong vehicle life and ensure operator safety while conducting research. Moreover, given the complexity of the systems within the vehicle, any graduate students wishing to perform research with this vehicle require a comprehensive understanding of vehicle functionality.

Figure 41: JimmE-V full-scale electric vehicle conversion.

Before operating or performing maintenance on the JimmE-V, one should ensure that necessary precautions have been taken to mitigate High Voltage (HV) hazards. The JimmE-V has a 330 VDC battery pack that poses a significant high voltage risk. Improper maintenance on the HV system (battery pack, charger, motor, controller, and contactors) can result in serious injury or death. Remove all jewelry (rings, necklaces, bracelets, etc.) before working on any part of the JimmE-V. While working on the HV system, there is a rubber mat to help isolate the individual from potential grounding. Additionally, there are rubber gloves accompanied by rubber coated socket wrenches when working on the battery pack.

Along with personal safety, it is important to know the parameters of the batteries to further an individual's safety while working with the JimmE-V. Failure to operate the batteries within their safe design parameters can result in catastrophic failures including fire, explosion, toxic fumes, excessive heat, the release of caustic or poisonous materials, and other potentially lethal situations. The JimmE-V utilizes lithium iron phosphate ($LiFePO_4$) batteries that have proved to be inherently safer than lithium ion batteries [28]. However, this does not mean that they should be treated any differently. Due to the potential risks and hazards of working on or around batteries, it is advisable that more than one person be present while working with high voltage systems along with both personnel wearing eye protection. NEVER touch anybody while they are working on high voltage systems or battery packs. Additionally, never allow more than one person to work on the same high voltage system at the same time. If two or more people are touching parts of the system, it is easier to complete a circuit and cause electrocution. In the event of an electrocution, the individual being shocked may not be able to let go of the electrical source. The extra person present can safely disconnect the electrical source or get help. If the properly insulated equipment is available, the extra person can use a device, such as an insulated human hook, to pull the effected person away from the electrical source. Under no circumstances should contact be made with a person being electrically shocked. If such tools are not available, sturdy pieces of wood can also be used to remove an individual from an electrical source. Figure 42 shows the proper safety tools for working on Electric and Hybrid Vehicles. The rescue hook is non-conducting and can be used to pull personnel off an electrical power source. The face shield and safety glasses are necessary to protect one's face in the event of a short circuit. The rubber gloves provide additional high voltage isolation.

Figure 42: Electrical hook, isolating gloves, facemask, and other proper safety tools for working on Hybrid and Electric Vehicles.

The high voltage system is isolated from the rest of the vehicle. This means that there are no risks of grounding high voltage through an individual via events like static shocks. The Battery Management System (BMS) is responsible for monitoring HV isolation. HV isolation can be manually checked with a multimeter set on the 'continuity' setting. Place one probe on a source of high voltage, and place the remaining probe on the vehicle chassis or a ground wire. If properly isolated, continuity should not exist. Along with electrical hazards, the JimmE-V should be treated like any other automobile.

The JimmE-V is a mid-sized Sport Utility Vehicle (SUV) with a weight of 4400 lbs. This is a significant amount of mass that has potential to damage vehicles, buildings, or individuals. While operating the JimmE-V always wear a seat belt, and do not operate the vehicle without a legal driver's license and automotive insurance. Additionally, since the JimmE-V is an electric vehicle, it is inherently quieter than a traditional vehicle. Use extreme caution while in parking lots, as pedestrians may not hear the vehicle and walk out in front of the vehicle. Before discussing individual components or systems, a general vehicle overview will be provided to illustrate the key features of the JimmE-V.

3.3 Vehicle Overview

The JimmE-V is a Battery Electric Vehicle (BEV) that utilizes 104 lithium iron phosphate ($LiFePO_4$) batteries in series to provide a nominal voltage of 330 VDC to the motor. The vehicle initially started as a 1997 GMC Jimmy (Chevy Blazer equivalent), and before the EV conversion could take place the entire vehicle was completely disassembled. The vehicle was initially a police impound vehicle that was involved in an accident. Consequently, the vehicle's structural integrity needed to be examined. Upon inspection the frame was twisted and not suitable for use. The 2010-2011 JimmE-V (EcoHawks) team sourced and purchased a recycled frame from a salvage yard and began preparing the vehicle chassis for the EV conversion. Anticipating a larger weight load from the battery pack, the suspension was upgraded to an air suspension in the rear along with the addition of an extra leaf in the rear leaf springs. The rear brakes on the vehicle were converted from drum to disc brakes, and the three-phase AC motor was installed in the front of the vehicle. To connect the motor to the rear differential, a custom driveshaft was

fitted. The vehicle was set up as a direct drive system as per the recommendation of Azure Dynamics. Azure specified that the AC55 motor not be used in conjunction with a transfer case or transmission due to the torque produced by the motor [24]. With the removal of the vehicle's original six-cylinder internal combustion engine (ICE), vehicle amenities needed to be evaluated.

A typical ICE in a vehicle is responsible for powering auxiliary features like the power steering pump, air conditioning compressor, generating vehicle electrical power, and providing a vacuum for the power braking system. To account for the loss of the vehicle ICE, the JimmE-V features an electric power steering pump from a Toyota MR2, an all-electric air conditioning compressor, and an electric vacuum pump for the brake booster. It should be noted that in both cases of the ICE and EV, these systems are parasitic losses. In the case of the JimmE-V, the air conditioning compressor is powered off the high voltage battery pack; whereas, the power steering and vacuum pump are powered off the auxiliary 12 VDC battery. However, the 12 VDC battery is charged through a DC-DC converter that steps down the 330 VDC to 12 VDC. As a result, these systems require energy that removes potential from the battery pack to power the vehicle's motor. The auxiliary 12 VDC batteries are necessary to power standard automotive circuits, such as lights, turn indicators, and fans. The 12 VDC batteries additionally power the ECU, BMS, contactors, and the motor controller.

The battery pack in the JimmE-V is composed of 104 $LiFePO_4$ batteries. These batteries were chosen over other lithium ion batteries for safety reasons. Even though the battery composition is safer, there is still a significant amount of voltage potential. To hold these cells safely, two Polyvinyl Chloride (PVC) battery boxes were lined with recycled rubber mats to ensure that the battery pack was isolated from the vehicle. The battery pack is charged through a Manzinita Micro PFC 20 battery charger that converts AC power into DC power for the battery pack. In order to ensure safe charging and discharging, an Elithion Lithiummate Pro BMS has been programmed with limits specific to the JimmE-V application. This BMS uses cell boards to monitor the individual cell and overall pack status. In addition to the BMS, there are additional safety features in the high voltage system including high current fuses, and an additional contactor that can be operated to disconnect the high voltage from the motor and controller.

The motor controller in the JimmE-V serves as both a motor controller and inverter. The inverter is necessary to convert the DC power into three-phase AC power for the motor. The motor and controller models are the Azure Dynamics AC55 and DMOC445 respectively. The controller is CAN controlled and requires the use of an ECU to function. Chapter 2 of this thesis contains further information regarding CAN and ECUs. For research purposes, several components in the JimmE-V are capable of data logging. The motor controller, ECU, and BMS can each individually log events and different data parameters. From a research perspective, the JimmE-V is a desirable research platform due to access for all of the vehicle's components. With a brief vehicle outline presented, each of the components will be discussed in further detail. While the focus of the author was the motor, controller, and ECU, since these systems require a comprehensive vehicle understanding, the vehicle chassis will be discussed next.

3.4 Vehicle Chassis

The chassis of the JimmE-V is the foundation that supports all of the vehicle systems. From an operation and maintenance standpoint there are minimal actions required; however, there are a few systems for the chassis that should be monitored and maintained. The JimmE-V frame is a fully boxed ladder frame. The thick walls of the tubular structure provide structural rigidity, but result in a heavy structure. For this application, having a structurally rigid frame allows larger error tolerances. Lastly, since the frame is fully accessible, modifications can be added if necessary [22]. The completed vehicle chassis is shown in Figure 41. To ensure that the converted JimmE-V would be able to handle the additional battery weight, modifications were performed on the stock suspension. Monroe Max Air shock absorbers were added for further adjustability, and have a pressure operating range from 20-150 psi. The air pressure in the suspension was set at 140 psi. The system does not leak; however, the air pressure should be checked on a monthly basis. The air pressure valve is accessible underneath the rear of the vehicle above the differential (Figure 43).

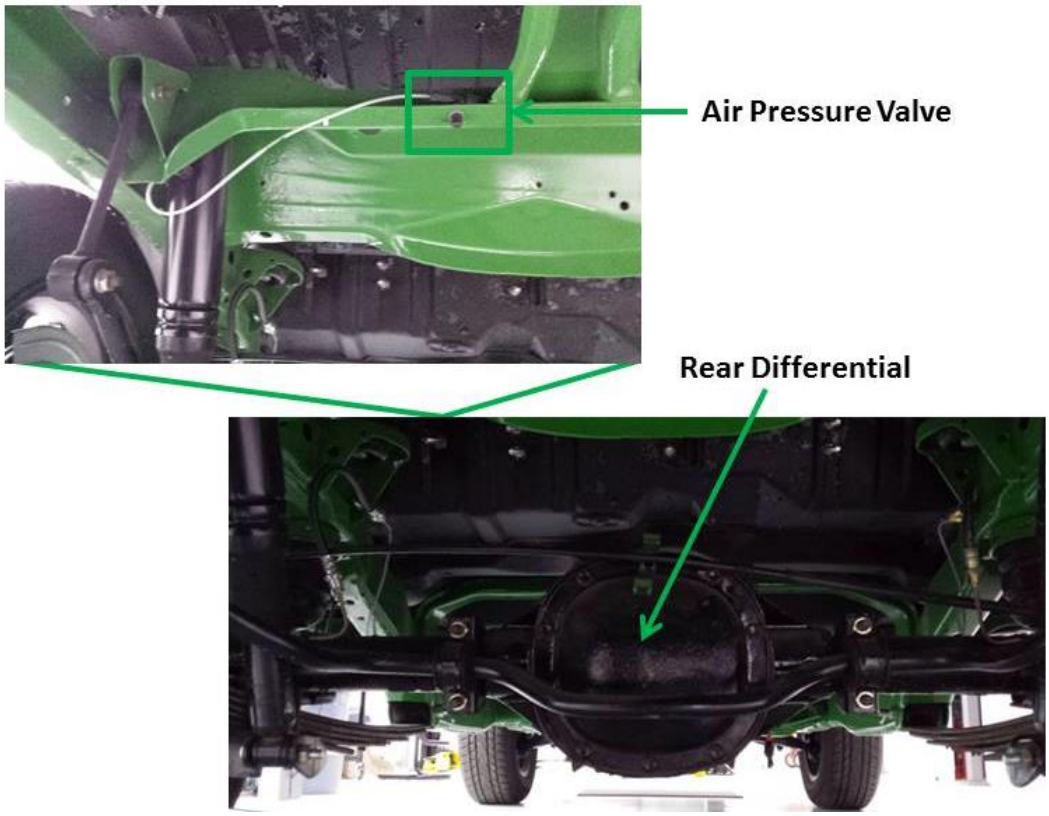

Figure 43: Air suspension adjustment valve location. The valve is located above the rear differential towards the left wheel.

In addition to the air shock absorbers, an additional leaf spring was added to the factory leaf springs. This modification allowed an additional 900 lbs of suspension support over the rear axle [22]. Along with modifying the vehicle's suspension, brake upgrades were performed to allow the vehicle to safely decelerate under both normal and emergency situations.

Figure 44: Completed JimmE-V chassis [22].

Braking within the JimmE-V is accomplished through the factory master cylinder and brake booster. These components were recycled from the original vehicle allowing the factory brake pedal to be implemented. With the added battery weight over the rear axle, the rear factory drum brakes were

converted to disc brakes. Upon completion of this conversion, the JimmE-V has a full disc brake system. In order to understand how the braking system functions, the system operation will be discussed.

Automotive braking systems apply hydraulic fluid pressure to actuate pistons. These pistons apply pressure to a high-friction material (i.e., brake pads) that contacts the braking surface (i.e., brake rotor). To assist the driver with braking, an engine vacuum is applied to a brake booster to multiply the vehicle's braking force [9]. However, since the engine was removed for the JimmE-V conversion, there is no vacuum source for brake booster. To account for the vacuum loss, an electric vacuum pump was implemented to ensure that the vehicle's braking power remained unchanged. The pump functions automatically when the brake pedal is depressed. When the brake pedal is engaged, there is an audible noise from the vacuum pump that was installed under the hood of the JimmE-V to the right of the master cylinder and brake booster. The master cylinder and brake booster are shown in Figure 45, and the electric vacuum pump is shown in Figure 46.

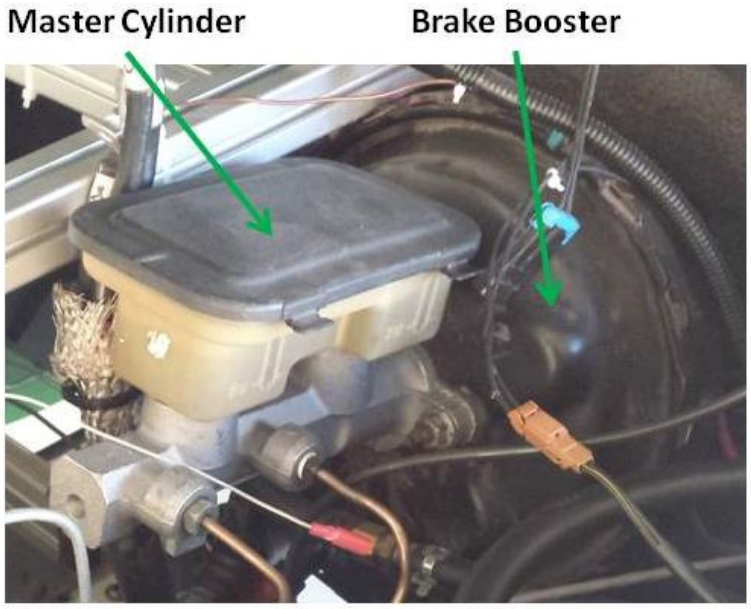

Figure 45: JimmE-V master cylinder and brake booster.

Figure 46: JimmE-V electric vacuum pump.

This location was desirable to keep the vacuum hose lengths short to allow instant response from the system. The vacuum kit implemented was the EV Source Vacuum Assist Kit. The kit included the vacuum pump, tubing, relays, fuses, a one-way check valve, and a vacuum switch. The components and schematic of the vacuum system will be discussed next to understand how it operates.

A schematic of the brake assist system is shown in Figure 47. When pressure is applied to the brake pedal, the brake light switch is engaged. The brake light switch is installed behind the brake pedal underneath the vehicle dashboard. When this switch is engaged, the relays in the relay kit are actuated to provide the vacuum pump power. The pump operates until ample vacuum pressure has built up. Once the vacuum pressure has been achieved, the vacuum switch disengages the relay causing the pump to power off. While decelerating the JimmE-V, the pump may operate for one or two seconds before shutting off. This indicates that the required pressure has been achieved. If more braking force is desired, the pump may switch back on. The one-way check valve ensures that desired vacuum pressure only flows in one direction and does not leak. In the event of a system malfunction, check the fuse located next to the battery. If the fuse is not blown, proceed to checking the relays in the relay kit. The two relays are located just past the fuse for the brake pump close to the 12 VDC battery. When parking the JimmE-V, or in an emergency, another curtail component to the braking system is the vehicle park brake.

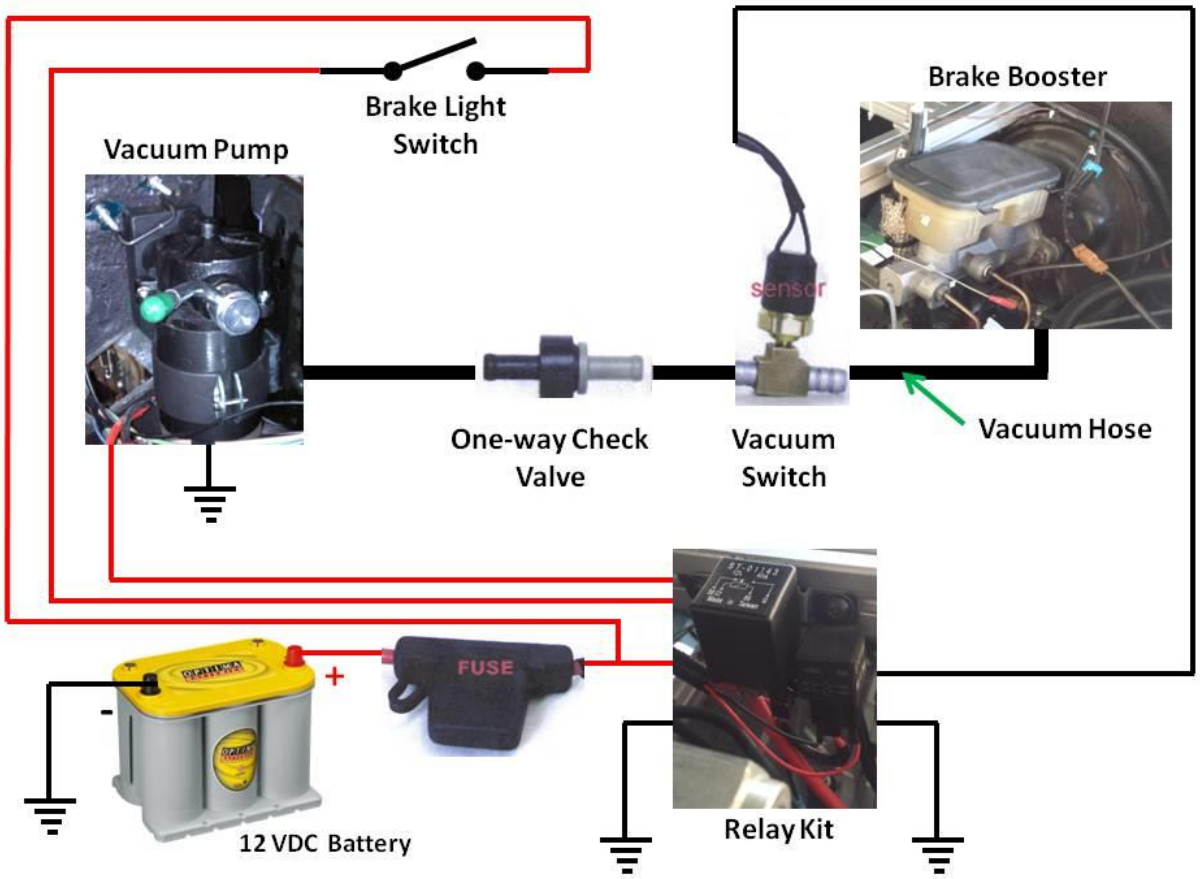

Figure 47: Vacuum brake assist system schematic.

The park brake holds the JimmE-V in place while not being driven or parked on a hill. Vehicle park brake systems are often mechanical systems consisting of levers and cables. The JimmE-V has a park brake pedal located to the left of the brake pedal (Figure 48). The park brake is engaged when the pedal is fully depressed. To release the park brake, there is a release handle. When the release handle is pulled, the park brake pedal actuates back to the disengaged position. In the event of an emergency, the park brake will assist in decelerating the vehicle. However, the park brake does not have the braking power of the power braking system. An additional safety feature on the JimmE-V is an Anti-lock Brake System (ABS) control module. The ABS module was installed (Figure 49), but does not function due to a high degree of difficulty required to set up and program the system. The ABS module is a BOSCH four channel ABS module that requires speed sensor input from the wheels, and a custom control algorithm to

operate effectively. Since the JimmE-V is a research vehicle, the expansion and research involved with this component allows for further development. Along with knowing how the brake system operates, it is also important to know how to maintain the brake system.

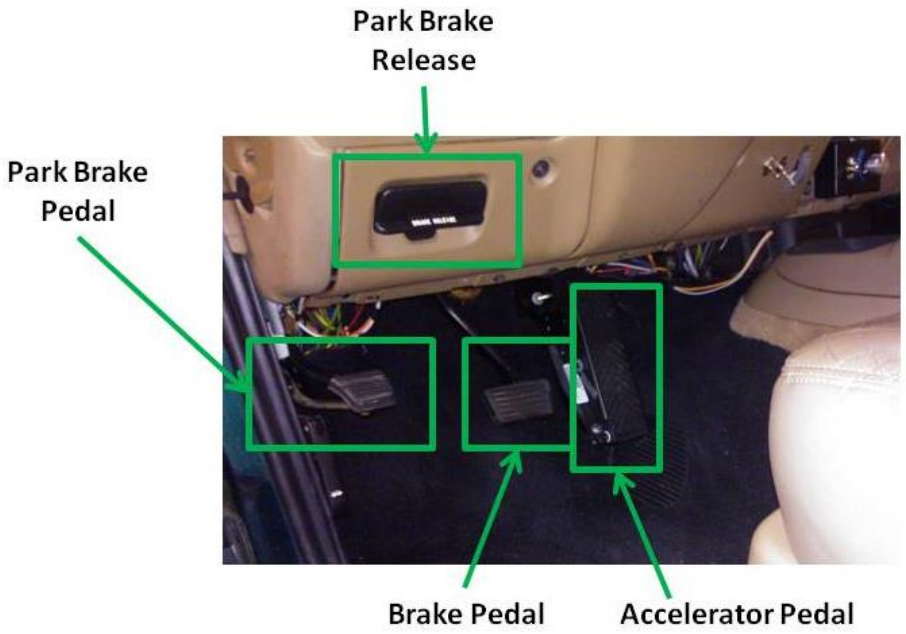

Figure 48: JimmE-V pedal layout including the braking system.

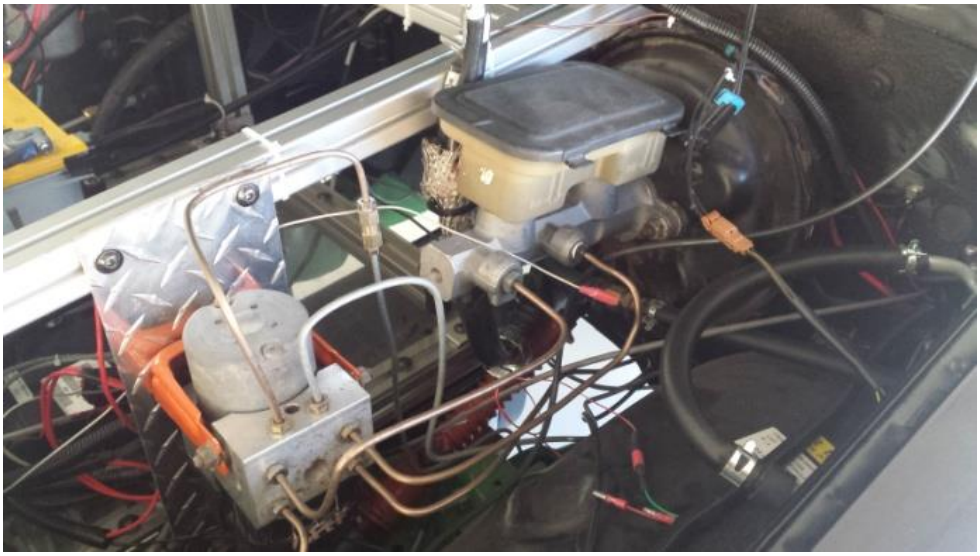

Figure 49: The Bosch four-channel ABS module is installed forward of the master cylinder and brake booster. Even though the system does not function, brake fluid passes through the controller to the brake calipers.

Maintenance on a vehicle's braking system is concentrated in two main areas, maintaining proper brake fluid level, and replacing the brake pads. Additional issues can arise if there is a leak in the brake lines. In the event of a brake line failure, the fluid will exit the system, and the recommended action is to replace the brake line. Maintaining the fluid level is achieved by first monitoring the fluid level on the side of the master cylinder. If the fluid is below the indicated region, add fluid by removing the black cover on the master cylinder. Take caution to not overfill the system. Only use Department of Transportation (DOT) three and four brake fluid. DOT three and four fluids are compatible, and are safe to mix in the same system. The other area of maintenance concern is the brake pads. When the brake pads wear out, there is a metal indicator tab that will contact the rotor as the pad thickness decreases. This results in a loud metallic noise that should alert concern. When this occurs, the brake pads need to be replaced. A trained mechanic or an individual with prior knowledge and experience replacing brake pads can complete this procedure. Along with maintaining the brake system, there are additional chassis features that require maintenance.

The remaining features of the JimmE-V chassis include the tires and the rear differential. The tires on the JimmE-V have a maximum inflation pressure of 50 psi. Varying tire pressure can affect the vehicle range. Higher pressure favors lower rolling resistance, but decreases the tire's contact area with the road. Additionally, maintaining proper tire pressure will ensure that the tires wear properly and last longer. The proper tire pressure for the JimmE-V is between 35 and 40 psi. When the tires need to be replaced, it is important to select the proper size of tire. Figure 50 shows the sidewall of a tire on the JimmE-V. The first characteristic to consider is the tire width. Failure to get an equivalent width will result in an improper fit on the wheel. The aspect ratio indicates the ratio of the height of the tire's cross section to the tire width. The larger the aspect ratio, the larger the tire's sidewall [29]. For maintenance purposes, replacement tires should have an aspect ratio of 65. The last factor to consider when replacing the tires on the JimmE-V is wheel diameter. The wheel diameter indicates the size of the wheel that the tire is intended to fit. The wheels on the JimmE-V are 17 inch tires and should be the only type installed

on the JimmE-V. Any other size will not fit properly onto the wheels. The final aspect of the chassis to discuss from a maintenance standpoint is the rear differential.

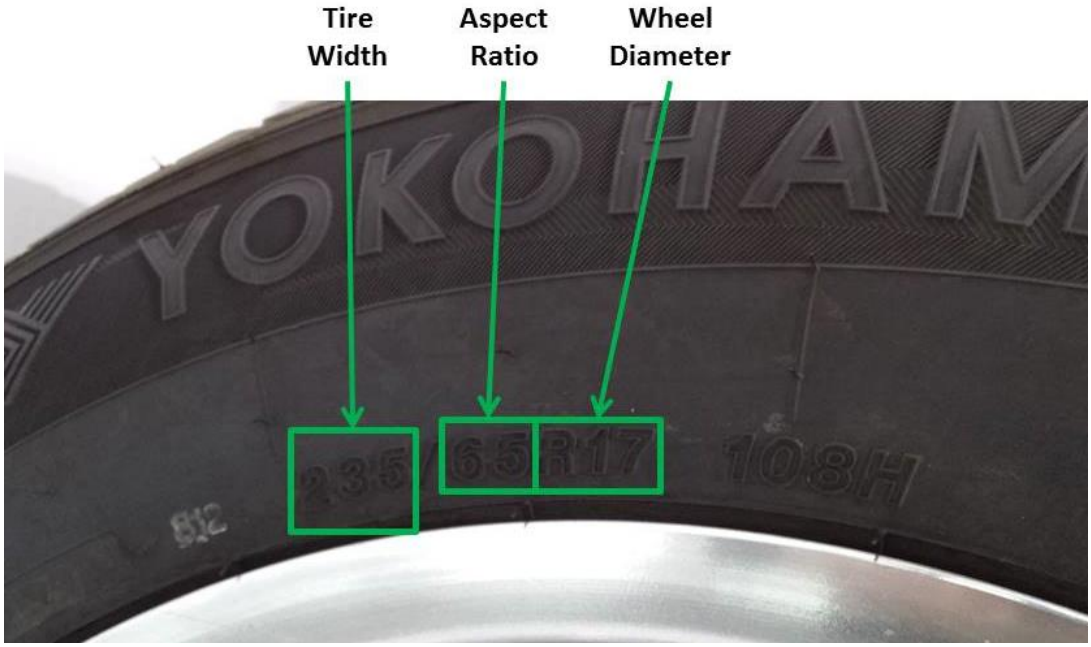

Figure 50: The tire size is indicated on the sidewall of the tire. Tire width, aspect ratio, and wheel diameter must all be considered when replacing the tires.

The rear differential of a vehicle allows the wheels to rotate at different speeds while maneuvering a turn. In order for a vehicle to turn, the wheel on the outside of the turn needs to rotate at a faster speed that the wheel on the inside of the turn. This is accomplished through a vehicle's differential with the JimmE-V's version in Figure 51 having a final drive ratio of 3.08 [22]. If desired, this ratio can be changed by swapping gears in the rear differential. Changing the final drive ratio may be desirable to optimize the vehicle to operate in the motor's peak efficiency regions. However, changing the final drive gear is not simple and should be left to a professional mechanic. Additionally, differentials need to be serviced every 30,000 to 50,000 miles depending on the vehicle application. It is recommended that the JimmE-V differential be serviced every 30,000 miles. Due to the differential being directly driven by the motor, the differential takes all the torque produced by the electric motor directly. This concludes the

chassis maintenance section. Next, the motor characteristics and maintenance requirements will be examined.

Figure 51: The JimmE-V rear differential. The motor directly drives the wheels through the rear differential. This allows the rear wheels to rotate at different speeds while turning.

3.5.1 Three-phase AC Induction Motor

A motor is a means to convert electrical energy into mechanical energy [30]. Motors have a variety of applications in today's industry from automotive applications, driving hoists, fans, pumps, and pitch and yaw motors in wind turbines. Electric motors utilize one of two types of power, alternating current (AC) and direct current (DC). The JimmE-V utilizes an AC induction motor. Before discussing the specific motor in the JimmE-V, the theory behind AC induction motors will be reviewed.

The theory of AC motors is the same as AC generators. They are built the same way that allows them to act as a motor or a generator. Induction motors are the most commonly used electrical machines because they are cheaper, more durable, and generally easier to maintain when compared to other motors available. When an AC current is run through winding coils, the coils produce a rotating magnetic field. When a conducting object is placed in the rotating magnetic field, current is induced in the object (rotor). The electromagnetic forces reacting between the rotating magnetic field produced by the coils and the rotor produce an Electromotive Force (EMF). The EMF applies a torque to the rotor that results in a change in rotor speed and causes rotation [30]. Since AC induction motors can be both a motor and a

generator, an AC motor is a desirable choice for an electric vehicle. Regenerative braking is achieved through the motor acting as a generator to recover energy while simultaneously slowing the vehicle down.

The motor selected for the JimmE-V was the Azure Dynamics' AC55 induction motor with specifications provided in Table 2. The AC55 was chosen due to the drive train simplicity. Azure recommended that the AC55 motor be implemented in a direct drive application. By directly providing power to a differential, the need for a transmission and transfer case is eliminated. Additionally, the torque produced from the motor could result in damage to the gears in the transmission [24].

Table 2: Azure Dynamics AC55 motor and DMOc445 controller specifications [24].

Peak Torque	280	Nm
Continuous Torque at Nominal Speed	140	Nm
Nominal Speed	2000	rpm
Maximum Mechanical Speed	8000	rpm
Maximum Current	250	A rms
Continuous Shaft Power at 1500-2500 rpm	25	kW
At a voltage of	312	VDC
Peak Efficiency	87	%
At a voltage of	312	VDC
AC55 Weight	106	kg
Minimum Recommended Nominal Battery Voltage	312	VDC
Maximum Nominal Battery Voltage	336	VDC
Minimum Operational Voltage	100	VDC
Maximum Operating Voltage	400	VDC
Minimum Operating Temperature	-40	°C
Maximum Operating Temperature	60	°C

To install the motor, the 2010-2011 JimmE-V team fabricated a steel plate to mount the motor in-between the frame rails as shown in Figure 52. This location was desirable to keep the mass of the motor low and centered, resulting in increased handling performance. Additionally, this location resulted in simple drive-shaft routing. Additional drive-shaft and differential information can be found in Section 3.4 of this Chapter. The motor wiring requires minimal connections and is discussed next.

Figure 52: AC55 motor installation location between the frame rails.

The three-phase AC motor only has two primary connections. The first connections are the three-phase wires that go from the motor to the controller. These wires were insulated and shielded by Azure. The final connection to be made is the encoder and sensor communication harness. This harness is responsible for relaying the encoder and motor temperature signals to the controller. These connections are illustrated in Figure 53.

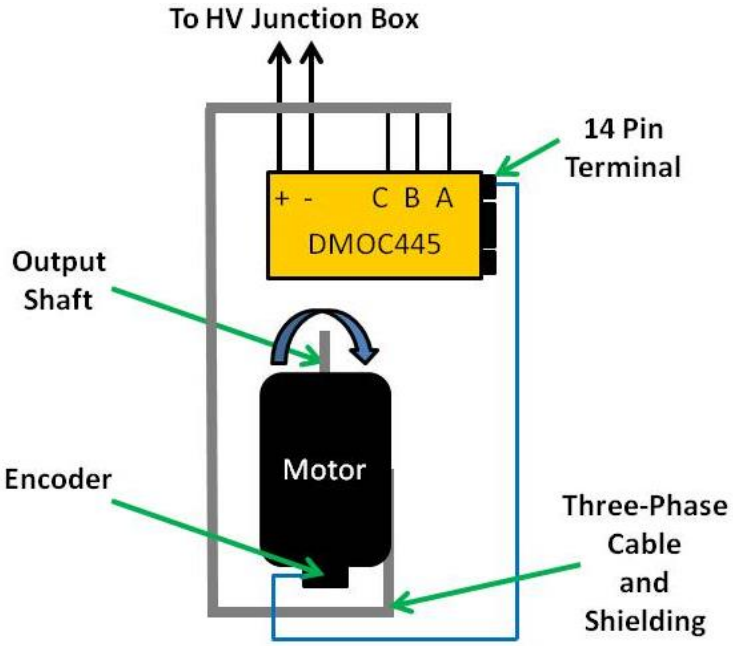

Figure 53: Motor wiring schematic for the Azure Dynamics AC55 motor.

To connect the three-phase cables to the controller, the access cover has four Phillips screws that need to be removed. The access cover is located on the top side of the controller behind the cooling fans. Connecting the wires is accomplished by fastening the terminals to the proper electrical post on the

controller. Each three-phase wire is labeled "A, B, and C" respectively, and each wire corresponds to a labeled terminal as illustrated in Figure 54. The shielding for the three-phase cables is grounded through the controller chassis. A cord grip provides support for the three-phase cables, and the large fastening nut grounds the shielding to the controller frame (Figure 55).

Figure 54: DMOC445 three-phase AC connections.

Figure 55: The shielding is grounded through the controller chassis by fastening the large nut on the cord grip.

The final connection for the motor is the wire harness that couples with the 14-pin connector on the DMOC445 motor controller. This cable originates at the front of the motor, and relays encoder and motor temperature information to the controller. In order to prevent signal interference with the three-

phase cables, this harness is routed towards the front of the vehicle and connects to the controller. The wire terminals on the DMOC445 are mist rated. There are locking tabs on each harness connection to keep the terminals secured to the controller.

Figure 56: Motor encoder harness connected to the 14-pin connector on the DMOC445.

Overall, AC induction motors require minimal maintenance. However, Azure's AC55 motor has a reputation of rough (i.e., "jumpy") starts. The rough starts can be attributed to the factory encoder on the motor. At low motor speeds, the encoder relays the motor speed to the controller. Once the motor is above 1000 rpm, the controller uses the three-phase power data for motor speed. In the event encoder modifications are desired, the encoder is located on the front of the AC55 motor (side opposite of the drive-shaft) as shown in Figure 57. The encoder can be accessed without requiring motor removal by turning the steering wheel all the way to the right. This allows the steering linkages to move away from the encoder cover allowing it to be removed. Figure 58 shows the exposed AC55 motor encoder and the encoder wiring will be discussed in the following section. In order to control the motor, the AC55 was paired with Azure's DMOC445 motor controller and inverter. The DMOC445 will be the next topic of discussion.

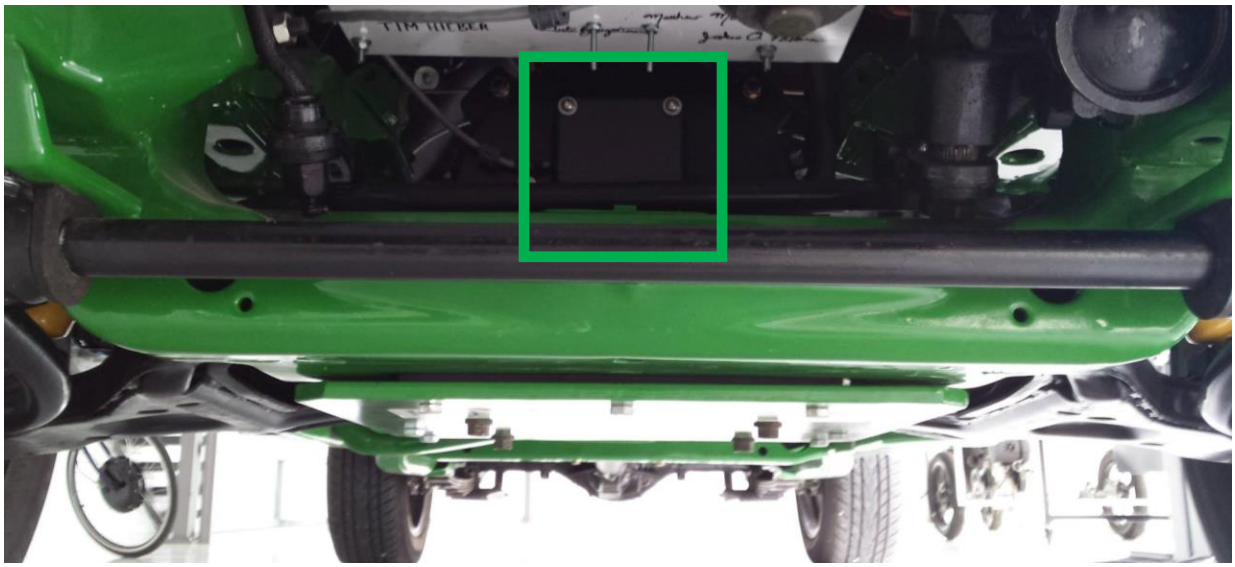

Figure 57: The AC55 encoder is located on the front of the motor.

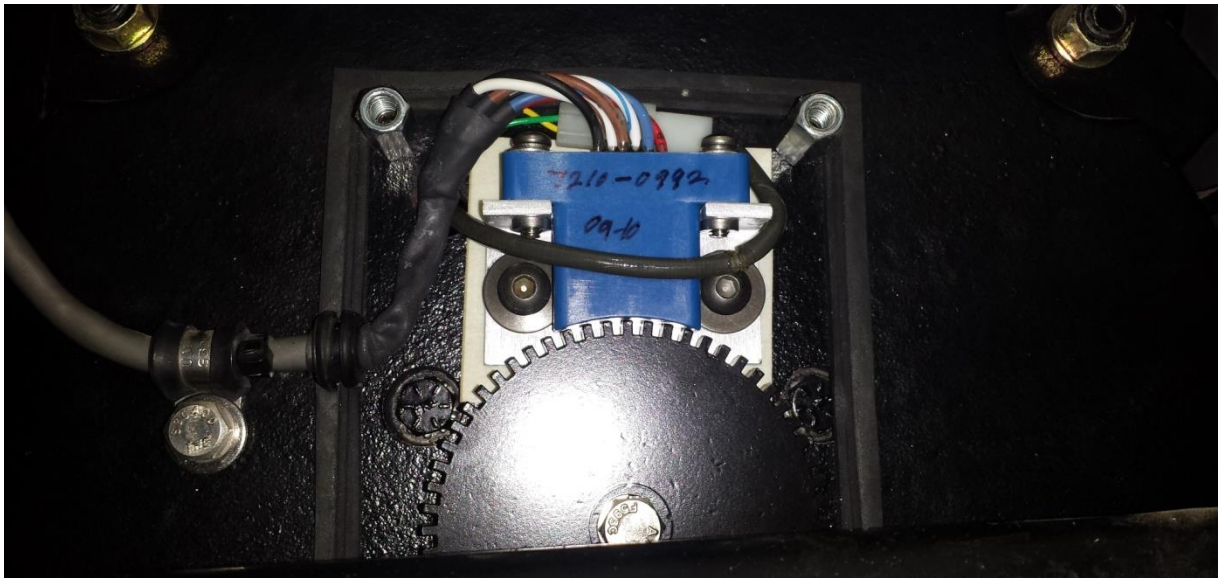

Figure 58: Exposed AC55 encoder.

3.5.2 JimmE-V Motor Controller & Inverter

Chapter 2 covers the theory behind how the CAN controlled DMOC445 (DMOC) operates. This section will be focused on the setup, operation, and maintenance of the Azure Dynamics DMOC445 inverter and controller (Figure 59). Before interfacing with the DMOC it is important to understand how the controller is installed in the JimmE-V.

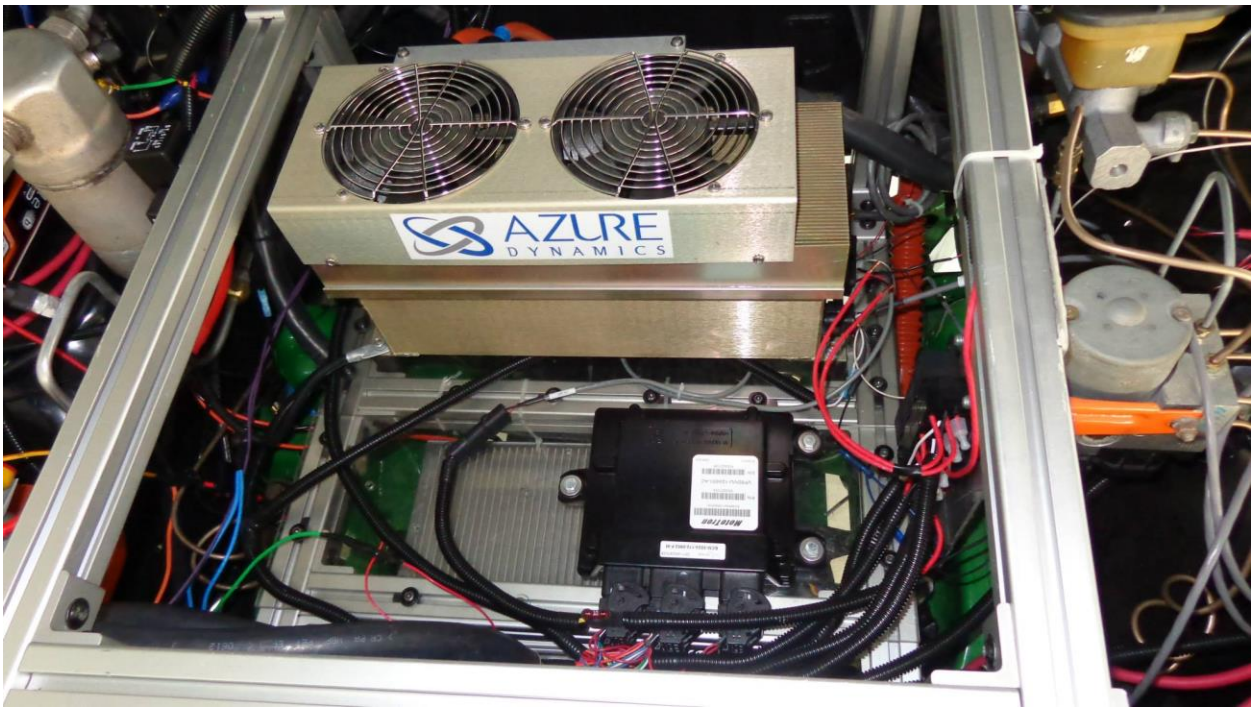

Figure 59: The Azure Dynamics DMOC445 AC motor controller and inverter under the hood of the JimmE-V.

In order to mitigate vibrations being transferred from the vehicle to the controller, the Azure DMOC is fastened to the vehicle using vibration isolation mounts. There are four mounts located at the each corner of the DMOC (Figure 60). The mounts are fastened to the polycarbonate platform under the hood of the JimmE-V; however, the controller can be removed by only removing the nuts located at each corner. The controller chassis is additionally grounded to the vehicle using a ground strap on one of the controller's corners. The different pin connectors are discussed further in Chapter 2 of this thesis; however, to further understand how the controller operates, the 35-pin interface terminal and the 8-pin communication terminal will be discussed next.

Figure 60: The DMOC has four vibration isolating mounts located at each corner of the controller.

The 8-pin communication terminal on the DMOC is responsible for communicating with the ECU via CAN bus, and communicating with a laptop via RS-232. The 35-pin connector allows the ECU to interface with different control aspects with the DMOC. Only the used pin connections will be discussed; for a full description of all the pins available on the DMOC, see the Azure user manual.

As previously mentioned, the 8-pin connector is responsible for transmitting and receiving communication information from the ECU and laptop. The pins used in the JimmE-V application are shown in Table 3. The pin numbering is indicated on the connector with pin 1 at the top left and pin 8 at the bottom right. The first three pins are for RS-232 communication to the computer. Pins four and six are for CAN communication, and the termination resistor is present on the two CAN wires adjacent to the controller. Pin 5 is a CAN communication ground used for shielding, and pin 8 is connected to the vehicle's chassis ground. While the 8-pin connection is responsible for communication, the 35-pin connector allows multiple components to interact with the controller.

Table 3: DMOC445 8-pin connections used on the JimmE-V [24].

Pin #	Function
1	RS-232 Tx
2	RS-232 Rx
3	Communication Gnd
4	CAN High
5	Communication Gnd
6	CAN Low
8	Chassis Gnd

The 35-pin terminal allows the DMOC to interface with the ECU and BMS through digital inputs. This is also the connector where the controller receives the 12 VDC from the auxiliary batteries. This is important to know because in order for the controller to operate, both 12 VDC and HV need to be present. Additionally, in the event of an emergency situation, the 12 VDC can be disabled using the vehicle's ignition switch. By removing the 12 VDC power, the controller immediately shuts down. The pins used in the JimmE-V application are shown in Table 4. The pins related to 12 VDC power are pins 1 and 13. Pin 1 is positive 12 VDC while pin 13 is the 12 VDC ground connection. It should be noted that the positive 12 VDC wire leading to the controller has a 10 A fuse to prevent excess current from entering the DMOC. If the DMOC is not receiving power when expected, check to ensure that the fuse is not blown before proceeding with further system diagnostics. The remaining pins interface with the BMS and ECU to ensure that the controller is not exceeding design parameters.

Table 4: DMOC445 35-pin connections used on the JimmE-V [24].

Pin #	Function
1	Key 12 VDC Source
7	Regen Disable
8	Drive Disable
13	Key 12 VDC Sink (Gnd)
19	Digital Gnd
30	Drive Enable
35	Digital Gnd

Pins 7 and 8 on the 35-pin connector communicate with the BMS through opto-isolators (Section 3.6.2) and are active low. Active low means that when the circuit is completed between the pin and a digital ground the pin becomes active. When the battery pack is full, the BMS completes the regen disable circuit telling the controller that regenerative braking is prohibited. Similarly, when the pack is depleted the BMS completes the drive disable circuit prohibiting further battery pack discharge. The drive enable function on pin 30 is controlled by the ECU once the shifter is moved from park to drive position (i.e., reverse or drive). When the shifter is in neutral, the drive enable relay is switched off. When the drive enable circuit is complete, the DMOC's internal contactors will engage indicating to the driver that the

vehicle is ready to drive. If the contactors do not engage while in a drive position ensure that the controller has 12 VDC. Also ensure that the ECU and shifter are operating correctly (Section 3.5.3). For troubleshooting purposes, the drive enable wire can be directly connected to a digital ground bypassing the ECU relay. Lastly, it is important to understand the hierarchy of the commands.

When drive is enabled, and the BMS indicates that the battery pack is low, drive disable is active at the same time as drive enable. In this situation drive disable has priority over drive enable, and the internal contactors will switch off preventing further motor operation. Regen disable does not interfere with a drive command, thus it can be active at the same time as drive enable. These interface connections can also be viewed using a computer via RS-232 communication. Communicating with the DMOC over RS-232 will be the next area of discussion.

Communicating with the DMOC via RS-232 communication allows the operators to change controller parameters in real-time in addition to viewing, monitoring, and logging data. Before communication with the controller is established, it is important to understand where to connect the controller to the computer since multiple components can be hooked up and monitored simultaneously while the JimmE-V is operating.

The RS-232 communication from the DMOC ends in a DB-9 connector. In order to adapt the DB-9 connection to a modern computer connection, the ATEN USB to RS-232 converter is implemented (Figure 61). The DMOC and ECU USB cords are located in the glove box of the JimmE-V. This adapter allows the user to connect the controller to a laptop when a serial terminal is not available. This adapter is also used with the Elithion BMS (Section 3.6.2). The BMS is capable of auto-configuring the COM port setting; however, the DMOC and ECU are not. As a result, it is important that the correct USB port be used for each component. If a different USB port is used, the COM port settings will need to be altered for the specific component. The DMOC COM port is COM 6 on the vehicle's laptop (Figure 62). The BMS uses COM port 8. The BMS adapter uses a USB extension cord, and as a result has a different plug compared to the DMOC cable. However, in the even the COM ports are mixed up it is important to understand how to correct the COM port settings in order to establish communication with the controller.

Figure 61: The ATEN USB to RS-232 adapter is located in the glove box of the JimmE-V.

Figure 62: Connect the DMOC USB cord to COM 6 on the vehicle's laptop. COM 8 is used for the Elithion BMS.

Communicating with the DMOC is accomplished through Azure's ccShell software utility. Before parameters can be viewed, altered, or logged the proper communication port needs to be selected since the DMOC cannot auto-configure COM ports. Once a COM port has been established it can be used subsequent times without having to re-establish the COM port settings. The ccShell program can be opened three ways: from the start menu, from the icon on the taskbar, or from the shortcut on the desktop screen. The taskbar and shortcut options are shown in Figure 63.

Figure 63: ccShell can be opened from the desktop shortcut or taskbar icons.

Once ccShell has been opened, a blank screen will be displayed. The current COM port settings are displayed at the bottom of the window as shown in Figure 64. In order to change the COM port settings the configuration menu at the top of the ccShell window needs to be selected. Figure 65 shows the different options available in the configuration menu. The first option is used to change COM port settings, while the auto-save option allows the user to select which port is saved as the default COM port.

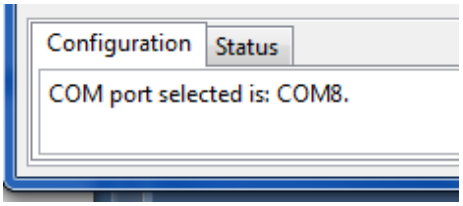

Figure 64: The current COM port selection is displayed in the bottom left of the ccShell window.

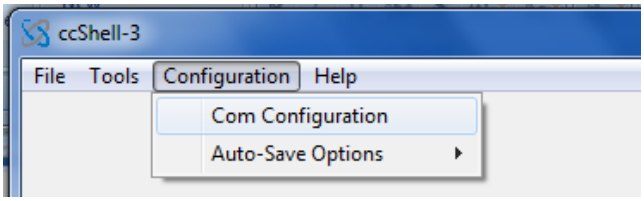

Figure 65: The configuration menu is used to alter the current COM port settings.

In order to change the COM port settings, select the Com Configuration option. Once this option is selected, an additional window will open prompting the user to select the serial port (Figure 66). Once the new COM port has been selected, clicking OK returns the user to the main ccShell window.

Figure 66: COM Port configuration window [31].

With the correct COM port selected, communication can now be established with the DMOC controller. In order to establish communication with the DMOC, the .ccs file needs to be opened using the file menu. The program should default to the file's location; however, if the .ccs file is not immediately displayed it is located on the C drive in the Azure Dynamics program file (Local disk C:/Program files (x86)/Azure dynamics). This file is crucial for modifying the controller settings. Consequently, multiple copies of the file were saved in the event it becomes lost. The .ccs file tells ccShell the name of each variable, the data type, length, and where it is located in the controller's memory. *The .ccs file for the JimmE-V DMOC445 is named CND-03FB-302A-003-0024.ccs*. Once the file has been located, double click the file name to open it in ccShell. If the file has been opened successfully, the main window of the program will be populated with four different options to select on the left side of the display window. Figure 67 shows the different options available for the user to select once the .ccs file has been successfully opened.

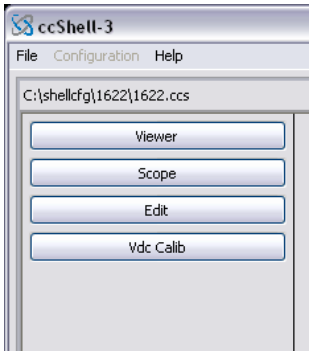

Figure 67: Once the .ccs file has been successfully opened there will be four options available to select in the ccShell window [31].

In addition to showing the options in Figure 67, the user can also monitor the connection time and status in the top right of the ccShell display window. If the DMOC is connected with the laptop, ccShell will display that it is "Connected" followed by the connection time (Figure 68). If the DMOC loses connection it will display "Disconnected" followed by the time the controller has been disconnected. Connection with the DMOC can be re-established by simply re-opening the .ccs file. If the file cannot be opened, ensure that the controller is powered on (i.e., the shifter is in a drive position, the 12 VDC batteries are charged, and HV is turned on). As previously mentioned, the controller needs both 12 VDC and HV from the battery pack in order to power on.

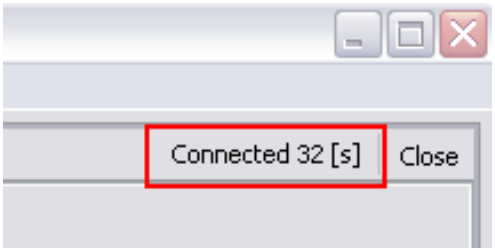

Figure 68: The connection time is displayed at the top right corner of the ccShell window [31].

With a connection established between the laptop and the DMOC, the user can use the "Viewer" option to view variables and log data from the controller. Figure 69 shows the ccShell window with the "Viewer" option selected. When viewing controller parameters, only 20 variables can be viewed at the same time. Variables can be added or removed using the options on the right side of Figure 69. The top window displays the selected variables to monitor. These variables can be removed using the remove button. Removing a variable returns it to the list below the selected variables. Variables can be selected and then added using the add button. The "Filter" box can be used to search for the desired variables. A full list of variables and descriptions are available in the Azure DMOC445 user manual and the CAN controller user manual. Along with viewing variables, the "Viewer" option can additionally be used to log controller data.

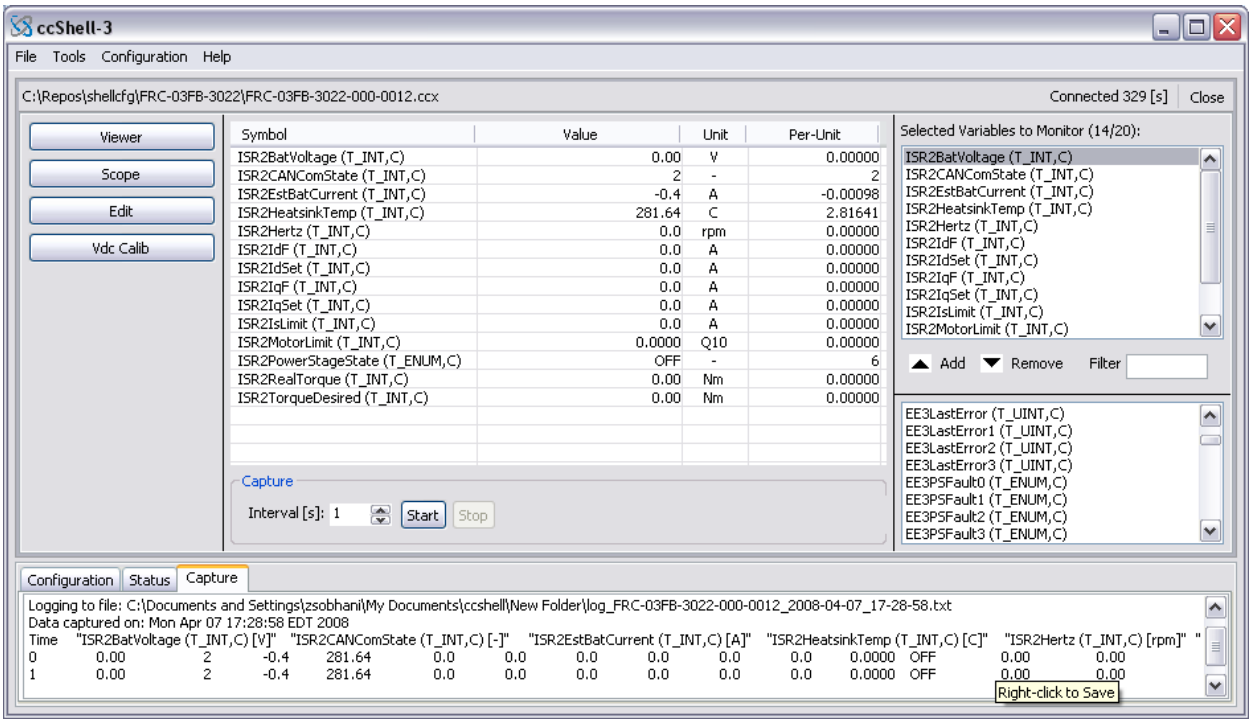

Figure 69: Selecting the "Viewer" option allows the user to view parameters in real-time and log controller data [31].

The bottom part of the ccShell window in Figure 69 is used for data logging. Once data logging is started, the controller will log the selected variables shown in the main ccShell window. Logging intervals can be selected by changing the time (in seconds). One second is the fastest data capturing rate for the DMOC. Clicking the “Start” button begins data logging. Similarly, clicking “Stop” ends data logging. Once data logging has been started, the capture tab in the bottom of the window begins to be populated with the different variables at the selected time step. Once logging has been completed, the text can be selected, copied, and pasted into a notepad or excel file. The file can also be saved when the user right clicks the text in the capture window (at the bottom of the logged data). At the top of the ccShell capture window the program also displays the directory where the logging file is being saved. The user can then take the logging file and use any desired program for post processing the data recorded by the controller. While logging data it is important to monitor the controller connection status. If the controller disconnects, connection will need to be re-established and a new logging file started. For this reason it is helpful to have two people present during drive cycle testing. This allows one person to focus on driving

the vehicle, and the second person to focus on data acquisition from the DMOC and BMS. The next tool in ccShell to examine is the "Scope" tool.

The Scope tool is used to view what is happening with different variables at a faster rate than the Viewer tool. Similarly to the Viewer, the user selects the desired variables to view on the right side of the ccShell window (Figure 70). Next, the Scope tool needs to be armed by selecting the "Arm" option. Arming the Scope tool simply starts a pre-trigger buffer. When the desired event occurs (i.e. vehicle acceleration) trigger the Scope tool using the trigger button adjacent to the Arm button. If the Scope tool is armed and an Error occurs in the DMOC, the tool will automatically be triggered to record the parameters during the error. Thus, the Scope tool can be used to record recurring faults to aid in diagnostics. Additionally, there is a pre-trigger percent that can be used to adjust where the data is collected relative to when the tool is triggered. For example, a pre-trigger percent of 100% would indicated that when the operator clicked the trigger button (after an event occurred), and would mark the end of the event logging. The next option to discuss is the voltage calibration tool.

The voltage calibration option in ccShell should not have to be used; however, if the voltage measurement needs to be recalibrated, the Voltage Calibration tool provides access to adjust the voltage sensor calibration. Before recalibrating the voltage sensor, it is important that the voltage be close to the operating voltage (after the vehicle has been charged). In order to compare the DMOC measure voltage to the actual voltage, an additional voltage measurement will need to be taken using a multimeter or the BMS software utility. The DMOC will show its measured voltage while the user measures the voltage independently and then selects calibrate. The DMOC should then adjust the sensor reading accordingly to match the independently measured voltage. Once the sensor has been recalibrated ensure that all changes are saved to the DMOC's EEPROM so that the new calibration settings are stored in the controller's memory. The last topic to discuss in ccShell is the Parameter Editor tool.

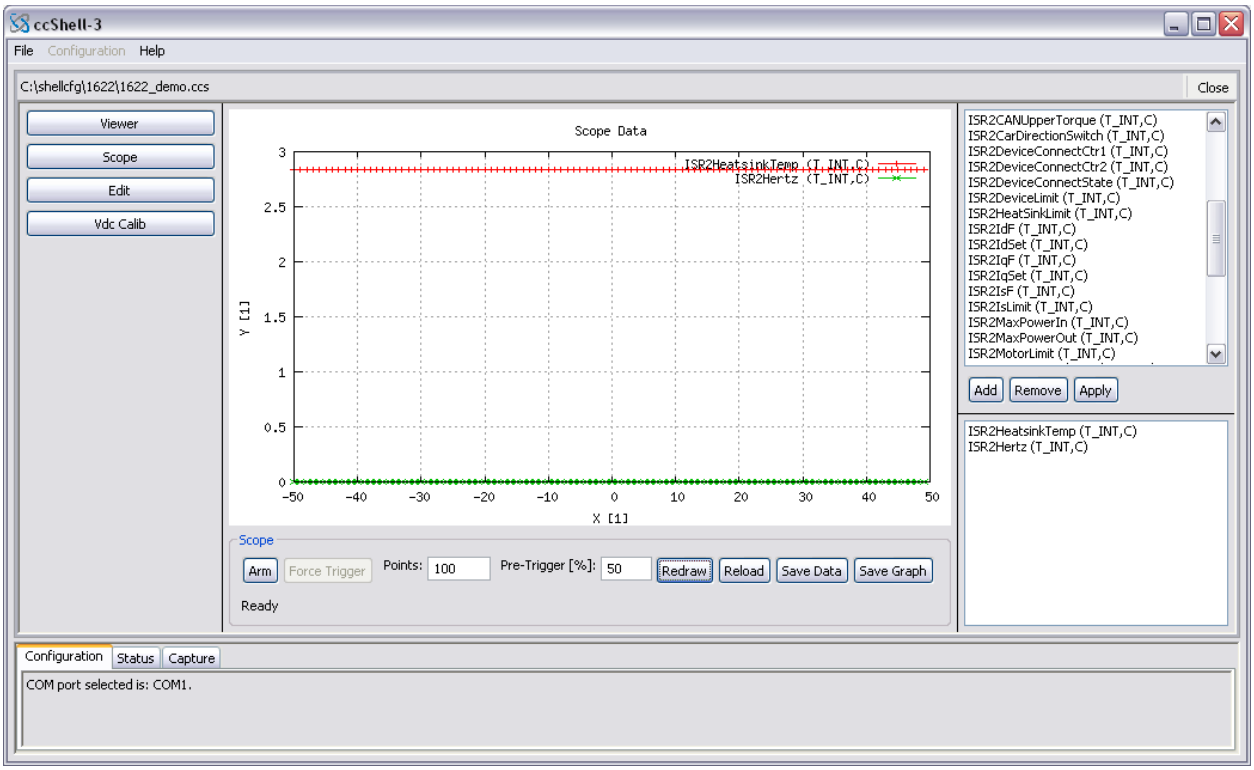

Figure 70: The Scope tool can be used to view what is happening with variables at a faster rate than the Viewer tool [31].

The Parameter Editor tool is used to access and modify the controller's variables. Once selected, the variables will begin to populate the ccShell window; however, this may take a minute or two to fully load the parameters. If an error occurs while loading a variable, the actual value of the variable will show "Rxd Error" reflecting a receive error. The display can be refreshed, or the .ccs file can be closed and then re-opened to ensure that all variables are properly loaded. Figure 71 shows an example of the parameter editor window with an Rxd error. Once the variables have loaded, the actual value is displayed with the specific unit associated with that variable. Minimum and maximum values are also provided to ensure that variable limits are not exceeded. The scroll slider can be used to view the different variables that can be changed. *Do not change variables until all the Azure user manuals and this thesis have been fully studied*. The DMOC445 .par file settings are show in the Appendix of this thesis (Figure 186 - Figure 191).

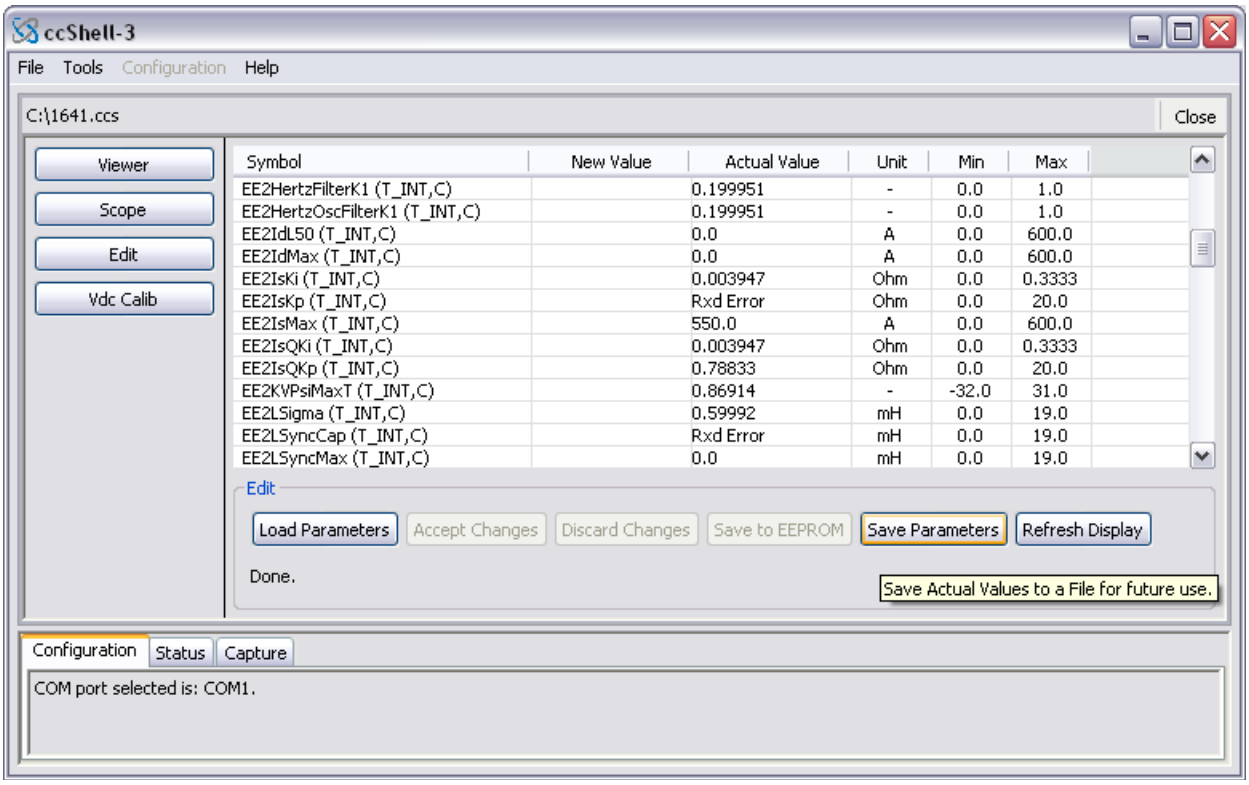

Figure 71: The ccShell parameters edit tool with and Rxd error. In this instance, the .ccs file can be closed and reopened, or the display can be refreshed [31].

In order to change a variable, select the desired variable and type in the new value in the "New Value" cell next to the variable and hit enter. However, hitting enter does not effectively change the variable. The program will provide an opportunity for the user to double check that the new desired value is a wanted change. This process is illustrated in Figure 72. If the change is wanted, select "Accept Changes" to approve the new variable value. Conversely, if the change is not wanted, select "Discard Changes" to cancel the variable change.

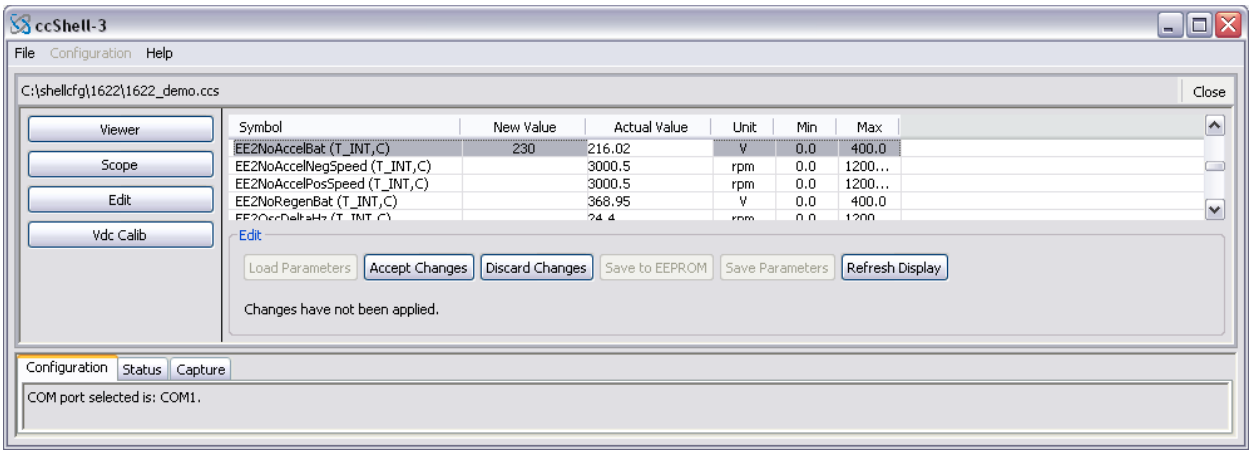

Figure 72: To change a variable type in the new desired value and hit enter. After reviewing the proposed change, select accept change to approve the new value, or select discard change to cancel the variable change [31].

Accepting the new variable change only temporarily changes the variable in the DMOC. If an error occurs during the variable change, the actual value will read "Txd Error" indicating a transmit error. In order to ensure that the new changes are effective the next time the vehicle is operated, ensure that the new changes are saved to the controller's EEPROM (Figure 73). Of importance, whenever a CAN related variable is altered it needs to be stored to EEPROM, and the controller power needs to be cycled with the ignition switch. However, if the new changes are not desirable after further testing, the 12 VDC power to the controller can be cycled and the memory will restore the previous value. If the new value was saved to EEPROM then it will need to be manually reset by changing the variable again. When changing variables, it is helpful to record the original value before accepting the new variable changes. This allows the user to revert to the previous variable if desired. Another method of saving the controller's parameters is using the "Save Parameters" option. This generates a .par file that can be saved in a desired location on the computer hard drive. Multiple .par files can be generated and loaded using the "Load Parameters" option and selecting the desired .par file. When a new .par file is loaded, the parameters need to be saved to EEPROM to remain in effect the next time the controller is powered on. Now that the calibration process for the controller has

been discussed, monitoring the powertrain temperature is of importance to confirm the components are not being operated beyond their limits.

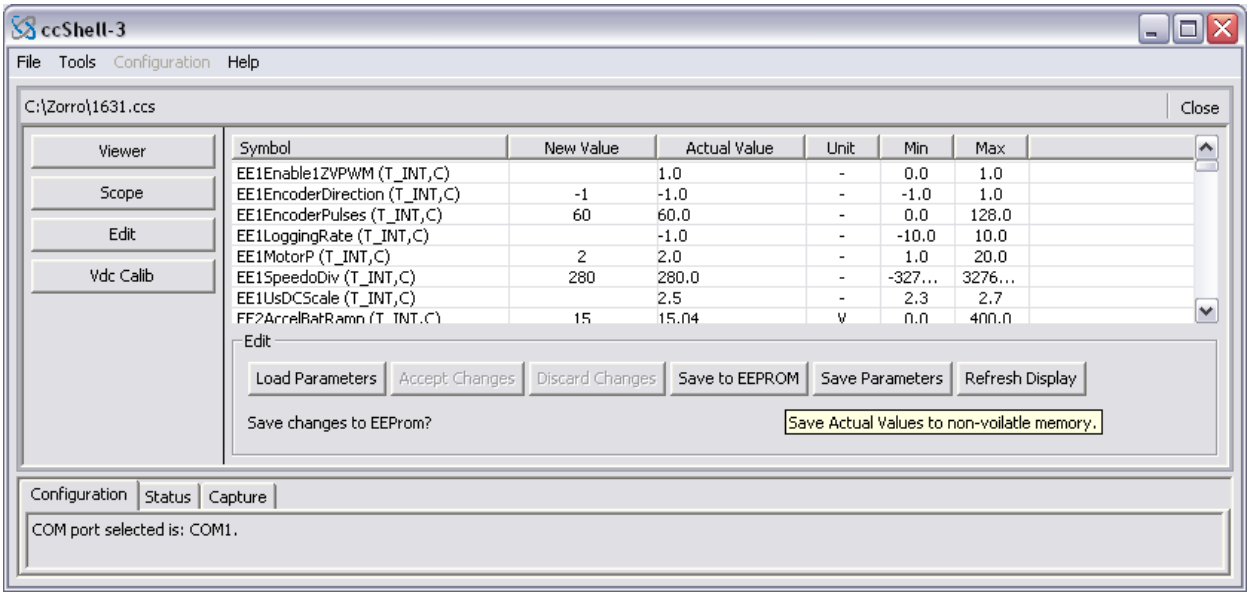

Figure 73: Variable changes can be stored to the DMOC's internal memory by selecting the "Save to EEPROM" option in ccShell [31].

While the motor can be operated slightly above the rated power, the combination of low motor speed and more power results in the motor quickly overheating. Fortunately, the DMOC monitors temperature in four critical locations; the insulated gate bipolar transistors (IGBTs), the motor, the DMOC heat sink, and the DC voltage terminals. The vehicle operator can monitor these temperatures using the *ISR2ThermCurrentLimitCause* variable in ccShell. While this variable does not specify the current temperatures, it does show if any thermal limiting is occurring in the powertrain system.

The IGBT's act as high speed switches that can handle more power than conventional transistors [30]. When the IGBT's are the cause of thermal limiting *ISR2ThermCurrentLimitCause* will display THERMAL_LIMIT_IGBT or a 1 depending on how the variable is being viewed. If the motor is overheating, ccShell will display THERMAL_LIMIT_MOTOR or a 2. If the heat sink is overheating, the heat sink temperature limits can be adjusted to allow the cooling fans to come on at lower temperatures to reduce overheating. THERMAL_LIMIT_HEATSINK or a 3 indicates that the DMOC heat sink is too

hot. Lastly, the DC voltage connections are also monitored. Excess temperature on the DC connections could indicate that excessive current is entering the DMOC. Additionally this could indicate that the DC wiring is getting too hot. If the DC wires get too hot, the insulation on the cables could be compromised resulting in a loss of HV isolation between the battery pack and operators. When the DC voltage terminals are the limiting cause, THERMAL_LIMIT_DC_VOLTAGE or a 4 will be displayed in ccShell. If both the DMOC and motor have reached their thermal limiting state, *ISR2ThermCurrentLimitCause* will only display the component that is being limited the most. Additionally, it is important to note that at zero motor speed the variable will reflect that the IGBTs are limiting. This occurrence is normal. Along with monitoring the powertrain component temperatures, it is additionally important to understand the procedure involved for removing the controller in the event it needs to be serviced.

In the fall of 2014, the Azure DMOC445 controller experienced issues with the internal contactors. After diagnosing the system, it was determined that the issue was rooted internally with the controller. In the event an internal controller issue arises, it is important to know how to remove the controller safely from the JimmE-V. Do not attempt to open the controller while it is hooked up to the HV system. Additionally, only experienced electronics personnel should attempt to perform service on the controller.

The first step is ensuring that the key is in the off position (Figure 74). While inside the vehicle, disable the high voltage power supply by depressing the emergency contactor control button (Figure 75). This ensures that no high voltage will be present at the controller when removing it from the vehicle. Next, unplug the three wire terminal on the right side of the DMOC (the 8, 35, and 14-pin connections). Unplugging these connections removes the 12 VDC source from the controller preventing operation.

Figure 74: The ignition switch in the off position (left), and in the on position (right).

Figure 75: The contactor control button is in the 'OFF' position on the left, and in the 'ON' position on the right.

Next, the electrical cover behind the cooling fans can be removed using the proper sized Philips screwdriver. Once the cover has been removed, proceed with caution due to the HV connections to the controller. At this point, the voltage on the positive and negative terminals can be checked with a multimeter. The voltage should read zero. If it is not zero, double check that the contactors have been disengaged. It is important to note that this version of the DMOC contains anti-EMF X and Y capacitors inside the controller. These capacitors connect to the positive, negative, and chassis of the controller. Consequently, when a multimeter is used to measure from the positive (or negative) terminal to the controller's chassis a large voltage will be present. If a wrench shorts either terminal to the controller chassis it can shock the individual working on the controller. However, there is no power behind the charge and the capacitance is not high (0.01 µF). At this point, it is best to let the capacitors inside the controller bleed off before resuming work. Let the controller sit for approximately 30 minutes before

checking the voltage between the DC terminals and the controller chassis. If there is still voltage present, continue to let the capacitors bleed off until the voltage is no longer present.

While the controller is bleeding off the capacitors, the DC-DC converters can be disabled (Figure 76). Shutting off the DC-DC converters ensures that the HV source is not providing power to the 12 VDC system. Once the capacitors have bled off, the DC connections can be removed by removing the nuts and bolts with wrenches. In order to remove the cables from the controller, the black plastic nuts that prevent water from entering the controller can be removed. Only remove one wire at a time, and once the HV cable has been removed, cover the exposed terminal with sufficient electrical tape. Once the two HV cables have been removed and taped, the three-phase AC cables can be removed by removing the nuts and bolts with wrenches. To remove the three-phase cables from the controller, the shielding nut (Figure 55) needs to be loosened using channel lock pliers until it can be loosened by hand. With the wire terminals unplugged and the AC and DC cables disconnected from the controller, the nuts fastening the controller to the vibration dampening mounts (Figure 60) can be removed. Once the four nuts at each corner of the controller have been removed, the controller can be lifted out of the JimmE-V by hand. The controller weighs approximately 30 lbs. Seek assistance if necessary. If the controller is in need of repair, there is contact information for individuals who have worked on the JimmE-V DMOC445 controller in the Appendix of this thesis. As evident from this section, it is important to understand how to operate and calibrate the DMOC445 in order to collect quality research data. In addition to the DMOC, knowing how to operate and calibrate the JimmE-V ECU is additionally important since the ECU is responsible for communicating driver commands to the DMOC for motor operation. The vehicle's ECU is discussed next.

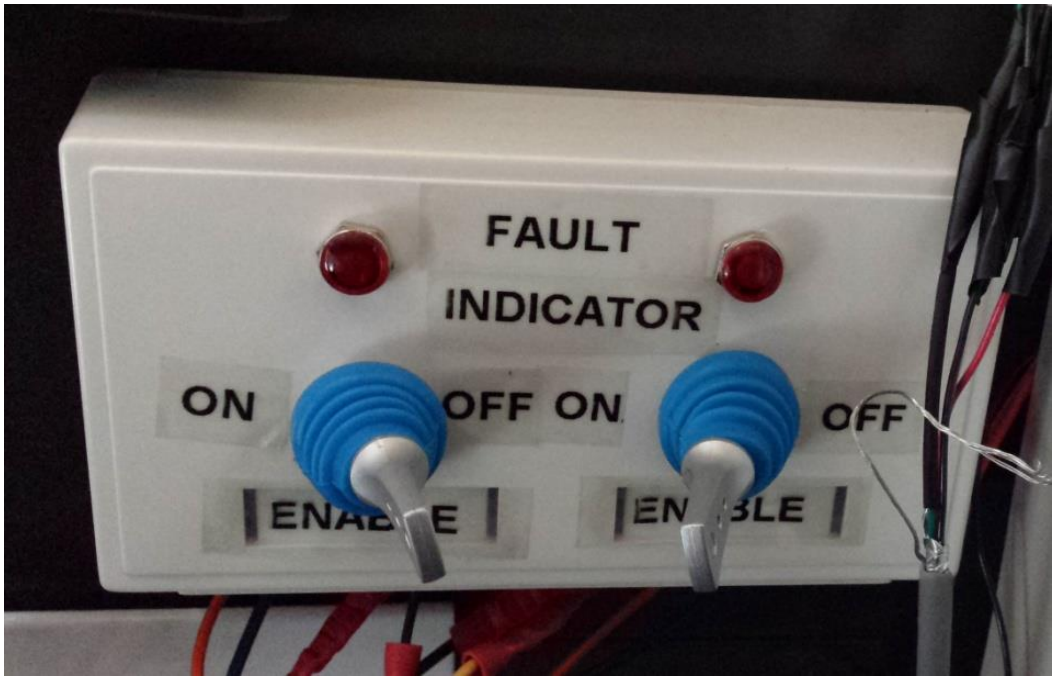

Figure 76: DC-DC converter enable switch box located behind the passenger seat.

3.5.3 JimmE-V Electronic Control Module

The JimmE-V ECU plays an integral role in operating the JimmE-V. As mentioned in Chapter 2 of this thesis, the ECU serves as a gateway between the operator and motor controller. Since the DMOC445 is CAN controlled, the ECU is needed to turn the analog signal from the dual potentiometer accelerator pedal into a digital torque command. The torque command is then relayed via CAN bus where it is received by the motor controller. The motor controller then applies the necessary electrical power from the battery pack to accelerate the vehicle. Additionally, the ECU assists in the regenerative braking procedure ensuring that the regen commands are sent to the controller when desired. This section focuses on the processes involved to communicate, calibrate, and view real time data from the ECU.

The ECU was installed under the hood of the JimmE-V forward of the motor controller Figure 77). In order to mitigate vibrations, the ECU is secured to the sub-frame's polycarbonate platform using three bolts and rubber bushings. Having these two components located in close proximity reduced the wiring length for the CAN bus. Before interfacing with the ECU, there are additional components to discuss to ensure the operator can properly interface with the control module. New Eagle's Mototune

software package is used to interface with the ECU and requires a license. The license information is contained on a Crypto-Box USB drive. Before the program can be opened, ensure that the Crypto-Box key has been inserted into the laptop's USB port. The license key accompanies the laptop for the JimmE-V, and the USB drive is left in the back right corner of the laptop (Figure 78). With the license key inserted into the laptop, the next step is to connect the laptop to the JimmE-V CAN bus using the Kvaser CAN to USB adapter.

Figure 77: The JimmE-V ECU.

Figure 78: The Mototune software license information is contained on the Crypto-Box USB drive.

In order for the Kvaser adapter to interface with the JimmE-V's CAN bus, it is connected to the Smartcraft connector located in the vehicle's glove box. The Smartcraft connection junction is wired to a DB9 connector that mates with the Kvaser adapter. The USB end of the CAN adapter connects to the

laptop. In order to eliminate COM port communication issues, the USB port adjacent to the Mototune license key is used for accessing the ECU.

Figure 79: The Kvaser Leaf Lite CAN to USB connection.

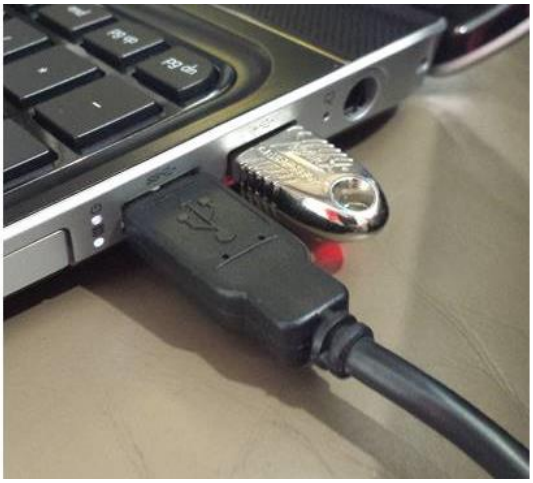

Figure 80: The Kvaser CAN adapter is connected to the laptop using the USB port next to the Crypto-Box USB drive.

The Kvaser adapter has two LEDs on it to indicate that it has power and that the device is connected to the CAN bus. Figure 81 shows the different LED indicators. Once all the USB connections have been made with the vehicle's laptop, the ECU can be powered on by switching the ignition switch to the on position (Figure 74). This provides the ECU with 12 VDC power from the auxiliary batteries. With

the ECU powered on, the Mototune software can now be opened to interface with the ECU. Mototune can be accessed through the start menu, or the icons located on the desktop screen shown in Figure 82.

Figure 81: The green LED indicates that the adapter is powered; while the amber LED indicates the CAN bus connection has been established.

Figure 82: Mototune can be accessed by selecting the icon or shortcut on the desktop screen.

Figure 83 shows the initial display window once Mototune has been opened. The top left of the Mototune window registers the license and displays "New Eagle LLC". If the license is not recognized, "Unlicensed" will be displayed. To get the license to be recognized, close Mototune, remove the Crypto-

Key, turn off the ignition switch, re-insert the Crypto-Key, turn on the ignition switch, and open Mototune. Once the license is registered, the user can select if they want to open a calibration file or display file. Calibration files allow the user to modify and save ECU settings, while displays only allow the operator to view parameters while the ECU operates. The explorer windows on the left side of Figure 83 allow the user to navigate through the various parameter folders available in the ECU. In order to calibrate the parameters in the ECU, a calibration file needs to be opened. Calibration files can be opened using the open folder icon, or under the file menu. Once selected, an open window will display what files are available to open. Figure 84 shows the main open window options; calibration files are located in the Cals folder, while display files are located under the Displays folder. The display option will be discussed after ECU calibration has been discussed in this section.

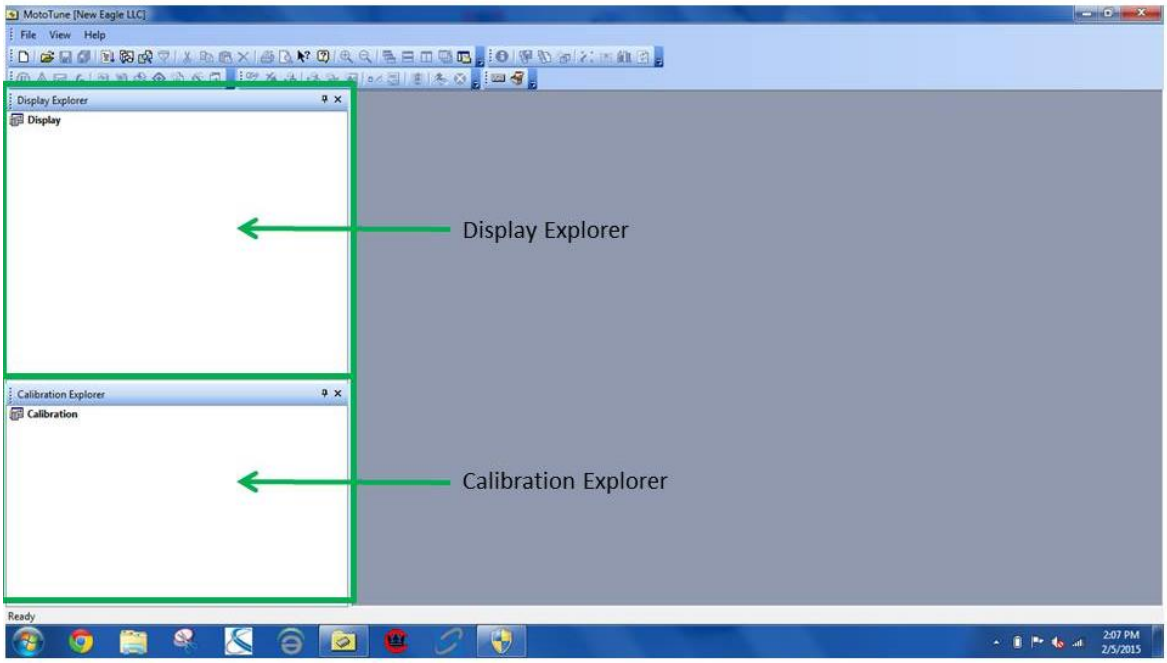

Figure 83: Initial display window when Mototune is opened.

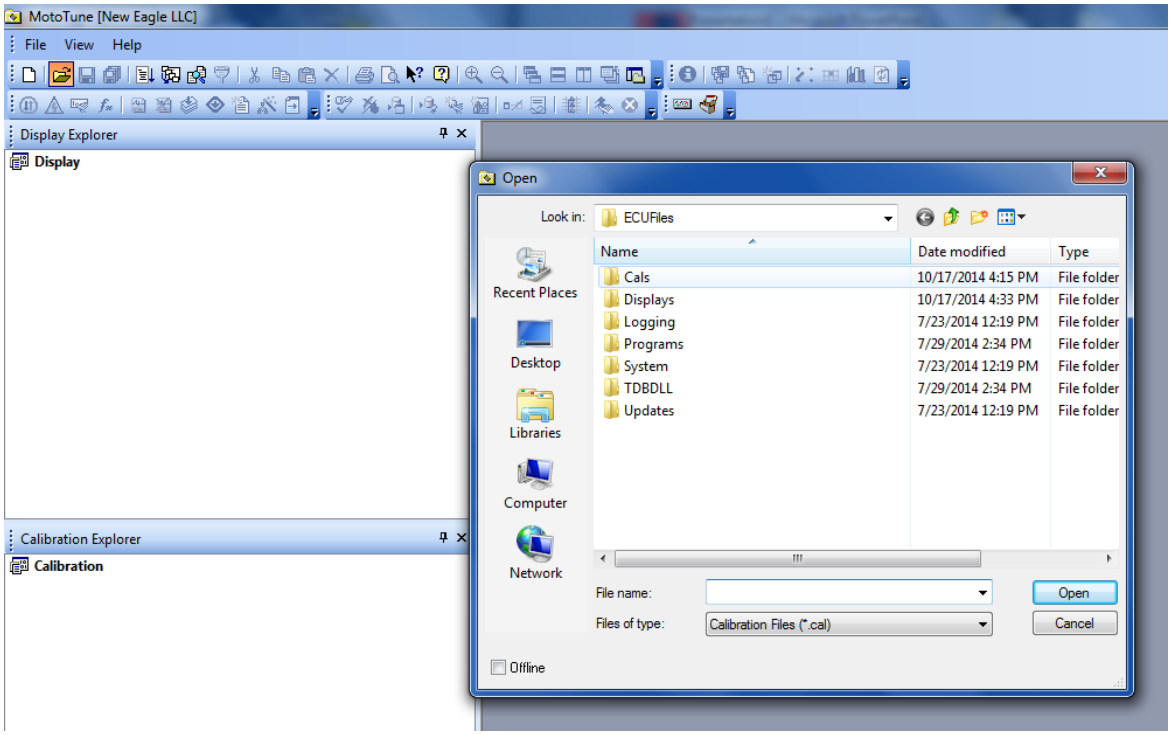

Figure 84: ECU calibration files are in the Cals folder.

To open the ECU's calibration file, select the Cals folder. In order to view the calibration files, ensure that the file type is .cal (default open option). The Cals folder contains each iteration of the ECU's calibration; however, in order to change parameters in real time, the most recent iteration should always be opened. Figure 85 shows the available calibration files. These files include files to the non-programmable ECU. In order to ensure that the most recent file is opened, the file names should be sorted by date. The most recent iteration ECU calibration file that should be used is named *Kansas_902_32mrg000.cal*. Once the calibration file has been opened successfully, the calibration explorer window is populated with folders and recently viewed calibrations open in the main window next to the explorer bar. It should be noted that New Eagle used a very similar ECU in the Ford Transit. As a result, there are unused parameters in the ECU's programming (e.g., AC control, contactor control, and heater control). The ECU is only used to communicate with the controller and motor. Figure 86 shows an example of what Mototune displays once a calibration file has been opened. Recently viewed parameters will often be displayed. If there are no parameters displayed, they can be accessed and viewed using the calibration explorer window for the desired parameters.

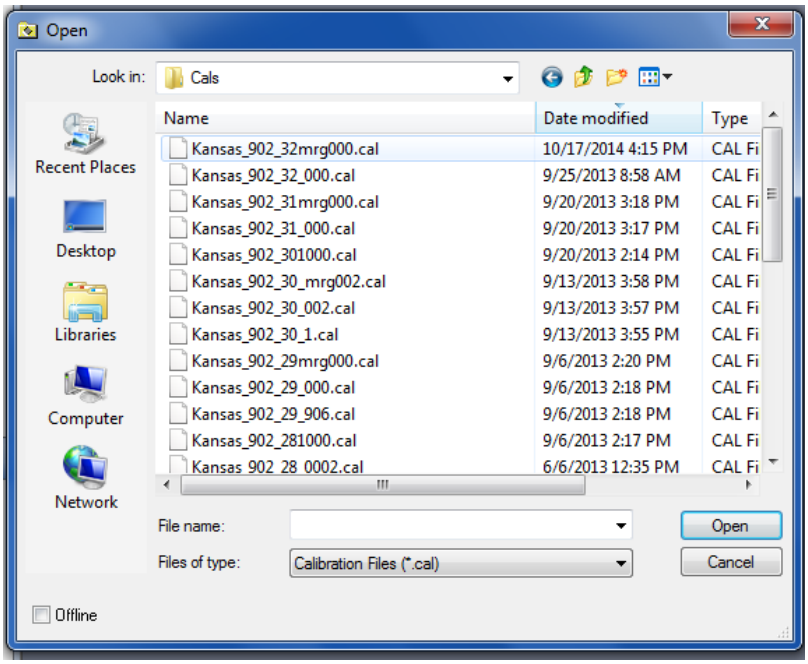

Figure 85: To view current ECU calibration parameters and alter parameters, the most recent calibration file should be opened.

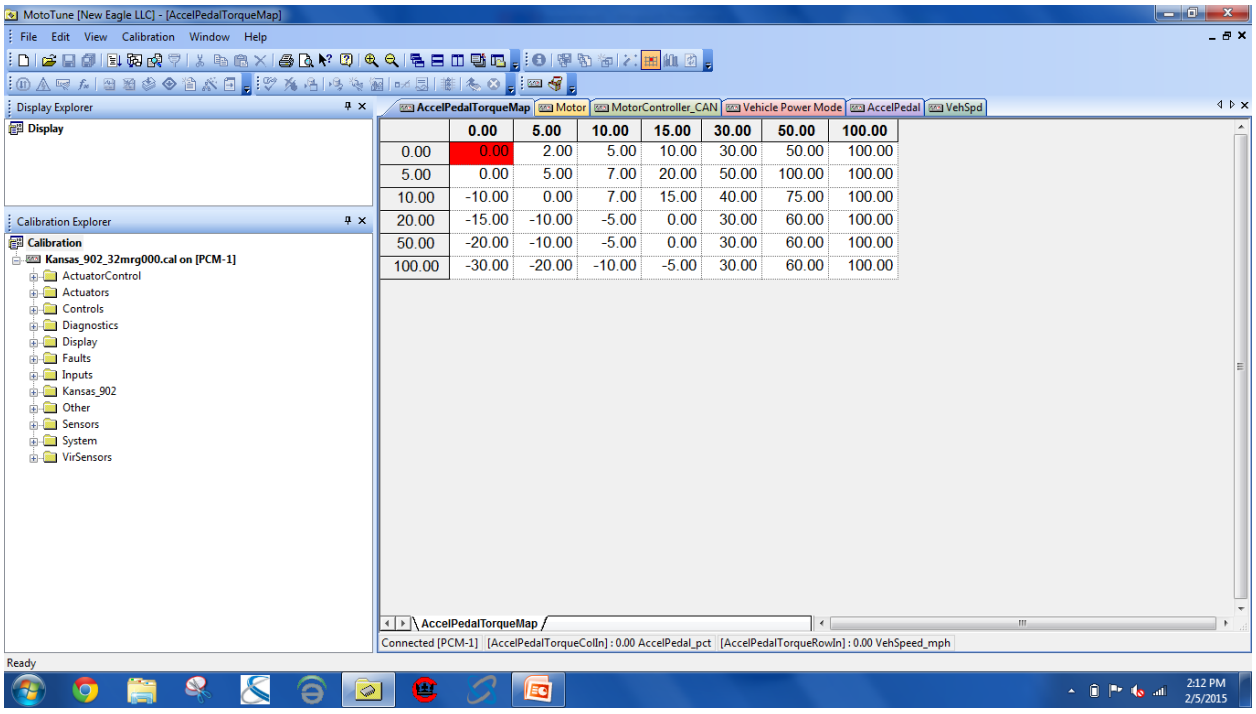

Figure 86: Once a calibration file is opened, the calibration explorer window is populated with parameter folders. Additionally, recently saved paramterers will be displayed in the main window.

With the calibration opened, some of the main ECU calibration parameters will be examined. When calibrating the ECU, it is important to understand that the motor controller has the final say in

regards to what happens with the motor. For example, the AC55 motor is rated at 280 N-m of torque. If the ECU requests a torque value of 350 N-m with the controller max torque set to 300 N-m, only 300 N-m will be commanded from the motor. This setup provides checks and balances to the powertrain system to ensure that the motor is not operated beyond its rated specifications. The first calibration parameter that will be examined is the accelerator pedal torque map.

The accelerator pedal torque map is responsible for varying the torque applied to the motor as the vehicle speed changes. Figure 87 shows the JimmE-V's accelerator pedal torque map. The top row of numbers represents the amount the accelerator pedal is pressed (i.e., 0%, 5%, 10%, 15%, 30%, 50%, and 100%). The far left row is the vehicle speed in miles per hour. Positive numbers in the map indicate positive torque applied to the motor drawing power from the battery pack, while negative values indicate that the motor is in a regenerative braking state. The numbers that populate the map are percent values of the motor's rated torque (i.e. if the ECU has the motor's rated torque at 300 N-m, when the pedal is pressed 30% at 10 mph, the ECU will command 40% of the motor's rated torque). This also applies to the negative percent values in the map for calibrating regenerative braking. The displayed map calibration in Figure 87 has been relatively unchanged other than the first two rows. The first two rows were altered using trial and error to ensure that the vehicle had smooth starts similar to a production vehicle.

AccelPedalTorqueMap | Motor | MotorController_CAN | Vehicle Power Mode | AccelPedal | VehSpd

	0.00	5.00	10.00	15.00	30.00	50.00	100.00
0.00	0.00	2.00	5.00	10.00	30.00	50.00	100.00
5.00	0.00	5.00	7.00	20.00	50.00	100.00	100.00
10.00	-10.00	0.00	7.00	15.00	40.00	75.00	100.00
20.00	-15.00	-10.00	-5.00	0.00	30.00	60.00	100.00
50.00	-20.00	-10.00	-5.00	0.00	30.00	60.00	100.00
100.00	-30.00	-20.00	-10.00	-5.00	30.00	60.00	100.00

Figure 87: The JimmE-V accelerator pedal torque map.

Before discussing the ECU display feature, there are some additional parameters that are important to discuss. As previously mentioned, the ECU needs to know the motor's rated torque (Figure 88), power limits (Figure 89), and final drive ratio (Figure 90). The rated torque should match the torque programmed into the DMOC in order to have a consistent pedal torque map. It should be noted that the

displayed values in these figures may not align with the current calibration in the ECU. They are simply displayed for discussion purposes. The motor power limit and regenerative braking limit are additional parameters that can be used to tune the power limits commanded from the ECU. For initial vehicle testing, the regen power limit was reduced to 0 kW to ensure the motor was functioning properly. This value can be calibrated as desired, with the DMOC having the final say in what is actually generated from the motor (i.e., can be set to max value in the ECU, and limit the regen power in the DMOC). The gear ratio tab is important in determining vehicle speed. The ECU and controller communicate the current motor speed in revolutions per minute (rpm). This value is then used with the final drive ratio to determine the vehicle's current speed. However, tire size is not an available parameter in the ECU. As a result, the final drive ratio parameter needs to be adjusted using trial and error, and then compared with GPS indicated speed.

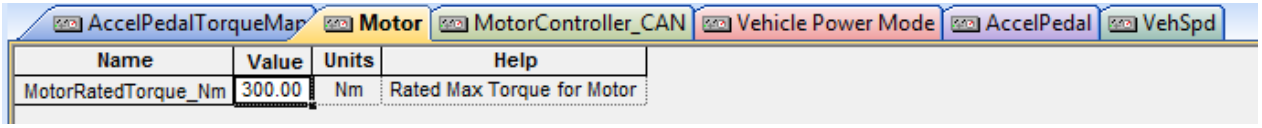

Figure 88: The ECU motor rated torque parameter.

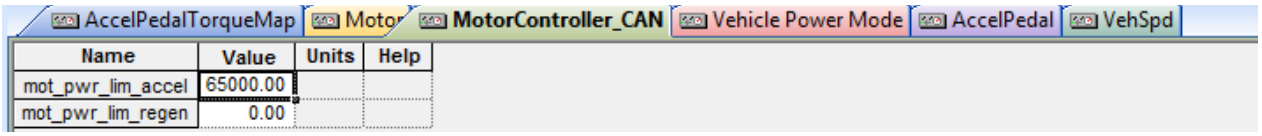

Figure 89: The ECU motor acceleration and regenerative power limits.

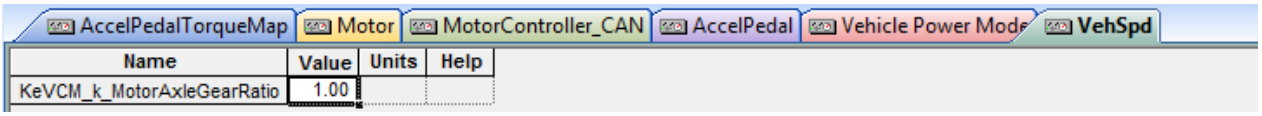

Figure 90: The final drive ratio parameter used to determine the vehicle speed.

Lastly, once a parameter is changed it is important to save the current setting. This ensures that the ECU memory will reflect the new value the next time the vehicle is operated. Files can be saved using the save icon (adjacent to the open icon), or by using the file menu. The next area of discussion is viewing ECU displays.

Viewing the ECU display is useful when operating the vehicle to ensure that the systems are operating as expected. Opening a display file is similar to opening a calibration file; however, instead of

selecting the Cals folder, the Displays folder is selected. Since the .cal is the default file type, the file type needs to be changed to .dis before any files will appear in the folder. This process is shown in Figure 91.

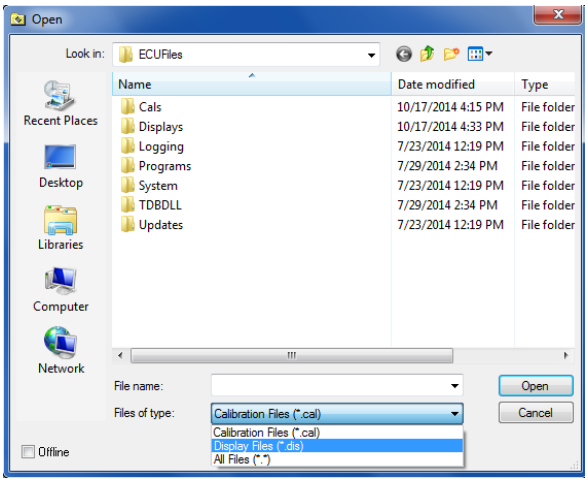

Figure 91: In order to view and open display files, the file type needs to be changed to .dis.

The major difference between display and calibration files is that the display files are user generated, and they are not dependent on the current calibration (i.e., several different displays can be made; whereas, the ECU only has one calibration file). The ECU only has one main calibration file, and Mototune will warn the user by indicating that the desired file and ECU do not match. This is not the case with display files. Starting a new display is accomplished through the new icon (to the left of the open icon) or through the file menu. From there, the user can select desired parameters to view by dragging and dropping the parameter into the new window. Once the parameters have been moved in to the desired cells, the cells can then be adjusted similarly to how cells are adjusted in Microsoft Excel. The most recent display file, *Display3.0.dis*, provides a good starting display for operators as it shows the majority of desired parameters used to indicate the ECU and vehicle are operating correctly. Figure 92 shows an example of a display file. The display file shows ECU power states, the current shifter position, accelerator pedal percentage, vehicle speed, and the output torque command. Additionally, variables can be overridden by changing the pass-through option to manual. Using manual entry can be beneficial in troubleshooting relays to ensure they are functioning properly (i.e., if the fault condition is changed to manual entry with the value changed from 0 to 1, the fault relay should engage illuminating the fault

light). The ECU relays will be covered later in this section. In the event the ECU is not communicating with the computer, the communication port settings need to be checked to ensure the Kvaser CAN adapter is functional.

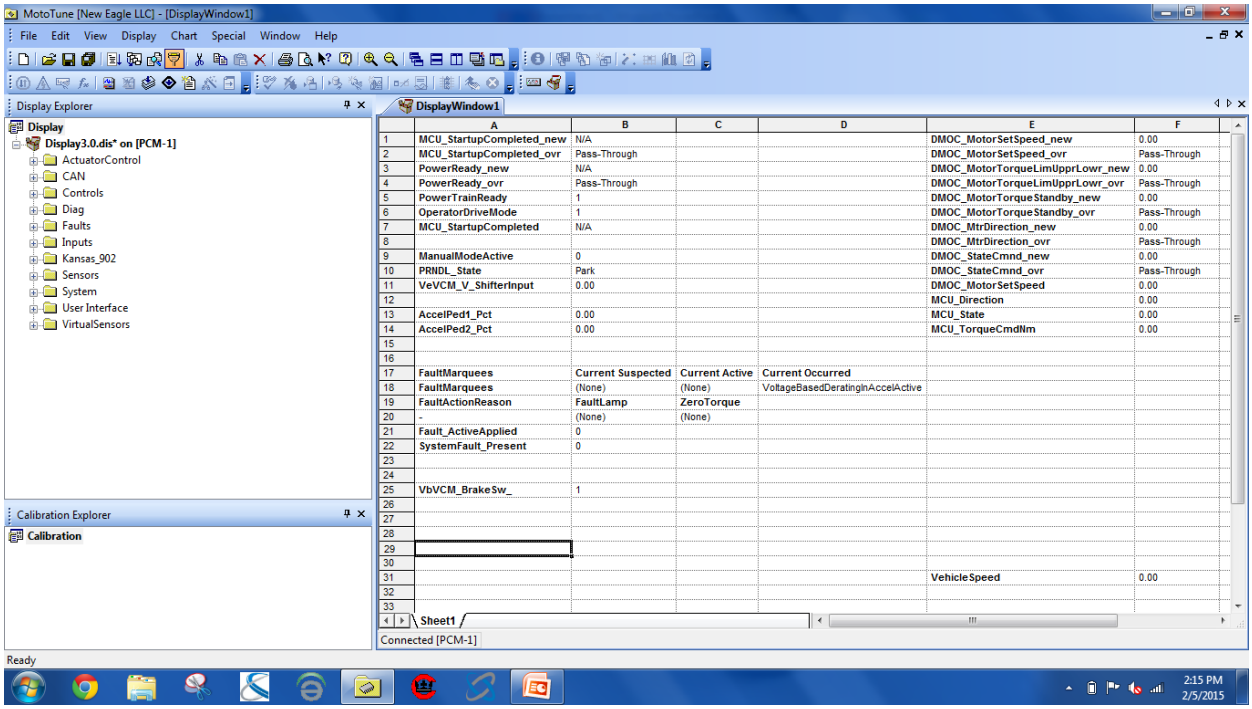

Figure 92: The display window allows users to view ECU parameters during vehicle operation.

In order to check the communication port settings, there is a MotoServer icon (a satellite dish) located in the bottom right next to the time and date on the taskbar. Right clicking the icon produces a settings list. This process is illustrated in Figure 93. When the ports option is selected, a port configuration will open showing the different options available (Figure 94). To communicate with the ECU, PCM-1 needs to be checked for the Kvaser CAN adapter. Lastly, the baud rate needs to match the ECU baud rate of 500 kbit/sec. These settings can be modified by selecting the port and clicking modify. Before closing the configuration box, apply needs to be selected for the new changes to take effect.

Figure 93: The MotoServer icon is located on the far right end of the taskbar. To view the connection settings, select the ports option.

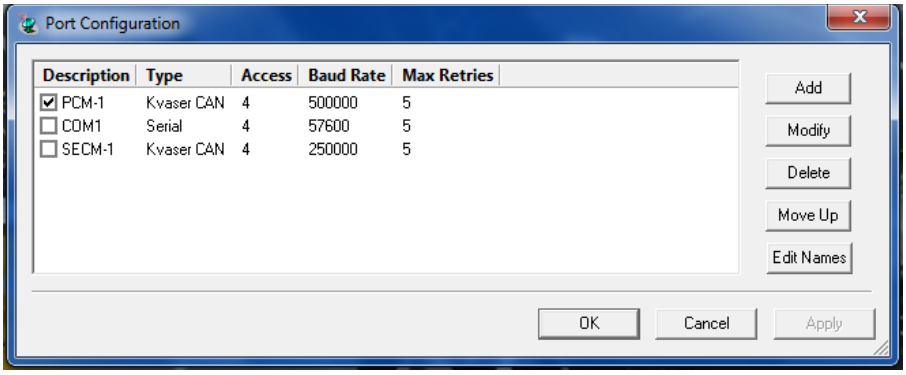

Figure 94: MotoServer port configuration window.

In addition to knowing how to access, calibrate, and view data in the JimmE-V ECU it is also important for the driver to understand how to operate the ECU. As previously mentioned, the ECU is responsible for taking the driver inputs and relaying the proper signals to the DMOC controller. The main inputs provided by the driver are the shifter, accelerator pedal, and brake pedal. In order to ensure proper vehicle operation, each of the main inputs will be discussed.

The first input to discuss is the shifter. Typically, automotive shifters have been mechanically linked to a manual or automatic transmission. Due to the lack of a transmission, it is important to note that this shifter does not mechanically place the vehicle in park. The shifter in the JimmE-V is simply an electrical five position switch with each position indicating a drive position. As vehicles begin adopting more electronics, manufacturers are already implementing electronic shifters into their vehicles (Figure 95). The shift positions follow typical automotive shifter setup; the shifter order is Park (P), Reverse (R),

Neutral (N), Drive (D), and Low (L). A similar shifter arrangement is implemented in the JimmE-V (Figure 96).

Figure 95: Electronic shift knob in the 2015 Chrysler 200 [32].

Figure 96: The JimmE-V shift knob is located on the vehicle's dash board.

Each shift position in the JimmE-V results with different motor operation. The shifter should only be operated with the vehicle's ignition switch in the on position. If the vehicle is turned on with the shifter out of park, the shifter will need to be returned to park and have the ignition switch cycled. The different shift positions are illustrated in Figure 97. When the shifter is in park, the ECU is on, but the ECU has not switched on power to the DMOC. When the position is moved to reverse, the drive enable relay will engage providing 12 VDC to the DMOC and enabling the drive mode. At this point, the driver should hear an audible switching sound from the DMOC. This sound is the main internal contactors engaging. Before backing up the JimmE-V, ensure that the path behind the vehicle is clear of obstacles and persons. Once the driver depresses the accelerator pedal, the ECU will request a negative torque command from the motor causing the motor to spin in the opposite direction accelerating the vehicle backwards. When

the neutral shift position is selected, torque commands will not be sent to the ECU, and the drive enable is disconnected. The final position is drive; this is the position the shifter needs to be in for the vehicle to move forward. Once the accelerator pedal is depressed, the ECU will send a positive torque command to the DMOC resulting in forward acceleration. The low position is not used, but is displayed to the driver to display the switch position. The JimmE-V will not operate in low. Just below the shifter is the Miniview display.

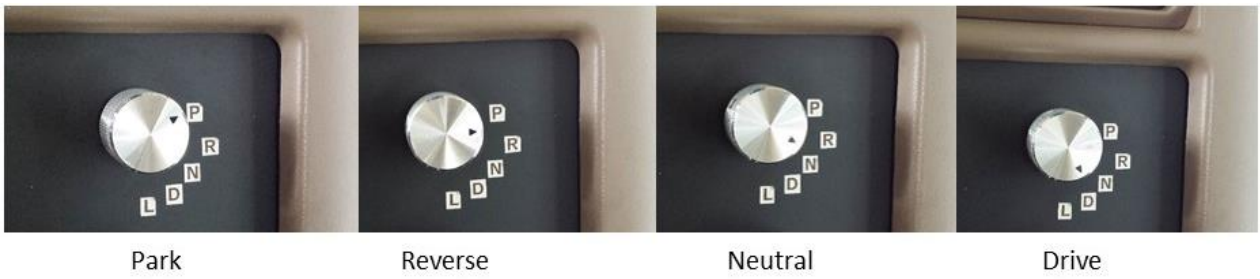

Figure 97: The different JimmE-V shifter positions to operate the vehicle.

The Miniview gauge display is used to provide feedback to the operators of the JimmE-V when a laptop is not in use. The display has three parameters available to display; however, only two are in use leaving the third for future expansion. The two parameters the gauge displays are accelerator pedal position (APP), and the requested torque command. The displayed parameter can be changed by pressing the up or down buttons below the display until the desired parameter is shown. Figure 98 shows the Miniview gauge displaying accelerator pedal percent (left) and the torque command (right). In addition to the Miniview gauge, there is also a toggle switch for regenerative braking in the JimmE-V.

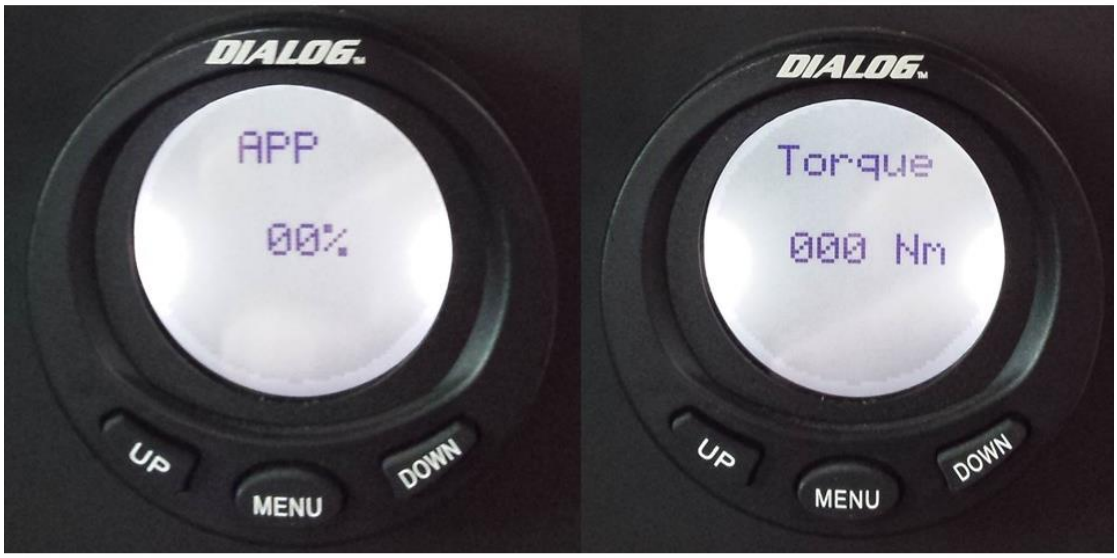

Figure 98: The Miniview display shows the operator accelerator pedal position and the current torque command from the ECU.

The regenerative braking switch is located below the light switch on the left side of the JimmE-V's steering wheel (Figure 99). The switch controls the voltage input to the ECU when the brake pedal is depressed. The 12 VDC signal from the brake pedal is routed through the voltage regulator mentioned in Chapter 2 of this thesis to reduce the voltage to no more than 4 VDC before entering the ECU input. When the switch is on, the voltage signal is allowed into the ECU. When the switch is off, the ECU input does not see a voltage signal. This signal lets the ECU know when the brakes are being applied, and whether or not regenerative braking should be applied. In addition to this switch, regenerative braking can be programmed on or off through the ECU or motor controller. Before using the toggle switch, ensure the desired parameters are established in the ECU and DMOC. Figure 89 shows the regenerative power limit set to zero. As a result, the ECU will not command any regenerative braking. If the ECU limit is set higher than the DMOC limit, the DMOC will enforce the lower limit. Conversely, if the DMOC is set higher than the ECU, the ECU will be the limiting regenerative power. The ECU in the JimmE-V is a low maintenance component; however, the ECU controls relays that eventually wear out due to the electromechanical nature of the component.

Figure 99: The regenerative braking toggle switch is located below the toggle switch for the vehicle's lights.

The relays used in the JimmE-V's ECU circuit are necessary to provide power to the ECU and DMOC. Additionally, the relays are used to cycle the controller's drive enable command. An additional relay was implemented for a fault lamp circuit. The four relays are shown in Figure 100. The fault lamp circuit will only be actuated in the event of an ECU fault. The other three relays see more use; as a result, if it is suspected that a relay has failed, the fault relay can be switched with the worn out relay to determine if that is the issue.

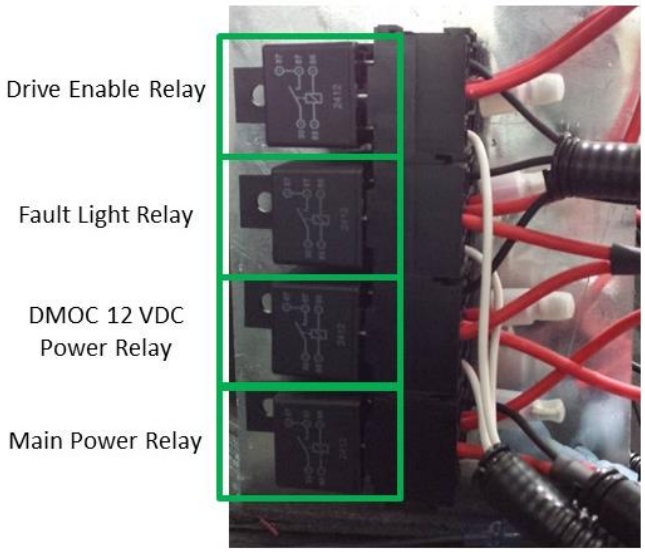

Figure 100: The ECU relays are located under the hood of the JimmE-V next to the ECU.

In the event of an ECU fault, the fault lamp will be illuminated. The fault lamp is located on the vehicle's dashboard above the 12 VDC gauge (Figure 101). Overall, the ECU in the JimmE-V has proven to operate reliably and consistently. It is important that the ECU calibrations be examined and compared

with the DMOC parameters before taking drive cycle data to ensure the vehicle operates as desired. Once the parameters are input and saved, they will remain unchanged allowing the ECU to communicate with the DMOC reliably and consistently. This allows the DMOC to operate while recording data. Along with knowing how the JimmE-V powertrain components work together, the controller and motor also interact with the high voltage battery pack. The high voltage system and its associated components will be discussed next.

Figure 101: The fault light is located on the dashboard above the 12 VDC gauge.

3.6.1 Vehicle Traction Battery Pack

Before discussing the JimmE-V's batteries, some context will be provided to further understand how batteries function. A battery consists of an anode, cathode, and an electrolyte solution. When the metal anode and cathode are immersed in the electrolyte an electron release occurs. There are a variety of batteries; however, this section will primarily focus on lithium iron phosphate ($LiFePO_4$) batteries as they are the batteries that power the JimmE-V.

Lithium batteries are desirable from an EV standpoint due to their light weight and high energy density. $LiFePO_4$ batteries offered a low cost cathode that is stable during discharging and recharging. Additionally, $LiFePO_4$ show no obvious capacity fading, and they have a low thermal conductivity at room temperature [28]. Due to these characteristics, these batteries were ideal to be implemented by undergraduate students for the JimmE-V conversion project.

The JimmE-V uses 104 CALB 100 Amp-hour (Ah) $LiFePO_4$ batteries installed in series to provide a nominal voltage of 330 VDC to the motor and controller with additional cell specifications given in Table 5. In the event a cell failure occurs, replacement cells need to have the same specifications and to avoid slight differences between battery manufacturers, only CALB batteries should be used. In order to maintain the battery pack properly, the battery pack construction will be discussed to illustrate the vehicle's HV isolation and safety.

Table 5: CALB $LiFePO_4$ cell specifications [33].

Nominal Voltage	3.20	VDC
Operating Voltage	2.50-3.65	VDC
Recommended Charging Voltage	3.65	VDC
Minimum Voltage	2.50	VDC
Maximum Discharge Current	2	-C
Minimum Operating Temperature	-20	°C
Maximum Operating Temperature	55	°C

The JimmE-V battery pack construction began during the second year of the project. Steel brackets and a support shelf were designed, fabricated, and installed into the vehicle to support the weight of the battery pack. For discussion purposes, the front battery pack refers to the battery pack located in the rear passenger compartment of the vehicle. The rear battery pack is located in the rear cargo section of the JimmE-V with battery packs shown in Figure 102. In order to provide electrical isolation, the battery boxes were constructed from polyvinyl chloride (PVC), and secured together using PVC specific adhesive to eliminate the use of metal fasteners. Additionally, the corners are reinforced with fiberglass brackets. To dampen vehicle vibrations and oscillations, each battery box was lined with a recycled rubber mat. The battery packs are covered with clear polycarbonate to prevent debris from falling in the battery packs. The covers each have four high-density rubber posts accompanied with nylon screws to further limit the amount of metal near the batteries and provide structural support for the covers. Each row of the battery pack is held in the battery box with a pair of locking bars.

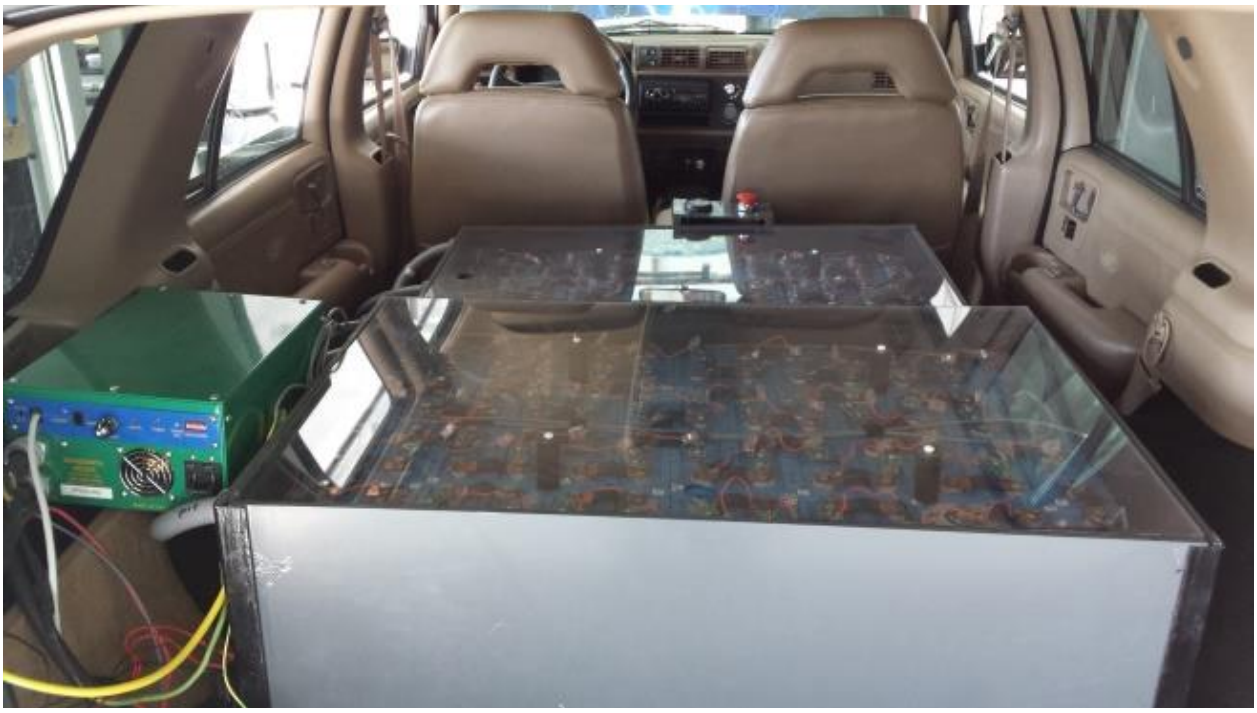

Figure 102: The JimmE-V battery packs in the rear passenger compartment (far) and rear cargo section (near).

These bars were an ideal method to use based on the cell construction with Figure 103 illustrating how the locking bars function. The bars interlock with channels on the batteries to secure the batteries to the neighboring rows of batteries. The locking bars also use the sides of the battery boxes to secure the cells to the boxes (Figure 104). These features are important to understand in the event a battery cell needs to be replaced. However, before removing cells, it is important to understand the layout of the HV voltage system to prevent personal injury or death.

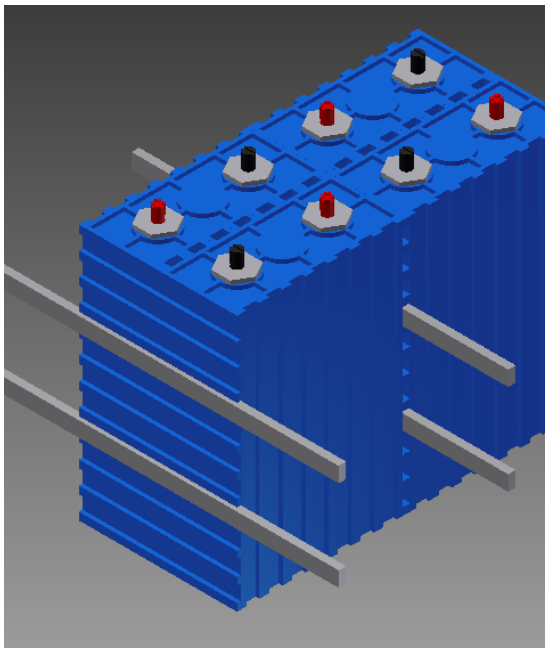

Figure 103: CAD drawing illustrating how the locking bars function [34].

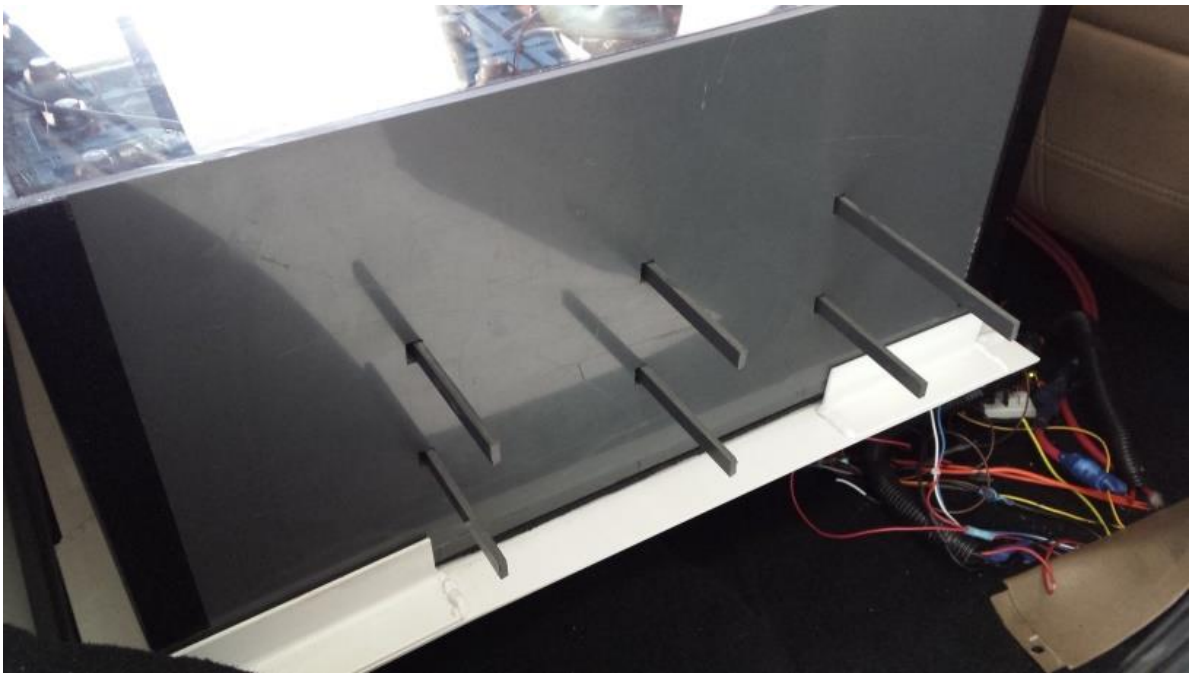

Figure 104: The locking bars can be accessed from the sides of the battery boxes. They safely secure the batteries to the boxes.

In order to safely operate and maintain the JimmE-V, high voltage safety is of the utmost importance. Figure 105 illustrates all the components connected to the HV circuit in the JimmE-V. For safety purposes one should assume that an orange wire located in the HV system carries voltage of 330

VDC or greater. The battery charger, DC-DC converters, motor controller, motor, and AC system each have additional sections in this chapter to examine each area in more detail. The purpose of this section is to provide information on how each system is linked with the HV system so that it can be safely maintained. The battery charger provides the input power to charge the battery pack. There are HV cables that connect the charger to the battery pack at the high voltage fuse junction. The two HV fuses are shown in Figure 106. In addition to the HV fuses, a HV junction box is responsible for completing the HV circuit and transferring HV to other vehicle components.

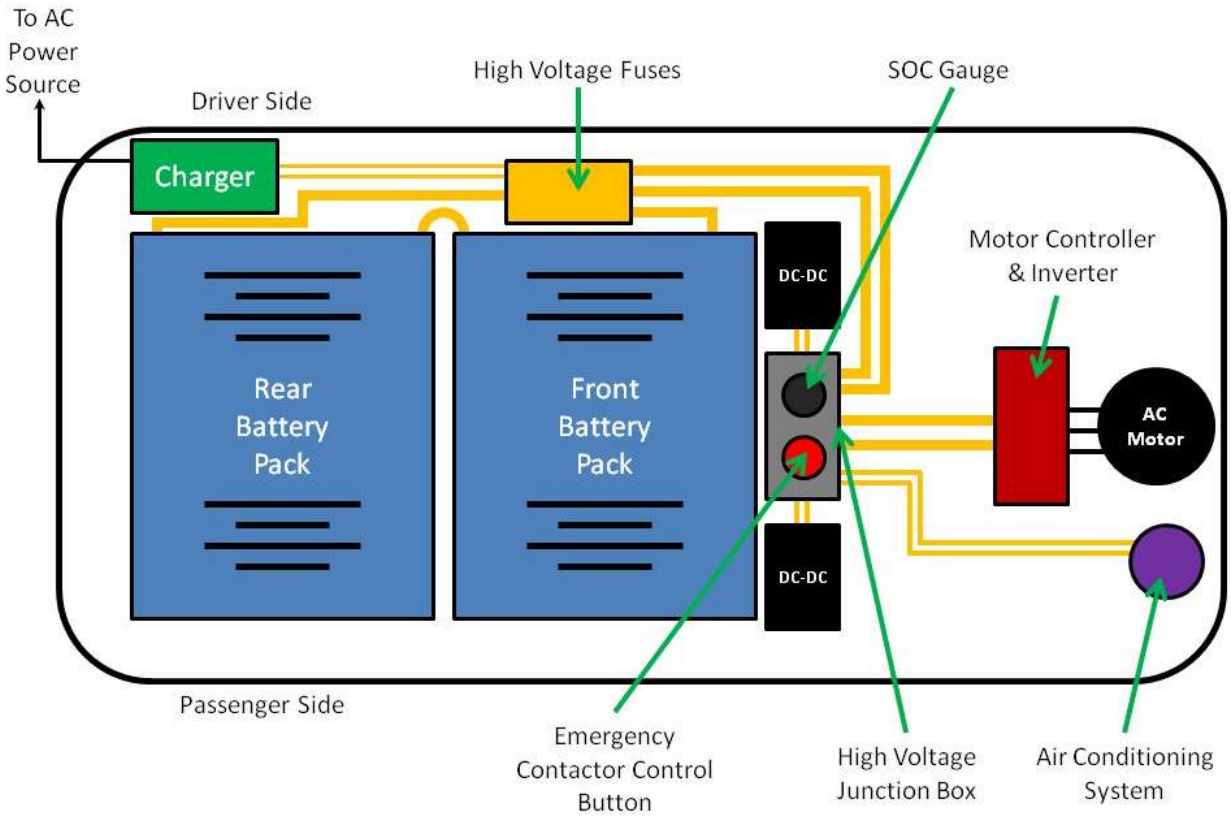

Figure 105: High voltage schematic illustrating all the components on the isolated high voltage circuit.

Figure 106: The HV fuses are located inside the driver's side passenger door.

The HV junction box is located in-between the two front seats of the vehicle. This junction box cannot be accessed unless both seats are fully forward, and the center console has been removed. The center console can be removed by lifting it out of the vehicle. The console was not secured to the vehicle since HV cables are routed underneath the console. The console acts as an additional barrier between the HV circuit and the vehicle operators. The HV junction box (Figure 107) contains two contactors and two junction blocks. The two contactors are located towards the top of the junction box, while the junction blocks are located at the bottom of the box. These junction blocks allow high voltage cables to be fastened together securely. The DC-DC converters, AC controller, and the motor controller all receive HV from this junction point. This area should never be serviced or exposed without first disengaging the main HV contactors. These contactors serve as a HV switch for the vehicle. Exercise extreme caution when servicing this area, and always check that the emergency contactor control button is depressed to disengage the HV system. In addition to switching off the HV contactors, always double check HV sources with a multimeter and take the necessary precautions to avoid the risk of electrical shock. Specific procedures for removing the motor controller from the HV source are outlined earlier in this chapter. The next topic of discussion will focus further on the use of the HV contactor switch.

Figure 107: HV junction box illustrating the two contactors (top) and two junction blocks (bottom).

As previously mentioned, when servicing the HV system in the JimmE-V, it is imperative that the HV be disengaged. This is accomplished through the emergency contactor control button. This button is located on top of the HV junction box in-between the two front seats where either vehicle occupant can access the switch. When the button is in the up position, 12 VDC is supplied to the contactor's control circuit. This results in the contactors engaging and switching on the HV circuit. When depressed (for servicing or in an emergency), the 12 VDC contactor control voltage is cut off disengaging the HV circuit. The different switch positions are shown in Figure 75. The next topic of discussion in maintaining the HV battery pack is replacing bad cells.

A bad battery cell will be indicated by the vehicle's BMS (Section 3.6.2), or by manual measurement with a multimeter. In the event this occurs, the first step is to disengage the HV circuit by depressing the red contactor control button. In addition to disengaging the HV contactors, ensure that no external power sources are present (i.e., unplug the vehicle and power down the battery charger). For further safety, turn the ignition switch to the off position. This ensures that the motor controller will not engage. The DC-DC converters also need to be shut off. This is accomplished through the enable switches outlined in the DC-DC converter section later in this chapter. With all the potential loads disengaged, it is safe to proceed with replacing the bad battery cell. While working around the HV battery packs, HV

isolating rubber gloves should be worn at all times. Additionally, a socket wrench was rubber dipped specifically for working on the JimmE-V battery packs. These tools are shown in Figure 108. Never use a tool that has not been rubber dipped. Failure to heed this warning can result in an electrical short if the tool is dropped in the battery box (of note, this has happened prior). Once the proper tools have been obtained, it is safe to start disconnecting the isolated cell from the battery pack. Begin by removing the battery box cover and set it aside.

Figure 108: HV isolating gloves, and the rubber dipped tool for working on the JimmE-V battery pack.

The batteries in the battery pack are connected in series through bus bars secured with bolts, washers, and lock washers. Figure 109 shows a magnified view of the battery pack showing the terminal bolts, the BMS cell board, and battery cells. Before removing the cell, observe the polarity of the cell to be removed. The red plastic tabs indicate the positive side of the battery. Cell polarity is also stamped in the plastic housing of the cell. When a cell is replaced, the same polarity needs to be maintained in order for the system to function. A positive terminal on one cell should be connected to the negative post on the neighboring cell. Conversely, the negative terminal should only be connected to the neighboring cell's positive terminal. Failure to connect the new cell properly can damage the battery, BMS, or harm the individual servicing the battery pack.

In order to remove a battery cell, the negative terminal bolt should be removed first. When this bolt is removed, the attached cell board will also be removed. To prevent the BMS cell board from damage, wrap the terminal with electrical tape. The next step is to remove the positive terminal bolt. Similar to the negative post, there is a terminal ring on the positive post. This terminal ring should also be covered with electrical tape to prevent electrical shorts. With both terminal bolts removed, the cell is almost ready to remove. Since the bus bars overlap each cell, the bus bars on the neighboring cells need to be removed to allow the bad cell to be removed. Remove the desired terminal bolts, and cover the BMS terminal rings with electrical tape. The last step to be completed before removing the battery cell is to uninstall the locking bars that affect the particular cell. Cells in the middle of the pack require four locking bars to be removed, while cells on the edges only require two bars to be removed. Once the desired locking bars have been removed, the cell can be removed.

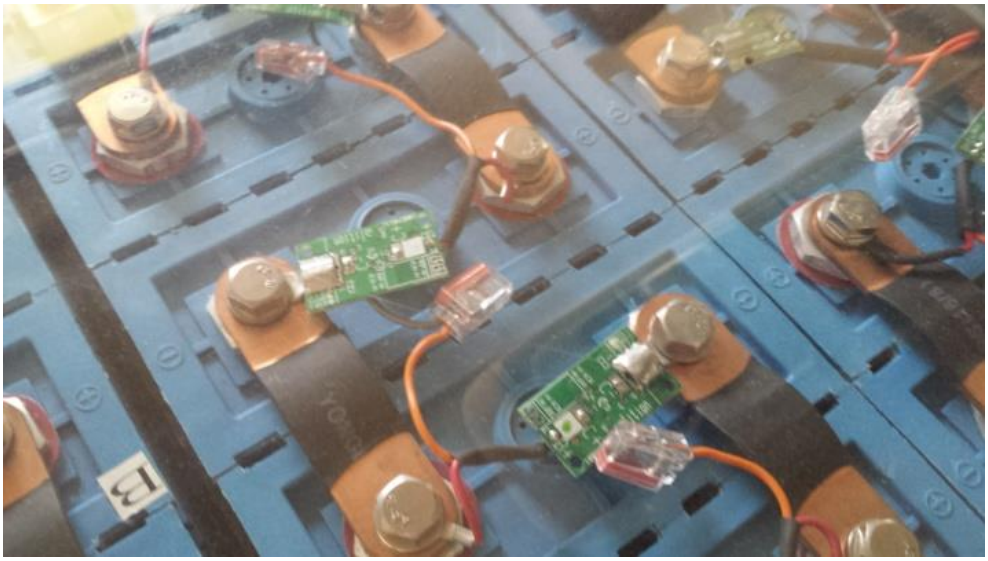

Figure 109: The JimmE-V battery pack consists of cells connected in series with bus bars, bolts, washers, and lock washers.

Upon inspection, the batteries appear to be difficult to remove; however, cells can be removed by threading the terminal bolts back into the cell. Do not entirely thread the bolts back into the cell. Approximately, a quarter to half the way is sufficient. Threading the bolts back into the cell allow the technician to grip each bolt and lift the cell vertically out of the pack. The new cell can now be installed

and simply be lowered into place, or bolts can be inserted into the terminals to lower the cell the same way the old one was removed. Once the replacement cell is installed with the proper polarity, the bus bars and BMS ring terminals can be re-installed. Ensure that the cell board ring terminal is installed on the negative terminal. If a cell board is installed on the positive terminal, the cell board will be damaged and need replacement (see Section 3.6.2). The remaining terminal ring should be installed on the positive battery post. Tighten the bus bars securely, but do not over tighten the bolts. The allowable torque on the battery terminals is 20 N-m (14.75 ft-lbs) [35].

With the new cell installed in the battery pack, re-install the locking bars and battery box cover. To verify that the new cell is functioning, the HV contactor should needs to be engaged by pulling up on the contactor control button. In addition to replacing bad battery cells, it is important that the JimmE-V battery pack be properly maintained.

Maintaining the JimmE-V battery pack is accomplished through the vehicle's BMS. The JimmE-V should be plugged in with the battery charger on. Since the BMS controls pack charging, the BMS can allow or disable charging when desired. This ensures that the cells stay charged and balanced. Failure to plug-in the vehicle after use or in periods of not being used can result in battery back depletion or damage. In the event the charging environment is cold, an external heating mat can be placed over the batteries to keep them warm. The JimmE-V BMS has been mentioned previously throughout this chapter, and it is the next component in the vehicle to discuss.

3.6.2 JimmE-V Battery Management System

An EV's BMS is a crucial component for controlling and regulating the battery pack during charging and discharging events. Further discussion on BMS theory of operation can be found in Chapter 2 of this thesis. The goal of this section is to focus on the operation and maintenance of the Elithion Lithiumate Pro BMS unit installed in the JimmE-V.

The Elithion BMS operates similarly to the Orion BMS discussed in Chapter 2; however, the Elithion BMS does not utilize cell taps to monitor the battery cells. In the application of the JimmE-V, the

Lithiumate BMS uses cell boards installed above each cell, as seen in Figure 110, to monitor and balance each cell locally. This results in a smaller BMS unit, but operation of the JimmE-V has shown that these cell boards are susceptible to wear and tear from vehicle vibrations. It is not uncommon for the BMS to cease communication with different banks in the battery pack. These communication issues are generally resolved by checking the cell board communication wiring. This issue is discussed later in this section. In order to understand how the BMS monitors the battery pack, the BMS wiring and pack distribution will be discussed.

Figure 110: The BMS cell boards are installed between the positive (right) and negative terminal (left) of each cell.

In order to monitor the JimmE-V battery pack, the Lithiumate BMS breaks down the battery pack into smaller banks of batteries. As mentioned in Section 3.6.1, the JimmE-V has 104 cells installed in series equally divided between two battery boxes. The BMS further breaks each box into an array of four rows of 13 cells (i.e., 4 × 13). Thus, the total pack is an array of eight by thirteen (i.e., 8 × 13). Each one of the eight rows in the battery pack represents a bank of batteries that the BMS controls. However, the bank numbering in the BMS graphic user interface (GUI) begins at zero. As a result, the BMS communicates with banks zero through seven. The row closest to the front of the JimmE-V corresponds to Bank 0, while the row closest to the rear of the vehicle corresponds to ‘Bank 7’. Furthermore, each cell

is assigned a number within each bank. Figure 111 illustrates the BMS bank numbering while also showing how the cells in the battery packs are numbered. The lowest number in each bank represents the most negative cell, while the highest number indicates the most positive cell in the bank. The battery pack positive and negative terminals are located at cells 103 and 0 respectively. While the BMS does not identify individual cells with issues, knowing the bank number or the cell numbers will aid in troubleshooting issues with the battery pack. In order to further understand how the BMS monitors the JimmE-V battery packs, the system wiring will be discussed next.

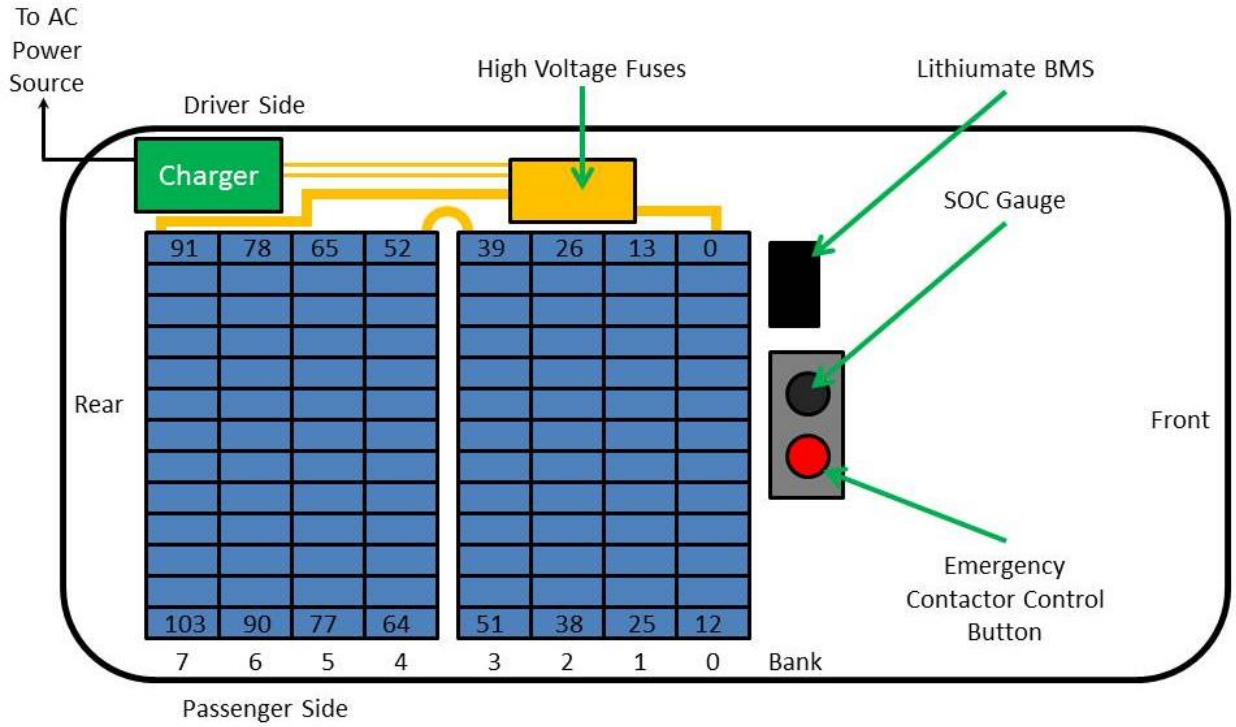

Figure 111: Schematic showing the BMS location, and the cell and bank numbering used for the BMS in relation to other components in the JimmE-V.

The BMS wiring is composed of three sensing and control areas: the current sensor, cell boards, and the BMS control pins. The current sensor for the Elithion BMS is a Hall effect sensor that is installed in the front battery pack. The sensor is installed in-between cell one and two with a bus bar running through the center of the sensor. The JimmE-V current sensor is shown in Figure 112. In the event this sensor ceases to respond and display data via the BMS graphic user interface (GUI), replace the current sensor with a cable mounted sensor from Elithion (part number: 2CS0400K). The maximum current for

the motor and controller is 250 A; however, to ensure that any excessive current situations can be monitored, the current sensor is capable of reading current up to 400 A. When servicing the external current sensor, ensure that all HV safety precautions are utilized (see Sections 3.2 and 3.6.1). The current sensor wiring simply unplugs from the sensor. When re-connecting the wiring, ensure that the black wire is connected to the top pin of the current sensor. The next topic of discussion will be the cell board wiring.

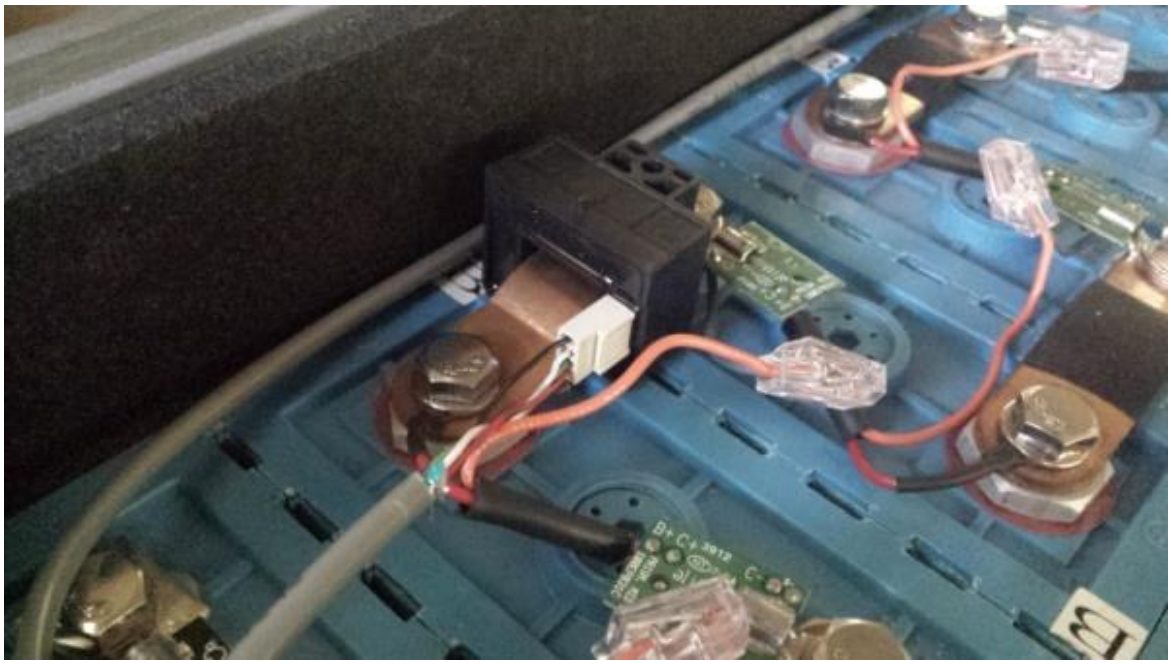

Figure 112: The BMS Hall effect sensor is installed in-between cells one and two.

The cell boards are the crucial component for the Elithion BMS. Each of the 104 cells in the JimmE-V has a corresponding cell board that monitors the cell voltage, resistance, and temperature. These measurements are then relayed back to the BMS controller where minimum, average, and maximum values are presented to the vehicle operator. Each battery bank is composed of three different types of cell boards: negative, positive, and middle cell boards. The negative cell board (part number: 106N/1PR0106N) are installed on the cell with the lowest potential (i.e., most negative cell in the bank). Similarly, the positive cell board (part number: 106P/1PR0106P) is installed on the most positive cell in the bank. The middle cell boards (part number: 106M/1PR0106M) are installed in-between the positive and negative cell boards in each bank. The cell boards are connected using molex socket connectors, as

shown in Figure 113. These connectors are only used once. As a result, if a cell board is replaced, new connectors will need to be installed surrounding the effected cell board. The connectors and cell boards can be ordered by contacting Elithion. Additionally, each bank has a wiring harness that connects the cell boards with the BMS. In the event cell boards need to be replaced (discussed later in this section), make sure that all connection wires are stripped prior to the cell board installation. This eliminates the use of metal wire stripers over the HV battery pack. In addition to properly wiring the cell boards, the controller wiring ensures that the BMS can control the load and source power. The Lithiumate Pro BMS wiring will be discussed next.

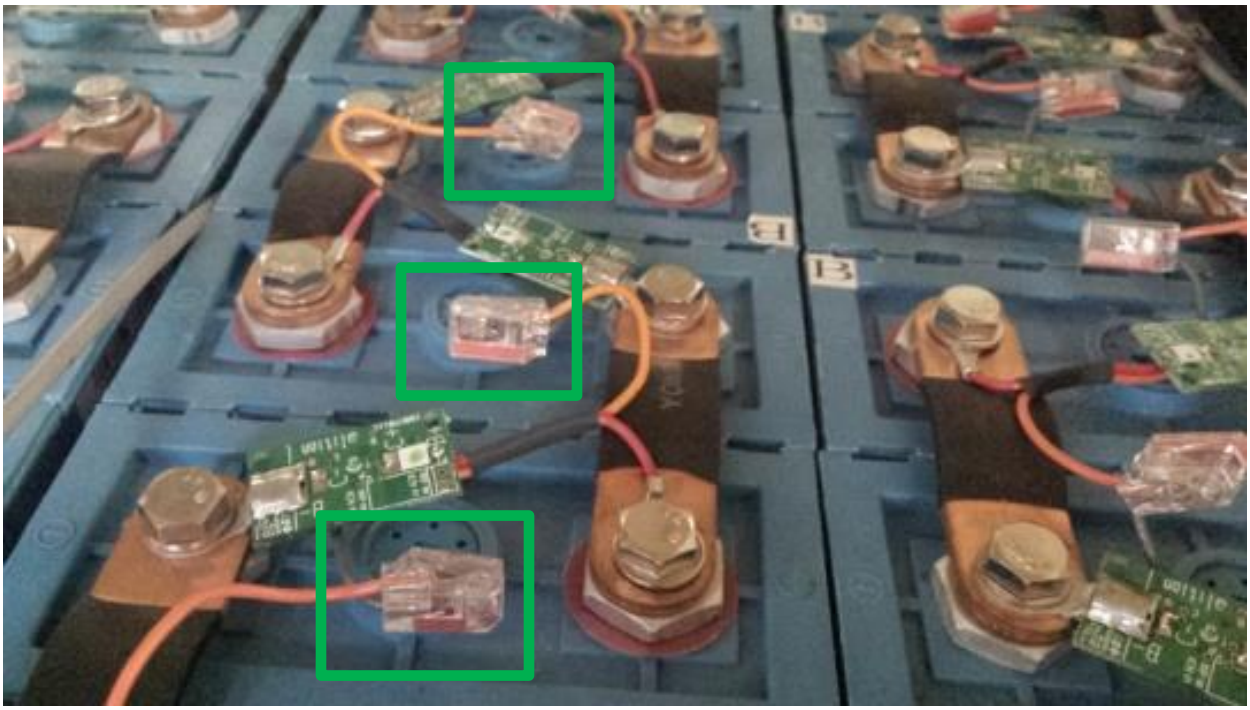

Figure 113: The cell boards in each bank are connected using the molex connectors.

The Elithion BMS controller is located behind the driver's seat in the JimmE-V. The BMS controller has four main areas; the battery bank wiring, the BMS control pin wiring, the external current sensor wiring, and the RS-232 connection. As previously mentioned in this section, the BMS monitors the battery pack in the JimmE-V by breaking the HV pack into smaller banks. Each bank has a wiring harness to connect the cell boards to the BMS. Figure 114 shows the different wiring areas for the BMS controller. The battery bank wiring is on the top side of the controller, and the JimmE-V uses banks zero

through seven. Occasionally, the BMS will report that it cannot communicate with a battery bank. This error can be resolved by checking the bank connection at the BMS. If this does not correct the error, a bad cell board may be present. The procedure for testing cell boards is discussed later in this section. In addition to the battery bank wiring, the external current sensor has its own connection on the BMS controller. In the event current measurements are not being displayed; double check the wiring before proceeding to replace the current sensor. The BMS controls the load and source power through the control pins. These pins ensure that the high and low voltage limits of the battery pack are not exceeded.

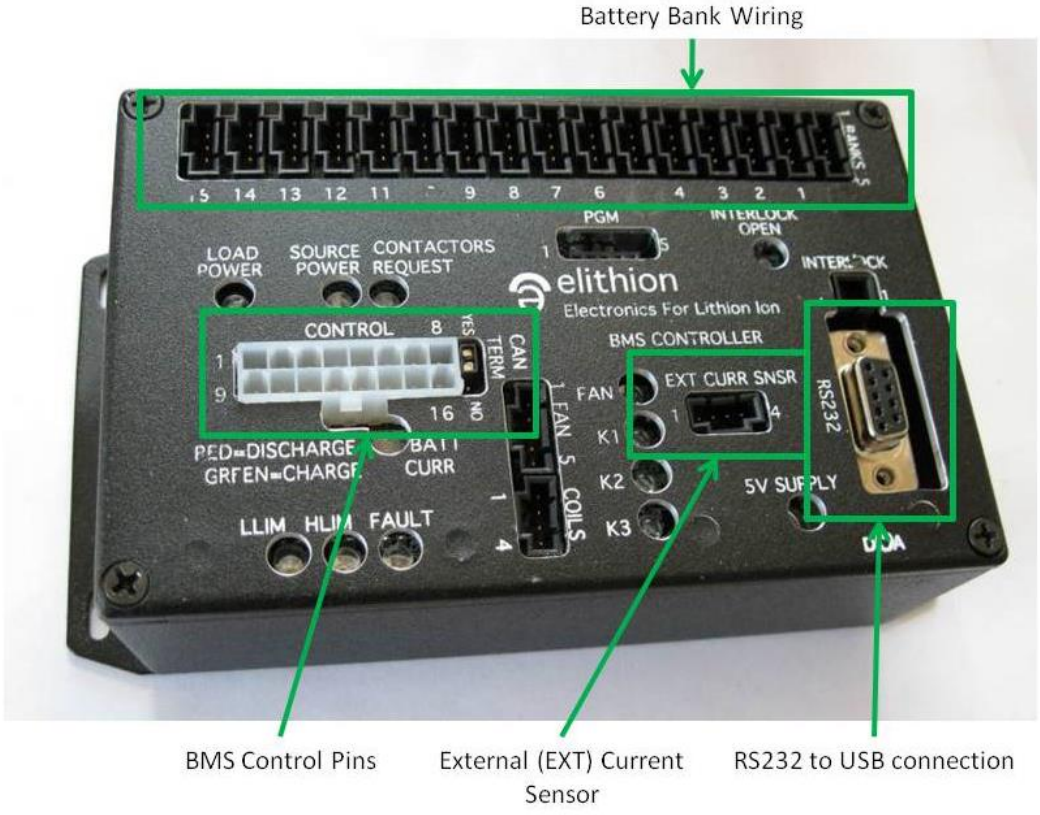

Figure 114: BMS controller wiring connections [36].

The Elithion Lithiumate BMS has an extensive user manual available online. In order to understand how the BMS functions in the JimmE-V, only the used control pins will be discussed. The occupied control pins are presented in Table 6, and an image of the wiring in the JimmE-V is shown in Figure 115. Pin 1 corresponds to the pin on the top left, while Pin 8 corresponds to the top right pin. The lower rows of pins are for pins nine through sixteen.

Table 6: BMS Control Pins [37].

Pin #:	Function:
1	Signal Ground (GND)
2	Full voltage utility supply (12 VDC out)
3	Power in from load (12 VDC)
4	Power in from source
8	CAN Bus low (CANL)
9	Power common
10	Low limit (LLIM)
11	High limit (HLIM)
16	CAN Bus high (CANH)

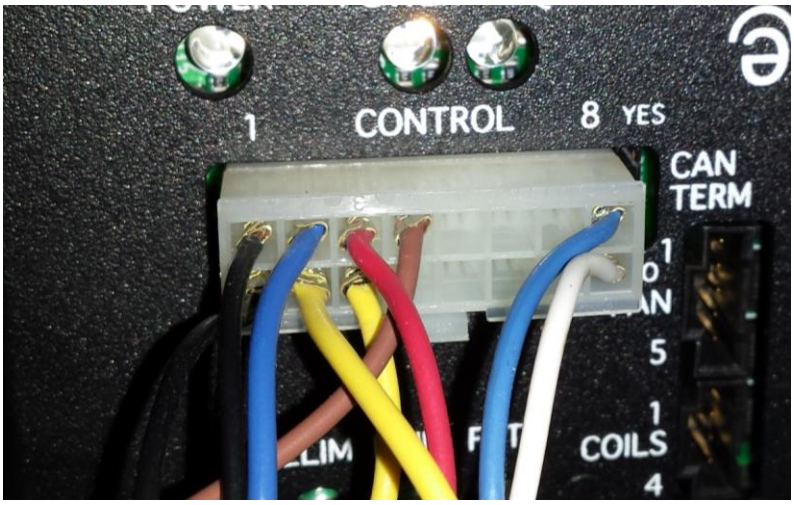

Figure 115: The control pin wiring for the JimmE-V BMS.

The two black wires at Pins 1 and 9 correspond to ground connections. Pin 2 represents a 12 VDC output from the BMS. This allows 12 VDC to be supplied to various relays that are controlled by the BMS, or any additional circuitry that needs to be supplied with 12 VDC. As indicated by the red wire, Pin 3 supplies the BMS with 12 VDC to operate the BMS. This wire comes directly from the battery and is protected by the main 12 VDC fuse. The BMS receives power when the ignition switch is on, or when the vehicle is plugged into a power source, which is discussed in the following section. Pin 4 (brown wire) is what powers the BMS when the source (i.e., plug-in) power is present. The limit connections on Pins 10 and 11 (both yellow wires) are responsible for controlling the motor and load power. The high limit prevents the battery pack from being overcharged. When the battery pack is fully charged, this

prevents regenerative braking from further charging the battery pack. The low limit is the converse of the high limit control. Once the low limit of the battery pack is reached, this control pin ensures that the drive function of the motor controller is disabled. This prevents the batteries from being over-discharged; however, this disables the vehicle until the batteries are charged. Figure 116 shows that the high and low limits are controlled using an opto-isolator. A larger view of this schematic is available in Figure 192 in the Appendix. An opto-isolator is an electronic part that transfers electric signals with light waves to provide electrical isolation between the input and output. These isolators allow the two systems to be electrically isolated.

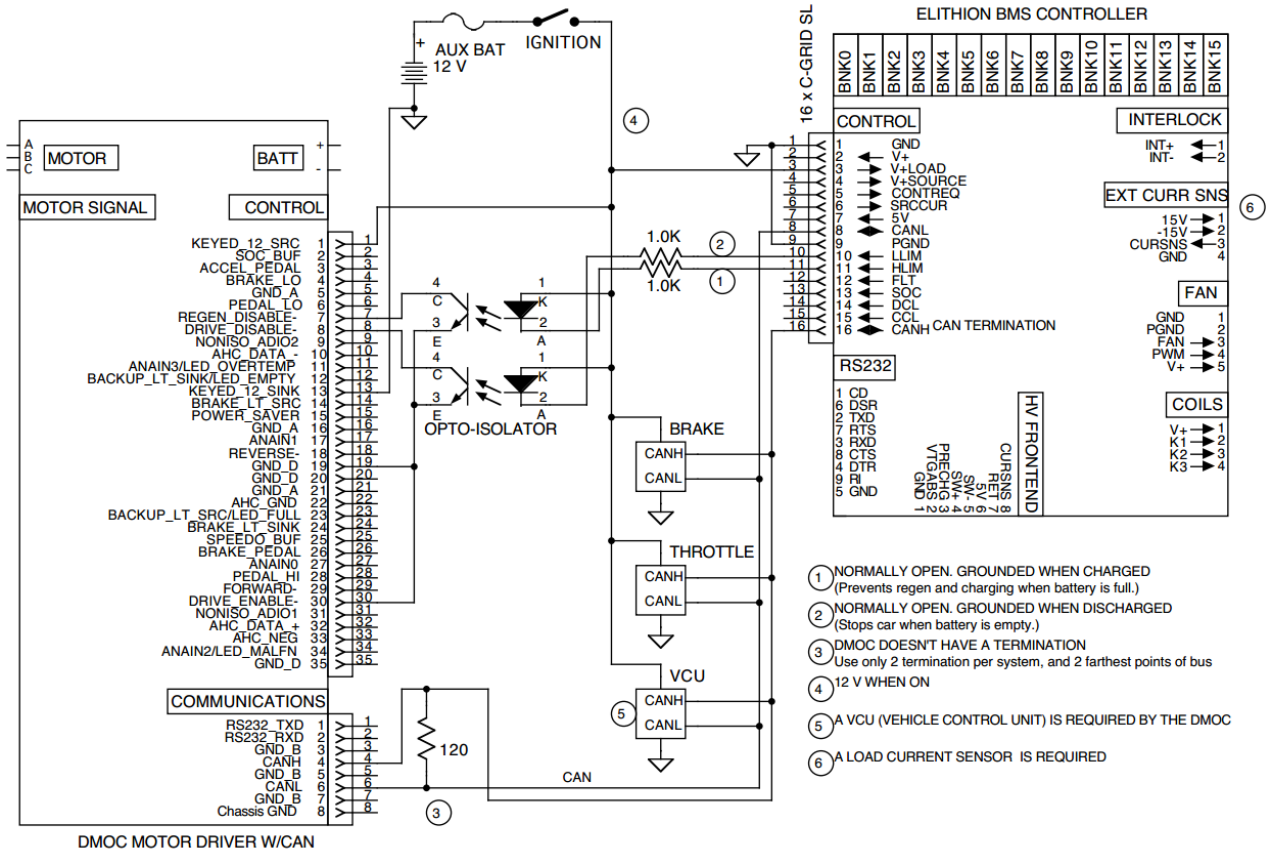

Figure 116: DMOC445 schematic showing how the BMS interfaces with the motor controller to control the high and low limits [38].

The opto-isolators in the BMS circuit control the regenerative braking disable and drive disable pins on the motor controller. The high limit is normally open, and is grounded when the battery pack is

charged. This prevents regenerative braking when the pack is full. Similarly, the low limit pin is also normally open. The low limit pin is grounded when discharged, and stops the vehicle when the batteries are low to prevent the controller from over-discharging the batteries. Figure 116, additionally shows that the drive enable pin on the DMOC is permanently wired to the digital ground pin. However, in the JimmE-V, there is a drive enable relay controlled by the New Eagle ECU (Section 3.5.3). When the drive enable circuit is completed, the DMOC's internal contactors engage. However, it should be noted that the drive disable pin has priority over the drive enable pin. As a result, when both pins are activated, the drive function will be disabled. The final control pin connections to discuss are the CAN bus options for the BMS.

The schematic shown in Figure 116 also shows that the CAN bus lines are connected to the DMOC. However, these connections are not present in the JimmE-V because the BMS was occupying network bandwidth and transmitting errors that were not relevant to the system. Additionally, the brake, throttle, and VCU parts of the schematic are all accomplished through the New Eagle ECU. The CAN bus wiring for the BMS is simply unplugged from the main vehicle network that allows for later expansion if desired. The BMS does utilize the CAN bus connections to display SOC to the vehicle operators. Along with being connected to the 12 VDC key power, the SOC gauge is wired to the CAN bus connections on the BMS controller (Pins 8 and 16). The SOC gauge is shown in Figure 117. The gauge is located above the HV junction box adjacent to the HV contactor control button. Along with showing the battery pack's current SOC, the gauge indicates when there are faults or warnings present with the BMS. If a fault or warning is present, the BMS GUI should be examined to resolve the issue. Navigating the BMS GUI is discussed later in this section. The SOC gauge will also indicate when load and source power is present. Load power refers to the key ignition switch, while source power indicates the vehicle is plugged into an outlet for charging. The most common fault is the plug and drive fault that occurs when both load and source power are present. This fault will not prevent operation and can easily be cleared using the BMS utility. The final connection to the BMS controller in Figure 114 to discuss is the RS-232 communication connection.

Figure 117: The SOC gauge displays the current SOC along with displaying additional faults and warnings when present. The source power light indicates when the vehicle is plugged into an electrical outlet.

The RS-232 connection allows the user to connect the BMS to a computer to monitor data and errors in real time. In addition to monitoring the batteries in real time, the RS-232 connection can be used in conjunction with a computer to log battery pack data and calibrate the BMS. The connection is made by correctly inserting the RS-232 plug into the BMS controller (Figure 118). When the BMS utility is in use, do not disconnect either end of the RS-232 to USB connection. In the event that the RS-232 to USB cord needs to be replaced, the model used is the ATEN UC-232A. With the BMS connections discussed, the next area of discussion will be using the RS-232 connection to interface with the BMS using a computer.

Figure 118: The ATEN RS-232 to USB connection on the BMS controller.

Before operating the BMS software utility, the RS-232 to USB cord needs to be connected to a computer. In order to ensure proper operation, a laptop was set up with all the necessary programs to

access, calibrate, and take data from the Elithion BMS controller. As previously mentioned, this laptop is additionally used to connect to the DMOC and ECU. The RS-232 to USB cord is connected to the COM 8 port on the laptop. The BMS utility automatically scans all available COM ports; however, some of the other software utilities do not. As a result, it is best to use the predestinated COM ports specified in this Chapter.

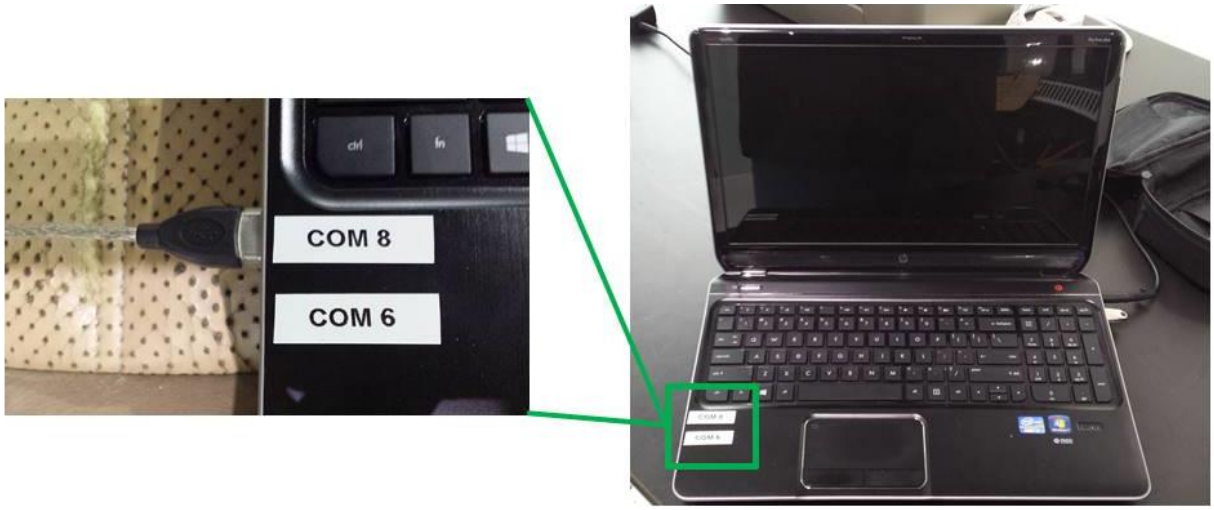

Figure 119: JimmE-V laptop with the BMS plugged into COM port 8.

The BMS can be connected to the laptop regardless if the laptop is on or off. However, it is important that the BMS utility not be opened until the BMS is connected to the computer. With the BMS connected to COM port 8, the Elithion BMS utility can be opened from the start menu, or the shortcuts present on the desktop screen (Figure 120). Once the BMS utility is opened, it is important to understand how to navigate the program to ensure that the BMS is operating correctly and that the user can properly monitor and record data from the battery pack. When the BMS utility is opened, the screenshot shown in Figure 121 will be displayed. This tab is one of three tabs the user can use to monitor the battery pack. The meter tab is convenient to use while driving the JimmE-V due to its large easy to read gauges. The battery pack SOC is displayed as a percent value, the current pack amperage is displayed (positive for discharging, negative for charging), and the current pack voltage is displayed. In addition to these gauges, there is a kilowatt hour (kWh) meter that can be used to monitor the total energy used during a trip. Just below the meter is a trip reset button. Before driving the JimmE-V, reset the meter to zero to ensure the

drive cycle power consumption is properly recorded. Conversely, this meter can monitor vehicle charging to record the power input. Once the drive cycle power consumption has been noted, the trip meter can be reset and the BMS will monitor the power consumption from the electrical source. Lastly, the bottom of the GUI displays when the load and source powers are present, and provides icons to notify the operators when there are any warnings for faults present. In the event of a fault, switch from the meters tab to the status tab (still under the main monitor tab). The status tab (Figure 122) shows more detailed battery pack data such as cell voltage, temperature, and resistance (minimum, average, and maximum). The status tab is also useful in determining faults, which will be discussed later in this section. The remaining tab in the monitor section of the BMS GUI is the graph tab.

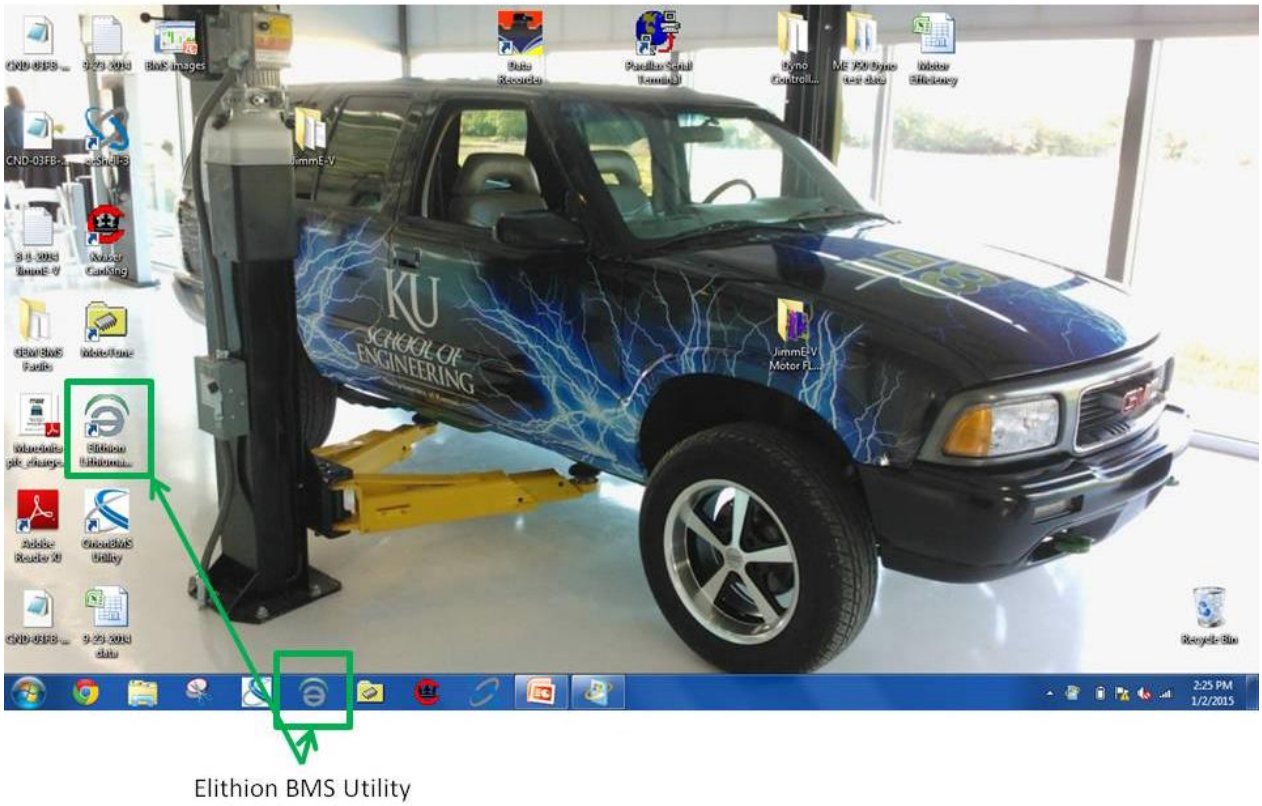

Figure 120: JimmE-V laptop desktop screen showing the Elithion BMS utility shortcuts.

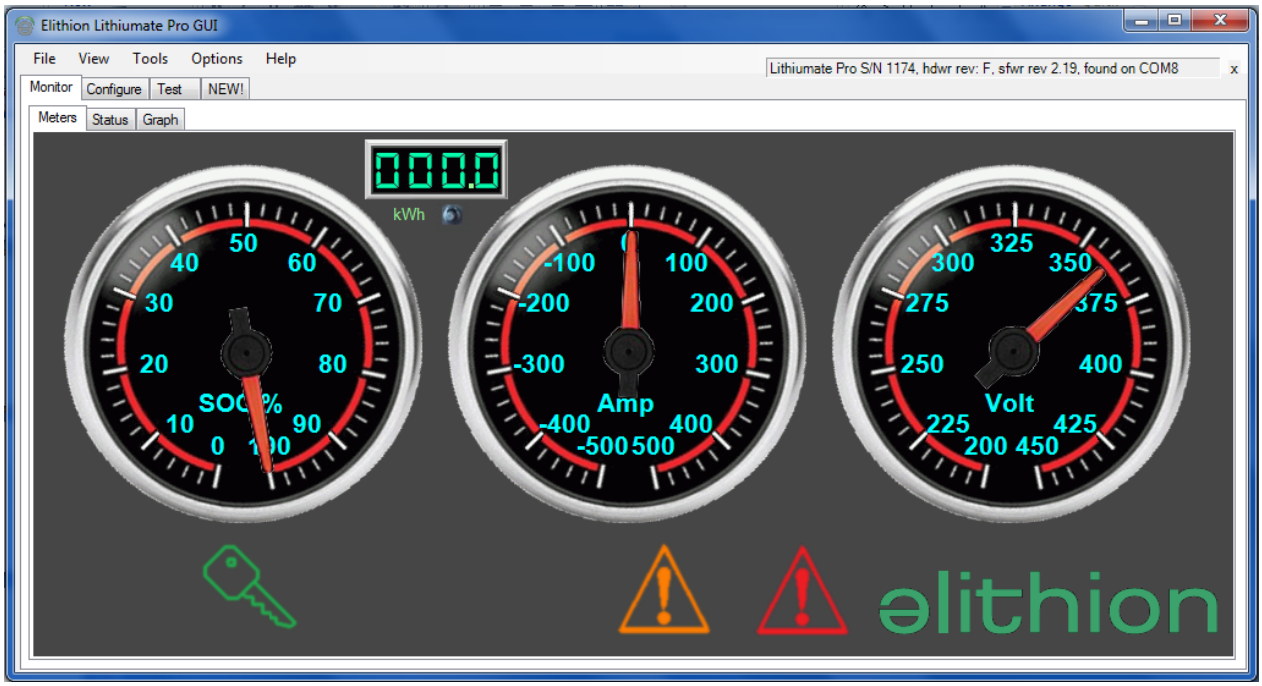

Figure 121: The main screen of the BMS GUI. In this screenshot, load power is present along with a warning and a fault.

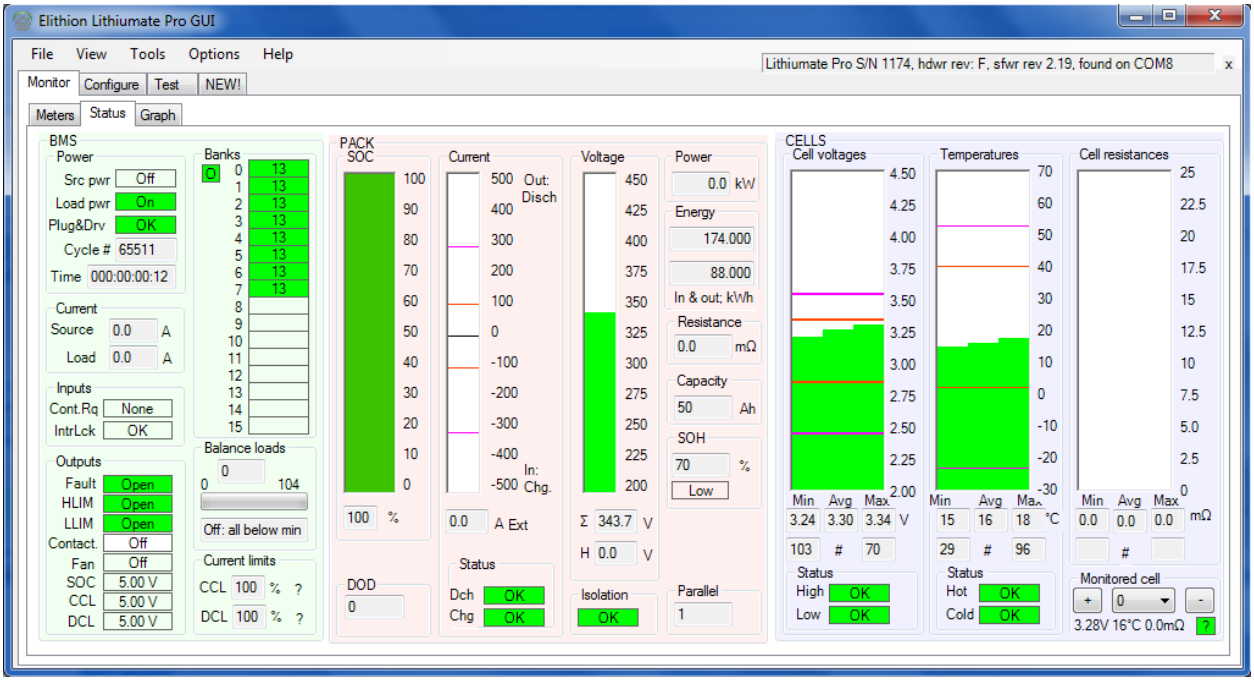

Figure 122: The BMS GUI status tab without errors present. The status tab can be used to see battery pack information in greater detail than the meters tab.

The graph tab is the main tab to select parameters to data log. This tab additionally shows a histogram of the desired parameters. The graph parameters can be selected above the graph area as shown in Figure 123. When data logging is desired, the data capture section below the graph should be utilized. This part of the GUI allows the user to set the desired output file, the data capture rate, and allows the user to start or pause the data recording. During normal operation of the JimmE-V, these are the main tabs of the GUI to be utilized by the operators. The remaining tabs in the BMS utility software are for setting up and testing the BMS to ensure that it is functioning properly. In the event the battery pack is altered in any way, some of the main calibration tabs should be changed as discussed next. The original JimmE-V complete configure tab information for the BMS utility can be found in the Appendix (Figure 194 - Figure 200) of this thesis.

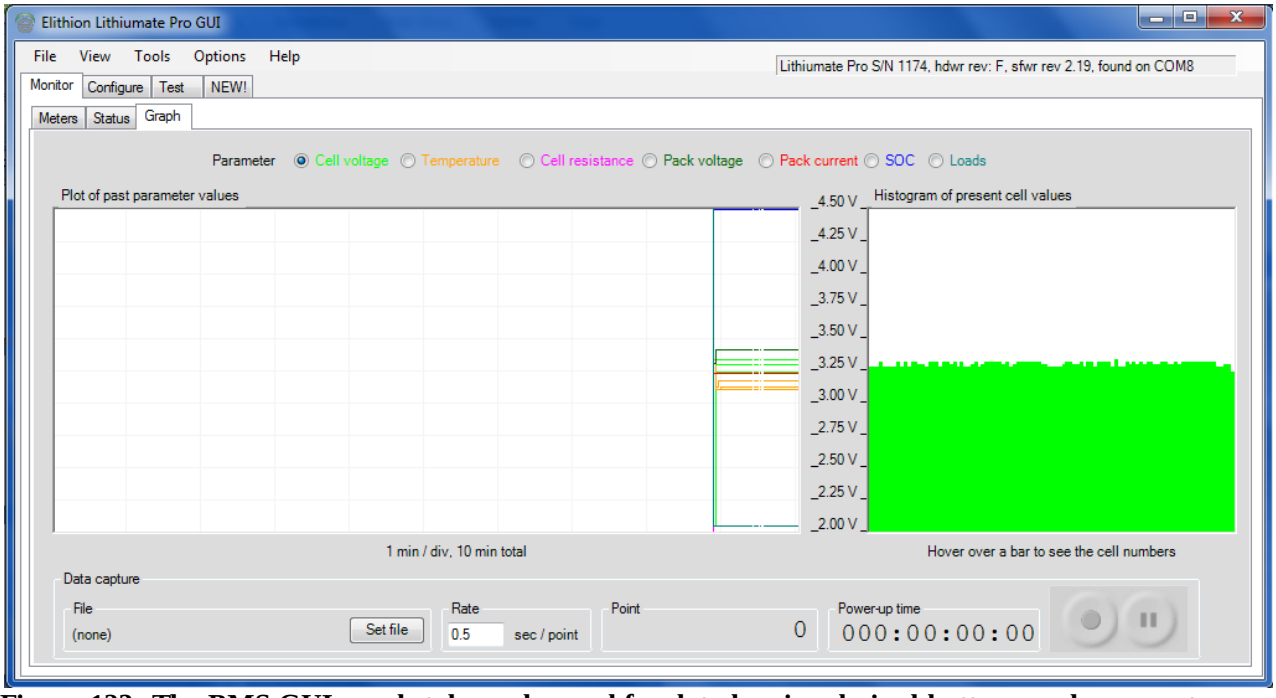

Figure 123: The BMS GUI graph tab can be used for data logging desired battery pack parameters.

The configure tab in the BMS GUI is used for setting up the cell specifications. The tabs within the configure tab allow the user to set up a BMS profile based on the cell specifications (Table 5). Figure 124 shows the first tab under the configuration tab. On the basic tab, the user selects the battery chemistry and capacity. One important aspect of the configure tab is the explanation of the options available in the

bottom right corner of the GUI. To explain these options further, Figure 125 shows an enlarged view of the BMS configuration options. These configuration options allow the user to read, write, load, or save BMS profile options. The read from BMS option loads the currently programmed BMS profile to the GUI. This feature is useful to ensure that the currently displayed profile matches what is programmed in the BMS controller. In the event any modifications are made to any of the configure tabs, the modified profile needs to be written to the BMS by selecting the write to BMS option. Saving the BMS profile allows the parameters to opened or transferred to additional BMS units, or to back up the most recent BMS configuration. In the event the profile is modified, the load option can be selected to restore the profile to previous versions. In the event the entire system needs to be reset, Elithion also provides a factory default option. Always make sure that the most recent profile has been saved before restoring the BMS to its factory defaults. Lastly, there is a password option that can be selected to secure the BMS profile settings. This option has not been previously used because driving the JimmE-V and using the vehicle's laptop already require approval. The laptop is password protected, but if it is desired to password protect the BMS, the lock can be selected to set a password on the BMS. Similarly, for some of the options shown in the GUI, these options are also available in the file, view, tools, and options menus above the tab section of the GUI. A help tab is additionally provided that directs the user to the online user manual to provide further assistance. To illustrate how Table 5 was used to program the BMS, the cell voltage tab will briefly discussed.

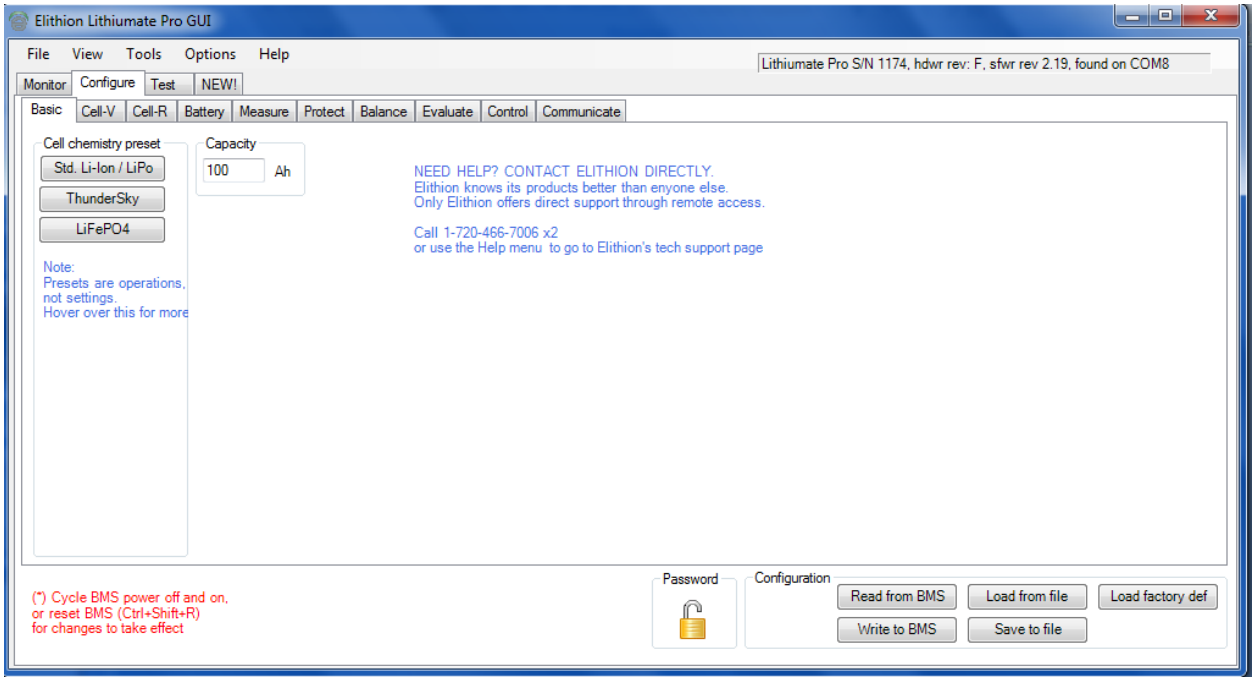

Figure 124: The configuration tab is used to program the BMS with the cell specifications.

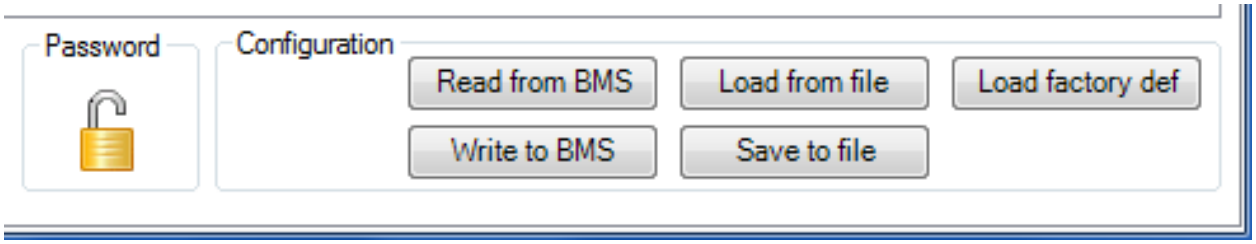

Figure 125: BMS configuration options available for the user to select.

The cell voltage (Cell-V) tab is used to program the cell voltage specifications (Table 5) into the BMS to ensure that the controller can properly measure and control the battery pack. Figure 126 shows the cell discharge profile and settings for the CALB 100 Ah cells used in the JimmE-V. In addition to setting the cell voltage, the SOC limits are additionally set in this tab. Once the BMS has been programmed and set up using the cell specifications, the GUI provides a test page to allow operators to test the controller to ensure it acts according to how it was programmed.

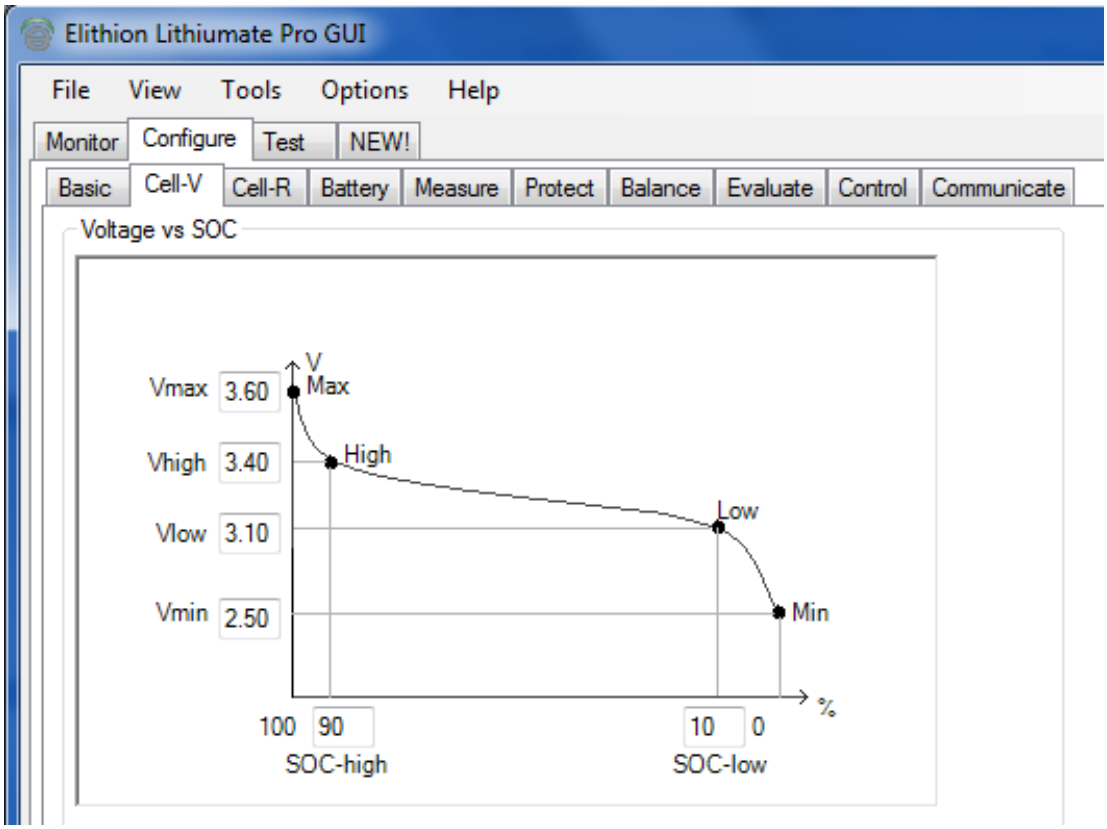

Figure 126: The Cell-V tab is used to program the cell voltage parameters in the BMS.

The test tab (Figure 127) should only be used when the vehicle is stationary. The test tab allows the user to individually (or simultaneously) select the enforcement of the control limits. For example, while the vehicle is charging, the user can select to enforce the high limit control. If properly set up, the HLIM relay should switch and prevent the battery pack from being charged. Similarly, the LLIM can be closed to prevent the controller from operating the motor. The last option is the fault switch. The BMS is currently set up such that when a fault occurs HLIM, and LLIM are turned off preventing vehicle operation. This option can be changed in the protect configure tab. However, due to the high voltage safety risk, it is advised that any BMS faults be diagnosed and corrected before proceeding to drive the vehicle to ensure that the operator's safety is not compromised. The fan option is not used in the JimmE-V application. Once BMS testing is complete, it is important that the restore automatic control button (bottom left of Figure 127) be selected to return control to the BMS. The final BMS topic to discuss is how to determine and diagnose faults in the BMS.

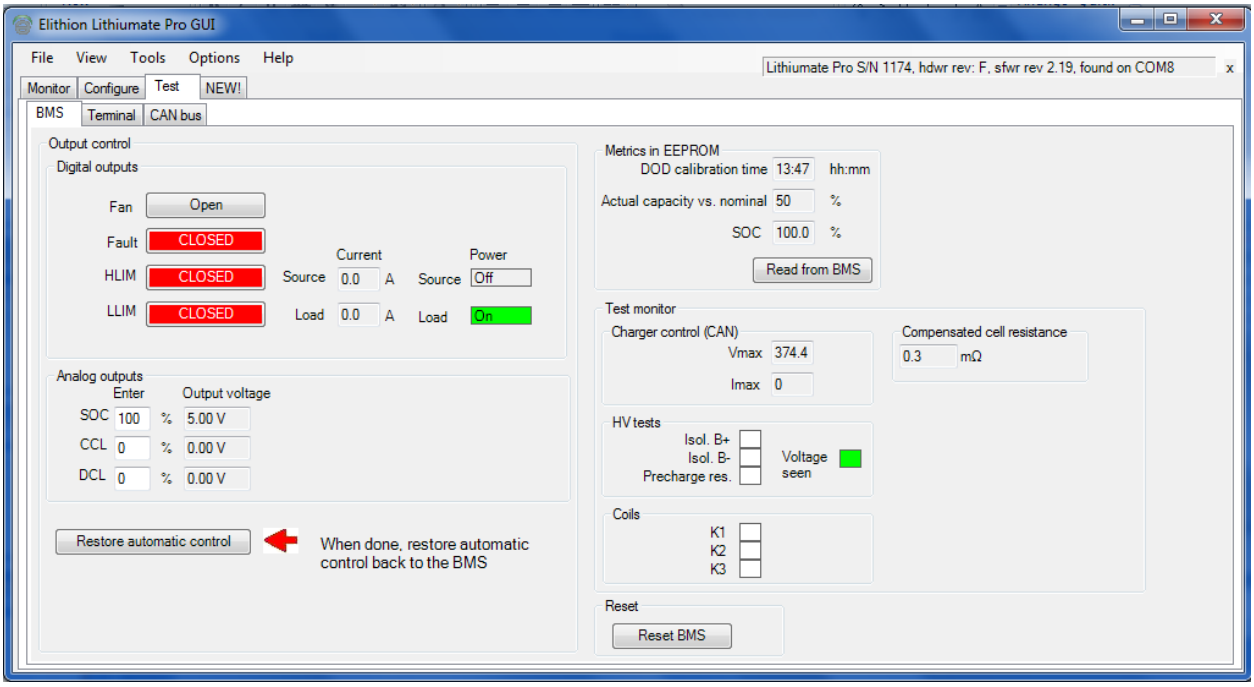

Figure 127: The BMS test tab allows the current profile configuration to be tested to ensure it responds correctly.

Throughout normal vehicle operation, the Elithion BMS has proved to be troublesome for the JimmE-V application. The cell board wiring connections can be unreliable at times due to vehicle and road vibrations. The most common fault that occurs with the Lithiumate BMS is a non-responsive battery bank. When this fault occurs, the BMS is not communicating with the total expected number of cells. This error can be due to poor wire connection, faulty cell board, or a defective battery cell. However, being able to interface with the BMS through a computer aids the user in pinpointing and fixing the issue. Figure 128 shows what the BMS GUI looks like when a fault is present while viewing the status tab. Figure 129 shows how faults are indicated while viewing the meters tab. A red exclamation mark indicates a fault, while the orange exclamation mark indicates a warning (i.e., cell with low or high voltage). When a fault occurs, the status tab of the GUI provides the most feedback to the operator to assist in pinpointing and repairing the issue.

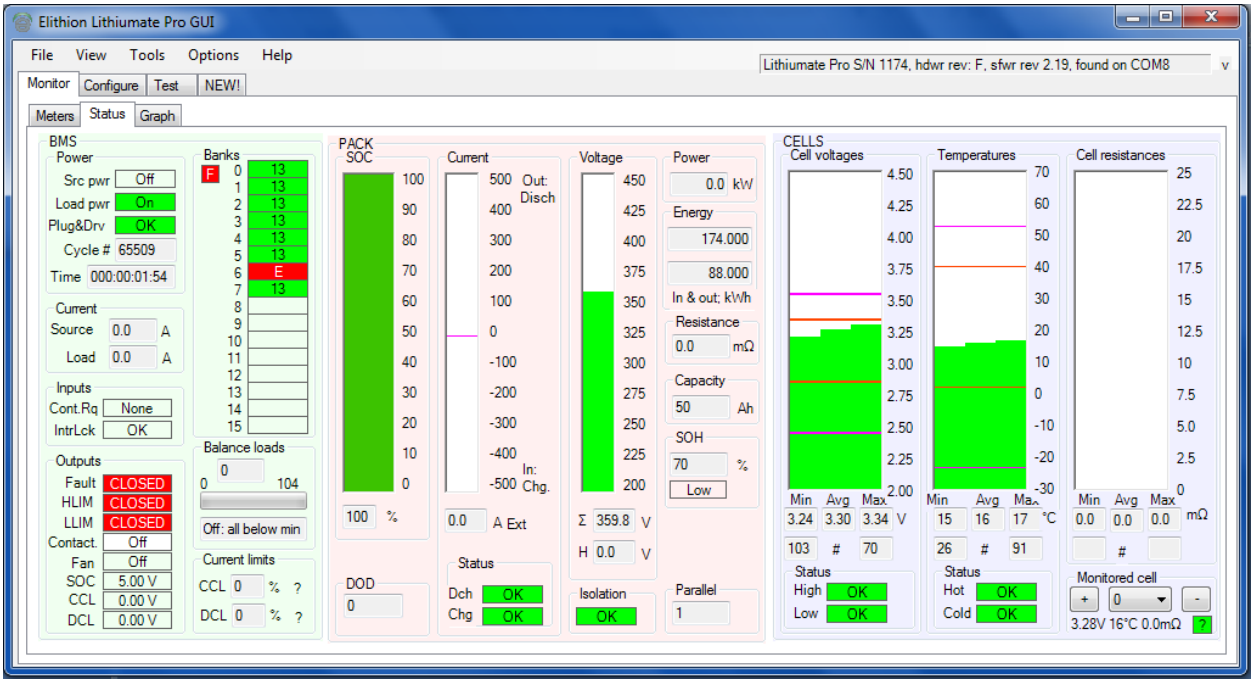

Figure 128: The BMS GUI with a fault condition present.

Figure 129: While viewing the meters tab, a fault is indicated by a red exclamation mark. The orange exclamation mark indicates a warning is present.

When a fault is present in the BMS, the fault output will be closed and change color from green to red (Figure 130). As previously mentioned, when a fault is present, the controller outputs close preventing vehicle operation. The next step is to determine what caused the fault. From Figure 130, it is observed that a red "F" is present in the square next to the battery banks. This indicates a communications fault with the battery banks. When the mouse is placed above the box, the GUI provides feedback to further indicate the cause of the fault (Figure 130). When further examining the state of the battery bank communication, it is observed that bank six now has changed color from green to red. The number 13 that is displayed in the box reflects the number of cells communicating with the BMS. The expected number 13 is now displaying an "E" showing the operator that bank six is in an error state (Figure 131).

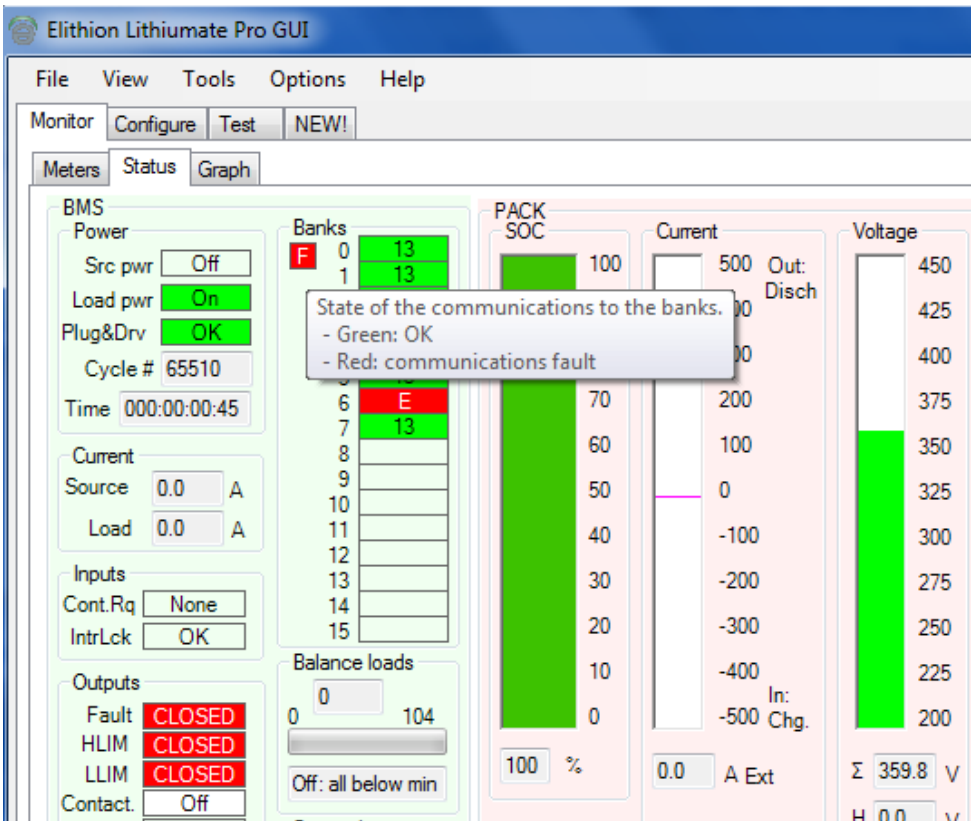

Figure 130: When a fault is present, the fault output changes from opened (green) to closed (red).

When the mouse is placed above the effected battery bank (see Figure 131) the GUI displays the bank number, the bank's cell numbers, bank connection status, the expected number of cells in the bank, and an error code. The error code can be custom programmed depending on how the BMS is interfaced with other systems to prevent duplicate errors. Elithion provides a spreadsheet online with all the error code information. In this instance, the 255 code reflects a bank communication error. Battery banks not responding is a common error, and is likely the result of the wiring at the BMS controller. Unplug the effected bank from the BMS controller, plug the bank back in, and then clear the fault. Faults can be cleared two ways: Ctrl + Shift + K, or by cycling power to the BMS (i.e., key ignition). If the bank is not responding, double check the wire connections to the cell boards on either side of the battery bank. If that does not resolve the issue, use a multimeter to measure the cell voltage of the batteries in the bank. However, the BMS typically indicates when one cell in a bank is not communicating, or has no voltage (i.e., the GUI would reflect an error and only show 12 cells reporting). Another cause can be from a loose bus bar. Use rubber gloves and the dipped socket wrench to double check that all the bus bars are secure.

If a bus bar has become loose, the cell board could possibly be damaged. The next topic to discuss in the BMS section is how to determine if a cell board is damaged and needs to be replaced.

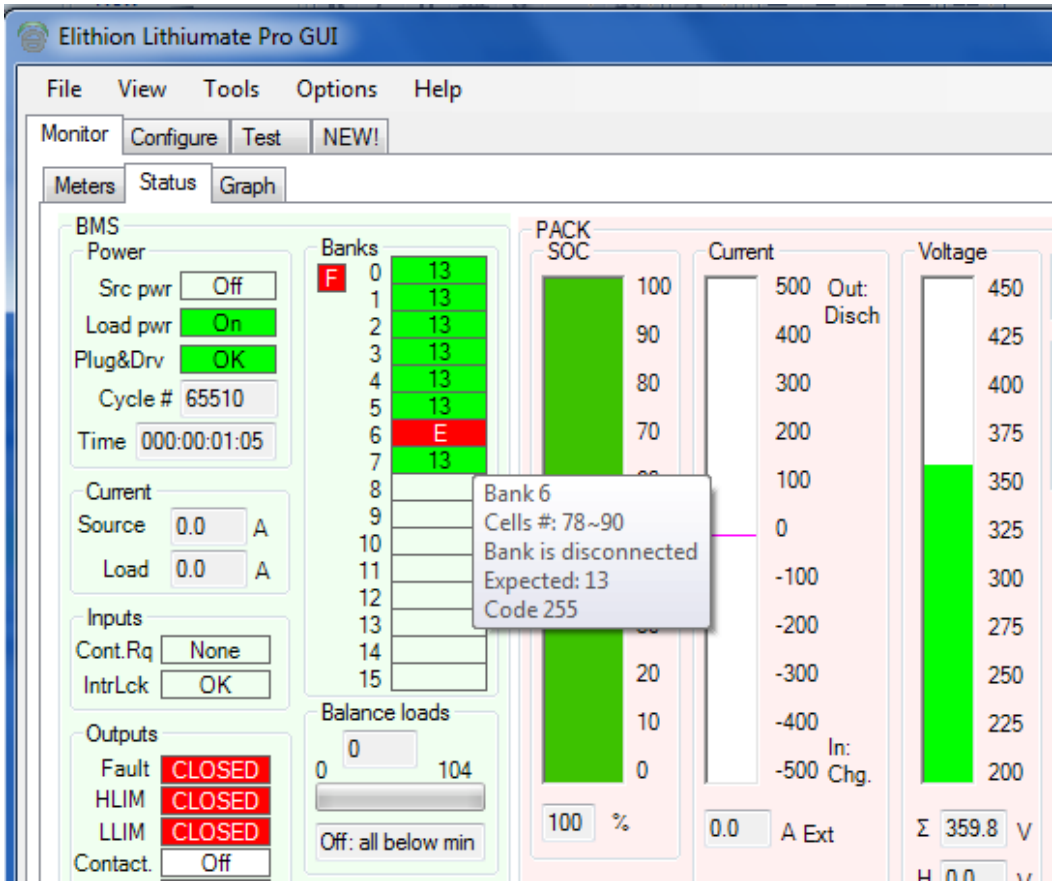

Figure 131: When the mouse is placed above the effected bank, the GUI shows additional information to assist the user in correcting the fault condition.

In order to test a cell board to determine if it has been damaged, the cell board and accompanying battery need to be removed from the battery pack. Detailed battery removal instructions are provided in Section 3.6.1 of this Chapter. It is imperative that all HV precautions be followed while working on the JimmE-V HV system. Ensure the key is in the off position, depress the emergency contactor control switch to shut off the vehicle's HV, remove the battery box cover, uninstall the effected cell board and bus bars to remove the cell, remove the locking bars from the battery box, and then remove the cell.

With the cell board and battery removed from the HV battery pack, the cell board can now be tested to determine if it has been damaged. Testing is performed with a multimeter installed in series with the cell board. In order to ensure that the meter is functioning, the internal fuse should be checked before

testing. If a fuse is blown, the multimeter will not measure any current and display all zeros. Checking the internal fuse is accomplished by placing the multimeter probe in the voltage input terminal. Switch the meter on to measure resistance. If the meter displays ‘OL’ (open loop) the internal fuse needs to be replaced. If the resistance measures less than 0.5 Ω the fuse is good. The multimeter can also be switched to measure circuit continuity with the probe in the voltage input terminal. Insert the probe into the current input terminal, if the circuit is complete (indicating a good fuse), an audible noise will be emitted from the multimeter. A bad fuse will not emit a sound from the meter and display ‘OL’ on the display. Figure 132 displays how to check the multimeter’s internal fuse.

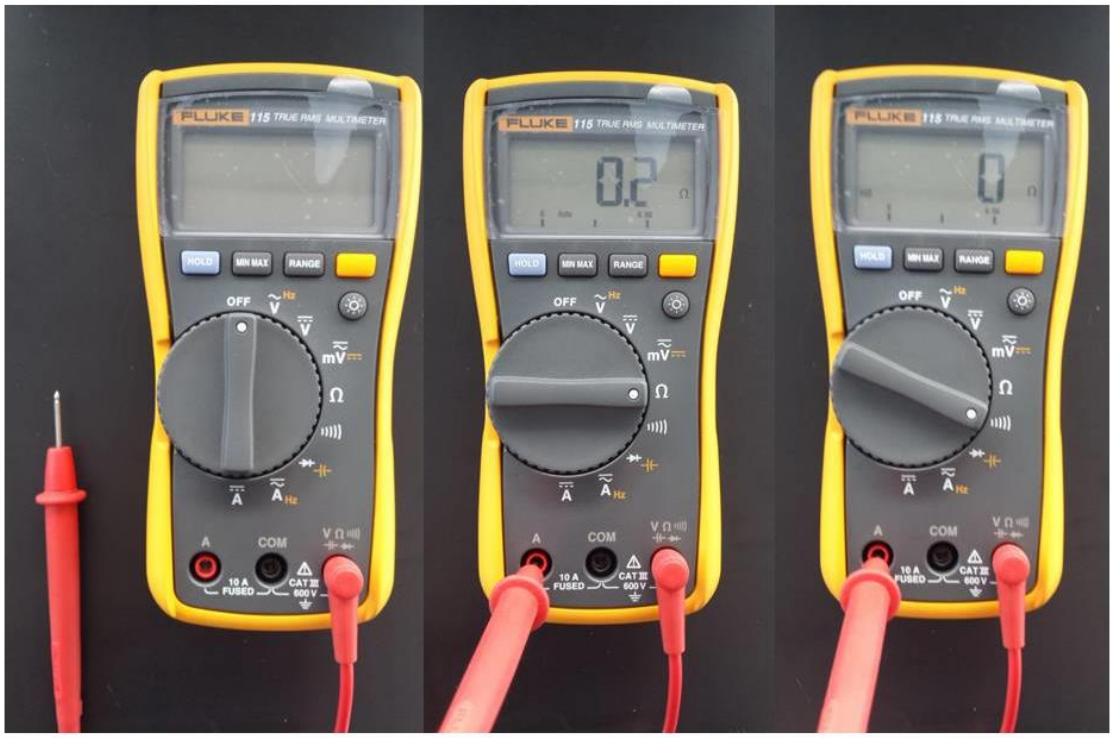

Figure 132: The multimeter fuse can be checked using the resistance or continuity options.

Before testing a cell board, prepare the multimeter to measure DC current. Figure 133 shows the multimeter probe's setup to measure current. To measure DC current, the dial needs to be rotated 180 degrees. When the cell board is removed, the accompanying battery can be removed and used to test the cell board. However, if the cell has no voltage, a different battery will need to be used. Before installing the multimeter in series, the cell board orientation will be discussed.

Figure 133: To measure current, ensure the probes are inserted into the current input terminal before rotating the dial to the indicated position.

Figure 134 shows one of the Elithion BMS cell boards. Before testing a cell board, it is important to note the orientation of the cell board. Reversing the cell board's polarity can result in damaging the cell board. The negative side of the cell board has the negative terminal directly soldered to the cell board. The red wire indicates the cell board's positive side with the terminal ring attached to the cell board.

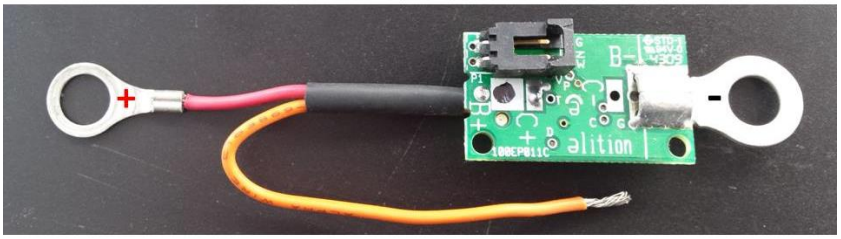

Figure 134: Elithion BMS cell board polarity.

To test the cell board, the negative probe on the multimeter needs to be attached to the battery's negative terminal. The positive multimeter probe needs to be connected to the negative terminal on the cell board. The remaining connection to complete is connecting the positive end of the cell board to the cell's positive terminal. Figure 135 shows the completed testing circuit. Once the circuit is completed, an LED will flash on the cell board. Once the LED has finished blinking, the multimeter should read 0.000 A. This indicates that the cell board is not damaged. If the multimeter displays a non-zero current measurement after the LED has stopped flashing, the cell board is damaged and should be replaced. This concludes the operation and maintenance topics for the JimmE-V BMS system. The next section is related to the vehicle's battery charger.

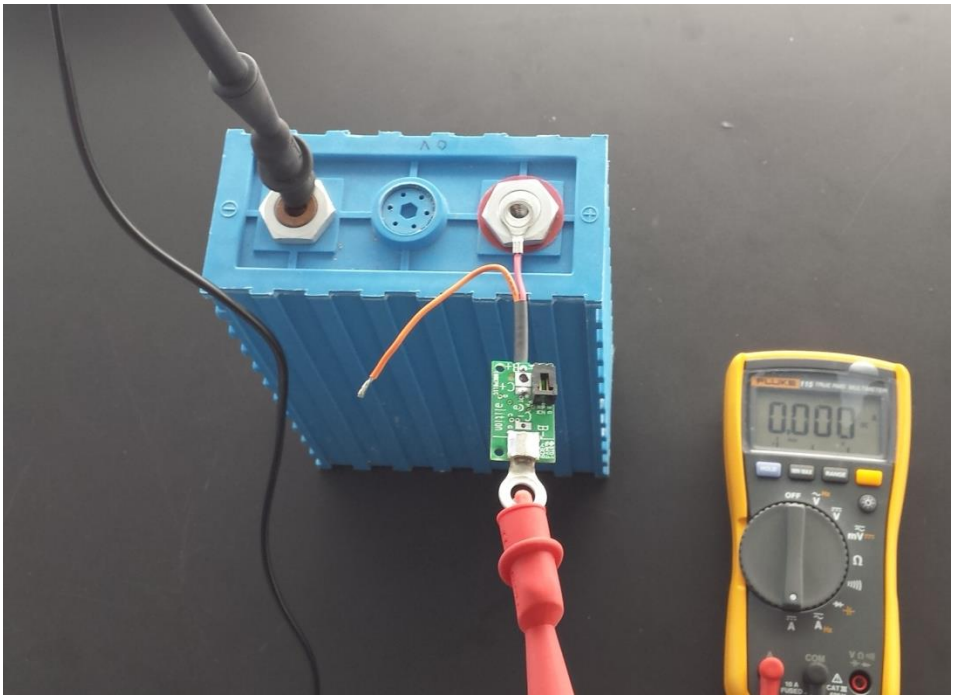

Figure 135: The completed cell board testing circuit.

3.6.3 Manzanita Micro PFC Battery Charger

Since the JimmE-V is a purely electric vehicle, an electrical source is needed to recharge the battery pack. The electrical source needs to be an Alternating Current (AC) source which can be achieved through grid tied solar panels, generators, or the electrical grid. However, AC power cannot directly charge a DC source. The battery charger in the JimmE-V transforms the AC power into usable DC power to charge the battery pack.

The selected battery charger was the Manzanita Micro PFC-20 battery charger. The PFC-20 charger is a powerful and efficient battery charger that can operate on input voltages ranging from 100 to 240 VAC, and can output 12 to 450 VDC. Further charger specifications are provided in Table 7. Additionally, the PFC-20 charger is Power Factor Corrected. Power factor correction is achieved through circuitry within the charger that ensures that voltage and current are drawn in unity. This results in the apparent power, measured in Volt-amps, almost equaling the real power, measured in Watts. The ratio of apparent power to real power equals the power factor. Power factor is expressed as a number between zero and one and a value closer to one indicates that less energy is being wasted [39].

Table 7: Manzanita Micro PFC 20 Charger specifications [39].

Input voltage range	100-250 VAC
Line frequency	40-80 Hz
Output voltage range	12-450 VDC
Input current range	0.2-20 Amps AC
Standard output	0-20 Amps DC
Standby current	0.2 Amps DC
Input protection	30 Amp 240 VAC breaker
Output protection	30 Amp 450 VDC clip mount fuse
Charge algorithm	Constant current then constant voltage

Before using the battery charger, it is important to understand the controls and features of the Manzanita PFC-20 charger to ensure proper operation. Along with reviewing the information presented in this document, the Manzanita Micro PFC manual should be reviewed additionally to ensure proper operation of the battery charger. The battery charger is accessible through the rear door on the JimmE-V.

The charger is installed above the driver's side wheel well adjacent to the rear battery pack. The charger can be installed in any orientation as long as there is adequate airflow to cool the charger. In the event the charger exceeds designed temperatures, the charger enters a thermal cutback mode to prevent damage to the charger. Figure 136 shows the PFC-20 operating panel. This panel is where all charger operations occur. The AC power input is located on the left side of the charger. The protected hole in the center functions as a hot air exhaust. The air intake is on the opposite side of the charger and is accompanied by two cooling fans. The circuit breaker on the right side of the charger is the main power on or off switch. The charger model and serial number are located below the Manzanita company information. In the event the sticker should become lost, the charger model and serial number, respectively, are PCF20 442. Lastly, along the top of the charger are the controls for the battery charger. Figure 137 shows a detailed layout of the controls for the battery charger.

Figure 136: Manzanita Micro PFC-20 charger operating panel

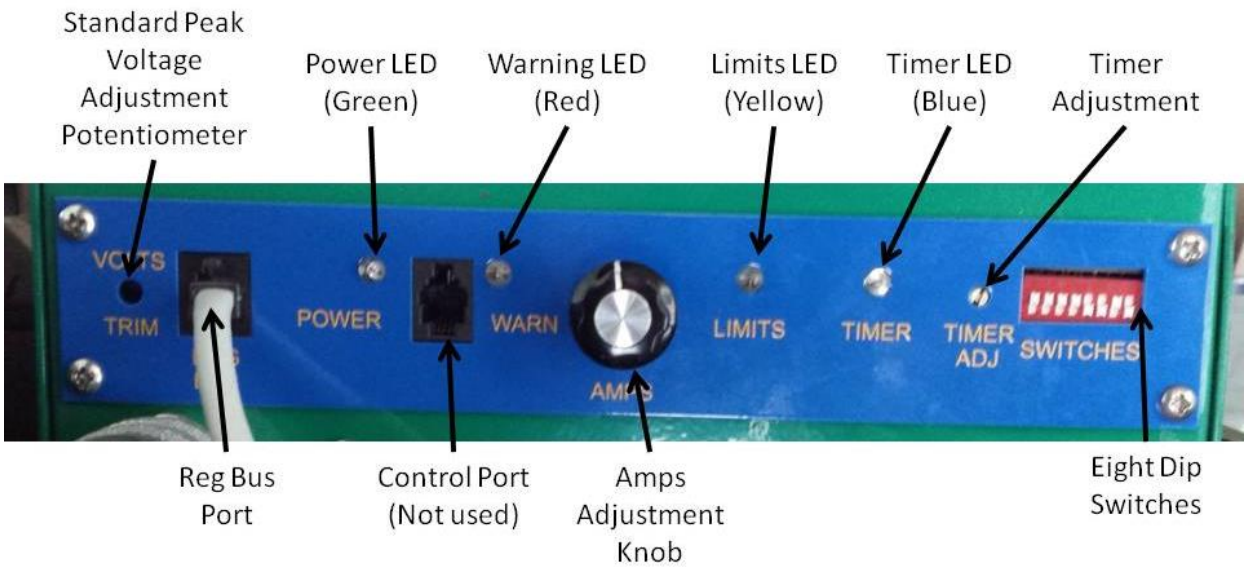

Figure 137: Charger controls layout.

On the left side of the control panel in Figure 137 is the "Standard Peak Voltage Adjustment Potentiometer". This potentiometer controls the peak DC voltage limit that the charger will allow the battery pack to reach before limiting the charging current. Trimming the potentiometer clockwise increases the voltage limit, while counter clockwise decreases the limit. Continuing to the right of the voltage adjustment is the "Reg Bus Port". The Reg Bus connection is a six-pin jack that is used to plug BMS communication into the charger. The Reg Bus wiring is discussed later in this section. Next, the Power LED is illuminated green when the power switch is in the 'ON' position while additionally indicating that input power is being supplied. If the switch is on but the vehicle is not plugged in, the LED light will not be lit. In this application, the "Control Port" is not used. If desired, the control port can be used for remote amperage control or J1772 control. J1772 refers to the Society of Automotive Engineers (SAE) standard for charging electric and hybrid vehicles. This charging standard is discussed later in this section. Adjacent to the optional control port is a red "Warn," or warning, LED. This LED blinks briefly when the charger is first powered on, and then the LED remains off during the charging process. In the event this LED remains on, immediately turn the "AMPS" knob all the way counter clockwise to the off or zero current position. Turn off the power switch to the charger and consult with Manzanita Micro or a qualified technician [39].

In the center of the control panel, there is an “AMPS” knob. This knob allows the user to control the amount of charging current entering the battery pack. This knob does not need adjusting as long as the vehicle is plugged into the same circuit. Setting the charging current higher than the electrical circuit will open a circuit breaker or fuse on the AC line into the charger, subsequently preventing battery charging. The user can adjust this knob in order to specify the charging current for the battery pack. To the right of the AMPS knob is the yellow “Limits” LED. This LED indicates that the charger has reached the peak voltage limit. This only happens at the end of the charge cycle once all of the batteries are fully charged. The Limits LED should be accompanied with the blue “Timer” LED. The blue Timer LED should be blinking that indicates the charger is in current cutback mode and the timer is counting down to the end of pack charging. If the yellow Limits LED is blinking, the charger is indicating that there is an over temperature condition and the charger is in thermal cutback mode [39]. The remaining two features are the “Timer Adjustment” (i.e., Timer ADJ) and the “Dip Switches.”

The Timer ADJ is a small 16 position rotary switch that allows the user to adjust the amount of time that the charger takes in constant voltage mode while the charger cuts current back at the end of the charging cycle. If the timer adjustment is in the ‘0’ position, the three o-clock position when viewed from the front, the timer will time out instantly. This position should not be used. Each additional tick after the ‘0’ position will add ten minutes to the charge cutback time. Turning the switch all the way clockwise provides the maximum amount of cutback time before the charger shuts down. For the JimmE-V, the maximum amount of cutback time setting is used. The last feature on the battery charger is the eight “Dip Switches” in Figure 138.

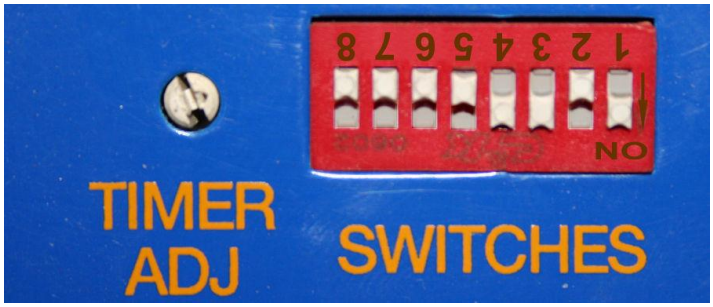

Figure 138: Magnified image of the timer adjustment and dip switches on the battery charger.

The red and white dip switches are located on the upper right end of the battery charger. The dip switch module contains eight switches; the switches are numbered from one to eight, with the number one switch being on the far right. It is important to understand how these switches function, because improper set up may cause undesirable charger performance. Switches in the down position represent an 'ON' position. Under no circumstances should the forth dip switch be adjusted. That switch must remain in the 'ON' position at all times. Manzanita specifies that the forth switch is for a future feature and must always remain on. The first dip switch (switch #1) engages the timer at the peak voltage limit set point. This switch should be 'ON,' and if the pack voltage drops below the peak voltage limit, the timer will turn back off. The second dip switch starts the timer as soon as the charger is turned on. This switch can be used for timed charging; however, the switch is currently in the 'OFF' position. The third dip switch starts the timer based on the Reg bus commands. This switch should be in the 'ON' position. In the event the Reg bus signal stops, the timer will turn off. The forth switch was previously discussed and should always remain in the 'ON' position. The fifth position is an additional future low battery detection feature, and should remain in the 'OFF' position. The sixth dip switch is primarily for the use of Absorbed Glass Mat (AGM) batteries. This switch is not applicable to the initial JimmE-V battery pack, and as a result, this switch is 'OFF.' The seventh switch bypasses the use of the timer and stops providing power when the high voltage limit is reached. This is not a desirable feature for the lithium battery pack, and the switch is in the 'OFF' position. The final dip switch is for an auto restart function. With this enabled, the charger is allowed to restart charging the battery pack when the pack reaches the low voltage set point. Manzanita recommends that this switch remain 'OFF' unless using the auto restart feature that is set behind the faceplate of the charger. The auto restart feature was not desirable in the JimmE-V. However, further information regarding this function can be viewed in the Manzanita PFC Charger Manual [39]. The battery charger has been properly set up for the initial $LiFePO_4$ battery pack. In the event the battery pack composition should change, or battery cells are added or deleted, the charger will have to be set up again based on the adjustments made.

Final battery charger tuning is best accomplished when the battery pack is fully charged. If the current SOC is low, the user will need to monitor and adjust the charger during the initial charge cycle. When tuning the voltage trim, ensure that an electrical isolating regular screwdriver be used to adjust the potentiometer. The first step in tuning the charger is to turn the amps knob all the way down (counterclockwise until it stops). With the amps knob turned down, make sure that the charger is plugged into the battery pack and that there are no open circuit breakers or fuses in the DC battery circuit. Ensure that the battery charger power switch is off before plugging in the AC power source. Once the charger is plugged in, turn on the charger. The cooling fans should turn on if operating properly. The final step requires the voltage trim potentiometer (pot) to be adjusted until the threshold where the yellow limits LED changes state. If the yellow LED is off, turn the trim pot counterclockwise until the LED turns on. If the yellow limits LED is on, turn the pot clockwise until it goes off. Once the threshold has been found, the cutoff voltage is set to the actual battery voltage and the charger will not charge the pack above this voltage. Once ready to charge, the pot will need to be turned clockwise to raise the voltage ceiling to allow charging. The last set to charge the batteries is to adjust the amps knob until the desired amount of current is being used. It is important to follow the battery specifications as to not exceed voltage and current limits. Failure to do so can result in damage to the charger, batteries, or the user. Current can be viewed using a multimeter with a high current clamp, referred to as an Amp Clamp (Figure 139), or through the BMS utility tool on a laptop computer as discussed in the previous section of this document.

Figure 139: Fluke multimeter for measuring high current.

In order for the BMS to function while the battery charger is on, an AC relay, referred to as an ice cube relay, is used to cycle 12 VDC power to the BMS when AC power is detected on the coil side of the relay. The coil side of the relay uses AC power; whereas, the switching side of the relay uses DC power. Once the JimmE-V has been plugged into an AC power source, this relay should switch. This allows the BMS to be powered on regardless of the charger operation. The ice cube relay in the JimmE-V is shown in Figure 140, and is located next to the battery charger.

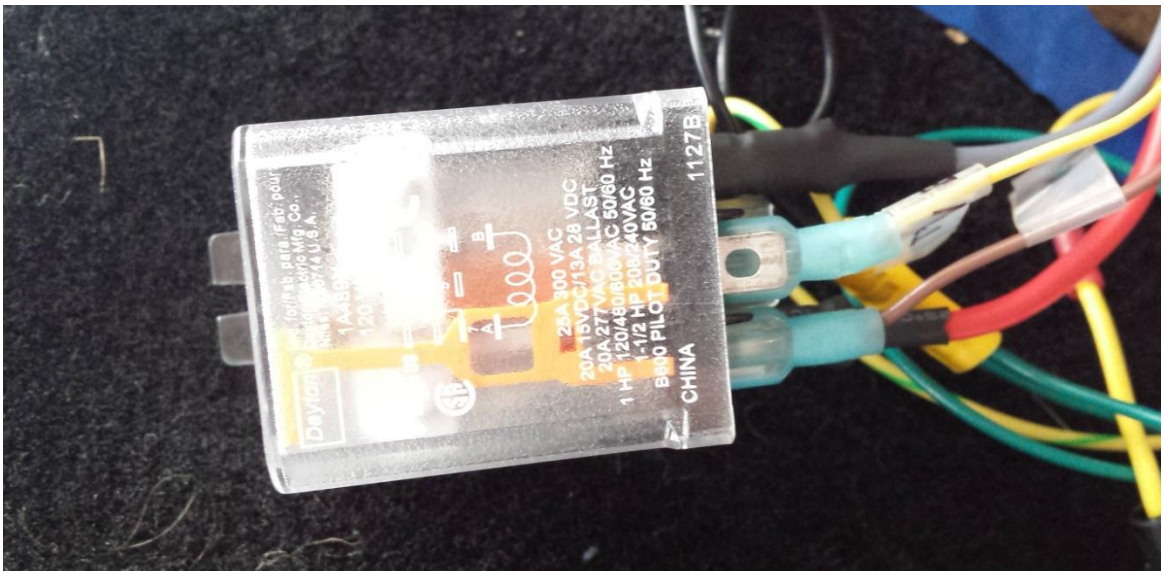

Figure 140: The ice cube relay provides the BMS with 12 VDC power when an AC power source is present. This ensures that the BMS can actively balance cells as needed.

There are two different methods for providing AC power to the JimmE-V battery charger. The first option is through the SAE J1772 plug. SAE J1772 is the standard for DC charging for plug-in electric vehicles [40]. These plugs are found on public charging stations and the two vehicle charging stations found at the Hill Center for Engineering Research and Development. Figure 141 shows the JimmE-V J1772 charging plug. The plug is located where the gas tank filling cap was previously located.

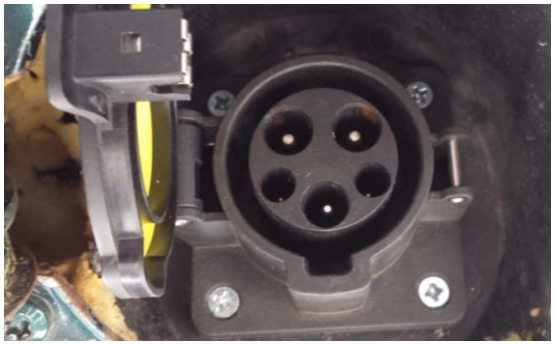

Figure 141: The SAE J1772 charging plug on the JimmE-V. The plug is located where the gas tank filling cap was previously located.

In order for the J1772 plug to work with the Manzinita battery charger, an AVC2 board was used. The AVC2 board is a small circuit board that monitors and controls the pilot signal from the J1772 inlet connector. The AVC2 board performs the necessary controls to tell the charging station that the car is connected, and when the connector is fully latched to request electrical power. The circuit monitors the proximity pin in the J1772 connector that indicates that the connector is latched. This ensures that power is either fully off when the connector is mated or disconnected to the vehicle [41]. Figure 142 shows the AVC2 board that is used in the JimmE-V. The AVC2 board is located near the ice cube relay and the battery charger. There is an additional automotive relay installed in-between the BMS and the battery charger on the Reg Bus line. This additional relay is a 12 VDC 40 amp relay that is typically found in vehicles. This relay allows the BMS to control the battery charger through the Reg Bus connection. The 12 VDC relay is shown in Figure 143.

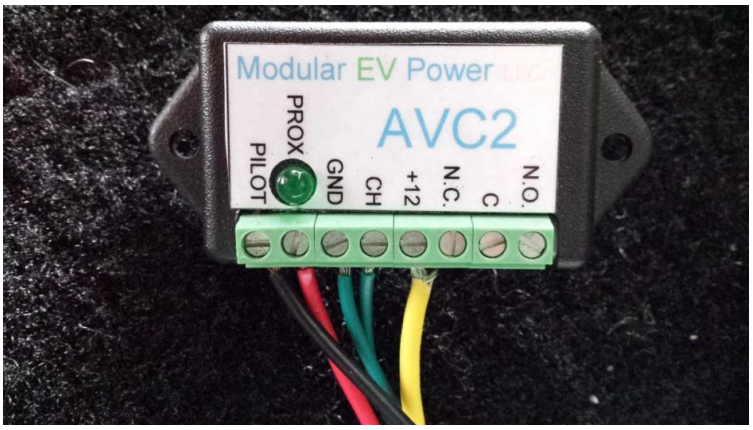

Figure 142: AVC2 Board for controlling the J1772 pilot signal.

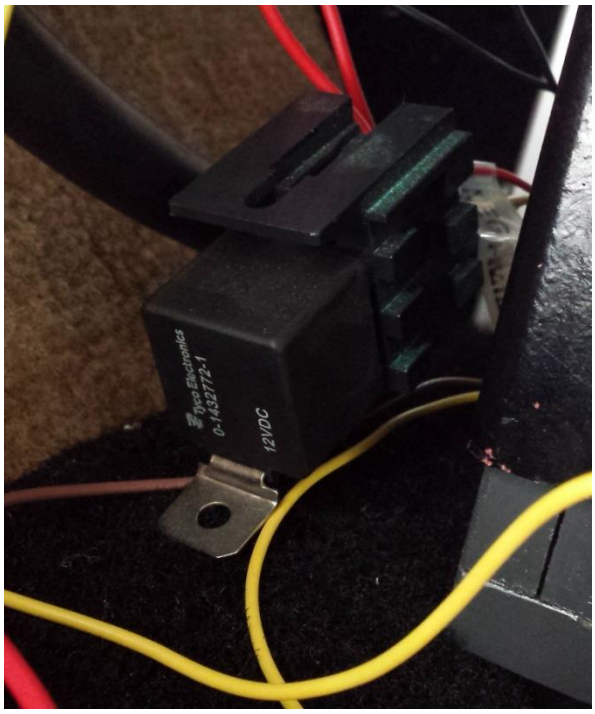

Figure 143: 12 VDC automotive relay for the BMS to control the battery charger through the Reg Bus connection.

Along with the J1772 plug, the JimmE-V can additionally be charged using a 240 VAC outlet with the fabricated extension cord. This allows the vehicle to be charged when J1772 plugs are not available. An Anderson Connector was employed to make switching between the two charging methods simple. When switching between charging methods, ensure that the charger is off, and the vehicle is disconnected from the AC power source. Figure 144 shows the plug for the 240 VAC extension cord along with the gray Anderson Connectors that can be used to switch between the two different charging

methods. With each component of the battery charging system examined, the entire system will be examined to demonstrate how it works as a whole.

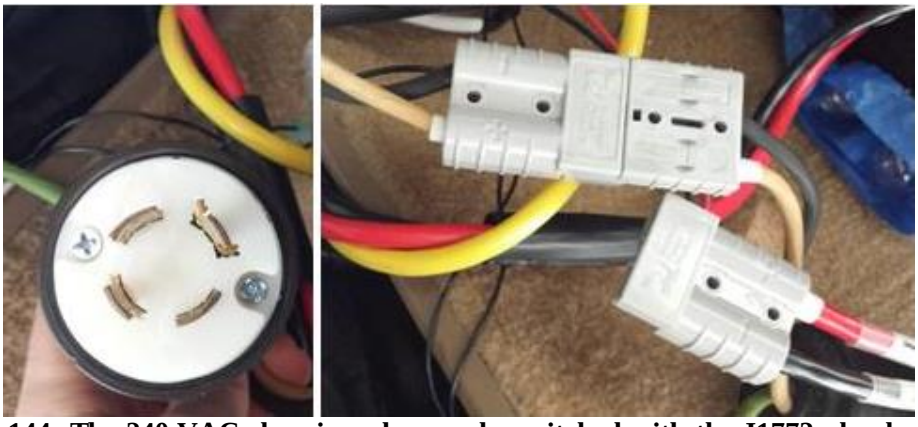

Figure 144: The 240 VAC charging plug can be switched with the J1772 plug by safely disconnecting the gray Anderson Connectors and re-connecting the desired charging plug.

The battery charger in the JimmE-V is just one of several components to ensure that the battery pack is safely and reliably maintained. Figure 145 shows the entire system schematic for the battery charger. The DC-DC converter is responsible for stepping down the battery pack voltage to approximately 12 VDC for automotive use. The DC-DC converter is discussed further in the next section. The BMS was discussed in the previous section, and only the connections concerning the battery charging system are shown. From Figure 145, it can be seen how power enters at the J1772 plug (or the optional 240 VAC plug). AC power goes into the charger, and the netural wires have been locally grounded to the chassis of the battery charger. The high voltage circuit is indicated by the orange lines connecting the pack to the DC-DC converter and battery charger. As previously discussed, it is seen here that the high voltage system is isolated from the rest of the vehicle to prevent risk of high voltage shock. The two smaller plugs on the J1772 pinout are for the proximaty and pilot signals for the AVC2 board. Lastly, the two relays in the system are shown in order to show how the BMS controlls the battery charger to ensure safe charging. Even though the battery charger has been set up to not exceed voltage limits, the BMS has the overall control athority and can prevent overcharging based on the input from the cell boards and current sensor. In addition to the high voltage battery pack, the JimmE-V has an auxilliary 12 VDC

system to operate the motor controller and traditional automotive components. The 12 VDC system is the next topic of discussion.

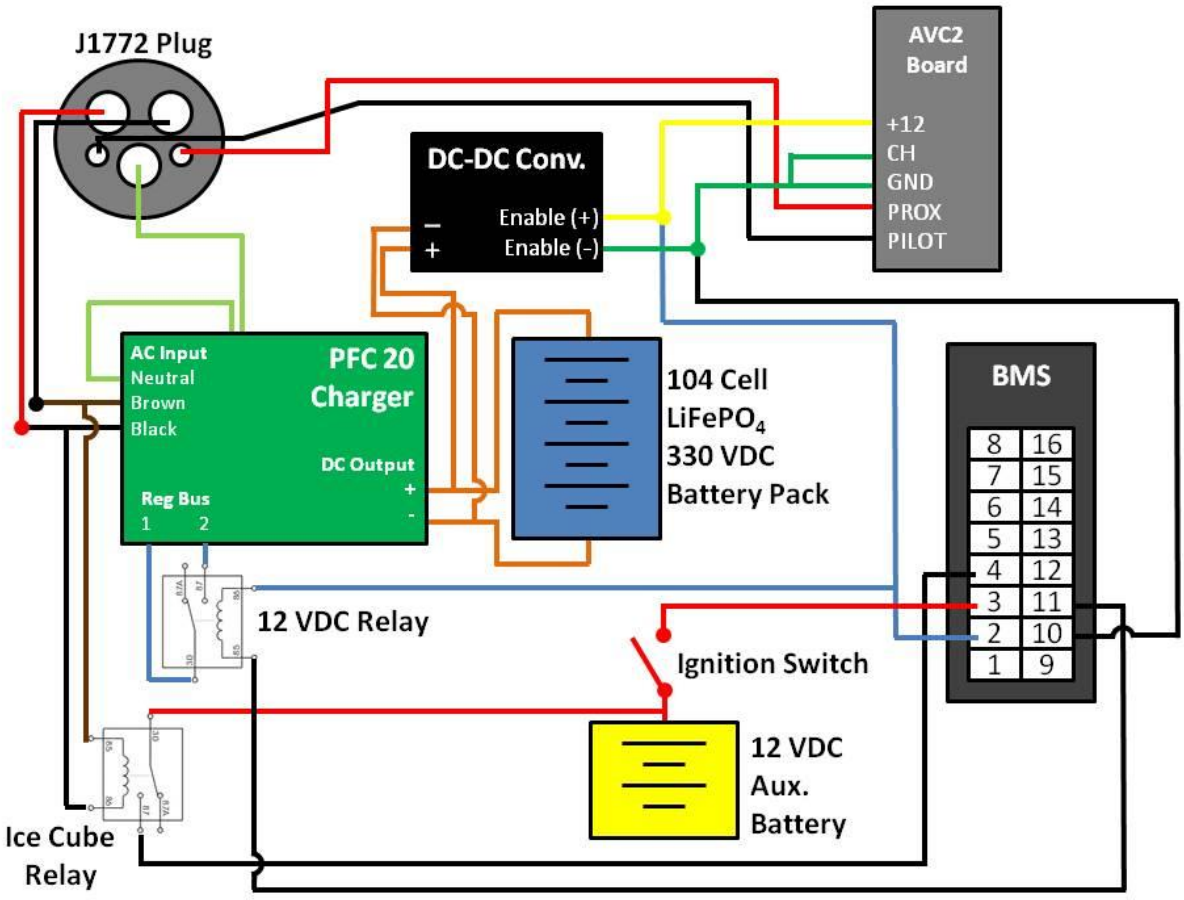

Figure 145: Schematic showing how the battery charger interfaces with the charging plug, AVC2 board, battery pack, BMS, DC-DC converter, and the 12 VDC system.

3.7 JimmE-V 12 VDC System

In addition to the HV system the JimmE-V has a standard automotive 12 VDC system. This system is necessary to run the vehicle's lights, fans, horn, motor controller, ECU, BMS, HV contactors, and various relays throughout the vehicle. Typical automotive 12 VDC systems are powered from the vehicle's alternator driven off the engine crankshaft. Since the ICE was removed, the JimmE-V utilizes DC-DC converters to step down the high voltage from the battery pack to approximately 13-14 VDC. Of note, the DC-DC converters are discussed further in following section in this chapter. This voltage range

is what a typical belt driven alternator generates for standard ICE vehicles. The focus of this section is to discuss the maintenance topics involved with the JimmE-V's 12 VDC system.

The first maintenance topic involves the vehicle wiring. The original Jimmy wiring harness was removed during the conversion process, and a new wire harness was sourced from Painless Performance. There are several different colors of wires in the JimmE-V. To create consistency, red wires indicate +12 VDC, and all black wires indicate the vehicle's ground. The vehicle is used as a ground in order to reduce the costs of a negative return wire in the 12 VDC circuit. Figure 146 shows the negative terminal of the 12 VDC grounded to the body of the vehicle. Another important aspect to the 12 VDC system wiring are the relays and fuses in the vehicle.

Figure 146: The 12 VDC circuit is grounded through the body of the vehicle.

Relays and fuses offer inexpensive overcurrent protection for vehicle components. Relays act as electromechanical switches and are covered in more detail in Chapter 2 of this thesis. The relays in the JimmE-V are 40 A relays. In the event current exceeds 40 A, the relay coil will fail preventing power distribution to the affected components. Fuses are similar to relays in their ability to prevent overcurrent situations; however, fuses do not have any switching components. The fuses in the JimmE-V have ratings from 5 A to 30 A depending on the circuit. The vehicle's main fuse block is located to the left of the steering column inside the JimmE-V (Figure 147). In addition to housing the vehicle's fuses, the turn indicator flasher and horn relay are part of the fuse block.

There are additional fuses beyond the fuse block located throughout the JimmE-V for specific requirements. In specific, there is a fuse for the ECU located close to the 12 VDC battery, and in between the ECU and motor controller. An additional fuse is located by the blower motor for the AC system. For specific fuse locations for the previously mentioned components, additional information is provided in the respective component's section in this Chapter. If a fuse in the main fuse block has been compromised, the fuse block can be accessed by gently removing the plastic trim by the fuse block. The trim piece has two Philips screws above the gauges that need to be removed prior to removing the trim piece. The two toggle switches have a retaining nut that also needs to be removed; however, there is enough wire slack on the switches to allow the plastic trim piece to be removed prior to replacing the fuses. When replacing a fuse, never use a higher amp fuse than the removed fuse. In some situations, a lower amp fuse can be used short-term; however, it is recommended that the fuse be replaced with a matching fuse. The next maintenance topic for the 12 VDC system is the auxiliary 12 VDC battery.

Figure 147: The main 12 VDC fuse block is installed in the dashboard to the left of the steering column.

The JimmE-V utilizes two deep cycle Optima batteries wired in parallel to provide power to 12 VDC components. The two batteries are wired in parallel to double the capacity of the system. Never wire 12 VDC batteries in series because batteries in series double the voltage. This would result in 24 VDC being supplied to a system designed to handle 12 VDC. To wire the 12 VDC batteries in parallel, connect the two positive terminals and the two negative terminals. This allows the voltage to remain constant while doubling the battery capacity. Moreover, in order to use two batteries in parallel, the specifications of both batteries need to be identical. In the event one battery fails, either a matching battery is used or two new matching batteries be installed. The Optima D75/25 battery specifications are found in Table 8. In the event either or both batteries need replacement, a similarly rated battery can be used. It is recommended that only deep cycle batteries be used in the JimmE-V due to their ability to provide a steady amount of current over a long period. Deep cycle batteries also allow repeated deep discharges [28]. Since the DC-DC output current can vary, these characteristics are desirable for use in the JimmE-V.

Table 8: Optima D75/25 deep cycle battery specifications.

Cranking Amps (CA)	770
Cold Cranking Amps (CCA)	620
Amp Hours (Ah)	48
Reserve Capacity (RC)	100

In addition to being a deep cycle battery, the Optima batteries are Advanced Glass Mat (AGM) batteries. This composition was desirable because AGM batteries use a glass mat to contain the electrolyte. This construction prevents the battery from spilling when damaged. AGM batteries have a relatively low electrical resistance combined with delivering higher power and efficiency compared to typical lead acid batteries. AGM batteries are maintenance free and completely sealed; however, the higher construction quality results in a higher cost [28]. Knowing these characteristics is important to properly charge and maintain the 12 VDC batteries.

When charging the 12 VDC batteries, only use a 12 VDC battery charger. Automotive battery chargers often have different charging options depending on the battery construction. In the instance of

the 12 VDC Optima batteries, the AGM option should be selected when charging the batteries. With respect to the charging rate, two to 20 A can be selected based on the demand for the battery. In most instances 10 A can be selected, which would charge one 48 Ah battery in just under five hours. Since the capacity has been doubled to 96 Ah, completely charging the system would take just under ten hours. During periods of not being used, the 2 A option can be used to maintain the batteries to ensure the system will be charged when used next. The 20 A option would be the fastest charging option for the 12 VDC batteries when the system needs to be recharged quicker. When hooking up a battery charger it is important to hook up the terminals properly. The positive connector is attached to the positive post, and the negative connector is attached to the negative terminal. Most battery chargers will prevent charging if hooked up improperly and signal an error message that they are fastened to the battery improperly. Properly maintaining the 12 VDC batteries will prolong the battery life; however, the 12 VDC batteries will need to be replaced during the vehicle's lifetime.

When replacing the 12 VDC batteries, safety is still an important consideration despite the lower voltage. While working around the 12 VDC batteries, the positive terminals can be grounded through metal tools, causing the battery to short directly to the ground. In order to prevent this, disconnect the negative connections before performing maintenance on the 12 VDC system. In the event a metal tool contacts the vehicle chassis ground while disconnecting the negative terminal, no short will occur. Once the negative terminal has been disconnected, the only way to cause a short is to directly connect the battery's positive and negative terminal. When re-installing a 12 VDC battery, the reverse process should be followed. First, connect the positive terminal, followed by the negative terminal. This process minimizes the risk of causing an electric short that could damage the battery, system, or user. Ensure that all 12 VDC connections to the batteries are tightened properly. Loose connections can result in the system not functioning reliably, or losing power while operating the vehicle. The main power switch for the 12 VDC system is controlled through the vehicle's ignition switch.

The JimmE-V ignition switch is located on the steering column on the right side of the steering wheel. This switch is referenced throughout this Chapter as it is the primary power switch for the 12 VDC

system. Since other systems such as the ECU, motor controller, and BMS also rely on 12 VDC power, the ignition switch can be used to cycle power to these components. In an emergency situation, this is relevant information because turning the key to the off position will result in the motor and controller shutting down. Typical ignition switches have multiple positions to allow the engine to be cranked until it is started. Despite using the original vehicle ignition switch, only two positions are functional. The ignition switch is either in the on or off position. This is demonstrated in Figure 74. Rotating the key ignition switch clockwise will result in turning the vehicle on. Rotating the key counterclockwise will shut the vehicle off. Knowing how to operate the vehicle's ignition switch is the first step in driving the vehicle. When vehicle operation is not desired make sure that the key has been returned to the off position to prevent the vehicle from draining the batteries. In addition to the ignition switch, knowing how to operate the JimmE-V's other 12 VDC components ensures safety while operating the vehicle on the road.

The JimmE-V is equipped with both low and high beam lights. Generally, these lights do not need to be used during vehicle operation; however, in the event the vehicle is driven at night or in dimly light situations, the vehicle lights allow the operator to maintain proper vision of the road while being visible to drivers surrounding the vehicle. For simplicity, the light switch in the JimmE-V is a three-position toggle switch that is installed on the polycarbonate cover for the fuse block. Figure 148 shows the light switch location and different operating positions. When the switch is centered, the lights are off. The high beams are operated by moving the switch to the up position. It should be noted that the vehicle's high beams draw more current from the 12 VDC system. While operating the vehicle's high beams, monitor the 12 VDC gauge to ensure the power is not being depleted too rapidly. Operating the high beams in conjunction with the power steering pump and additional 12 VDC components may cause the controller to lose power resulting in loss of motor operation. If this occurs, the system can be reset by shifting the shift knob back to park and cycling the key ignition switch. If the DC-DC converter does not reset, the enable switch may need to be toggled. The vehicle's low beams are operated by moving the switch to the downward position. These lights draw less power than the high beams and allow for longer

operation. In addition to the vehicle lights, the vehicle's turn indicators are essential for communicating the driver's intentions when turning.

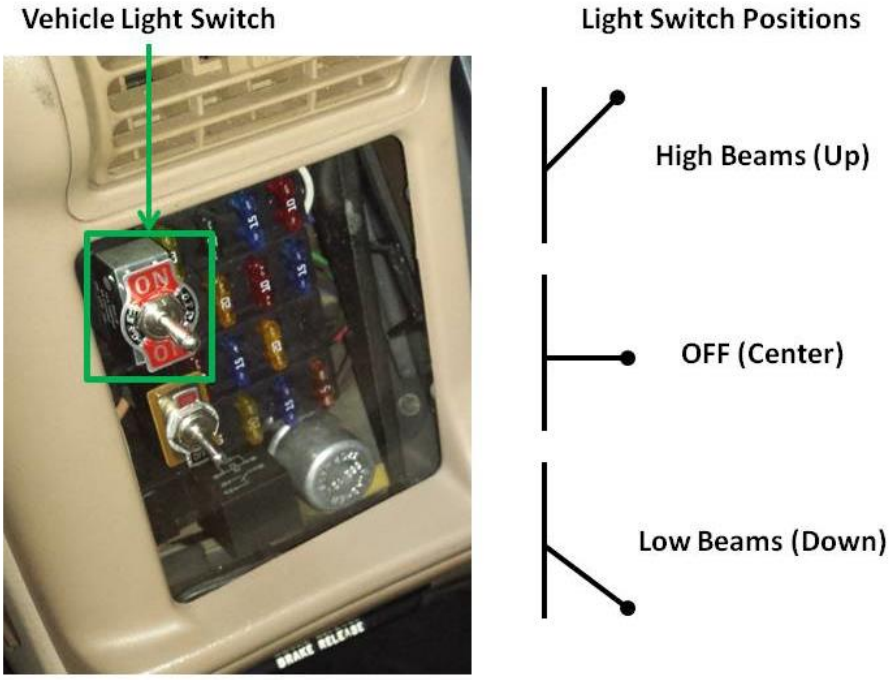

Figure 148: JimmE-V light switch location and operating positions.

The turn indicators on the JimmE-V function identically as traditional automobiles. The turn indicator switch is located on the vehicle's steering column, and is used to signal turning intentions to other drivers on the road. The right turn indicator should be used when turning right, similarly with the left turn indicator. The switch is auto-canceling; once the turn has been completed the switch returns to the off position. The windshield wipers are additionally controlled from the turn indicator switch.

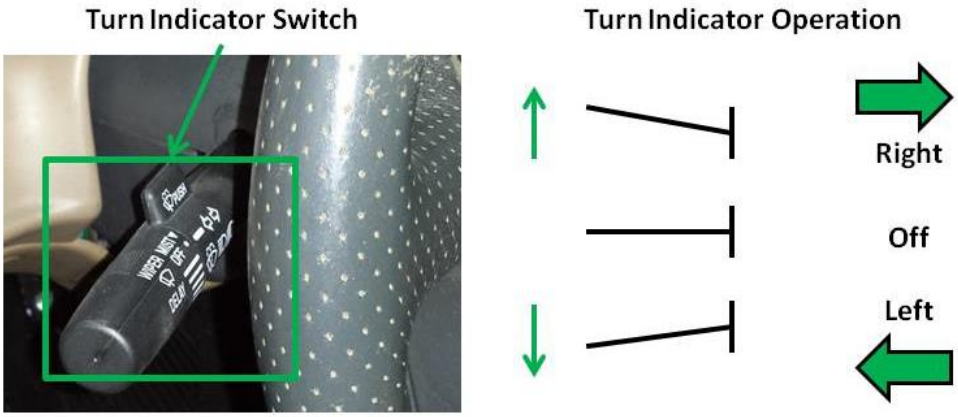

Figure 149: Turn indicator location and operating instructions.

In the event of inclement weather, the JimmE-V has functional windshield wipers. The JimmE-V has numerous mist rated components that allows the vehicle to be operated during wet weather. However, it is advised that the JimmE-V not be operated during extreme weather scenarios (i.e., thunderstorms, heavy rain, ice, or snow). If the windshield wipers are desired, the wiper controls are located on the end of the turn indicator switch. The wipers are operated by twisting the end of the turn indicator switch until the desired wiper speed is achieved (Figure 150). When no longer desired, return the wipers to the off position. In the event the vehicle becomes inoperable, the JimmE-V is equipped with hazard lights to indicate that the vehicle is disabled.

Figure 150: The wiper speed is controlled by rotating the end of the turn indicator switch.

The hazard lights are controlled through the factory hazard light switch that is a part of the turn indicator switch assembly. The switch is located on the top of the steering column as shown in Figure 151. When the switch is depressed, both the left and right turn indicator lights operate simultaneously to flash the hazard lights. When no longer desired, the lights are switched off by depressing the switch again. The final aspect to examine in the 12 VDC system is the solar panel system that provides an additional charging option for the 12 VDC batteries.

Figure 151: The hazard light switch is on top of the steering column.

The theory behind the solar panel system in the JimmE-V is that the system provides charging power to the 12 VDC batteries. However, this only occurs if the voltage output from the solar panels is greater than the current 12 VDC battery voltage. If the voltage cannot be supplied from the solar panels, a microprocessor controls a relay that switches between the DC-DC converter and the solar panels. Having more than one DC-DC operating simultaneously can cause back feeding issues. As a result, the solar panel DC-DC converter is off the majority of the time. The DC-DC converter can be switched on when the vehicle is not operating only if the main DC-DC converter is switched off. For further information regarding the DC-DC converters, see Section 3.8 of this document. In order to charge the batteries, the solar panels were installed in parallel. Solar panels in parallel are similar to batteries in parallel, keeping the voltage constant (relative to the solar input). In order to maximize their solar exposure, the six solar panels were installed on the forward section of the JimmE-V roof (Figure 152). The solar panels have the ability to output a maximum voltage of 15.4 VDC and 200 mA of current [42]. During vehicle operation, it was discovered that the initial panel installation was inadequate. This resulted in the panels disconnecting from the vehicle at higher speeds. To prevent further issues, silicon adhesive RTV and Gorilla tape were used to secure the cells to the roof and minimize the aerodynamic drag. In addition to the solar panels, a solar controller, relay, and microprocessor are additional components in the system.

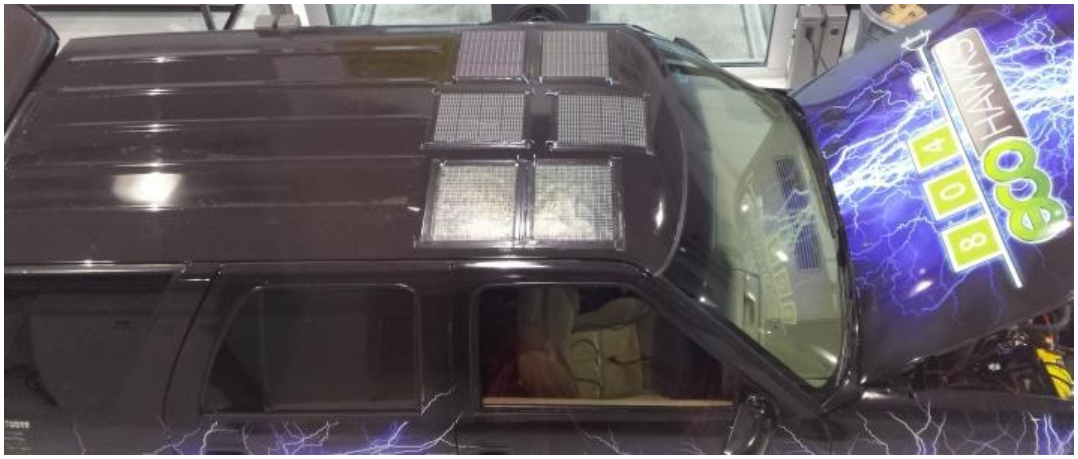

Figure 152: The JimmE-V solar panels on top of the roof.

In order to protect the microprocessor and 12 VDC battery, a HQRP solar controller was implemented. The controller regulates the solar panel output voltage to 14.4 VDC, and is rated at 10 A of current to prevent excessive current from flowing into the battery. Both the solar controller and relay are installed on the front battery box just behind the passenger seat in the JimmE-V (Figure 153). The final aspect to the solar charging system to discuss is the microprocessor.

Figure 153: HQPR solar controller and system relay.

The microprocessor used in the solar charging system is the Parallax Propeller microprocessor that is programmed using propeller's SPIN code v1.3.2. The program uses an analog to digital converter to read the incoming voltage signal from the solar panels, and determines if the voltage is sufficient to charge the 12 VDC batteries. If the voltage can charge the batteries, then the microprocessor toggles the

relay to allow the panels to output voltage to the batteries. If not, the relay says in the position favoring the HV battery pack to output voltage to charge the batteries [42]. The microprocessor is located behind the passenger seat in the JimmE-V (Figure 154). If desired, the program can be modified through a USB cord, a computer, and Parallax's Propeller Tool software that is available online. This concludes the discussion of the 12 VDC system in the JimmE-V. Given that the 12 VDC system will most likely be charged from the DC-DC converter, it is important to understand how this component functions in the JimmE-V.

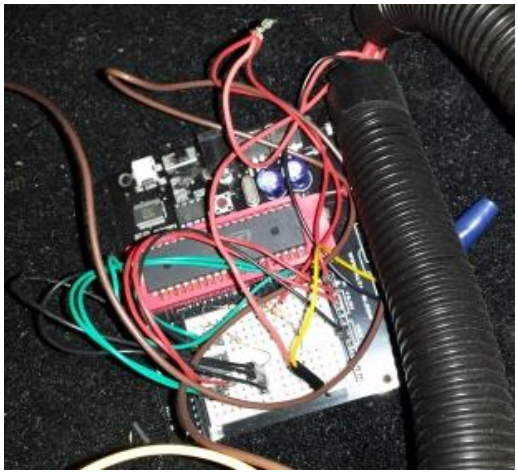

Figure 154: Propeller microprocessor and analog to digital converter.

3.8 DC-DC Converters

As mentioned throughout this thesis, the purpose of the DC-DC converter is to step down the 330 VDC to 12 VDC. By using a DC-DC converter, the systems can additionally get power from the larger capacity high voltage pack instead of relying on small capacity lead acid batteries, or an external heavy lead acid battery pack.

The DC-DC converters used in the JimmE-V are the MES-DEA 1000 Watt DC-DC converters. The converters are installed behind both the driver and passenger seats partially underneath the front battery box shelf. This location was selected due to the close proximity to the high voltage source, and because the converters are *not* mist or weatherproof. The specifications for the DC-DC converter are provided in

Table 9. Operation of the DC-DC converters is primarily automatic. To understand how the DC-DC converter is integrated into the JimmE-V, their wiring and operation will be discussed.

Table 9: MES-DEA 1000 W Specifications [43].

Input voltage	100-400 VDC
Output voltage (with 50 Ω charge)	14.5 VDC
Output voltage (full power) Vin > 190 VDC	13.3VDC
Maximum input current rms	6 Amps
Maximum continuous input current	75 Amps
Efficiency (full power)	>90%

The main wiring for the DC-DC converter requires an input connection to the high voltage source, and an output connection for the 12 VDC circuit. Additionally, the DC-DC converter has an enable positive and negative wire. When this circuit is completed (i.e., hard wired or through a toggle switch), the DC-DC converter is powered on. The high voltage connections for the DC-DC converters are made in the HV junction box (Figure 107). This is primarily done for safety reasons and to ensure HV isolation. The DC-DC provides power to the 12 VDC circuit through Anderson connectors and wire that is directly connected to the 12 VDC batteries. The remaining connections for operation are the enable signal connections. The input, output, and signal connections for the DC-DC converters are shown in Figure 155.

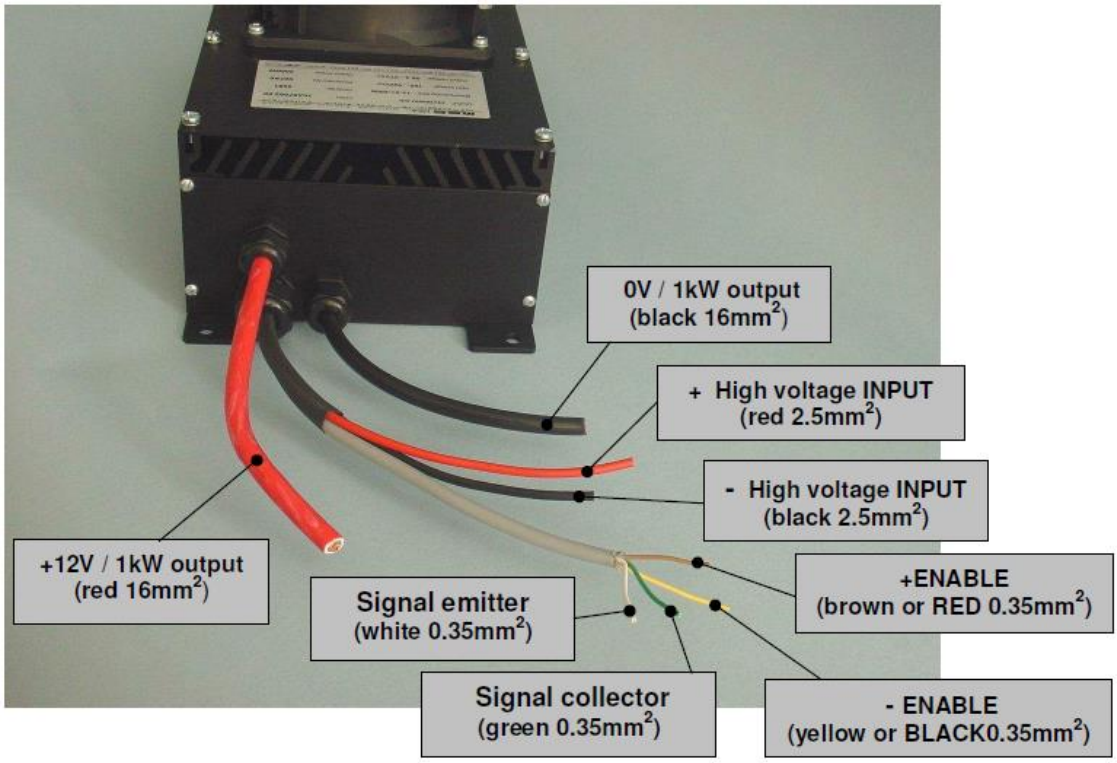

Figure 155: DC-DC converter wiring specifications [43].

For simple operation, these signals were routed to a switch box located behind the passenger seat. The switch box contains two toggle switches and fault indicator lights, as seen in Figure 76. When facing the switches, the left and right switches and fault lights correspond to the DC-DC converters to the left and right of the junction box. The right DC-DC converter is the primary DC-DC converter, while the left DC-DC converter is used in the auxiliary solar panel circuit. The signal emitter and collector connections are for the fault light connections. Operation requires the driver to select which DC-DC converter should be on or off. It is important to note that only one DC-DC converter should be used at a time. This is because DC-DC converters connected in parallel do not work like batteries in parallel. Operating more than one DC-DC converter simultaneously can cause current to flow into the output of the parallel DC-DC converter [43]. The DC-DC converters are connected to the 12 VDC system to charge the batteries while the vehicle is operating. Additionally, the 12 VDC batteries serve as a capacitor in the system because the DC-DC converters do not reliably output constant current. Having the batteries in the circuit

ensure that adequate current can be provided when demanded. In order to verify that the DC-DC converter is operating as desired, the 12 VDC system voltage is indicated on a gauge installed on the dash of the JimmE-V.

A properly operating DC-DC converter should produce an output voltage readout on the gauge higher than 13 VDC. Verification can also be observed directly at the battery. When measured with a multimeter, the voltage should read closer to 14 VDC (Figure 157). When the batteries are low or the DC-DC converter is not functioning, the gauge should show the typical 12 VDC reading. A low battery can be detected when the red warning light on the 12 VDC gauge is illuminated. Figure 156 shows 12 VDC gauge readings for a low battery and a charging battery. When the warning light is illuminated, the operator should immediately return the vehicle to charge the battery. When the 12 VDC battery starts getting low, the motor controller is often disabled causing the vehicle to not operate. The controller can be restarted by putting the shift knob in the park position and cycling the ignition switch. For further information regarding the DC-DC converter, consult the MES-DEA technical information document or contact the manufacturer. The next system to examine further is the electric power steering system.

Figure 156: The 12 VDC gauge indicating a low battery (left) and a charging battery (right).

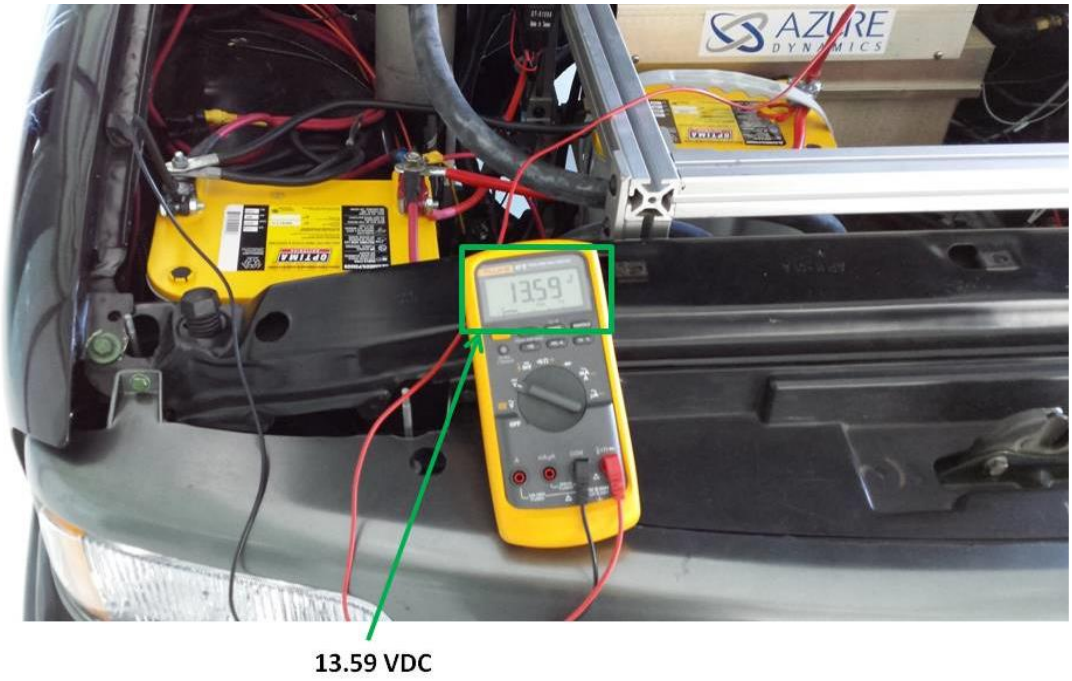

Figure 157: Verification that the DC-DC converter is functioning correctly. The voltage measured at the battery should approximately equal the output voltage of the DC-DC converter.

3.9 Electric Power Steering System

Without an ICE to power a traditional power steering pump, the JimmE-V relies on an electric power steering pump. Power steering uses hydraulic fluid pressure to minimize the effort exerted by the driver to steer the vehicle. The JimmE-V has an integral power steering system that applies fluid pressure inside the steering gearbox. From the hydraulic gearbox, the steering power is then transferred mechanically through a pitman arm to the steering linkage system [9]. Without the engine, there are two options for powering the power steering pump. The first method would require adapting a belt drive system to the electric motor, and the second method would require the use of a completely electric power steering pump. Due to the simplicity in design, an electric power steering pump was implemented.

The electric power steering unit contains all the necessary parts of the system contained into one unit. The power steering unit contains the electric motor, a controller, and the fluid reservoir as seen in Figure 158. In order to connect the power steering unit to the existing steering gearbox on the JimmE-V, the power steering unit had to be located close to the gearbox to allow the low and high-pressure hose

connections. To accomplish this, a steel plate was fabricated and installed in-between the frame rails in the front of the vehicle. The power steering pump is shown in Figure 159 to the right of the electric air conditioning compressor. The fluid reservoir can be accessed by opening the hood on the vehicle and using a funnel. When adding fluid to the system, it is imperative that only Toyota EH fluid be used: part number 08886-01206. This fluid is a specific electro hydraulic fluid for use only in this pump. Under no circumstances should any other type of power steering fluid be used. Failure to do so can result in damage to the power steering pump. In the event the pump becomes damaged, it can be removed by disconnecting the low and high-pressure fluid lines along with removing the three bolts that fasten the pump to the steel plate.

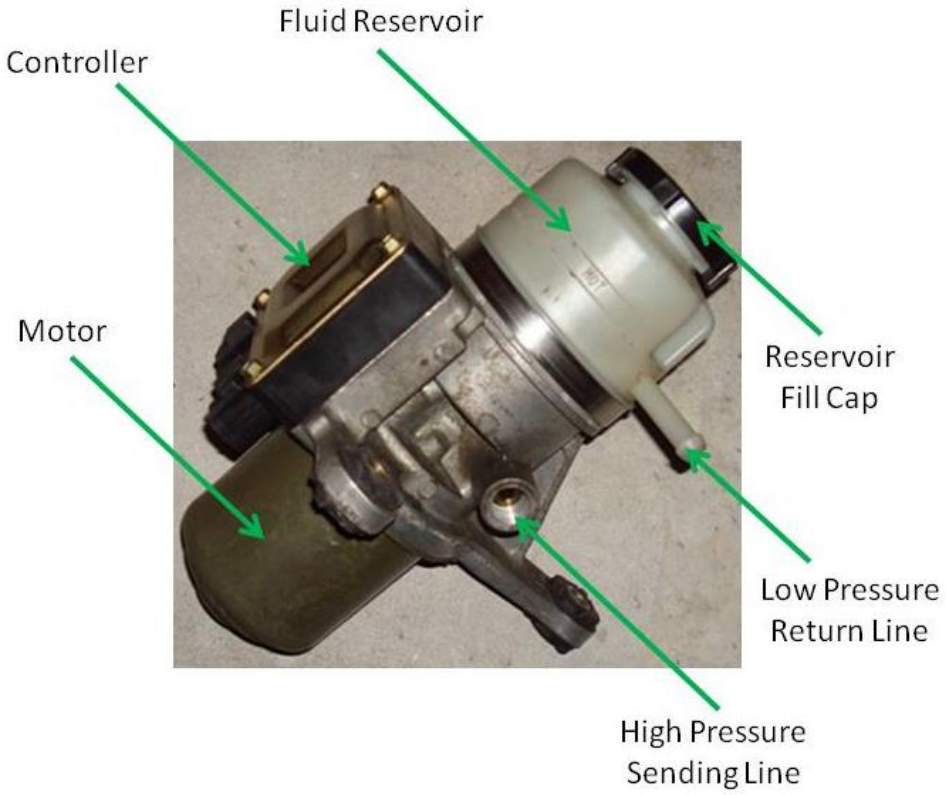

Figure 158: Toyota MR2 electric power steering unit.

Figure 159: The electric power steering pump was installed on a steel plate in the front of the vehicle to locate the pump close to the steering gearbox.

Since the power steering pump is electric, it is important to understand how the electric pump interacts with the other systems in the vehicle and an overall system schematic is provided in Figure 160. Originally, the electric pump was powered from a 12 VDC battery in the MR2; hence, the decision was made to run the pump using the DC-DC converter (this was the reason why two DC-DC converters were purchased, one specifically to be used for the power steering system). The MR2 pump puts out approximately 2500 psi when drawing 45 A from the batteries [22]. However, it was discovered during the third year of the project that the DC-DC converter does not necessarily put out constant current and the electric pump would not operate continuously. In order to ensure that the power steering system would have ample power, it was connected to the 12 VDC system. This allowed the battery to serve as a capacitor that the pump could draw from, and the DC-DC converter would re-charge the deep cycle battery from the main high voltage pack. Lastly, to ensure that the pump was protected from excess battery current, 50 A auto-reset circuit breakers were implemented along with a 100 A fuse to protect the DC-DC converter from a short within the system [42]. The system is operated by turning the ignition switch to the ‘ON’ position (normal vehicle operating position). Other than the ignition switch, no

additional operation is required from the driver. The remaining component to be discussed is the solenoid relay.

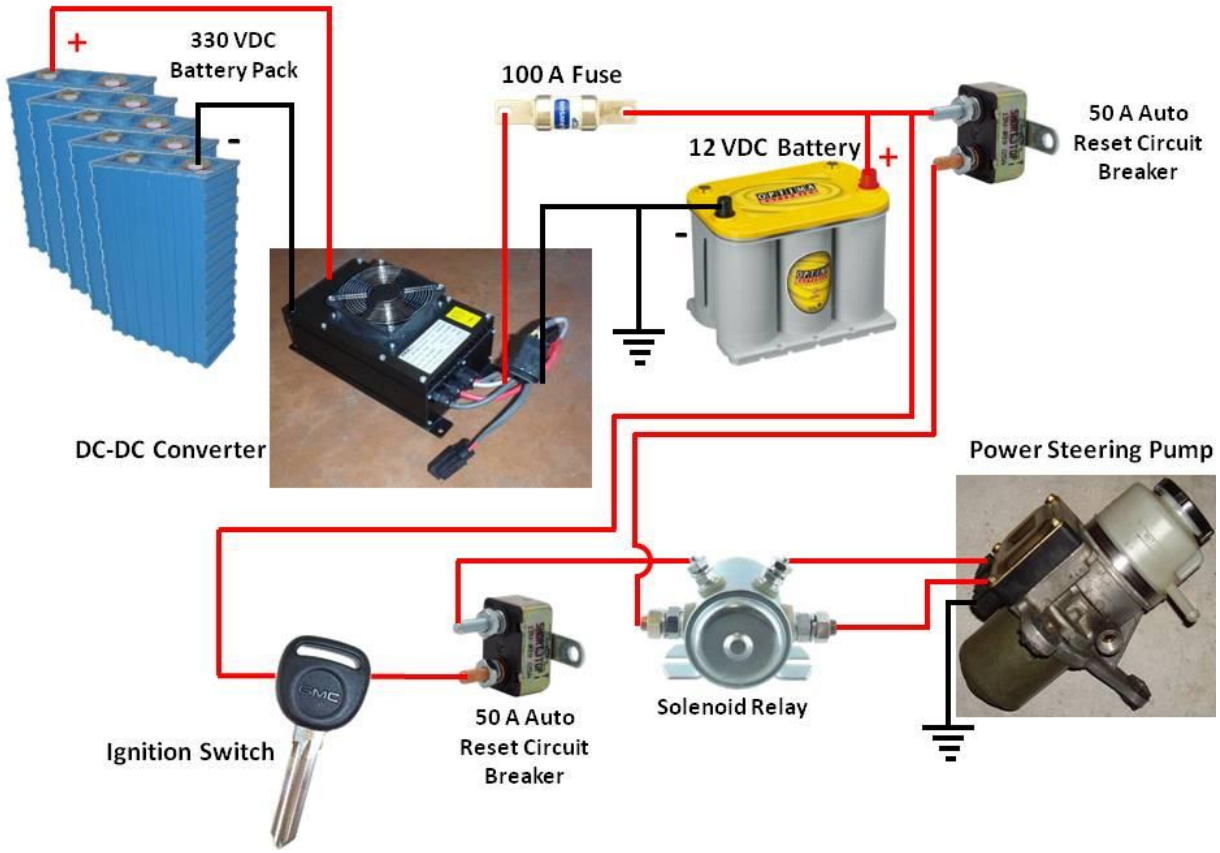

Figure 160: Electric power steering system schematic.

Wiring power to the power steering pump required the use of a 40 to 50 A relay. Due to part unavailability, the relay was replaced with a solenoid. Solenoids function similarly to relays and the implemented solenoid is used frequently in Dodge trucks. The power steering pinout with the 40-50 A relay is shown in Figure 161 with the solenoid taking the place of the relay. When the ignition switch is turned to the 'ON' position, the solenoid audibly engages followed by an audible noise from the pump motor indicating that the system is operating correctly. In the event no audible noises are heard from the solenoid or pump, check the fuses, circuit breakers, and the solenoid for proper operation before operating the vehicle. From the pump wiring schematic in Figure 161, it is seen that there is an additional pin for input from a speed sensor. This input reads the pulses generated from a speed sensor, and adjusts the pump speed so it is not operating at a constant speed. For simplicity, this feature was not implemented.

However, if future vehicle control schemes are altered this may be a desirable feature to utilize as the pump would consume less power at higher vehicle speeds.

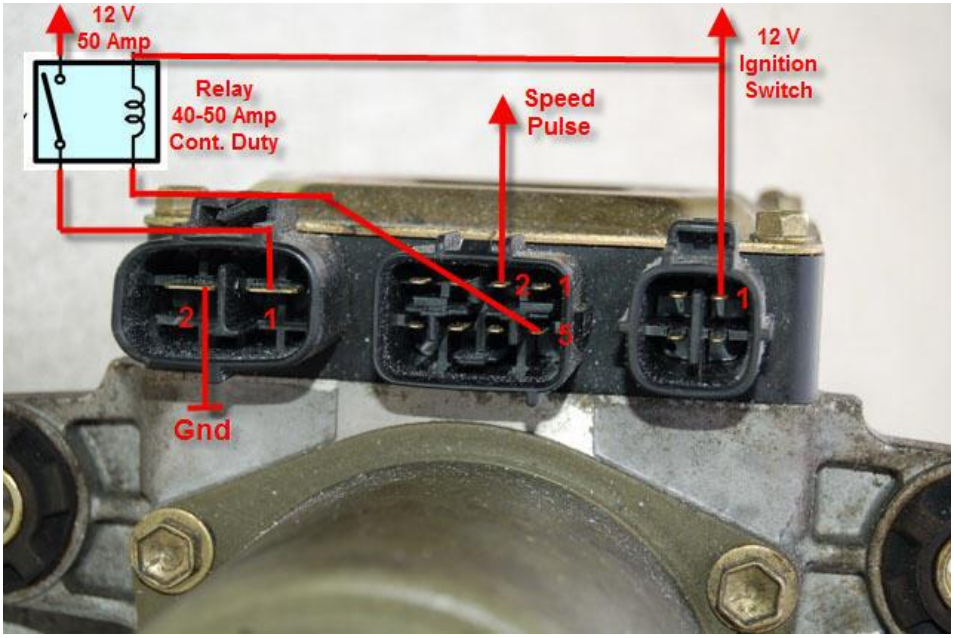

Figure 161: Toyota electric power steering pump pinout diagram [44].

In the event of a failure in the power steering system, it is important to note that the vehicle will still steer. However, without the assistance from the power steering pump more effort will be required from the driver to steer the vehicle. To further aid in any system diagnostics, the location of all the power steering components will be covered. As previously mentioned the power steering pump is located under the hood of the JimmE-V in the front driver's side of the compartment. Additionally, the DC-DC converter for the power steering system is located inside the rear passenger door on the driver's side of the vehicle. The DC-DC converter is just aft of the driver's seat partially under the front battery box shelf. The 100 A fuse is also located similar proximity to the DC-DC converter [43]. The circuit breakers and solenoid are located under the hood of the vehicle on the driver's side, as shown in Figure 162. The final system to be addressed is the air conditioning system.

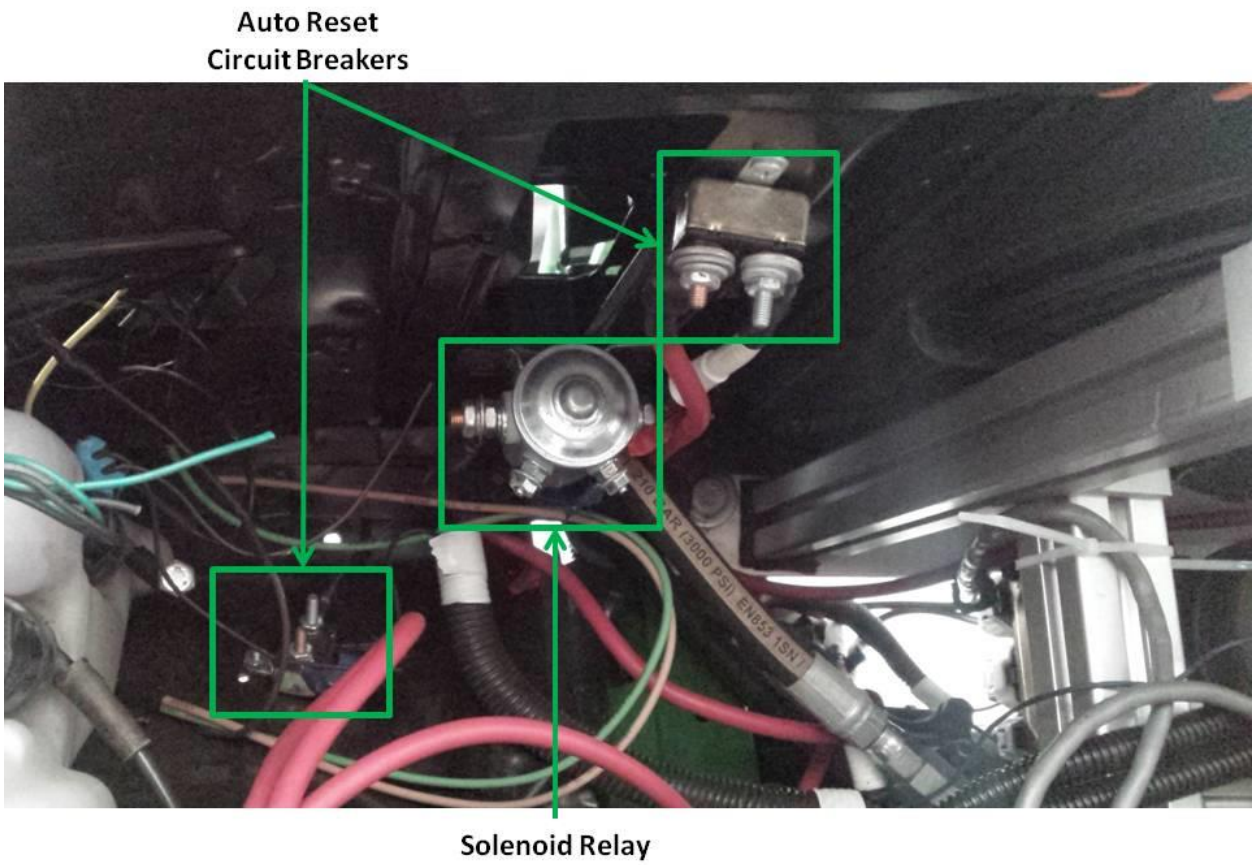

Figure 162: The power steering circuit components.

3.10 Vehicle Air Conditioning System

Similar to the vehicle power steering system, the standard methodology to power a vehicle's Air Conditioning (AC) system has been to power the compressor using a belt driven off the engine's crankshaft. Since the original ICE was removed, and a belt system was not implemented with the vehicle's motor, the JimmE-V uses an electric AC compressor to provide cooling for the vehicle. During the first year of the JimmE-V project, undergraduate student Nathaniel Mayhew conducted substantial research on the AC system for the JimmE-V. The focus of this section will be to provide a brief summary of the theory behind the AC system, along with operating instructions. For further information regarding the research conducted, refer to the (EcoHawks) Team JimmE-V 2010-2011 report.

Figure 163 shows an AC system schematic, and will be used as a guide to discuss the different processes involved in the cycle. From State 1 to 2, the refrigerant gas is compressed to a high temperature

and pressure. After being compressed, the refrigerant is then cooled by ambient air in a condenser (Process 3-4). The condensing process lowers the working fluid's temperature, but holds the pressure constant. In-between States 4 and 5, the refrigerant passes through a drier filled with a desiccant to remove moisture from the system. From State 5 to 6, the fluid passes through an expansion valve, causing a decrease in pressure. At this point, the refrigerant changes from a gas to a liquid. The low temperature liquid then passes through an evaporator (State 7 to 8). The blower is used to exchange heat with the air inside the vehicle cabin, thus cooling the vehicle [22]. This process is identical to the process used in the JimmE-V; however, the power input for the compressor comes from the HV battery pack instead of an IC engine. With a basic understanding of the process involved to remove heat from the vehicle's cabin, the specific components installed in the JimmE-V will be examined.

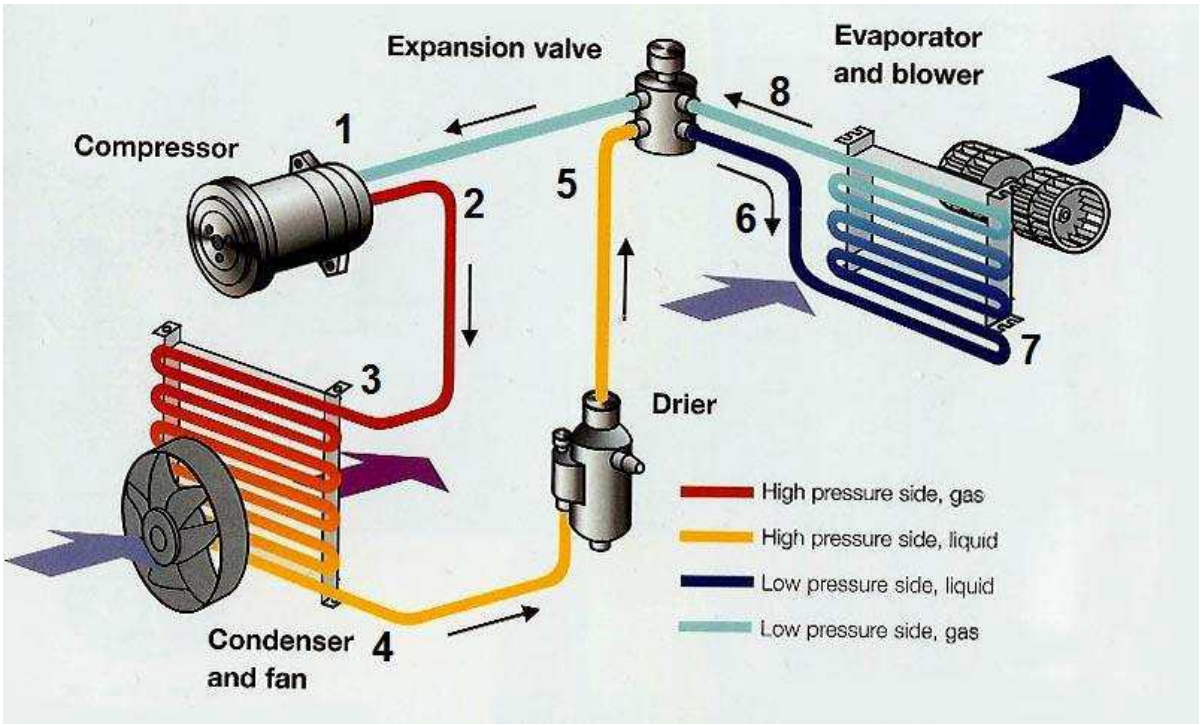

Figure 163: An automotive AC system schematic [38].

The AC compressor installed in the JimmE-V is the Sierra 06-0982Y3 Compressor. The compressor is powered exclusively off the HV battery pack. Thus, exercise caution when performing maintenance on the AC system. The AC compressor was installed next to the electric power steering pump under the hood of the JimmE-V (Figure 164). In addition to the drier, the compressor has an

additional liquid accumulator on the inlet side of the compressor (Figure 165). One difference between an IC engine powered compressor and the electrical compressor is that the electrical compressor requires an additional controller to modulate the electric compressor motor.

Figure 164: The electric AC compressor (left) and electric power steering pump (right).

Figure 165: The AC compressor inlet, accumulator, and outlet.

The electric compressor is controlled with a Masterflux 025F0140-003 controller. The compressor controller provides continuous thermal and electrical protection to the AC system, and it was designed specifically for the selected compressor. Selecting these components for the electrical AC system allowed the factory evaporator and drier to be implemented in the JimmE-V. This prevented additional parts from being scrapped or recycled. The controller was installed on the same steel plate as

the AC compressor, and can be seen behind the compressor in Figure 164. Access to the AC controller can be achieved by removing the polycarbonate ECU panel on the sub-frame under the hood of the JimmE-V. As previously mentioned, these components are on the HV system and extreme caution should be exercised when accessing these components. The orange wires that connect to the AC controller have HV potential. Ensure that all HV sources have been disabled before performing maintenance on the AC system (see Section 3.6.1). Figure 166 shows how the AC system is integrated with the HV system in the JimmE-V. Additionally, Figure 167 shows how the AC compressor is wired to the controller and note that there is a fuse located on the AC controller. In the event the system ceases operation, a blown fuse may be a possible source for the issue. As mentioned during the explanation of the AC system process, a condenser is necessary to lower the temperature of the working fluid.

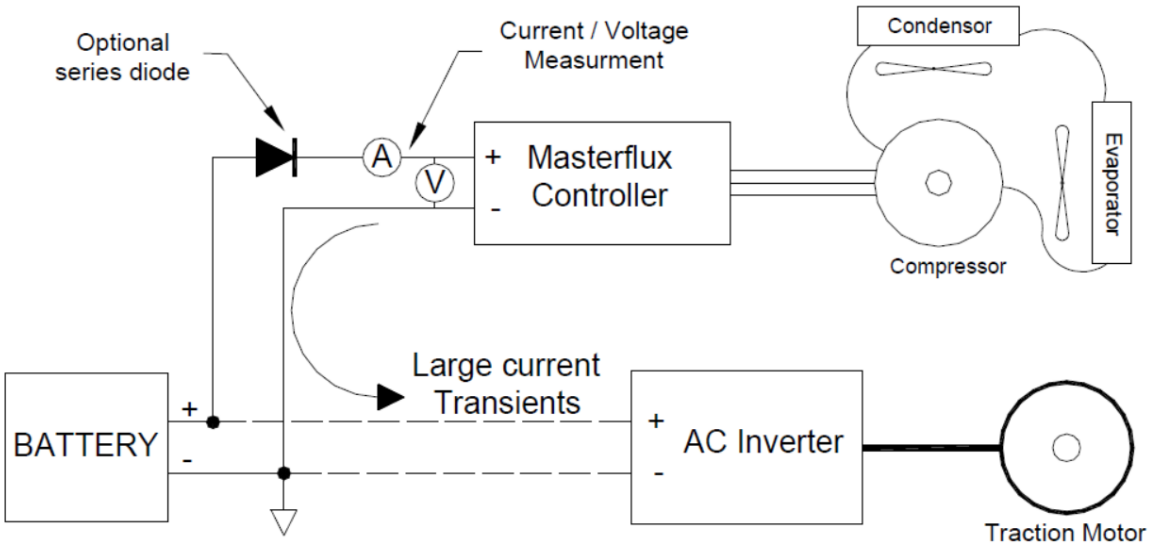

Figure 166: Schematic showing how the AC system is integrated into the HV system [45].

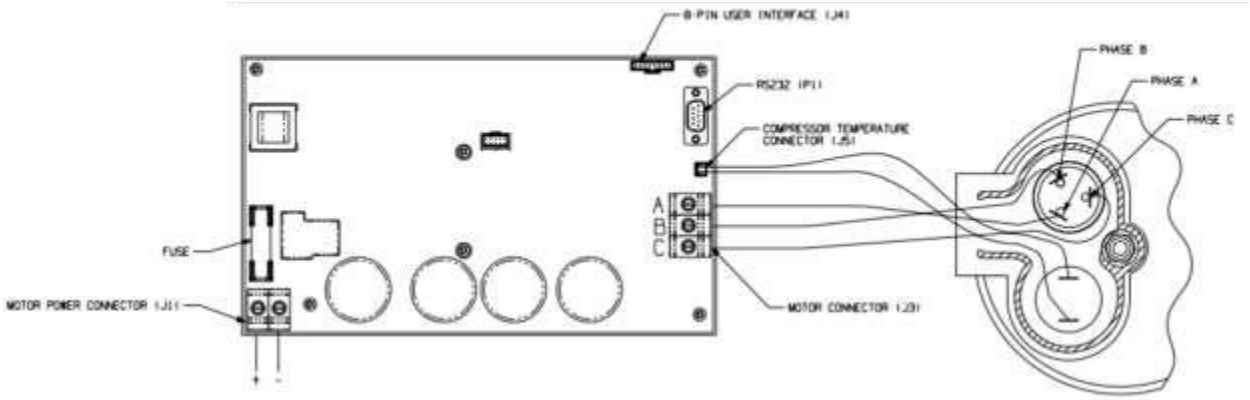

Figure 167: Schematic showing how the compressor is wired to the AC controller [45].

The condenser in the JimmE-V is located where a traditional vehicle's radiator and condenser would be located, as shown in Figure 168. This allows sufficient airflow through the condenser to cool the refrigerant. Two fans were also installed with the condenser to help pull airflow through the condenser. The condenser fans run off the 12 VDC system, and are controlled through a toggle switch and two relays. As previously discussed, the relays allow one switch to control two fans, and to provide overcurrent protection for the condenser fans. The relays are installed on the sub-frame under the hood of the JimmE-V by the AC compressor (Figure 169). Before discussing system operation, the blower schematics will be examined.

Figure 168: The AC condenser and fans are installed in the front of the JimmE-V. They are located behind the front grille to provide sufficient airflow.

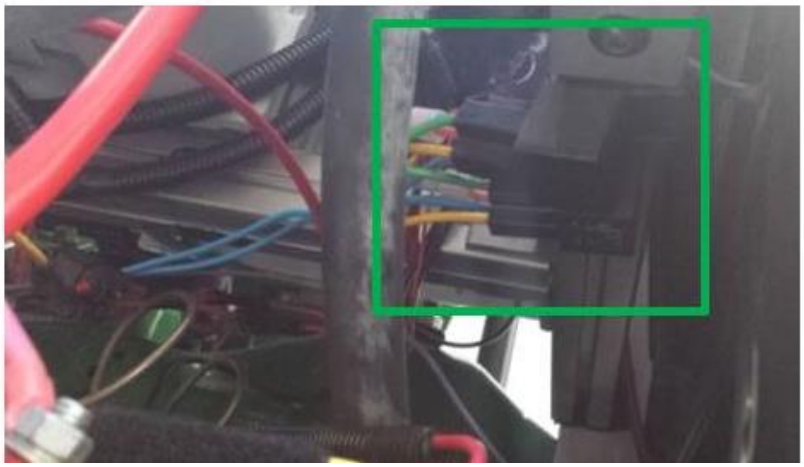

Figure 169: The condenser fan relays are installed on the sub-frame by the AC compressor.

As shown in Figure 163, during the process from 7 to 8, a blower is used to exchange heat with the vehicle's cabin to provide cooling for the vehicle's interior. The selected electric system allowed the original blower and evaporator to be utilized. Before operating the JimmE-V AC system, it is important to understand how the blower is integrated into the cooling system. The blower motor schematic is shown Figure 170. In addition to the schematic, Figure 170 additionally shows the locations of the components in the blower system.

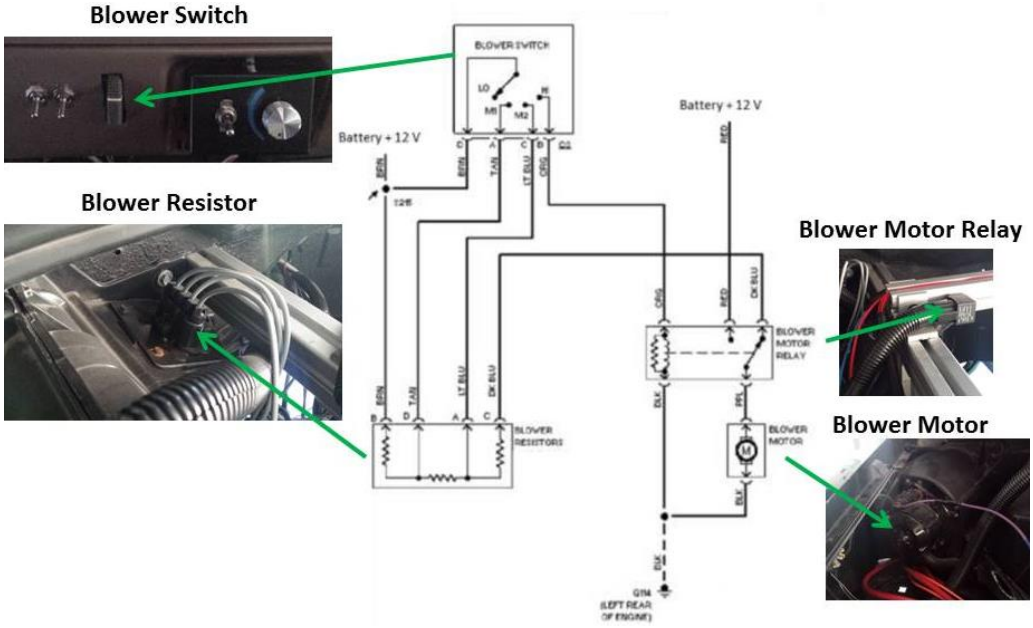

Figure 170: Blower motor schematic showing the components and their respective locations under the hood of the JimmE-V.

The blower motor speed is controlled through the blower switch that is located in the vehicle's interior on the dashboard of the JimmE-V. This multi-position switch allows different motor speeds based on the desired amount of cooling required. The white indicator line represents the current speed position. All the way down corresponds to the lowest speed setting while the highest speed setting is all at the top. These different speeds are achieved by changing the resistance in the circuit. The blower resistor is installed in the evaporator housing that also provides cooling to the circuitry. The evaporator housing is located under the hood of the JimmE-V on the passenger side next to the blower motor. The blower motor is the primary component in the blower system, and it is installed next to the evaporator by the passenger side front fender. The AC system components are located under the hood of the JimmE-V and can be seen in Figure 171. It should be noted that the top hose coming out of the evaporator housing is the low pressure side of the AC system that returns to the compressor. The expansion valve and drier are located inside the plastic cowling that also houses the evaporator. With an understanding of all the components involved in cooling the JimmE-V, AC system operation will be covered next.

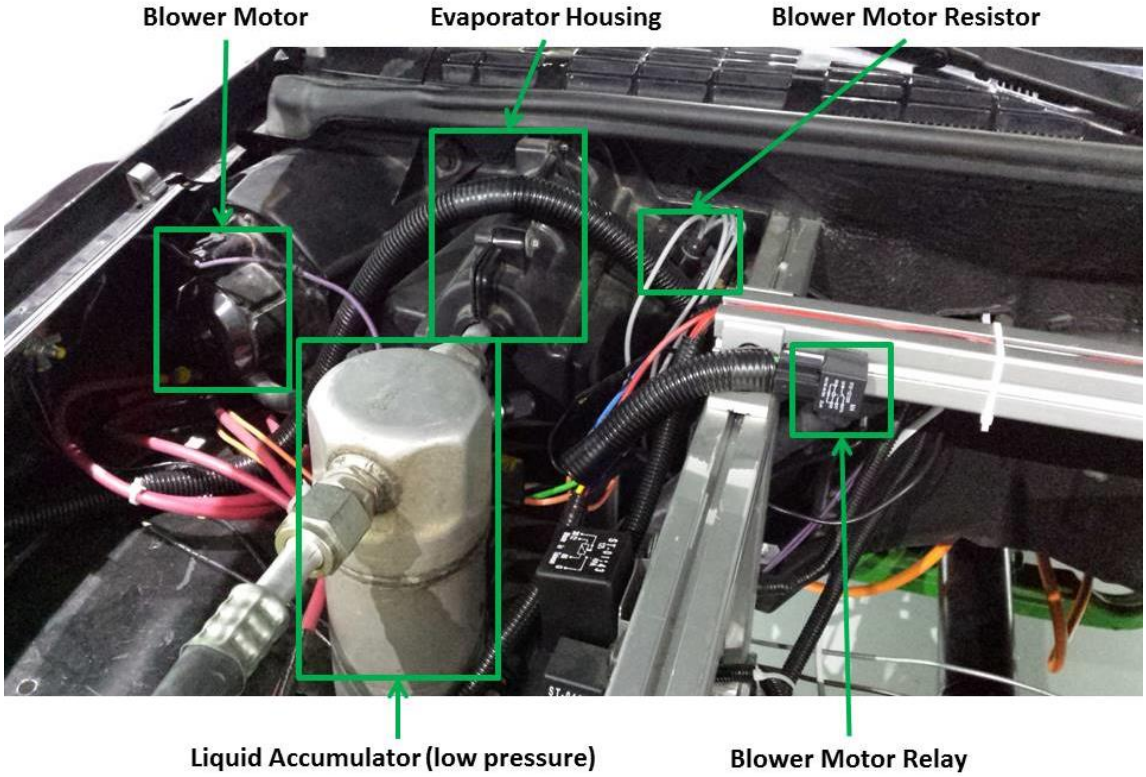

Figure 171: AC system components under the hood of the JimmE-V.

The AC system in the JimmE-V is operated from the interior of the vehicle. The system controls were placed such that either the operator or passenger can control the system. The controls are located on the lower portion of the vehicle's dashboard just above the center console. The different controls are shown in Figure 172. The switch closest to the driver is the condenser fan switch. The condenser fans should be on anytime that the AC system is operating. However, when the AC system is not operating, the condenser fans can provide additional airflow for components under the hood of the JimmE-V. The blower motor switch is to the right of the condenser fan switch. This switch toggles the blower motor on or off and can be operated with or without the AC system operating. Running the blower provides fresh air to the occupants of the JimmE-V when the windows cannot be rolled down. The controls located on the black box in Figure 172 correspond to the AC compressor. This control box is directly wired to the AC controller. The toggle switch cycles power to the AC controller and compressor, while the rotary dial controls the compressor speed. The amount of cooling is controlled by increasing or decreasing the compressor speed. Rotating the dial clockwise increases the compressor speed that results in increased vehicle cooling. The opposite holds true for rotating the dial counterclockwise. When not in use, ensure that all switches are in the off position. In addition to operating the JimmE-V AC system, maintaining the system is of equal importance.

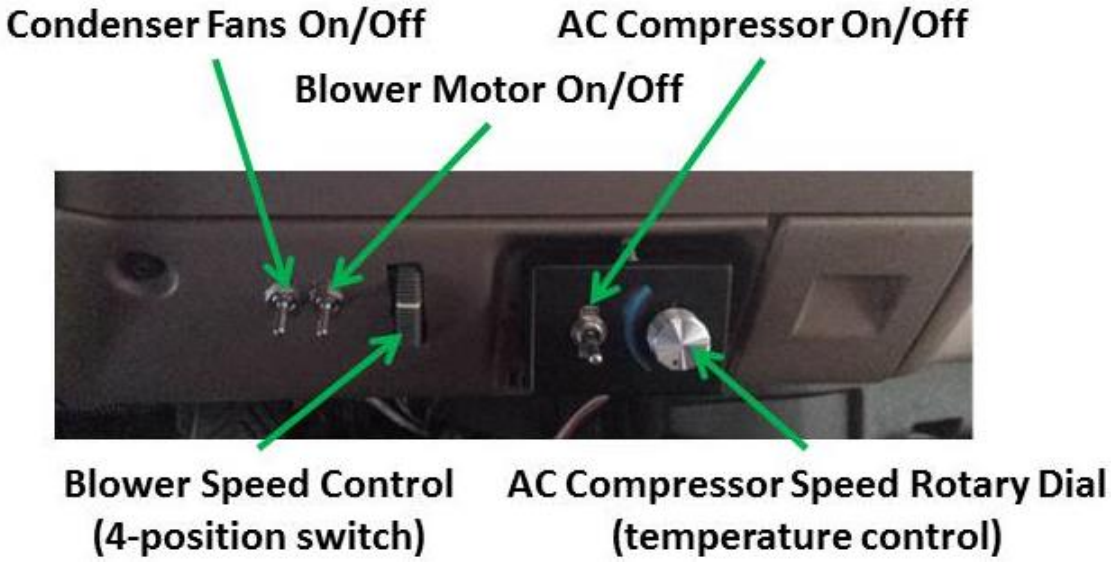

Figure 172: AC system operation panel inside the JimmE-V.

Due to the complexity of the AC system, only a trained automotive technician should perform maintenance on the JimmE-V's AC system. The Masterflux system should only be charged with R134a refrigerant. Do not charge the system with any other refrigerant. The compressor was pre-charged with oil from the factory. However, in the event more oil is needed it is imperative that only Idemitsu FVC68D oil be used [46]. Failure to heed this warning can result in the AC lines conducting high voltage. As a result, the system would no longer be HV isolating. Thus, this information should be provided to a trained professional before performing maintenance on the AC system in the JimmE-V. For additional compressor and controller specifications, refer to the product specification documents.

3.11 Causes for Vehicle Failure

Overall, the JimmE-V has shown to be relatively reliable; however, the vehicle has been known to have isolated issues within the vehicle's powertrain system. This section focuses on discussing previously known issues, and examines issues that could be a potential problem in the future. Only the powertrain system failure causes will be examined. Other mechanical failures will be similar in nature to standard automotive failures (i.e. failed bearings and universal joints) and are not discussed. As previously discussed, the powertrain system in the JimmE-V includes the motor, controller, ECM, HV battery pack, BMS, and the HV wire connections.

The first powertrain system to examine is the AC55 motor. Overall, the motor is relatively robust. However, during warmer temperature months in the summer the motor may overheat. In the event overheating occurs, the controller reduces power being sent to the motor to allow it to cool down. If this occurs during drive cycle testing the vehicle may need to be pulled over if it cannot maintain speed. Additionally, if overheating becomes a persistent issue electric fans may need to be installed to ensure adequate airflow across the motor's cooling fins. Another failure mode associated with the motor is related to the encoder located in the front of the motor. In the even the encoder fails low motor speeds will not be reported and will result in poor low speed operation (or no operation at all).

An additional area where a powertrain system failure could occur is the Azure motor controller. The main cause for failure are the controller's internal contactors. This issue occurred in the fall of 2014, and after being sent in for repairs the cause could not be determined. However, the controller has been functioning since its return in the spring of 2015. If the internal contactors fail the vehicle will not operate. Contact information for repairing the controller are provided in the Appendix of this thesis. Additionally, the controller could possibly overheat. However, if it does overheat the inverter cooling fans can be adjusted to power on at lower temperatures to mitigate excessive heat. Once the controller and ECM were initially synchronized over the CAN bus no further reprogramming is necessary. However, if the controller's default parameters are restored the CAN specifications outlined in the DMOC445 section will need to be reprogrammed. Similarly, if the ECM in the JimmE-V is removed or altered the CAN communication parameters will need to be reprogramed to allow vehicle operation. Other causes for failure with the motor controller include the loss of 12 VDC power. If the 12 VDC battery voltage gets too low the controller will power off and not turn back on

Other than the CAN communication settings the ECM has not experienced severe issues. However, the relays in the system are electromechanical switches that will eventually fail. If the main power relay and drive enable relay fail the vehicle will not operate. In the event the ECM experiences an unmentioned failure, contact information for New Eagle is provided in the Appendix of this thesis.

The main cause for powertrain failures is associated with the battery pack and BMS. Overall, as long as the circuit remains connected the vehicle will operate if a battery voltage drops too low (or to zero). However, if a short circuit occurs in the battery system (i.e. a punctured separator) the circuit will no longer be complete and operation will cease until the battery is replaced. The most common failure is lost communication with battery banks for the BMS. When this occurs the vehicle will still operate, but the BMS will indicate that a fault is present. While this is not an ideal situation, the vehicle can still be driven until it is safe to access the situation. Lost communication with the BMS is usually fixed by examining the wiring connections for the associated battery bank. If the fault is associated with a loose cell board not that the cell board may be damaged and need replacement. However, most instances can be

fixed by simply retightening the loose connection on the battery cell. An additional benefit of $LiFePO_4$ batteries in comparison to Li-ion batteries is the absence of thermal excursions. The CALB batteries in the JimmE-V have vents located on top of the batteries to prevent expansion. While temperature control is crucial for Li-ion batteries, $LiFePO_4$ batteries remain stable during charging and discharging. However, if the vehicle is ever stored outside in cold temperatures around freezing a battery heater should be used to keep the packs warm. The combination of cold temperatures and low voltage could potentially damage the vehicle's battery pack.

3.12 Conclusion

The JimmE-V is full scale EV designed and built by students that is representative of a modern EV. In order to take journal quality EV data, it is important to understand how the vehicle's systems operate and work together. To ensure that experiments will give repeatable results, proper operation and maintenance will prolong the vehicle's life. In addition, the operator's safety is of the utmost importance while working with HV systems in electric vehicles. The author's main contributions to the JimmE-V were the installation and calibration of the motor controller, and the establishment of a vehicle CAN bus. Additionally, the author was the main contributor to the research, installation, and calibration of the vehicle's ECU. Due to the bankruptcy of Azure Dynamics, getting the DMOC controller and ECU to operate as designed proved to be difficult without technical support. In addition to installing and calibrating the ECU and controller, the powertrain system relies on additional vehicle components, the author needed knowledge of the HV systems and 12 VDC systems. The author also made contributions to the AC system, vehicle assembly, and vehicle wiring.

Chapter 4: Well-to-Wheels energy and emissions analysis of a recycled 1997 GMC Jimmy converted into a battery electric vehicle.

4.1 Abstract

With the growing popularity of Electric Vehicles (EVs), it is important to understand the complete picture of their energy used and emissions generated from vehicle manufacturing through driving. To this end, a vehicle Life-Cycle Analysis (LCA) can provide these energy and emissions estimates for the vehicle manufacturing process and subsequent on-road usage. This study is a follow up effort to a previous LCA for a 1974 VW Beetle Parallel Hybrid Electric Vehicle (PHEV) conversion project. In specific, this effort follows suit by utilizing the Argonne National Laboratory's Greenhouse Gasses, Regulated Emissions, and Energy Use in Transportation (GREET) model to complete a LCA for the University of Kansas's second generation EV, the JimmE-V. The JimmE-V LCA provides estimates regarding the benefits of reusing the original vehicle's larger components. Additionally, the LCA examines two different lithium iron phosphate ($LiFePO_4$) battery cathode manufacturing processes. Lastly, the LCA examines the electricity energy and emissions needed to power the vehicle along with a full Well-to-Wheels (WtW) analysis over the vehicle's lifetime. This analysis includes two full electricity generation mixes, and two additional solar generation mixes. To further examine the efficiency of the JimmE-V, this work includes drive cycle data acquired through the vehicle's CAN bus system. Finally, this effort examines the solar generation capabilities of the Hill Engineering Research and Development Center.

4.2 Introduction

As Electric Vehicles (EVs) become more established in the automotive industry, it is important to educate students on the impact EVs have on the energy grid in regards to energy usage and emissions. To this end, Dr. Christopher Depcik established the University of Kansas (KU) EcoHawks in 2008 with the goal to provide engineering students with sustainable design projects that focus on transportation and its associated energy infrastructure. Two of the major EcoHawks projects have involved converting internal combustion (IC) engine vehicles into full-scale EVs.

The first project involving the EcoHawks was a full-scale Plug-in Hybrid Electric Vehicle (PHEV) conversion of a 1974 Volkswagen (VW) Super Beetle (Figure 173). The intent of this project was to design and fabricate a PHEV using recycled parts and a relatively simple vehicle powertrain. The VW Beetle can operate in three different modes: hybrid in EV mode (generator installed, but not running), series hybrid mode (generator installed and running), and Battery Electric Vehicle (BEV) mode (generator removed from vehicle). The Beetle is equipped with a NetGain Warp 9, 120 VDC Brushed Series Wound motor that is matched to the original VW five-speed manual transmission. The motor is powered by a 14.19 kWh lead acid battery pack with a total pack voltage of 120 VDC, and Amp hour (Ah) capacity of 115 Ah. From a controls standpoint, the Beetle is relatively simple. The motor is controlled using a NetGain Controls Classic DC Speed Controller that receives driver input via a potentiometer accelerator pedal. The motor and controller in this application do not provide any regenerative braking energy to the battery pack due to complexity issues with DC motors and regenerative braking [47]. Overall, the Beetle achieves approximately 106 miles per gallon equivalent (mpg_e) [16]. Along with providing a project for engineering seniors, the Beetle has additionally been used by previous graduate students for developing vehicle and battery models while examining the well-to-wheels energy usage of EVs.

Figure 173: KU EcoHawks 1974 VW Super Beetle

The second generation EV produced by the KU EcoHawks is a 1997 GMC Jimmy (aka Chevy Blazer) referred to as the JimmE-V with renovations starting in 2010. The JimmE-V uses an Azure Dynamics AC 55 three-phase Alternating Current (AC) motor, coupled to an Azure Dynamics DMOC445 motor controller and inverter. The DMOC445 is CAN controlled and requires the use of an ECU to relay accelerator pedal input to the controller. The advanced composition battery pack consists of 104 CALB lithium iron phosphate ($LiFePO_4$) batteries in series that provides 330 VDC to the controller with an overall capacity of 100 Ah for a total energy content of 33 kWh. Each cell is controlled by an Elithion Lithiumate Pro Battery Management System (BMS) to ensure that the batteries are properly charged, discharged, and maintained. The motor transfers power to the wheels of the vehicle by directly driving a drive-shaft through a differential to the rear wheels. In addition to a more advanced powertrain, the JimmE-V has additional amenities that make it comparable to a consumer available EV. The vehicle has electric air conditioning components, electric power steering, electric heating elements, two DC-DC converters to step down the high voltage source for automotive use (12 VDC), and solar panels on the roof to float charge the 12 VDC batteries needed to run traditional automotive components.

Figure 174: KU EcoHawks 1997 JimmE-V.

From an emissions standpoint, EVs offer zero local tailpipe emissions. However, it is important to understand that the required energy for re-charging comes from the electrical grid. Depending on the region, this could mean that the emissions come from coal, natural gas, nuclear, or alternative energy sources. As a result, this study will make the assumption that power is provided through the main coal power plant for Lawrence, Kansas. Additionally, both of the university's EVs are charged at the Hill Engineering Research and Development Center that provides a peak power output of 14.8 kW of grid tied solar generation. In order to further examine the energy and emissions impact of the JimmE-V and compare that with the prior VW Beetle efforts, a Life-Cycle Analysis (LCA) was performed using Argonne National Laboratory's (ANL) Greenhouse gases, Regulated Emissions, and Energy Use in Transportation (GREET) model.

GREET models the life cycle energy and emissions for different vehicle types. This type of investigation is also referred to as a Well-to-Wheels (WtW) emissions and energy use analysis. This is beneficial because it provides an overall inquiry into the vehicle's influence on the environment. GREET also allows the study of the extraction, enrichment, production, and transportation of fuels referred to as a Well-to-Pump (WtP) analysis. Since the JimmE-V is a BEV, the main fuel source is the coal used to generate electricity to charge the battery pack. Fuel consumption in the vehicle is additionally covered in GREET through a Pump-to-Wheels (PtW) analysis. GREET models these different processes for three different vehicle types: passenger cars, Light Duty Truck (LDT) 1 and LDT 2. These classes are separated

by vehicle weight. Passenger cars are used for typical consumer vehicles, while LDT 1 is used for trucks weighing less than 6,000 lbs. The remaining LDT 2 classification is used for trucks weighing less than 8,500 lbs but more than 6,000 lbs. Since the JimmE-V weighs 4,405 lbs, the LDT 1 classification was used to generate the energy use and emissions GREET model. Before discussing further assumptions used in the JimmE-V GREET model, previous LCA efforts on the 1974 VW Super Beetle were reviewed.

4.3 Previous Efforts for the 1974 VW Super Beetle

Strecker, et al. conducted a WtW energy and emissions analysis on the EcoHawks 1974 VW Beetle [48]. The vehicle implemented a compression ignition generator fueled by (used) canola oil biodiesel. Testing was conducted with the vehicle in three different modes: hybrid in EV mode, series hybrid mode, and battery electric vehicle (BEV) mode. Additionally, this study was also used to modify and validate electrified vehicle dynamics modeling techniques developed by Austin Hausmann [16]. Lastly, their efforts implemented a solar photovoltaic (PV) charging station to study the effects of renewable energy for the Beetle's LCA. The VW Super Beetle specifications are shown in Table 10.

Table 10: 1974 VW Super Beetle series hybrid specifications [48].

Transmission	Original four speed w/reverse
Drive motor	NetGain Warp 9, 120 VDC Brushed Series Wound
Motor controller	NetGain Controls Classic DC Speed Controller
Battery pack	Discover Energy EV31A-A 10S1P 120 VDC, 115 Ah
DC-DC converter	ElCon TDC-400-120, 400 W
Generator	Yanmar L100V 5.5 kW operating on 100% biodiesel
120 VAC charger	Elcon PFC 2500, 1.5 kW
230 VAC charger	Zivan NG3 F7-PH, 3 kW
Tire size	185/75R16
Weight with generator	1246 kg
Weight without generator	1149 kg

Overall, the comparison between the three different vehicle operating modes yielded that the VW Beetle was most efficient while operating in BEV mode as shown by the drive cycle route statistics in Table 11. The increase in efficiency was attributed to the lack of the generator and fuel tank in the

vehicle. In order to compare the efforts of the VW Beetle and the JimmE-V, only the BEV results for the Beetle will be discussed in this study. In addition to using drive cycle data to validate the electrified vehicle dynamics model, a vehicle LCA was conducted on the VW Beetle.

Table 11: 1974 VW Super Beetle route statistics [48].

	Test Time [s]	Energy Used [kWh]	Efficiency		Final Voltage [VDC]	Average Current [A]
			[kWh/mi]	[mpg_e]		
Hybrid in EV Mode (1)	3145	7.23	0.335	100.6	117	75.6
Hybrid in EV Mode (2)	3256	7.33	0.341	99.0	118	73.0
Hybrid in EV Mode (3)	3020	7.52	0.351	95.9	119	80.1
Series Hybrid Mode	2866	7.20	0.335	100.6	122	79.1
BEV Mode (1)	2788	6.84	0.318	106.0	120	74.2
BEV Mode (2)	2963	6.85	0.319	105.5	121	73.8
BEV Mode (3)	3002	6.82	0.318	106.1	120	72.5

The previous study utilized GREET 2.7 coupled to GREET 1.8c to analyze the processes for creating the VW Beetle components and materials. GREET 2.7 used the provided model information to calculate the energy use and total estimated emissions produced from these processes. GREET 1 was used to specifically calculate the transportation and distribution energy requirements [48]. Table 12 contains the GREET calculated energy and emissions offset during the component manufacturing process, and the assembly, disposal, and recycling (ADR) process. The totals shown in Table 12 reflect the calculated energy and emissions offset by reusing the stock VW Beetle components. GREET 1.8c was used to analyze a number of pollutants, including carbon monoxide (CO), carbon dioxide (CO_2), volatile organic compounds (VOC), oxides of nitrogen (NO_x), particulate matter smaller than 10 microns (PM_{10}) and smaller than 2.5 microns ($PM_{2.5}$), oxides of sulfur (SO_x), and methane (CH_4). GREET 1.8c also generates results total greenhouse gasses (GHG) as a CO_2 equivalent [48]. From the results shown in Table 12, one should note the high amounts of CO_2 emissions. These emissions are the result of the energy intensive process for manufacturing the vehicle components; however, these results include the transportation and distribution processes, along with the final disposal processes for the original Beetle.

Table 12: Calculated emissions and energy use avoided in the reuse of Beetle stock components [48].

	mmBtu or g per vehicle lifetime		
	Components	**ADR**	**Total**
Energy Use [mmBtu]:			
Total energy	18.1	12.8	30.9
Fossil fuels	16.7	11.6	28.4
Coal	6.9	5.9	12.8
Natural gas	8.2	5.5	13.8
Petroleum	1.6	0.2	1.8
Emissions [g]:			
CO_2	1425601.0	986942.6	2412543.5
CO_2 (VOC, CO, CO_2)	1441250.6	987284.1	2428534.7
CH_4	2550.1	1708.8	4258.9
N_2O	15.5	14.0	29.6
GHGs	1509633.1	1034181.4	2543814.5
VOC: Total	187.7	93.4	281.2
CO: Total	13808.5	301.3	14109.9
NO_x: Total	1509.8	1106.0	2615.8
PM_{10}: Total	2874.9	1089.0	3963.9
$PM_{2.5}$: Total	1164.5	304.2	1468.7
SO_x: Total	1941.7	1783.7	3725.4

The authors of the VW Beetle LCA developed emissions factors for electricity sources in GREET 1 to include coal, natural gas, petroleum, nuclear, hydroelectrical, geothermal, solar photovoltaic, wind, and biomass fired power plants [48]. Theses emissions factors are presented in Table 13 in the US 2010 Electricity Generation Mix column. To complement the US electricity mix, the authors then developed a second user defined electricity generation mix based on the available solar usage consisting of 70% solar, and 30% coal-fired electricity generation. This electricity generation mix was generated to simulate the original PV array employed (at an old manufacturing facility) and the North Lawrence Power Plant since the PV array was not sufficient to fully charge the vehicle (unlike the new array at the Hill Center). The generated emissions factors are shown in Table 13. For the previous GREET study, it is important to note that the solar energy was considered to be emission free. However, this assumption does not consider the energy and emissions generated by the production of the silicon solar panels that was beyond the scope of

the previous study [48]. Earlier versions of the GREET model were not conducive to modeling solar energy. Hence, the authors modified the U.S. mix emissions factors to simulate the solar PV generation at the previous manufacturing facility. For completeness, their emissions factors are included in this summary; however, recent updates to the GREET model make it easier to include solar PV generation. As a result, the emissions factors for this study are omitted because they were not modified beyond the GREET model's default assumptions.

Table 13: Emissions factors developed in GREET 1 2011 [48].

	US 2010 Electricity Generation Mix [g/kWh]	**Solar Photovoltaic/ Coal Mix [g/kWh]**
VOC	0.062	0.029
CO	0.589	0.337
NO_x	0.826	0.388
PM_{10}	0.913	0.603
$PM_{2.5}$	0.246	0.159
SO_x	1.2456	0.773
CH_4	1.828	0.490
N_2O	0.011	0.004
CO_2	693.478	360.339
CO_2 (w/ C in VOC & CO)	694.598	360.959
GHGs	743.423	374.278

When considering the different production mechanisms, it is important to differentiate between the Well-to-Pump (WtP) and Pump-to-Wheels (PtW) phases. The WtP phase includes the creation and distribution of the selected fuel source, while the PtW phase only includes driving the vehicle. In regards to electric vehicles, there are no PtW emissions [48]. Consequently, this is the reason the EPA designates electric vehicles as zero emissions vehicles [49].

After running the completed GREET model, emissions results for the US electricity consumption mix and for the solar PV/coal mix were generated as shown in Table 14. These results demonstrate the varying range of emissions for the VW Beetle when used as a BEV connected to the electrical grid or the

solar array. The main drawback presented is the lack of solar availability; as a result, the Beetle has to source energy from the coal-fired power plant to receive reliable and consistent power to charge the vehicle [48].

Table 14: Emissions results for US 2010 electricity consumption mix and the solar/coal mix [48].

	USCM EV Mode [g/mile]	Solar/Coal EV Mode [g/mile]
VOC	0.020	0.009
CO	0.190	0.109
NO_x	0.266	0.125
PM_{10}	0.294	0.194
$PM_{2.5}$	0.079	0.051
SO_x	0.402	0.249
CH_4	0.589	0.158
N_2O	0.003	0.001
CO_2	233.636	116.204
CO_2 (w/ C in VOC & CO)	223.997	116.403
GHGs	239.742	120.699

The last aspect of the 1974 VW Beetle LCA to examine is the final Well-to-Wheel (WtW) energy use. Table 15 contains the energy use for the electricity production. The results reflect the large amount of energy required in generating the electricity to power the VW Beetle in BEV mode. Overall, the solar energy source proved to be the most sustainable energy source of the different energy sources previously studied; however, the availability of the solar energy hinders it from being a reliable electricity source [48]. To accompany the VW Beetle LCA, the authors of the previous study provided literature reviews regarding the reuse of vehicle components. The next section will highlight their findings while discussing the recycled components used on the second generation EV.

Table 15: 1974 VW Beetle EV mode Well-to-Wheel energy usage [48].

	USCM EV Mode [Btu/mile]	Solar/Coal EV Mode [Btu/mile]
Total energy	2727.123	1079.173
Fossil fuels	2438.729	1078.539
Coal	1589.664	1061.137
Natural gas	789.130	2.795
Petroleum	59.935	14.606

4.4 Reuse of Vehicle Components

The previous study conducted by Strecker, et al. provided literature reviews discussing the main findings and benefits of reusing vehicle components. To help understand the impact of the reuse of materials in the JimmE-V, their main findings are presented.

Vehicle manufacturing consumes large amounts of energy, and is an important area to study when performing an EV conversion to determine which vehicle components to reuse. In 2010, ANL completed a study examining vehicle and vehicle component manufacturing in order to improve the GREET 2 model [48]. Their study yielded that the total energy use per 1532 kg vehicle was 33.9 GJ resulting in 2013 kg of CO_2 emissions [50]. The largest contributor to energy consumption and emissions was the material transformation process using 19.3 GJ of energy and emitting 1065 kg of CO_2 [50]. Previous studies conducted by the United States Council for the 1998 Automotive Research (USCAR) reported that for a traditional internal combustion engine vehicle (ICEV) 39.9 GJ of energy was consumed and 2610 kg of CO_2 emissions were produced [51]. Prior to that study, Kobayashi reported in 1997 that manufacturing a 1270 kg vehicle consumed 19.9 GJ of energy, and produced 1040 kg of CO_2 [50]. Sullivan and Cobas-Flores additionally concluded from other efforts that the vehicle manufacturing process produces 1800 to 7500 kg of CO_2 [52]. Vehicle assembly emitted 1039 to 2615 kg of CO_2, and end-of-life disposal resulted in 39 to 240 kg of CO_2 [52]. However, these results vary depending on the style and size of the vehicles [48]. To that end, the LCA for the JimmE-V is of interest because the vehicle is a larger SUV composed of more materials and components.

Reusing the larger vehicle components from an SUV prevents components from occupying landfills. Strecker, et al. additionally reviewed literature discussing the impact of the vehicle end-of-life processes due to the interest of component recycling around the globe. Daniels, et al. stated that 75% of automobile materials are recyclable, resulting in the deposit of 2.7-4.5 million tons per year of material accumulation in landfills across the United States [53]. Additionally, Chen discusses end-of-life vehicle recycling in China that resulted in an increase of reused parts rate from 22.5% to 31.7% [54]. As a result, vehicle end-of-life landfill deposits were reduced from 10% to 4% [54]. Lastly, Amelia, et al. identified component reuse as the most effective method of vehicle recycling. This method is effective due to not needing to remanufacture or reprocess the recyclable material. Consequently, component reuse is a relatively low energy intensive process because it does not require additional raw material extraction, reprocessing, and manufacturing [55]. Amelia, et al. concludes that recycling and reusing vehicle components leads to significant gains in the areas of energy, emissions, and landfill reduction. However, recycling and reusing outdated components develops safety and reliability concerns [55]. Due to the larger size of the 1997 GMC Jimmy, there is a greater potential to offset more energy and emissions by reusing the vehicle's larger components.

The original 1997 GMC Jimmy contained a 4.3 L V-6 gasoline spark-ignition engine. The engine was coupled to a four-speed automatic transmission and transfer case in order to achieve four-wheel drive. The vehicle was donated to the KU EcoHawks in 2010 after it had been involved in an accident. The original state of the vehicle is shown in Figure 175. The EV conversion process began by completely disassembling the vehicle to inspect the body and frame for damage.

Figure 175: The original 1997 GMC Jimmy prior to the EV conversion. The front end of the vehicle had been damaged in an accident prior to donation of the vehicle.

With the vehicle completely stripped of all its components, it was determined that the ladder frame had been structurally compromised, and not repairable. In order to maintain the project's suitability aspect, a frame was located from an identical vehicle in a salvage yard. This provided a net balance since the purchased frame was destined to be recycled. This allowed the damaged frame to take the place of the non-damaged frame to be recycled. The purchased frame was then cleaned and powder coated to mitigate rust and frame degradation. Before the body was fitted back to the frame (Figure 176), the chassis was updated with stiffer suspension to account for the added battery weight, and the three-phase AC motor was aligned and coupled to the rear differential.

Figure 176: The original body shell installed on the recycled frame.

Overall, the main body shell was still in usable condition; however, some of the front body panels and hood were damaged during the accident. As a result, the damaged parts were replaced with new parts,

as seen in Figure 177. Other than the front quarter panels, hood, bumper, and radiator support, all other body parts were reused (doors, windows, seats, and trim parts). To finalize the body of the JimmE-V, the entire vehicle was covered in a vinyl wrap. A wrap was chosen over paint primarily due to the cost to paint a vehicle of this size. However, wrapping the JimmE-V provided an additional sustainability feature.

Paint shops produce Volatile Organic Compound (VOC) emissions. While there are techniques in place to reduce paint booth VOC emissions, the best way to reduce VOC emissions is to reduce the amount of paint used [56]. As a result, the JimmE-V produced zero VOC emissions related to painting the body. The completed EV conversion is shown in Figure 178. As previously discussed, the JimmE-V employs a $LiFePO_4$ battery pack in contrast to the VW Beetle's lead acid battery pack. In order to further understand the well-to-wheels analysis of the vehicle, lithium battery production and recycling were examined.

Figure 177: The final body assembly with the new panels on the front of the vehicle.

Figure 178: The completed JimmE-V full-scale EV conversion.

4.5.1 Lithium Battery Production

Lithium is an ideal choice as a battery material in automotive vehicle because it is the lightest metal available. Additionally, lithium offers a high energy density while being significantly electropositive [57]. From an environmental standpoint, lithium has no noticeable toxicity effects, and has been successfully applied in treatment of mental disorders. However, excessive amounts can be fatal [58]. For an EV application, lithium iron phosphate ($LiFePO_4$) batteries offer a low cost cathode with plentiful elements, and are environmentally benign. Additionally, no obvious capacity fading is observed with these batteries, and they are stable during the charging and discharging process. Lithium iron phosphate batteries offer enhanced safety and reliable performance (Figure 179). As a result, this battery composition choice is ideal for student applications.

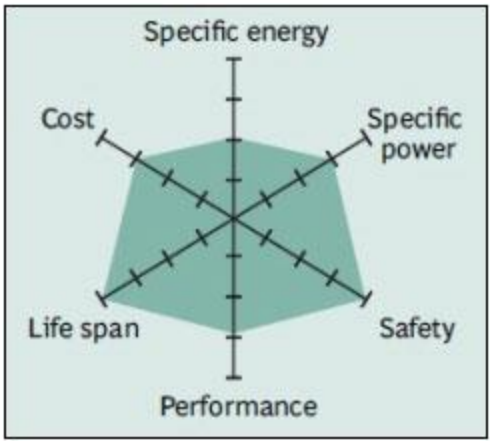

Figure 179: Overall snapshot of a typical $LiFePO_4$ battery [59].

From a production perspective, the main construction methods investigated were solid state synthesis (SS) and hydrothermal (HT) synthesis. There are other production methods available; however, ANL's GREET model only provides energy pathways for solid state and hydrothermal production synthesis production methods. Figure 180 displays the hydrothermal production path, while Figure 181 shows the solid-state path. The solid-state production pathway used in GREET follows the preparation method patented by Dai. This method combines a lithium compound, an iron compound, and a phosphorous compound [60]. Lithium iron phosphate cathodes are hydrothermally formed in an oxidizing environment by heating a hydroxide (OH) solution to 700 °C until crystalline phosphates are formed [61]. The iron sulfate needed for hydrothermal synthesis is provided from a waste product from the steel industry; therefore, this production method does not have any additional adverse energy or environmental influences [62].

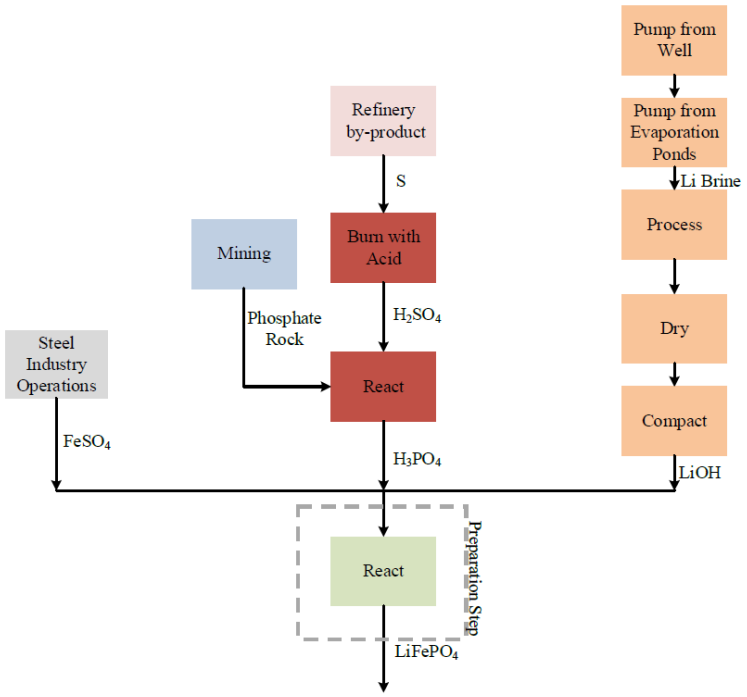

Figure 180: GREET hydrothermal production path for $LiFePO_4$ batteries [62].

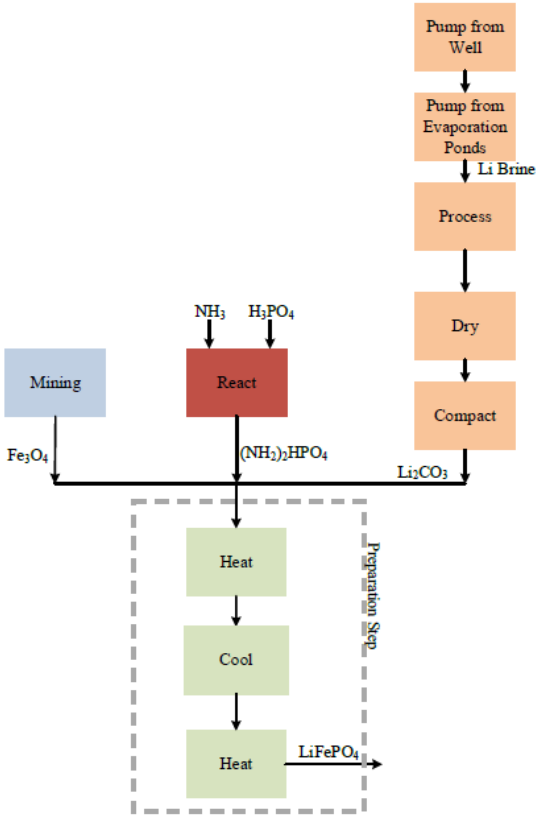

Figure 181: GREET solid-state production path for $LiFePO_4$ batteries [62].

Table 16 shows the energy consumption used in the two discussed production methods in this section. In addition to energy consumption, Table 16 also shows the energy consumption and percent contributions from the preparation step. Lastly, the major input factor and its contribution percent are shown for each process [62]. By comparing the HT results in Table 16 to the production path in Figure 180, it is observed that the preparation step for hydrothermal synthesis consumes the majority of the energy in the production path. This is attributed to the energy required to heat up and maintain the solution temperature until the phosphate crystalizes. Conversely, comparing the SS results in Table 16 to the solid-state production path in Figure 181 shows that the mining of the Fe_3O_4 is the largest energy consumption factor. From ANL's findings in Table 16, it is observed that the cathode preparation step for solid-state synthesis consumes less energy in comparison to hydrothermal synthesis. Therefore, it is observed that the hydrothermal production technique consumes more energy than the solid-state method. Understanding the difference between these results is important when considering the production technique to use in the developed GREET model. In order to further understand the sustainability of lithium used for battery applications, the recycling of lithium batteries will be examined.

Table 16: GREET total energy consumed for $LiFePO_4$ cathode material [62].

Cathode Material	Energy Consumption [mmBtu/ton]	Preparation Step		Major Contribution to Energy Consumption	Contribution [%]
		Energy Consumed [mmBtu/ton]	Contribution to Total [%]		
$LiFePO_4$ (HT)	48	35	71	$LiFePO_4$ preparation	71
$LiFePO_4$ (SS)	39	6	16	Fe_3O_4	40

4.5.2 Lithium Battery Recycling

As hybrid and electric vehicles begin to gain more of the consumer vehicle market share, another important aspect to consider is the recycling of the lithium batteries used in vehicle battery packs. Due to the availability of lithium, it is pertinent to review the literature regarding the techniques available for lithium battery recycling. In this area, lithium battery recycling is still in its infancy, but several authors

have identified the need to implement recycling processes and techniques for high-energy lithium based battery packs.

High voltage batteries for automotive applications are expected to increase over the next few years as hybrid and electric vehicle production continues to increase as a methodology of reducing CO_2 emissions while satisfying Corporate Average Fuel Economy (CAFE) standards. Consequently, concerns have been accumulating regarding the disposal of automotive batteries at the end of their in-vehicle lives. With increasing environmental regulations and a greater corporate responsibility focusing on sustainability, battery recyclability and use in secondary applications have been examined [63]. For example, Mackintosh mentions that due to the increased focus on sustainability, using landfills for discarded batteries does not appear to be a practical long term plan, and the European Union already prohibits batteries used in transportation from entering landfills [63].

Despite the potential use of large battery packs in secondary applications (e.g., grid storage [64]) after their in-vehicle life, there is a definitive end of life (EOL) for these batteries. As a result, they will need to be recycled to avoid landfills [63]. In order to address the EOL concerns of automotive batteries, the Society of Automotive Engineers (SAE) Battery Steering Committee set up a group focused on battery recycling. This SAE committee developed a standard regarding the recommended practice to identify battery chemistry. The goal of the standard, SAE J2984 Identification of Transportation Battery Systems for Recycling, is to help make the recycling infrastructure more efficient. Mackintosh suggests that a more efficient infrastructure, such as that proposed by SAE, will lead to an increased yield of EOL battery recycling [63].

Once removed from the vehicle, battery packs will appear as “black boxes” coming in a variety of shapes and sizes. Battery chemistry identification is the key to successfully recycling automotive batteries. For battery packs already in use, Mackintosh addresses the need for these packs to be identified at the service level. The service level offers an opportune time to identify previously unidentified battery modules in the event individual cells or the pack need to be replaced as the defective cells will need to be recycled as well [63].

Battery recyclers are generally set up to extract lead (Pb), nickel (Ni), and cobalt (Co) materials. Ni and Co are the present materials in many lithium-ion (Li-ion) batteries that recyclers are interested in extracting [63]. Furthermore, Mackintosh states that lithium iron phosphate (LFP) and lithium manganese dioxide (LMO) have no or little valuable metals to extract. Phosphate based batteries can cause contamination issues with other recycling paths and will likely need to be separated from other chemistries in order to mitigate corruption [63]. By identifying the chemistry, the battery owner will be enabled to find the best recycler, secondary application, or EOL process most suitable for the battery pack.

Current identification processes includes a National Electrical Manufacturers Association (NEMA)/American National Standards Institute (ANSI) standard that provides a single letter to designate the battery system. While this system provides high level identification of the battery system, Mackintosh states that this does not provide enough details for battery recyclers. The SAE Battery Recycling committee has recommended using a color coded system consistent with the Battery Association of Japan (BAJ) to avoid duplication efforts and end user confusion. While the SAE committee method is similar, it additionally expands on the BAJ method to provide more Li-ion chemistry and miscellaneous property information pertinent to battery recyclers [63].

Mackintosh concludes that a common battery identification system that provides sufficient chemistry information will serve as a significant asset to the recycling and secondary application industry. A more efficient recycling industry results in properly recycled batteries previously bound for landfills [63]. Similar to Mackintosh, Jody, et al. agree that hybrid vehicle battery materials are expensive, and without recycling, the raw materials could soon be in short supply [65]. While Jody, et al.'s focus is on the entire recycling and EOL process for lightweight materials and hybrid vehicle components, only the information regarding battery recycling is presented. Due to the increased demand for hybrid vehicles, increased amounts of nickel, cobalt, and lithium are required for high voltage battery applications. As a result, recycling these materials is necessary to maintain their economic availability while helping prevent environmental pollution [65]. While they highlight the percentage of recycled automotive materials, their

main findings are that the recycling industry is lacking the technology that will allow the recovery, purification, and recycling of hybrid vehicle materials [65].

In agreement with Mackintosh, Howes addresses the need to recycle advanced lithium batteries to meet the growing demand for hybrid and electric vehicles. He acknowledges that the lithium industry in in its infancy and in order to have a successful commercial lithium recycling industry, their performance needs to be comparable in scale to the lead-acid battery recycling industry [66]. In order for the emerging lithium recycling industry to be successful depends on four factors:

1. The cost of the recycled lithium needs to be equal or less than the cost of "virgin" lithium. At the time of this study, Howes indicates that this is currently not the case with recycled lithium exceeding the cost of virgin lithium by 10 to 20 percent [66].
2. For a large-scale lithium recycling industry to be successful, a large "pool" of batteries with a standardized design must exist so that lithium and other materials can be easily extracted [66]. This statement agrees with Mackintosh's premise of implementing a standard battery identification method. However, battery pack design has yet to become standardized amongst automotive manufacturers.
3. Additionally, a collection and delivery system needs to be established to supply facilities with sufficient volume flow of material. Currently, California, New York, and Rhode Island are moving aggressively to establish such collection and delivery systems [66].
4. The policies developed at the federal government level can have a large effect (positive or negative) on the success of lithium battery recycling initiatives [66]. The U.S. Department of Energy (DOE) and Environmental Protection Agency (EPA) will play vital roles in the development of an industry to recycle advanced batteries used in hybrid, plug-in hybrid, and electric vehicles. The DOE and EPA have supporters and detractors in their works to establish an advanced battery recycling industry. However, those in the public and private sectors are hopeful that the lithium recycling will achieve an equivalent performance rate equivalent to the lead-acid battery and vehicle recycling industry [66].

In order to further illustrate the hurdles that the emerging lithium battery recycling industry has to overcome, Howes discusses three main approaches to recycling advanced lithium batteries: pyrometallurgy, hydrometallurgy, and direct recycling. Both pyrometallurgy and hydrometallurgy are well established processes. Pyrometallurgy utilizes high temperatures to downgrade material to a metallic state for sale as base metals. Hydrometallurgy implements aqueous chemicals to solubilize material for precipitation or electrowinning in further processes [66]. Direct recycling requires specific unit operations that are utilized to separate different materials into concentrates that are then reintroduced back into the battery production process [66]. Despite Li-ion batteries being the conventional choice to provide portable consumer electronics power, recycling companies continue to struggle with developing recycling processes that accommodate a wide variety of feedstock types on a large scale.

Howes concludes by highlighting the success of the lead-acid recycling industry and its ability to provide a "closed-loop, life cycle process". With the use of lithium in automotive batteries and other consumer products, the need for a similar process for lithium will continue to become more apparent. The projected growth and sales of electric and hybrid vehicles will provide an abundant feedstock for the emerging lithium recycling industry allowing further growth and development. However, it is unknown whether lithium recycling can reach the scale of lead-acid recycling [66].

Based on the information available in the literature reviews presented, advanced lithium composition batteries are an ideal choice when designing and fabricating a modern EV. However, due to the lack of a recycling process, the EOL sustainability of lithium batteries is not an ideal choice when compared to the previous efforts lead-acid pack in the VW Beetle that is 99% recyclable [57]. With both the production and EOL processes examined for advanced lithium batteries, the outcomes of JimmE-V LCA study will be discussed next.

4.6 Outcomes of this Study

The objective of this study is to perform a LCA on the JimmE-V utilizing ANL's GREET2_2014 (GR2) coupled with GREET1_2014 (GR1). For further context on how GR1 and GR2 calculate a vehicle

LCA, Figure 182 shows the two different paths analyzed for the vehicle's LCA. GR2 calculates the vehicle manufacturing cycle, while GR1 calculates the fuel (i.e., electricity) cycle path. To finalize the LCA, GR2 imports data from GR1 to provide a complete LCA. It is important to note that since the JimmE-V is a BEV, the Pump-to-Wheels (PtW) analysis is simply the battery pack energy consumption with no emissions produced from the vehicle. The generated results will be used to examine the energy and environmental benefits from recycling the larger JimmE-V vehicle components. This study will additionally compare LCA results for both of GR2's recently added (October 2014) lithium production pathways focusing on $LiFePO_4$ cathode materials. Lastly, the modelled emissions produced from the electricity needed to charge the batteries in the JimmE-V will be examined. In order to compare this study to the previous Beetle LCA efforts, four electricity generation methods will be analyzed. These generation methods include the US generation mix, a regional electricity generation mix for the state of Kansas, a 70% solar and 30% coal mix to correspond to the previous study, and a 100% solar generation simulation to examine the benefits of the new Hill Center facility's larger solar array. JimmE-V drive cycle data will additionally be presented to examine the efficiency of the second generation EV produced at the University of Kansas.

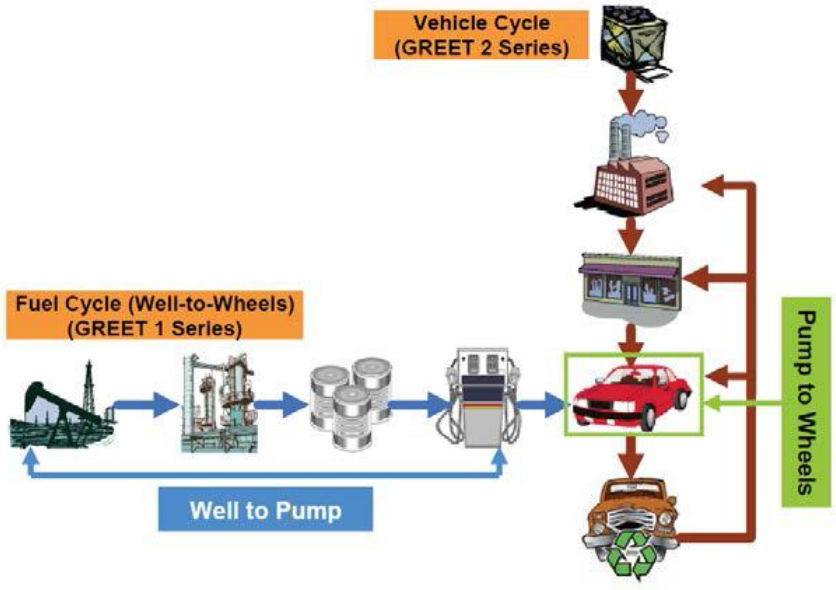

Figure 182: GREET model total energy cycle for transportation technologies [67].

4.7 GREET Recycling and Reuse Energy and Emissions Analysis

One of the efforts that this study examines includes the environmental benefits of recycling the larger JimmE-V body parts. This is achieved through a full energy and emissions analysis of GR2 coupled with GR1. GR2 calculates the energy and emissions over a vehicle's lifetime by using a by-weight ratio. The LCA calculated using GR2 includes the vehicle production stages including the material mining, processing, and final assembly [68].

In order to determine the by-weight characteristics of the JimmE-V, the default GR2 material assumptions for an LDT 1 were assumed. The gross vehicle weight (GVW) of the JimmE-V is 1,998 kg (4,405 lbs). This provided a reasonable starting point to change vehicle weight assumptions. The main assumptions employed centered on altering the powertrain component weights. The AC55 three-phase AC induction motor weighs 106 kg (233.7 lbs). Additionally, the DMOC445 motor controller and inverter adds an additional 14.7 kg (32.4 lbs) to the weight of the JimmE-V. GR2 does not require the weight of the batteries; however, it is important to note that each of the $LiFePO_4$ cells weights 3.2 kg (7 lbs). Overall, the batteries contribute 330.2 kg (728 lbs) to the total vehicle weight not including the battery box materials. This makes the batteries the largest weight component to the JimmE-V excluding the body and frame. GR2 does require the weight of any secondary batteries implemented in a vehicle. The JimmE-V utilizes two auxiliary lead acid batteries to power 12 VDC components. Overall, both of these batteries weigh 34.3 kg (75.6 lbs).

Once the powertrain assumptions were altered, GR2 automatically adjusts the weight percentage values to reflect the updated changes. After adjustment, GR2 re-calculates the body weight (excluding $LiFePO_4$ batteries) automatically to ensure that the total vehicle weight percent reflects 100%. Overall, the vehicle chassis is 32.8% of the total vehicle weight, and the body (including paint, interior, exterior, and glass) is 56.3% of the total vehicle weight. The GR2 calculated ADR results for the JimmE-V are presented in Table 17. The results presented have been separated by emissions species and energy type used in each process.

Table 17: GR2 calculated emissions and energy use avoided in the reuse of Jimmy stock components.

	mmBtu or g per vehicle lifetime		
	Components	**ADR**	**Total**
Energy Use [mmBtu]:			
Total energy	27.2	16.0	43.2
Fossil fuels	25.4	14.5	39.9
Coal	7.5	5.6	13.1
Natural gas	17.5	8.7	26.2
Petroleum	0.4	0.2	0.6
Total Emissions [g]:			
CO_2	1751438.9	1095190.6	2846629.5
CO_2 (VOC, CO, CO_2)	1759140.4	1101515.8	2860656.2
CH_4	4527.0	2347.4	6874.5
N_2O	41.9	23.2	65.2
GHGs	1906060.7	1178095.2	3084155.9
VOC: Total	1948.2	1749.5	3697.8
CO: Total	1036.9	555.3	1592.2
NO_x: Total	2162.9	1368.9	3531.8
PM_{10}: Total	448.5	310.9	759.4
$PM_{2.5}$: Total	271.9	187.0	459.0
SO_x: Total	2660.7	2068.9	4729.5

Overall, the final JimmE-V weight was reduced 202 kg (445 lbs) from the stock Jimmy's GVW of 2200 kg (4850 lbs) [69]. This includes the additional weight incurred by the two $LiFePO_4$ battery boxes and battery box materials. It is estimated that approximately 635 kg (1,400 lbs) was removed during the conversion process. This includes the IC engine, automatic transmission, transfer case, front differential, gasoline tank, and spare tire. Comparing the results from Table 17 and Table 12, it is observed that the JimmE-V consumes more energy and fossil fuels to manufacture than the VW Beetle; however, this results in a greater energy and emissions offset during the ADR process. This is attributed to the JimmE-V being a larger SUV as compared to the smaller VW Beetle. Of note, during the component manufacturing process, the Jimmy petroleum use and CO emissions are lower compared to the VW Beetle. Because of the length of time in-between these two studies, this may be attributed to advances in

technology and more stringent emissions restrictions along with a potentially lower amount of petroleum used during the vehicle manufacturing process (perhaps also better experimental data employed in the GREET model). Overall, the JimmE-V body and frame may have required more materials and energy to manufacture; however, by reviewing the literature and the previous efforts, these results provide additional support to the decision to reuse the original vehicle's larger components to avoid these energy intensive processes.

In addition to the energy and emissions offset by reusing the stock Jimmy components, this study examines the energy and emissions produced during the $LiFePO_4$ manufacturing process. These values are tailored specifically to the 35 kWh battery pack in the JimmE-V. Of note, the original Beetle LCA efforts do not include the energy and emissions produced during the lead-acid battery pack manufacturing process; hence, a direct comparison cannot be accomplished. The energy and emissions results for the two LFP cathode production methods are shown in Table 18. These results confirm the data shown in Table 16 showing that the hydrothermal production technique remains an overall more energy intensive process compared to solid-state production. However, the solid-state production method consumes more coal produced energy, and produces more VOC, CO, NO_x, PM_{10}, $PM_{2.5}$, and SO_x emissions.

Table 18: Energy and emissions associated with battery assembly per vehicle lifetime for HT and SS lithium cathode production techniques.

	mmBtu or g per vehicle lifetime	
	HT	SS
Energy use [mmBtu]:		
Total energy	28.47	26.71
Fossil fuels	26.34	24.33
Coal	10.06	10.58
Natural gas	12.14	9.84
Petroleum	4.14	3.90
Total Emissions [g]:		
CO_2	1832755.49	1734385.05
CO_2 (VOC, CO, CO_2)	1836386.95	1738232.60
CH_4	4630.90	4036.63
N_2O	36.66	30.55
GHGs	2019601.44	1901999.69
VOC: Total	455.73	519.11
CO: Total	1407.06	1418.87
NO_x: Total	2809.51	2916.11
PM_{10}: Total	1795.20	1826.19
$PM_{2.5}$: Total	943.28	987.93
SO_x: Total	14815.71	16301.99

4.8 GREET Electricity Energy and Emissions Analysis

In order to examine the energy use and emissions produced from the JimmE-V fully, GR1 and GR2 were utilized to analyze the electricity production. This work examines four different electricity generation methods: U.S. generation mix, Southwest Power Pool (SPP) mix, a 70% solar/30% coal generation mix, and 100% solar generation. The U.S. generation mix is an average electricity generation mix that implements coal, natural gas, nuclear, wind, solar, and other generation methods. The SPP mix was a regional mix selected for the state of Kansas (Figure 183). The 70% solar/30% coal mixture was created to simulate the previous effort's solar array. Lastly, the 100% solar generation method was created to simulate the larger solar capacity produced by the Hill Center.

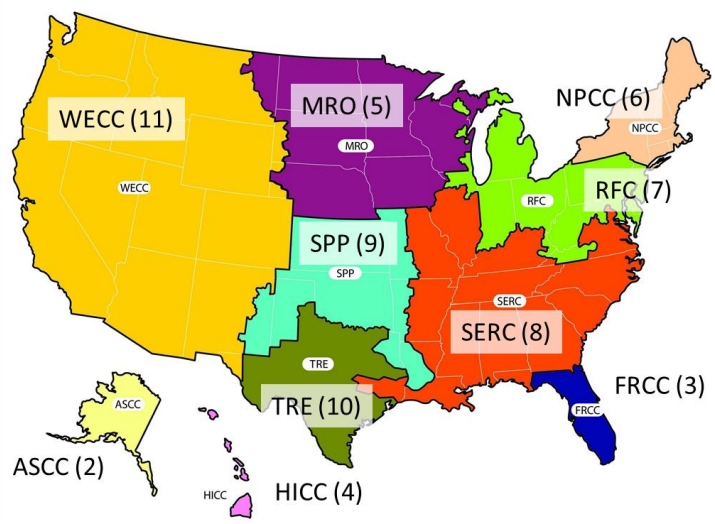

Figure 183: GR1 map for regional electricity generation mixes [70].

In order to complete the WtW analysis of the JimmE-V, every process up to the electrical outlet needs to be examined. Consequently, the analysis becomes a WtP analysis with the electrical outlet being the 'pump'. Once the vehicle is charged, no emissions are directly produced from the vehicle during operation. Solar energy is considered 'clean' aside from the solar panel production. The solar panel production is beyond the scope of this study because it requires the creation of the power plant (i.e., the solar panels). GR1 was used to analyze the electricity production for the vehicle LCA. The electricity generation does not vary between the battery manufacturing processes examined in this study. As a result, only the four main generation mixes are presented. Drive cycle data is not implemented in the GR2 model, but it is examined later to compare the efficiency of the JimmE-V to the Beetle under similar operating conditions. The GR2 model bases vehicle LCA calculations on the vehicle's lifetime mileage which was the default 180,000 miles provided by ANL's research. While the JimmE-V will not likely travel 180,000 miles, that mileage represents ANL's research on consumer vehicle lifetime mileage [68]. While the previous study does not mention the Beetle's lifetime mileage used in the GR2 simulation, discussions with the previous author indicate that the default assumption was used for a similar reason. Thus, both vehicles were modeled using similar lifetime mileage assumptions.

Table 19 shows the emissions results related to the electricity production including the mining, processing, transportation, and consumption of the power plant fuel. Similarly, Table 20 shows the electricity energy production results. From these results, it is observed that the 100% solar generation is the cleanest form of electricity production. This provides the ideal generation case for the Hill Center. However, since the solar panels are not constantly generating power, energy will need to be provided by a power plant. The 70/30 solar coal mix provides a reasonable energy and emission balance when the solar panels may not be at their peak generation capabilities (and aids consistency between the two LCA studies). During night hours and when cloud cover is present, the solar panels will be unable to provide power to charge the JimmE-V. To this end, the U.S. and SPP mix provides energy and emissions approximations for two different electric generation mixes. The main differences between the U.S. mix and SPP regional mix for Kansas is the distribution of electrical generation.

Table 19: GR1 WtW electricity production emissions results.

	U.S. Mix [g/mile]	**SPP Mix [g/mile]**	**70/30 Solar Mix [g/mile]**	**100% Solar [g/mile]**
VOC: Total	0.031	0.032	0.014	0.000
CO: Total	0.093	0.135	0.024	0.000
NO_x: Total	0.354	0.470	0.199	0.000
PM_{10}: Total	0.107	0.112	0.078	0.000
$PM_{2.5}$: Total	0.059	0.069	0.040	0.000
SO_x: Total	0.730	0.719	0.503	0.000
CH_4	0.479	0.483	0.226	0.000
N_2O	0.004	0.005	0.002	0.000
CO_2 (w/ C in VOC & CO)	282.631	286.721	154.256	0.000
GHGs	298.191	302.549	161.699	0.000

Table 20: GR1 WtW electricity production energy results.

	U.S. Mix [Btu/mile]	SPP Mix [Btu/mile]	70/30 Solar Mix [Btu/mile]	100% Solar [Btu/mile]
Total energy	3859.194	3975.843	2776.838	1752.896
Fossil fuels	3277.091	3275.517	1548.782	0.000
Coal	2113.001	2229.828	1520.159	0.000
Natural gas	1098.649	992.809	4.804	0.000
Petroleum	65.440	52.880	23.819	0.000

To compare the electricity generation emissions results with the VW Beetle results Table 19 should be compared with Table 14. When examining the electricity production emissions, it is important to note the difference in the battery pack size difference between the Beetle and JimmE-V. The Beetle battery pack is 14 kWh [16] in comparison to the JimmE-V's 35 kWh pack. GR2 takes the battery pack size into consideration for the vehicle LCA. The difference in battery pack size accounts for the larger emissions produced to charge the JimmE-V; however, the emissions are of a similar magnitude in comparison to the Beetle. Of note, CO, PM_{10}, $PM_{2.5}$, and CH_4 emissions are lower while the remaining species of emissions are higher for the JimmE-V.

In order to compare the electricity energy required to charge both vehicles, Table 20 was compared with Table 15. These results can appear to be misleading due to GR1 labeling them as WtW results. However, Figure 182 shows that these WtW results are the results specifically for the fuel path and are not overall vehicle WtW results. In order to get the overall emissions and energy use picture, the GR2 Total Energy Consumption (TEC) results need to be examined. It was observed that the previous study did not include TEC results; however, this study does include TEC results for the JimmE-V that are discussed later. With this understanding, the GR1 emissions and energy can be compared between the Beetle and JimmE-V. After comparing the two vehicle's energy required, the JimmE-V requires more energy from the different generation fuel types than the VW Beetle. Since the emissions produced and energy consumed are directly related, the higher energy use is attributed to the JimmE-V's larger battery

pack size. However, the JimmE-V is able to source electricity from the larger solar array which lessens the energy and emissions produced from non-renewable sources.

Examination of the U.S. and SPP mix electricity generation distributions (Table 21) accounts for the difference in energy and emissions required for each process. It should be noted that the information in Table 21 is provided to illustrate the distribution of electricity generation methods that will feed into the JimmE-V LCA presented later. The SPP mix produces more emissions other than SO_x as compared to the U.S. mix. The increase in emissions between the U.S. and SPP mix is attributed to the lower percentage of natural gas and nuclear generation, and a larger percentage of coal-fired electricity generation in the region. One benefit of the SPP mix is that it utilizes a larger percentage of 'other' energy sources. These energy sources include renewable energy sources such as wind, solar, and hydroelectrical generation. Overall, both mixes provide reasonable approximations on the impact of powering the JimmE-V.

Table 21: GR1 U.S. and SPP generation mix distribution from the Annual Energy Outlook 2013.

	U.S. Mix	**SPP Mix**
Residual oil	0.5%	0.2%
Natural gas	26.1%	21.5%
Coal	41.5%	43.4%
Nuclear power	19.5%	3.0%
Biomass	0.3%	3.0%
Others	12.2%	28.9%

After examining the electricity production emissions and energy results, the GR2 TEC results were examined. GR2 imports the emissions and energy results generated by GR1 to model an overall TEC vehicle analysis. The GR2 TEC energy results are shown in Table 22 and Table 23. Due to the absence of the previous study's TEC results, these results cannot be compared with the Beetle. Since the TEC analysis includes the vehicle production processes, both the HT and SS lithium cathode results (aka battery pack manufacturing) are shown to illustrate the differences in the energy consumption from each process. It should be noted that at this point the TEC results presented in GR2 additionally represent the

total WtW energy use for the JimmE-V. These results are the combination of both fuel and vehicle paths shown in Figure 182. This is also the reason why the solar energy results shown in Table 23 are not 'clean'. However, the 100% solar results provide an approximation of the energy required to produce a vehicle similar to the JimmE-V when the vehicle can be charged purely from solar energy.

Table 22: GR2 TEC energy results.

	US Mix		SPP Mix	
	HT [Btu/mile]	**SS [Btu/mile]**	**HT [Btu/mile]**	**SS [Btu/mile]**
Total energy	4607.659	4597.874	4734.178	4724.117
Fossil fuels	3977.260	3966.058	3977.693	3966.436
Coal	2427.453	2430.357	2552.580	2555.521
Natural gas	1414.977	1402.184	1303.715	1290.923
Petroleum	134.831	133.516	121.398	119.992

Table 23: GR2 TEC solar energy results.

	70/30 Solar Coal Mix		100% Solar	
	HT [Btu/mile]	**SS [Btu/mile]**	**HT [Btu/mile]**	**SS [Btu/mile]**
Total energy	3525.303	3515.518	2501.362	2491.577
Fossil fuels	2248.951	2237.749	700.170	688.967
Coal	1834.610	1837.514	314.451	317.356
Natural gas	321.132	308.340	316.327	303.535
Petroleum	93.209	91.895	69.391	68.076

Based on the information presented in Table 16, it is evident in the vehicle's TEC analysis that the HT cathode manufacturing method requires more energy than the SS procedure. As a result, it is important to consider both processes unless the direct manufacturing method is known. Hence, examining both methods provides a range of energy requirements to produce a BEV. An additional aspect to consider when examining the environmental benefits of a BEV is the WtP emissions produced from manufacturing the vehicle combined with the emissions produced from the electricity generation required to power the vehicle. The GR2 TEC emissions results for the JimmE-V simulation are shown in Table 24.

Table 24: GR2 TEC emissions results.

	US Mix		SPP Mix		70/30 Solar Coal Mix		100% Solar	
	HT [g/mile]	SS [g/mile]	HT [g/mile]	SS [g/mile]	HT [g/mile]	SS [g/mile]	HT [g/mile]	SS [g/mile]
VOC: Total	0.380	0.381	0.382	0.382	0.364	0.364	0.350	0.350
CO: Total	0.286	0.286	0.332	0.332	0.218	0.218	0.194	0.194
NO_x: Total	0.425	0.425	0.551	0.552	0.271	0.271	0.071	0.072
PM_{10}: Total	0.140	0.140	0.145	0.145	0.111	0.111	0.053	0.054
$PM_{2.5}$: Total	0.076	0.076	0.086	0.087	0.057	0.058	0.024	0.024
SO_x: Total	1.007	1.016	0.995	1.003	0.780	0.789	0.277	0.285
CH_4	0.602	0.599	0.606	0.603	0.349	0.346	0.123	0.119
N_2O	0.006	0.005	0.006	0.006	0.004	0.003	0.001	0.001
CO_2 (VOC, CO, CO_2)	336.587	336.041	341.092	340.543	208.209	207.664	53.953	53.408
GHGs	356.419	355.766	361.221	360.563	219.924	219.271	58.225	57.572

Similar to the energy results, the TEC emissions results also depend on the battery manufacturing technique implemented during the vehicle manufacturing process. By employing a rage of electricity generation methods, emissions estimates are their lowest when the vehicle is charging from the Hill Center's solar array (as expected). Conversely, emissions are at their maximum when relying on the U.S. or SPP generation mix. These results show the benefit of having the larger solar array due to its assistance in reducing the vehicle's emissions produced by power plants. Overall, the GREET model is a useful tool to provide energy and emissions estimates for different vehicle types, specifically the JimmE-V BEV. Another important aspect to consider along with the energy and emissions produced is how efficient the vehicle operates.

4.9 Drive Cycle Results

In order to determine and compare the driving efficiency between the VW Beetle and JimmE-V, the route used in this study is identical to the route used in the VW Beetle efforts. However, the route does deviate slightly due to a permanent road closure, and a different starting location. The route and elevation profile shown in Figure 184 was traveled clockwise and covers 22.3 miles; whereas, the route in the previous study was 21.2 miles. Overall, the route used in this study provides different vehicle speeds

ranging from 20 mph to 65 mph, along with a variety of elevation changes. The route drive cycles were data logged using different components installed in the JimmE-V with all component specifications provided in Table 25. The motor controller provides motor information via CAN bus, and the battery management system collects battery pack information via RS232 communication. The main component differences between the VW Beetle and JimmE-V is the transmission (or lack of), motor selection, and the battery pack chemical composition. Additionally, the JimmE-V has power steering, air-conditioning, and heating elements available for driver comfort. Of note, while regenerative braking is an option in the JimmE-V, it was not employed for this effort in order to quantify its effect in follow-up efforts.

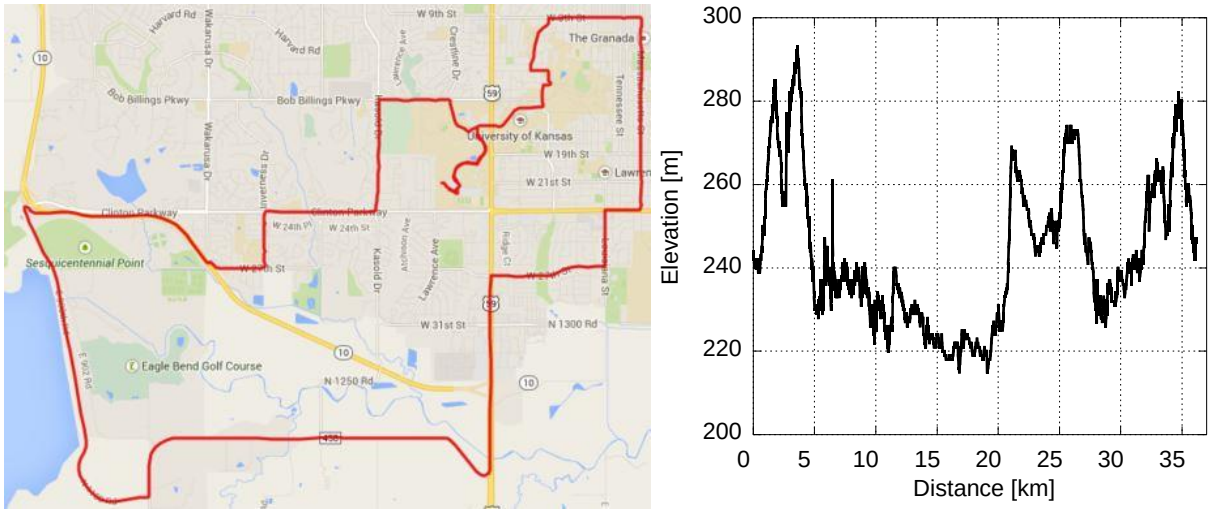

Figure 184: Drive cycle route map (left) along with elevation profile (right) for Lawrence, Kansas.

Table 25: 1997 JimmE-V specifications.

Transmission	None. Direct drive with final drive ratio of 3.08
Drive motor	Azure Dynamics AC55 three-phase induction motor
Motor controller	Azure Dynamics DMOC445, CAN controlled
Battery pack	CALB $LiFePO_4$ 330 VDC, 100 Ah
Battery management system	Elithion Lithiumate Pro
Battery charger	Manzanita Micro PFC-20
12 VDC battery	x2 Optima D75/25 deep cycle batteries in parallel, 48 Ah each
AC compressor	Masterflux 025F0140-003
Power steering pump	Toyota MR2 electric power steering pump
Heater	Road Worthy Back Seat Heater Plus
DC-DC converter	MES-DEA 1000 W
Tire size	235/65R17
Vehicle weight	1998 kg

The author drove the drive cycle route three times while a passenger accompanied the author to assist in data acquisition allowing the author to focus on consistently driving the vehicle (note: this was similarly done for the Beetle). Overall, the route's average speed was 30.3 mph covering 1,706 ft of climbing, 1,723 ft of descending, and a total cumulative elevation change of 3,429 ft. Due to the permanent road closure, this study had a larger change in elevation due to the new route's additional elevation changes to detour the closed road. The motor controller and BMS were set up to log vehicle data every second and produce a comma-separated value (CSV) file and text file for post processing. The drive cycle testing statistics are shown in Table 26. The average current drawn from the JimmE-V's battery packs was 30.6 A over the three testing cycles with a maximum current of 244.4 A, 243.4 A, and 234.8 A for each respective test. To examine the vehicle's efficiency, the kWh/mi ratio was calculated using the energy consumed and the total distance traveled. In addition to this ratio, another important metric of evaluating EV efficiency is its miles per gallon equivalent (mpg_e) rating. The Environmental Protection Agency (EPA) calculates the fuel economy of EVs using an equivalency factor of 33,705 Wh per gallon of gasoline [49]. Using the EPA's gasoline equivalency factor, the JimmE-V achieved a maximum efficiency of 0.390 kWh/mi and 86.4 mpg_e. Overall, the JimmE-V averaged 0.405 kWh/mi and 83.3 mpg_e over the three drive cycle tests.

Table 26: JimmE-V drive cycle route statistics from three driving tests.

Test date:	Test time [s]	Energy used [kWh]	Efficiency [kWh/mi]	Efficiency [mpg_e]	Starting voltage [VDC]	Final voltage [VDC]	Average current [A]	Avg. vehicle speed [mph]
3/20/2015	3236	8.7	0.390	86.4	345.4	327.9	30.8	26.3
3/27/2015	3419	9.3	0.417	80.8	345.2	326.6	30.9	23.7
2/28/2015	3414	9.1	0.408	82.6	345.1	327.4	30.0	24.3

During each drive cycle test, the author focused on maintaining the posted speed limits; however, weather conditions over the three testing cycles varied. Wind speed and direction can affect a vehicle's performance, while ambient temperature can affect the battery pack's performance [16]. To this end, the wind speed, direction, and temperature are presented in Table 27. Overall, there are not significant variations in the data, and the testing conditions were relatively similar.

Table 27: Drive cycle test weather conditions [70].

Test date:	Wind speed [mph]	Wind direction [-]	Temperature [°F]
3/20/2015	4	WSW	65
3/27/2015	8	N	45
2/28/2015	9	SE	54

Comparing these efforts to the previous efforts on the VW Beetle, the JimmE-V has a lower efficiency and mpg_e rating. However, considering that the original GMC Jimmy achieved 15 mpg city, 20 mpg highway, and 16 mpg combined, the vehicle's efficiency has been significantly increased [71]. The VW Beetle in BEV mode achieved an average efficiency of 0.318 kWh/mi and an average EPA fuel economy rating of 105.9 mpg_e. In comparison, the JimmE-V does not fall far from those standards considering the vehicle's larger size and weight. In order to examine a more direct comparison metric, a ratio of the vehicle's average mpg_e to the vehicle's weight was taken. The Beetle produces a $mpg_e/kg_{vehicle}$ ratio of 0.09, while the JimmE-V's ratio is 0.04. Based on this metric, the Beetle achieves a higher fuel economy rating per kg of vehicle weight making it more efficient than the JimmE-V. For completeness, the solar array for charging the JimmE-V is presented in the next section.

4.10 Hill Center Solar Array

The initial Beetle study implemented a 1.1 kW solar array consisting of six monocrystalline panels on top of an old barn at the University of Kansas [48]. In June 2013, the University of Kansas dedicated the Hill Engineering Research and Development Center to house the EcoHawks design projects. The Hill Center was designed and built by Studio 804 students who focus on implementing sustainability into their building designs. In addition to using recycled materials for the building project, the Hill Center additionally features a 14.8 kW grid tied solar array. Forty-five Suniva Optimus Series monocrystalline solar modules were installed on the roof of the facility, and twelve Lumos LSX250 Series monocrystalline panels were installed as an awning over the facility entrance as shown in Figure 185. In order for the solar panels to be tied to the grid, each panel utilizes the Enphase Energy M215 microinverter. These inverters have a maximum output of 215 W and have a peak efficiency of 96.3% [72]. While the solar panels on the awning are flat and affected by the building shade in the afternoon, the solar panels on the roof are tilted at ten degrees. The Suniva panels have a module efficiency of 16.02% [73], while the Lumos have a module efficiency of 15% [74].

Figure 185: The Hill Engineering Research and Development Center solar arrays. The roof panels (left) provide 11.7 kW, and the front awning (right) provides 3.1 kW.

The combined surface area of the solar array is important to consider when examining the energy availability from the Hill Center's solar array. The forty-five panels on the roof each measure 1.652 m by 0.982 m providing the roof with 73.00 m^2 of solar panel area. The twelve flat panels on the front awning each measure 1.664 m by 1.041 m resulting in a total surface area of 20.79 m^2. The total combined solar

panel surface area of the Hill Center is 93.79 m^2. This is a large improvement over the previous study's solar area of 8.06 m^2 [48]. Under ideal conditions, the solar panels on the roof of the Hill Center provide 11.7 kW of energy, and the awning provides 3.1 kW of energy. As a result, the larger solar panel area of the Hill Center has a larger power capacity (14.8 kW) when compared to the facility used in the previous study (1.1 kW) [48].

The previous effort implemented a Micro Circuit Labs SDL-1 Solar Data Logger to measure and record the solar irradiance for the previous EcoHawks facility. Data was collected over the course of 2011 and yielded an average daily solar irradiance of 4.44 kWh/(m^2-day) [48]. Since the Hill Center is less than half a mile away from the previous location, this data is considered valid for the Hill Center location. The Kansas Corporation Commission (KCC) reported that the yearly average for Topeka, Kansas (approximately 28 miles) was 4.07 kWh/(m^2-day) for a fixed tilt solar array [75]. The study conducted by KCC analyzed solar data from 1991 until 2005 to mitigate any variations in weather patterns. Overall, the larger solar array at the Hill Center provides a sustainable method for charging both vehicles at the University of Kansas.

4.11 Conclusion

This work provides a Well-to-Wheel energy and emission analysis of a plug in battery electric vehicle conversion from a 1997 GMC Jimmy generated by GREET2_2014 coupled with GREET1_2014. In addition to the JimmE-V life cycle analysis, lithium cathode manufacturing and recycling techniques were investigated to further examine the sustainability of lithium battery materials. This study highlights the benefits of reusing larger vehicle components in full-scale electric vehicle conversions. One drawback is that larger vehicles require more energy and materials to initially produce. Although EVs produce zero local emissions during vehicle operation, it is important to understand the energy and emissions on a global spectrum. To this end, this work examines the energy requirements and emissions produced based on four electricity generation methods for each lithium cathode manufacturing process. Overall, the generated results provide an estimated range of energy and emissions based on the amount of solar energy

produced by the Hill Center's solar array. To examine the efficiency of the JimmE-V further, drive cycle tests were completed using a nearly identical route to the previous study's efforts involving the 1974 VW Beetle PHEV conversion. Overall, the kWh/mi efficiency and mpg_e rating are smaller in comparison to the VW Beetle. However, due to the JimmE-V's larger size and weight, 83.3 mpg_e is a large improvement on the vehicle's original fuel economy specifications. Lastly, in order to examine the solar capabilities of the Hill Engineering Research and Development Center's larger solar array, information was provided in regards to the generation capacity and surface area required by the building's monocrystalline solar panels. Overall, the larger solar array provides a sustainable EV charging station when solar energy is available.

Chapter 5: Conclusions and Future Work

The 1997 GMC Jimmy EV conversion is the result of three years of design and research from the KU EcoHawks. While the JimmE-V is larger in comparison to the VW Beetle, the vehicle's size is representative of the SUV market in the United States. With low fuel economy and high emissions, these vehicles are suitable candidates for electric vehicle conversions. Of note the original Jimmy had a combined fuel economy rating of 16 mpg, while the EV conversion achieved 83.3 mpg_e.

With the project starting in 2010 and reaching completion in 2013, the author was involved with the JimmE-V project from 2011 until 2015. During this time the author was involved in many different aspects of the vehicle conversion process. While on the EcoHawks senior design team from 2011 to 2012, the author was focused on installing the vehicle's motor controller and getting it fully operational. The original team in 2010 had intended that a simple potentiometer be used as the vehicle's accelerator pedal; however, through the author's research that method would severely limit the functionality of the vehicle. This was an undesirable characteristic for a research institution, and as a result the author needed to further research the controller's specifications. After designing and installing the aluminum sub-frame under the hood of the vehicle and installing the motor controller, the author located the control system company New Eagle. Numerous phone and email conversations yielded results for the JimmE-V's ECM. Throughout the consulting process with New Eagle the author additionally contributed to the vehicle assembly process as needed and installed the vehicle's audio entertainment system. Through the author's research regarding CAN communication the ECM and DMOC445 controller were synchronized and first communicated in the spring of 2013. Once the ECM and controller were communicating, the motor was then provided power resulting in the rotation of the rear wheels. However, over the course of initial testing it was determined that the initial ECM was too simple for its application. Often New Eagle would need to be contacted to reprogram calibration files since that option was unavailable. During the summer of 2013 an upgraded ECM was sourced and installed using the existing wiring from the previous ECM. The new module allowed the JimmE-V ECM system to be monitored and calibrated in real-time during

vehicle operation. Once the high voltage system was installed and connected to the motor controller, the author's focus shifted to calibrating the powertrain system.

Vehicle calibration was achieved through testing. The author examined different parameters that effected vehicle drivability and systematically adjusted parameters until a desirable result was achieved. Since Azure Dynamics went bankrupt in 2012 this process was difficult due to the lack of technical support available for the JimmE-V motor and controller. However, through trial and error testing the author was able to resolve vehicle acceleration and top speed issues. Getting the vehicle's powertrain system fully functional was the author's significant main contribution.

Once the vehicle proved to be road ready, the author then assisted with the vehicle licensing process to provide the necessary information required by the state of Kansas to make the vehicle street legal. In addition to focusing efforts on the motor, controller, and ECM the author was simultaneously learning about the vehicle's battery pack. This knowledge proved valuable during vehicle drive cycle tests when batteries had to be replaced due to age issues. Additionally, the knowledge gained from the JimmE-V BMS was implemented on the GEM's BMS to beta test different software calibration options for Ewert Energy. Through the BMS recalibration and motor reconditioning, the range of the GEM increased from 7 miles to 16 miles. These results further supported the initially proposed research and battery pack design proposed by the EcoHawks GEM team.

In addition to the JimmE-V's powertrain, the author readily provided assistance where needed during the final year of the project. The author provided support during the installation process for the power steering system providing system wiring knowledge. Similarly, since the author was familiar with the vehicle's HV system assistance was provided during the installation process for the Air Conditioning system's controller. The author additionally worked on the battery pack as needed.

With the vehicle operational, the final contributions from the author were focused on drive cycle testing and vehicle efficiency evaluation. To that end, the author utilized an identical route used in evaluating the VW Beetle's efficiency. During testing the author was the driver of the vehicle, while lab colleagues assisted in monitoring the data acquisition systems. Through the vehicle drive cycle testing the

author then processed the drive cycle data to obtain the 83.3 mpg_e efficiency metric for the JimmE-V. This metric accompanied a full vehicle LCA calculated by ANL's GREET model to examine the vehicle's overall sustainability on an energy and emissions standpoint.

Looking towards the future of EV research and development at the University of Kansas, the JimmE-V will be used to further research and develop EV modeling techniques. In addition as the $LiFePO_4$ batteries continue aging, the different battery aging effects can be researched to further improve battery chemistry technology. Similarly, the further sustainability of the $LiFePO_4$ batteries will be examined in comparison to the VW Beetle's lead acid battery pack since the $LiFePO_4$ batteries have little to no recyclable material in comparison to lead acid battery recyclability. In addition to battery pack sustainability, the electric vehicles at KU can be used to develop and test battery management systems to eliminate the need to rely on proprietary components. The JimmE-V's larger capacity battery pack makes the vehicle suitable for Vehicle to Grid (V2G) research.

Overall, the 1974 VW Super Beetle provided a good introduction to electric vehicle design and manufacturing. The lessons learned from the VW allowed for a more complex vehicle to be developed. The second generation EV at the University of Kansas, the JimmE-V, represents a typical EV that would be available to consumers. In comparison to traditional IC engine vehicles, the JimmE-V has a relatively simple CAN bus with minimal components communicating via CAN. This results in a vehicle control system that is more accessible to students. Overall, by understanding how the different components on the JimmE-V operate the vehicle's energy use can be evaluated while being able to calibrate system components to operate efficiently. Additionally, after examining the vehicle LCA information it is observed that despite zero local emissions EVs require energy input for both the manufacturing and fueling processes. While this results in lower emissions per vehicle lifetime in comparison to ICE vehicles, the LCA information shows that EV fueling and production do produce emissions. Lastly, since the JimmE-V was designed and fabricated by students, the vehicle's components are easily accessible allowing the vehicle to be adapted for future sustainable research at the University of Kansas.

References

1. Agency, U.S.E.P. *About the EPA*. Available from: http://www.epa.gov/.
2. Agency, U.S.E.P., *EPA Sets Tier 3 Motor Vehicle Emission and Fuel Standards*, 2014.
3. Ramsey, M. *Bumpy Road for Elecctrics*. 2010 [cited 2015; Available from: http://www.wsj.com/articles/SB10001424052748704654004575517891616896222.
4. Depcik, C., *ME 790: History of Hybrid and Electric Vehicles*, 2014.
5. Motors, T. *Supercharger: The World's Fastesst Charging Station*. 2015; Available from: http://www.teslamotors.com/findus#/bounds/49.38,-66.94,25.82,-124.39?search=supercharger&name=us.
6. Instruments, N. *ECU Desigining and Testing using National Instruments Products*. 2007 [cited 2014 11/19/2014]; Available from: http://www.ni.com/white-paper/3312/en/.
7. Paret, D., *Multiplexed networks for embedded systems: CAN, LIN, Flexray, Safe-by-Wire*. 2007: John Wiley & Sons.
8. ISO, *CAN Specification Version 2.0*, 1991, Robert Bosch GmbH.
9. Bosch, R., *Bosch Automotive Handbook, 8th Edition*. 2011: Bentley Publishers.
10. Technologies, P. *Automotive multi-purpose ECU*. Available from: http://prodrive-technologies.com/ready-to-use-products/electronic-control-unit/.
11. *Orion BMS Wiring & installation Manual*, Ewert Energy.
12. Pazul, K., *Controller Area Network (CAN) Basics*, 1999, Microchip Technology Inc.
13. Baltusis, P., *On board vehicle diagnostics*, 2004, SAE Technical Paper.
14. Instruments, P., *Test Equipment.*
15. OBDTester.com, *OBD2 Connector.*
16. Hausmann, A.J., *Advances in Electric Drive Vehicle Modeling with Subsequent Experimentation and Analysis*, in *Department of Mechanical Engineering*2012, University of Kansas: Lawrence, Kansas.

17. Choate M., M.J., Christianson C., Collins P., and Depcik C. . *A Swappable Battery Pack for Short-Range Electric Vehicles*. in *ASME 2014 International Mechanical Engineering Congress & Exposition*. 2014. Montreal, Canada.

18. *GEM Owner & Repair Manual*, General Electric Motorcar.

19. Shukla, A.K., S. Venugopalan, and B. Hariprakash, *Nickel-based rechargeable batteries*. Journal of Power Sources, 2001. **100**(1–2): p. 125-148.

20. Digi-Key, *Signal Relays*.

21. *State of Charge Calculation with Dynamic Drift*. Available from: http://www.orionbms.com/features/state-of-charge-with-drift/.

22. Petty, J., et al., *Team JimmE-V ME 645 Report*, in *Department of Mechanical Engineering*2011, University of Kansas: Lawrence, Kansas.

23. Depcik, C., *ME 790: Vehicle Modeling* 2014. p. 2-100.

24. Inc., A.D., *DMOC445 and DMOC645 User Manual for Azure Dynamics DMOC Motor Controller*, 2009: Woburn, MA.

25. Woodward, *MotoHawk Control Solutions ECM-0554-112-0904-C/F Engine Control Modules Calibratible/Flash*, 2014: Fort Collins, CO.

26. Lakshmi, A.K. *Wheatstone Bridges*. 2008; Available from: http://www.ustudy.in/node/3622.

27. Tenergy, *Voltage Regulator Breakout Board*.

28. Depcik, C., *ME 790: Batteries*, 2014.

29. Goodyear. *Tire Size*. Available from: http://www.goodyearautoservice.com/content/content.jsp?pageName=TireSize.

30. Theodore, W., *Electrical Machines, Drives And Power Systems, 6/E*. 2007: Pearson Education India.

31. Dynamics, A., *ccShell Software Instruction Manual*, 2008: Woburn, MA.

32. Chrysler. *The All-New 2015 Chrysler 200*. 2015; Available from: http://www.chrysler.com/en/200/?sid=1037056&KWNM=chrysler+200&KWID=5856931466&TR=1&channel=paidsearch.

33. Power, G. *GWL/Power SE100AHA - Lithium Cell LiFePO4 (3.2V/100Ah) - CALB-PROMO*. Available from: http://www.ev-power.eu/CALB-40Ah-400Ah/SE100AHA-Lithium-Cell-LiFePO4-3-2V-100Ah.html.

34. Collins, P., et al., *Team JimmE-V: Large Scale Electric Vehicle Conversion*, in *Department of Mechanical Engineering*2012, University of Kansas: Lawrence, Kansas.

35. Works, E.M. *CALB CA100FI 100Ah LiFePo4 Cell*. Available from: http://store.evtv.me/proddetail.php?prod=ca100fi.

36. Elithion. *Lithiumate Pro Controller*. 2015; Available from: http://elithion.com/lithiumate_pro_controllers.php.

37. Elithion. *Lithiumate Manual: Installation - BMS Controller*. 2015; Available from: http://lithiumate.elithion.com/php/install_controller.php.

38. Elithion. *Lithiumate Manual: Using an Azure DMOC AC motor driver with a Lithiumate BMS*. 2015; Available from: http://lithiumate.elithion.com/php/azure.php.

39. Micro, M., *PFC-20, PFC-30 & PFC 40 Charger Owner's Manual*, 2013.

40. Toepfer, C., *SAE Electric Vehicle Conductive Charge Coupler, SAE J1772*. Society of Automotive Engineers, 2009.

41. Power, M.E. *SAE J1772:2010 Compatible Active Vehicle Side Control Board Module*. 2014; Available from: http://modularevpower.com/Active_Vehicle_Side_Control_development.htm.

42. Helton, K., et al., *Team JimmE-V: Large Scale Electric Vehicl Conversion*, in *Department of Mechanical Engineering*2013, University of Kansas: Lawrence, Kansas.

43. MES-DEA, *DC – DC CONVERTER 1000W 100 - 400VDC Input / 12VDC Output* 2005.

44. Hofstad, A. *Toyota MR-S Electric power steering pump conversion*. 2011; Available from: http://www.mazdaspeedy.com/2011/11/toyota-mr-s-electric-power-steering.html.

45. Masterflux, *Battery Powered Application Tips*.

46. Masterflux. *SIERRA06-0982Y3*. Available from: http://www.masterflux.com/products/sierra/?pid=51.

47. Depcik, C., *ME 790: Motors*, 2014.

48. Strecker, B., A. Hausmann, and C. Depcik, *Well to wheels energy and emissions analysis of a recycled 1974 VW Super Beetle converted into a plug-in series hybrid electric vehicle.* Journal of Cleaner Production, 2014. **68**(0): p. 93-103.

49. Agency, U.S.E.P. *Electric Vehicles - learn More About the New Label*. [cited 2015; Available from: http://www.epa.gov/carlabel/electriclabelreadmore.htm#7.

50. Sullivan, J., A. Burnham, and M. Wang, *Energy-consumption and carbon-emission analysis of vehicle and component manufacturing*, 2010, Argonne National Laboratory (ANL).

51. Sullivan, J.L., et al., *Life Cycle Inventory of a Generic U.S. Family Sedan Overview of Results USCAR AMP Project*, 1998, SAE International.

52. Sullivan, J.L. and E. Cobas-Flores, *Full Vehicle LCAs: A Review*, 2001, SAE International.

53. Daniels, E.J., et al., *Sustainable end-of-life vehicle recycling: R&D collaboration between industry and the US DOE.* JOM, 2004. **56**(8): p. 28-32.

54. Chen, M., *End-of-life vehicle recycling in China: now and the future.* Jom, 2005. **57**(10): p. 20-26.

55. Amelia, L., et al., *Initiating automotive component reuse in Malaysia.* Journal of Cleaner Production, 2009. **17**(17): p. 1572-1579.

56. Tong, E.H. and T.A. Loch, *Paint Usage Reduction in Automotive Paint Booths*, 2000, SAE International.

57. Depcik, C., *ME 790: Batteries*, 2014. p. 3-111.

58. Electropaedia. *Cell Chemistries - How Batteries Work*. Battery and Energy Technologies; Available from: http://www.mpoweruk.com/chemistries.htm.

59. University, B. *BU-205: Types of Lithium-ion*. 2015; Available from: http://batteryuniversity.com/learn/article/types_of_lithium_ion.

60. Dai, Q., J. Shen, and F. Xiao, *Lithium iron phosphate cathode material*, 2012, Google Patents.

61. Yang, S., P.Y. Zavalij, and M.S. Whittingham, *Hydrothermal synthesis of lithium iron phosphate cathodes*. Electrochemistry Communications, 2001. **3**(9): p. 505-508.

62. Dunn, J.B., et al., *Material and Energy Flows in the Production of Cathode and Anode Materials for Lithium Ion Batteries*, 2014, Argonne National Laboratory

63. Mackintosh, T.F., *Identification of Transportation Battery Systems for Recycling*, 2012, SAE International.

64. Sbordone, D., et al., *EV fast charging stations and energy storage technologies: A real implementation in the smart micro grid paradigm*. Electric Power Systems Research, 2015. **120**(0): p. 96-108.

65. Jody, B.J., et al., *Impact of Recycling Automotive Lightweighting Materials on Sustainability*, 2009, SAE International.

66. Howes, J., *Battery Recycling Interaction with Washington*. SAE Int. J. Mater. Manf., 2012. **5**(1): p. 150-159.

67. Keoleian, G., et al., *Life cycle material data update for GREET model*. Report No. CSS12-12, 2012.

68. Wang, M., *Argonne National Laboratory GREET2_2014*, 2014: Argonne, IL.

69. Trend, M. *Used 1997 GMC Jimmy Exterior Specifications*. [cited 2015; Available from: http://www.motortrend.com/cars/1997/gmc/jimmy/specifications/exterior.html.

70. Wang, M., *Argonne National Laboratory GREET1_2014*, 2014: Argonne, IL.

71. Energy, U.S.D.o. *1997 GMC Jimmy 4WD Fuel Economy*. 2015; Available from: http://www.fueleconomy.gov/feg/noframes/13949.shtml.

72. Energy, E., *Enphase M215 Microinverter*, 2014: Petaluma, California.

73. Suniva, *Suniva Optimus Series Monocrystalline Solar Modules*: Norcross, Georgia.

74. Lumos, *LSX Frameless Module with Integrated Mounting*: Boulder, Colorado.

75. Programs, K.C.C.E., *Kansas Solar Resource Map,* 2005.

Appendix

JimmE-V & Syngas laptop password: captainplanet

Azure DMOC445 repair contact information:

Wolf (WolfTronix): wolf@wolftronix.com

Note: As of 3-31-2015 Wolf has suspended his repair operations due to health issues.

Collin Kidder: collink@kkmfg.com

For additional assistance consult solectria_ev@yahooogroups.com

(yahoo group dedicated to keeping product alive)

New Eagle Contacts (ECM):

Rich Swortzel P.E.

New Eagle, Founder & Business Development

rswortzel@neweagle.net

Direct Number: 734-649-8156

Thomas Dougan (main designer and contact for JimmE-V ECM, not very helpful)

New Eagle, Sales Engineer

tdougan@neweagle.net

Direct Number: 734-585-1718

Office Number: 734-929-4557

Justin Goeglein (ECM support, very helpful)

New Eagle, Sr. Controls Engineer

jgoeglein@neweagle.net

Direct Number: 765-606-7908

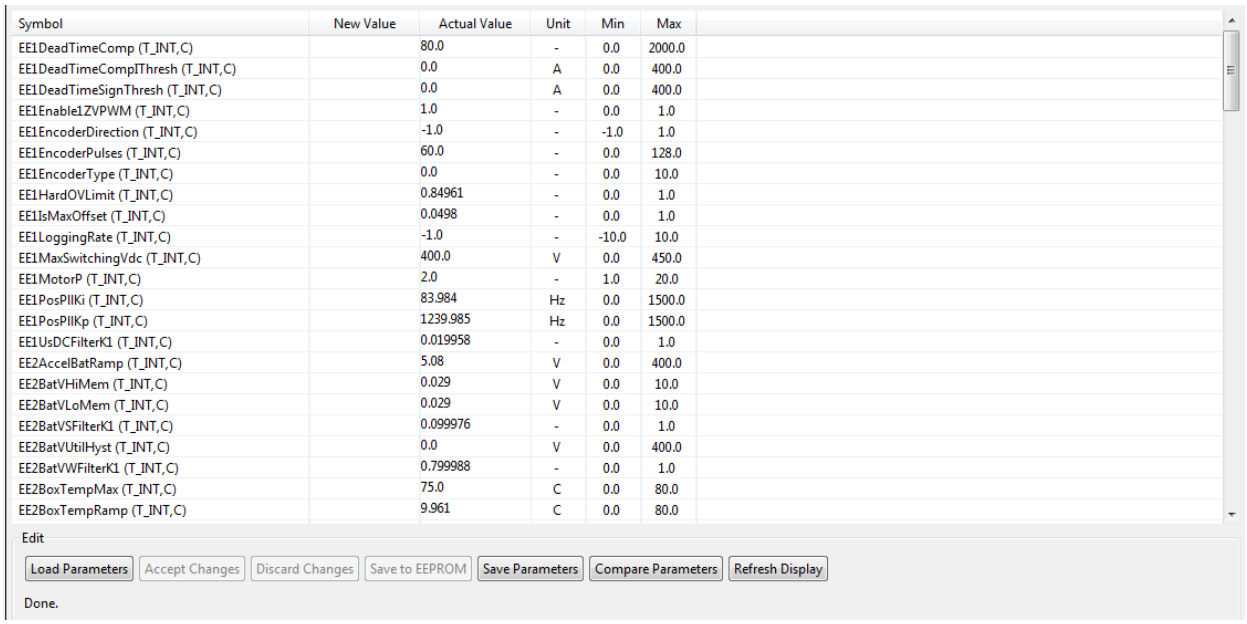

Symbol	New Value	Actual Value	Unit	Min	Max
EE1DeadTimeComp (T_INT,C)		80.0	-	0.0	2000.0
EE1DeadTimeCompIThresh (T_INT,C)		0.0	A	0.0	400.0
EE1DeadTimeSignThresh (T_INT,C)		0.0	A	0.0	400.0
EE1Enable1ZVPWM (T_INT,C)		1.0	-	0.0	1.0
EE1EncoderDirection (T_INT,C)		-1.0	-	-1.0	1.0
EE1EncoderPulses (T_INT,C)		60.0	-	0.0	128.0
EE1EncoderType (T_INT,C)		0.0	-	0.0	10.0
EE1HardOVLimit (T_INT,C)		0.84961	-	0.0	1.0
EE1IsMaxOffset (T_INT,C)		0.0498	-	0.0	1.0
EE1LoggingRate (T_INT,C)		-1.0	-	-10.0	10.0
EE1MaxSwitchingVdc (T_INT,C)		400.0	V	0.0	450.0
EE1MotorP (T_INT,C)		2.0	-	1.0	20.0
EE1PosPIIKi (T_INT,C)		83.984	Hz	0.0	1500.0
EE1PosPIIKp (T_INT,C)		1239.985	Hz	0.0	1500.0
EE1UsDCFilterK1 (T_INT,C)		0.019958	-	0.0	1.0
EE2AccelBatRamp (T_INT,C)		5.08	V	0.0	400.0
EE2BatVHiMem (T_INT,C)		0.029	V	0.0	10.0
EE2BatVLoMem (T_INT,C)		0.029	V	0.0	10.0
EE2BatVSFilterK1 (T_INT,C)		0.099976	-	0.0	1.0
EE2BatVUtilHyst (T_INT,C)		0.0	V	0.0	400.0
EE2BatVWFilterK1 (T_INT,C)		0.799988	-	0.0	1.0
EE2BoxTempMax (T_INT,C)		75.0	C	0.0	80.0
EE2BoxTempRamp (T_INT,C)		9.961	C	0.0	80.0

Edit

Load Parameters | Accept Changes | Discard Changes | Save to EEPROM | Save Parameters | Compare Parameters | Refresh Display

Done.

Figure 186: DMOC445 ccShell .par file parameters.

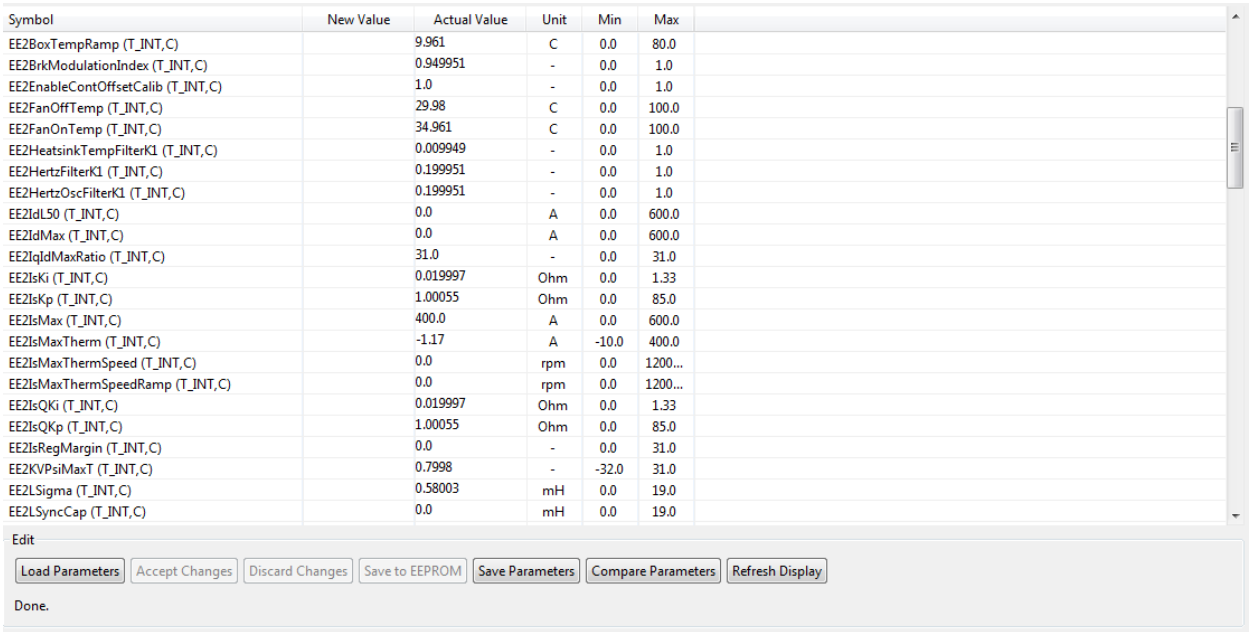

Symbol	New Value	Actual Value	Unit	Min	Max
EE2BoxTempRamp (T_INT,C)		9.961	C	0.0	80.0
EE2BrkModulationIndex (T_INT,C)		0.949951	-	0.0	1.0
EE2EnableContOffsetCalib (T_INT,C)		1.0	-	0.0	1.0
EE2FanOffTemp (T_INT,C)		29.98	C	0.0	100.0
EE2FanOnTemp (T_INT,C)		34.961	C	0.0	100.0
EE2HeatsinkTempFilterK1 (T_INT,C)		0.009949	-	0.0	1.0
EE2HertzFilterK1 (T_INT,C)		0.199951	-	0.0	1.0
EE2HertzOscFilterK1 (T_INT,C)		0.199951	-	0.0	1.0
EE2IdL50 (T_INT,C)		0.0	A	0.0	600.0
EE2IdMax (T_INT,C)		0.0	A	0.0	600.0
EE2IqIdMaxRatio (T_INT,C)		31.0	-	0.0	31.0
EE2IsKi (T_INT,C)		0.019997	Ohm	0.0	1.33
EE2IsKp (T_INT,C)		1.00055	Ohm	0.0	85.0
EE2IsMax (T_INT,C)		400.0	A	0.0	600.0
EE2IsMaxTherm (T_INT,C)		-1.17	A	-10.0	400.0
EE2IsMaxThermSpeed (T_INT,C)		0.0	rpm	0.0	1200...
EE2IsMaxThermSpeedRamp (T_INT,C)		0.0	rpm	0.0	1200...
EE2IsQKi (T_INT,C)		0.019997	Ohm	0.0	1.33
EE2IsQKp (T_INT,C)		1.00055	Ohm	0.0	85.0
EE2IsRegMargin (T_INT,C)		0.0	-	0.0	31.0
EE2KVPsiMaxT (T_INT,C)		0.7998	-	-32.0	31.0
EE2LSigma (T_INT,C)		0.58003	mH	0.0	19.0
EE2LSyncCap (T_INT,C)		0.0	mH	0.0	19.0

Edit

Load Parameters | Accept Changes | Discard Changes | Save to EEPROM | Save Parameters | Compare Parameters | Refresh Display

Done.

Figure 187: DMOC445 ccShell .par file parameters.

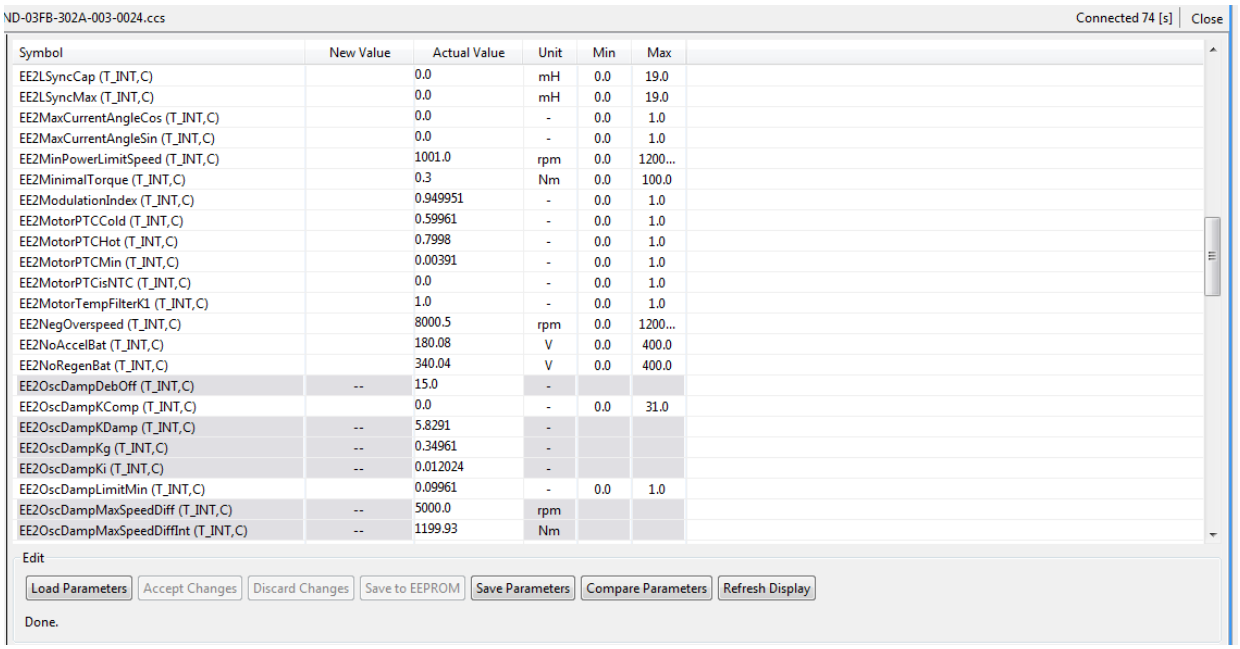

Symbol	New Value	Actual Value	Unit	Min	Max
EE2LSyncCap (T_INT,C)		0.0	mH	0.0	19.0
EE2LSyncMax (T_INT,C)		0.0	mH	0.0	19.0
EE2MaxCurrentAngleCos (T_INT,C)		0.0	-	0.0	1.0
EE2MaxCurrentAngleSin (T_INT,C)		0.0	-	0.0	1.0
EE2MinPowerLimitSpeed (T_INT,C)		1001.0	rpm	0.0	1200...
EE2MinimalTorque (T_INT,C)		0.3	Nm	0.0	100.0
EE2ModulationIndex (T_INT,C)		0.949951	-	0.0	1.0
EE2MotorPTCCold (T_INT,C)		0.59961	-	0.0	1.0
EE2MotorPTCHot (T_INT,C)		0.7998	-	0.0	1.0
EE2MotorPTCMin (T_INT,C)		0.00391	-	0.0	1.0
EE2MotorPTCisNTC (T_INT,C)		0.0	-	0.0	1.0
EE2MotorTempFilterK1 (T_INT,C)		1.0	-	0.0	1.0
EE2NegOverspeed (T_INT,C)		8000.5	rpm	0.0	1200...
EE2NoAccelBat (T_INT,C)		180.08	V	0.0	400.0
EE2NoRegenBat (T_INT,C)		340.04	V	0.0	400.0
EE2OscDampDebOff (T_INT,C)	--	15.0	-		
EE2OscDampKComp (T_INT,C)		0.0	-	0.0	31.0
EE2OscDampKDamp (T_INT,C)	--	5.8291	-		
EE2OscDampKg (T_INT,C)	--	0.34961	-		
EE2OscDampKi (T_INT,C)	--	0.012024	-		
EE2OscDampLimitMin (T_INT,C)		0.09961	-	0.0	1.0
EE2OscDampMaxSpeedDiff (T_INT,C)	--	5000.0	rpm		
EE2OscDampMaxSpeedDiffInt (T_INT,C)	--	1199.93	Nm		

Figure 188: DMOC445 ccShell .par file parameters.

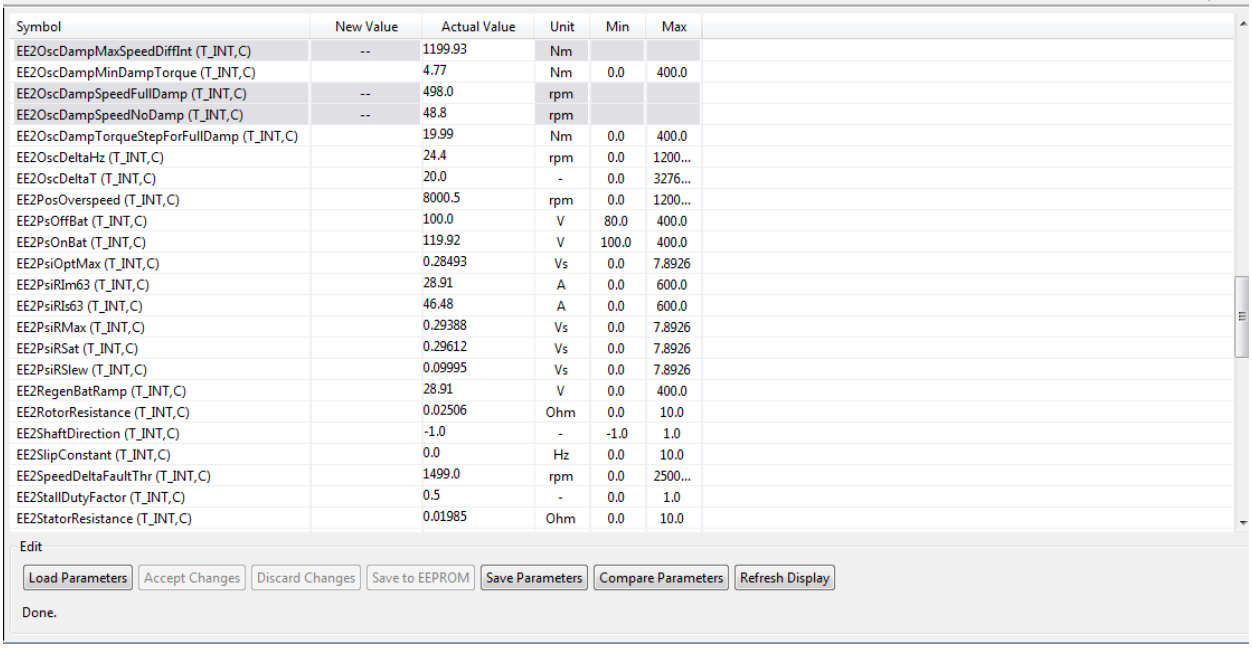

Symbol	New Value	Actual Value	Unit	Min	Max
EE2OscDampMaxSpeedDiffInt (T_INT,C)	--	1199.93	Nm		
EE2OscDampMinDampTorque (T_INT,C)		4.77	Nm	0.0	400.0
EE2OscDampSpeedFullDamp (T_INT,C)	--	498.0	rpm		
EE2OscDampSpeedNoDamp (T_INT,C)	--	48.8	rpm		
EE2OscDampTorqueStepForFullDamp (T_INT,C)		19.99	Nm	0.0	400.0
EE2OscDeltaHz (T_INT,C)		24.4	rpm	0.0	1200...
EE2OscDeltaT (T_INT,C)		20.0	-	0.0	3276...
EE2PosOverspeed (T_INT,C)		8000.5	rpm	0.0	1200...
EE2PsOffBat (T_INT,C)		100.0	V	80.0	400.0
EE2PsOnBat (T_INT,C)		119.92	V	100.0	400.0
EE2PsiOptMax (T_INT,C)		0.28493	Vs	0.0	7.8926
EE2PsiRIm63 (T_INT,C)		28.91	A	0.0	600.0
EE2PsiRIs63 (T_INT,C)		46.48	A	0.0	600.0
EE2PsiRMax (T_INT,C)		0.29388	Vs	0.0	7.8926
EE2PsiRSat (T_INT,C)		0.29612	Vs	0.0	7.8926
EE2PsiRSlew (T_INT,C)		0.09995	Vs	0.0	7.8926
EE2RegenBatRamp (T_INT,C)		28.91	V	0.0	400.0
EE2RotorResistance (T_INT,C)		0.02506	Ohm	0.0	10.0
EE2ShaftDirection (T_INT,C)		-1.0	-	-1.0	1.0
EE2SlipConstant (T_INT,C)		0.0	Hz	0.0	10.0
EE2SpeedDeltaFaultThr (T_INT,C)		1499.0	rpm	0.0	2500...
EE2StallDutyFactor (T_INT,C)		0.5	-	0.0	1.0
EE2StatorResistance (T_INT,C)		0.01985	Ohm	0.0	10.0

Figure 189: DMOC445 ccShell .par file parameters.

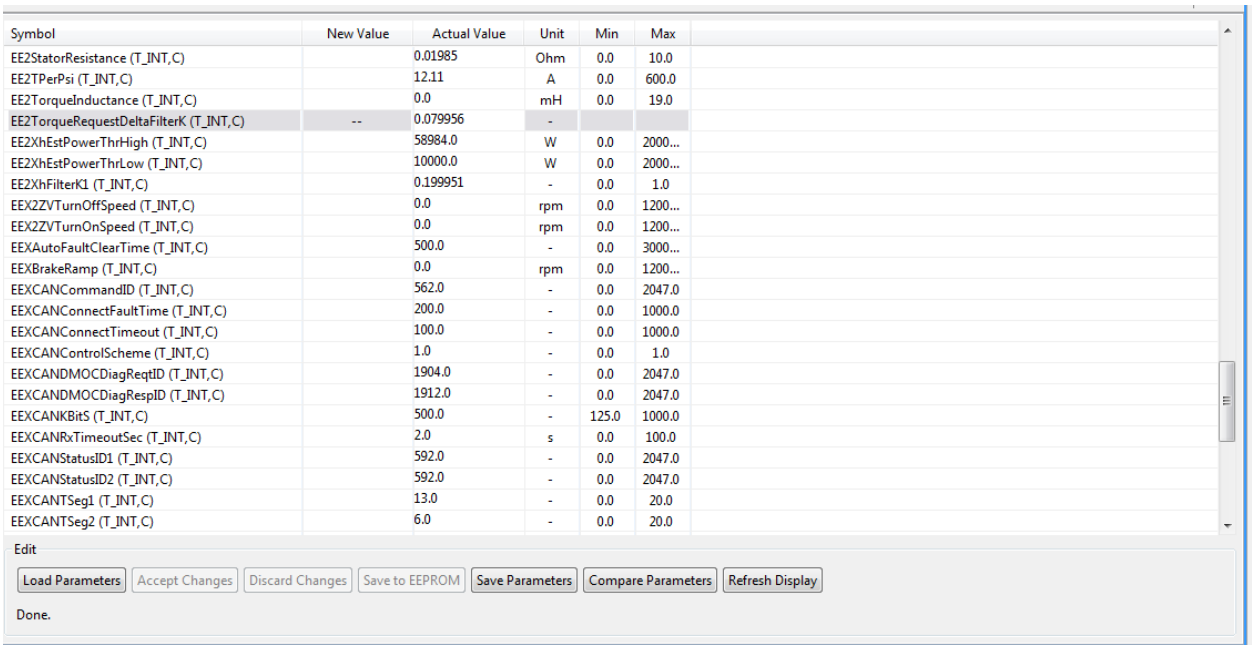

Symbol	New Value	Actual Value	Unit	Min	Max
EE2StatorResistance (T_INT,C)		0.01985	Ohm	0.0	10.0
EE2TPerPsi (T_INT,C)		12.11	A	0.0	600.0
EE2TorqueInductance (T_INT,C)		0.0	mH	0.0	19.0
EE2TorqueRequestDeltaFilterK (T_INT,C)	--	0.079956	-		
EE2XhEstPowerThrHigh (T_INT,C)		58984.0	W	0.0	2000...
EE2XhEstPowerThrLow (T_INT,C)		10000.0	W	0.0	2000...
EE2XhFilterK1 (T_INT,C)		0.199951	-	0.0	1.0
EEX2ZVTurnOffSpeed (T_INT,C)		0.0	rpm	0.0	1200...
EEX2ZVTurnOnSpeed (T_INT,C)		0.0	rpm	0.0	1200...
EEXAutoFaultClearTime (T_INT,C)		500.0	-	0.0	3000...
EEXBrakeRamp (T_INT,C)		0.0	rpm	0.0	1200...
EEXCANCommandID (T_INT,C)		562.0	-	0.0	2047.0
EEXCANConnectFaultTime (T_INT,C)		200.0	-	0.0	1000.0
EEXCANConnectTimeout (T_INT,C)		100.0	-	0.0	1000.0
EEXCANControlScheme (T_INT,C)		1.0	-	0.0	1.0
EEXCANDMOCDiagReqtID (T_INT,C)		1904.0	-	0.0	2047.0
EEXCANDMOCDiagRespID (T_INT,C)		1912.0	-	0.0	2047.0
EEXCANKBitS (T_INT,C)		500.0	-	125.0	1000.0
EEXCANRxTimeoutSec (T_INT,C)		2.0	s	0.0	100.0
EEXCANStatusID1 (T_INT,C)		592.0	-	0.0	2047.0
EEXCANStatusID2 (T_INT,C)		592.0	-	0.0	2047.0
EEXCANTSeg1 (T_INT,C)		13.0	-	0.0	20.0
EEXCANTSeg2 (T_INT,C)		6.0	-	0.0	20.0

Edit

Load Parameters | Accept Changes | Discard Changes | Save to EEPROM | Save Parameters | Compare Parameters | Refresh Display

Done.

Figure 190: DMOC445 ccShell .par file parameters.

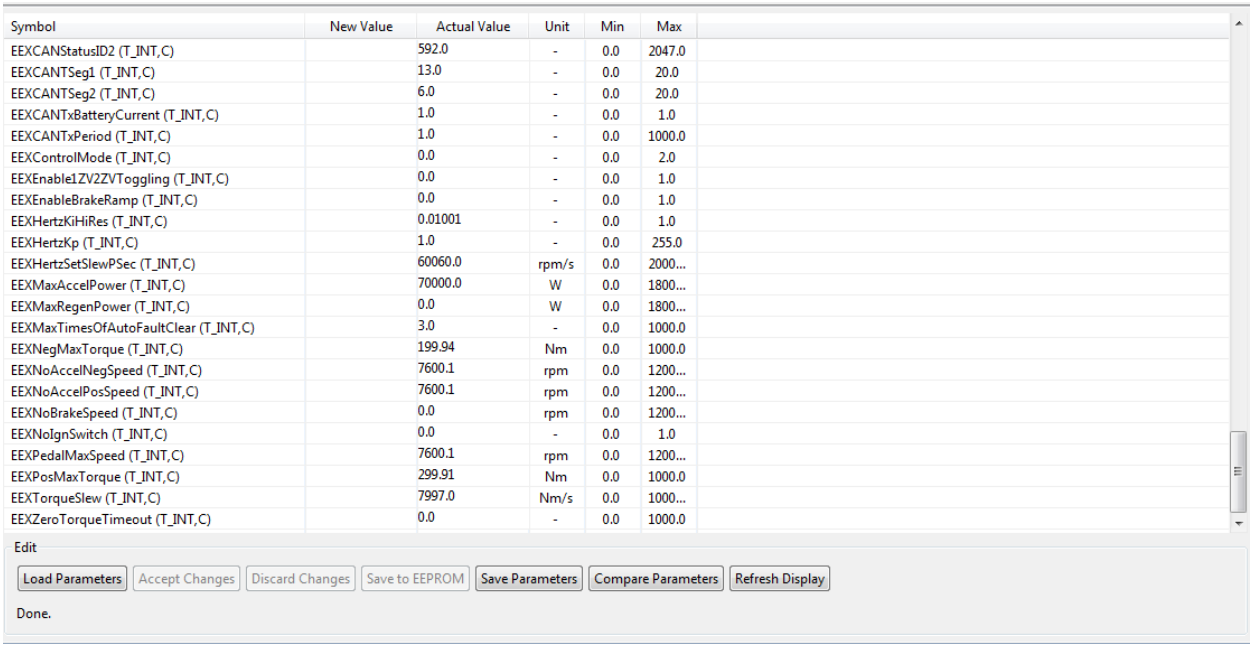

Symbol	New Value	Actual Value	Unit	Min	Max
EEXCANStatusID2 (T_INT,C)		592.0	-	0.0	2047.0
EEXCANTSeg1 (T_INT,C)		13.0	-	0.0	20.0
EEXCANTSeg2 (T_INT,C)		6.0	-	0.0	20.0
EEXCANTxBatteryCurrent (T_INT,C)		1.0	-	0.0	1.0
EEXCANTxPeriod (T_INT,C)		1.0	-	0.0	1000.0
EEXControlMode (T_INT,C)		0.0	-	0.0	2.0
EEXEnable1ZV2ZVToggling (T_INT,C)		0.0	-	0.0	1.0
EEXEnableBrakeRamp (T_INT,C)		0.0	-	0.0	1.0
EEXHertzKiHiRes (T_INT,C)		0.01001	-	0.0	1.0
EEXHertzKp (T_INT,C)		1.0	-	0.0	255.0
EEXHertzSetSlewPSec (T_INT,C)		60060.0	rpm/s	0.0	2000...
EEXMaxAccelPower (T_INT,C)		70000.0	W	0.0	1800...
EEXMaxRegenPower (T_INT,C)		0.0	W	0.0	1800...
EEXMaxTimesOfAutoFaultClear (T_INT,C)		3.0	-	0.0	1000.0
EEXNegMaxTorque (T_INT,C)		199.94	Nm	0.0	1000.0
EEXNoAccelNegSpeed (T_INT,C)		7600.1	rpm	0.0	1200...
EEXNoAccelPosSpeed (T_INT,C)		7600.1	rpm	0.0	1200...
EEXNoBrakeSpeed (T_INT,C)		0.0	rpm	0.0	1200...
EEXNoIgnSwitch (T_INT,C)		0.0	-	0.0	1.0
EEXPedalMaxSpeed (T_INT,C)		7600.1	rpm	0.0	1200...
EEXPosMaxTorque (T_INT,C)		299.91	Nm	0.0	1000.0
EEXTorqueSlew (T_INT,C)		7997.0	Nm/s	0.0	1000...
EEXZeroTorqueTimeout (T_INT,C)		0.0	-	0.0	1000.0

Edit

Load Parameters | Accept Changes | Discard Changes | Save to EEPROM | Save Parameters | Compare Parameters | Refresh Display

Done.

Figure 191: DMOC445 ccShell .par file parameters.

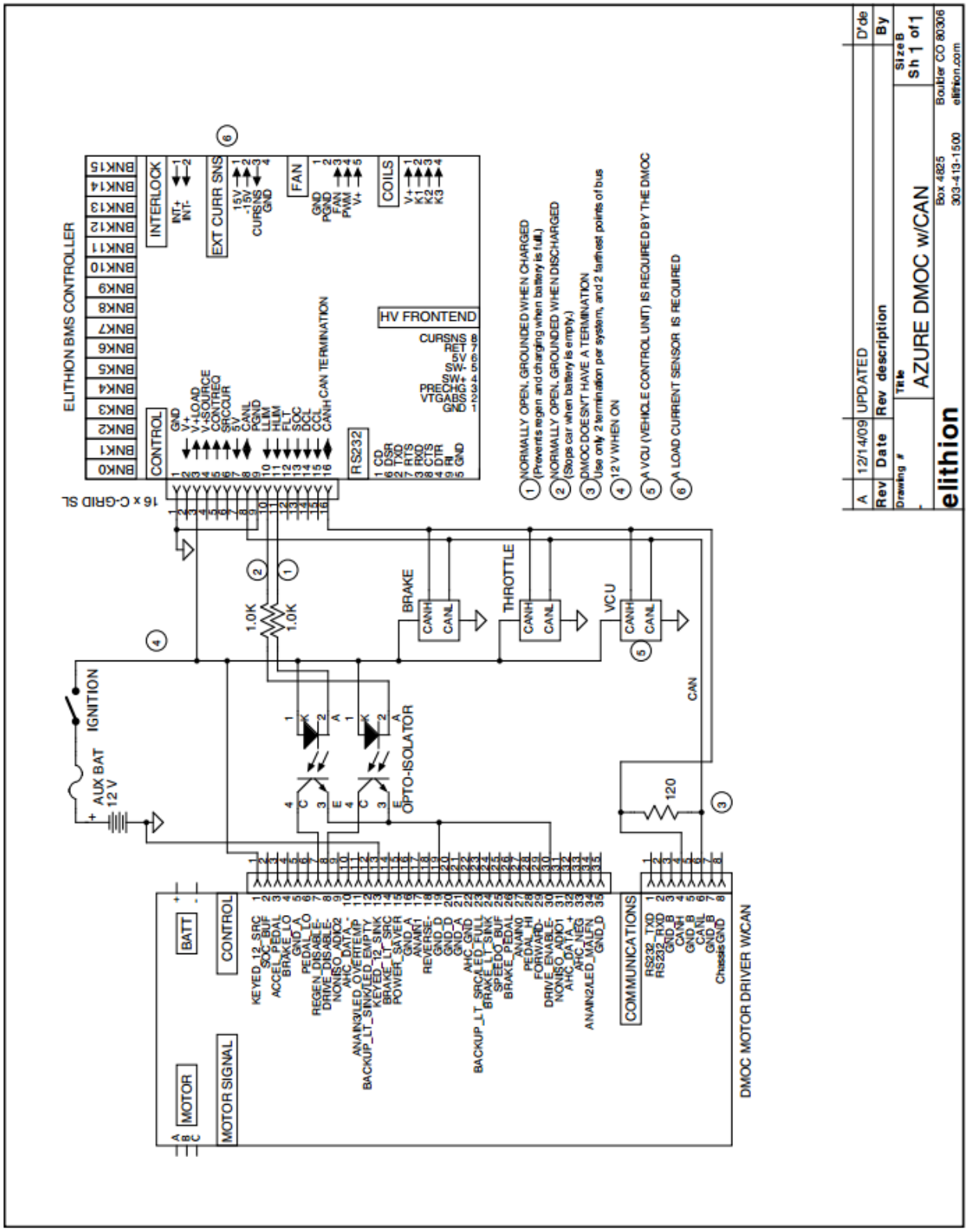

Figure 192: Elithion BMS schematic for Azure DMOC w/CAN.

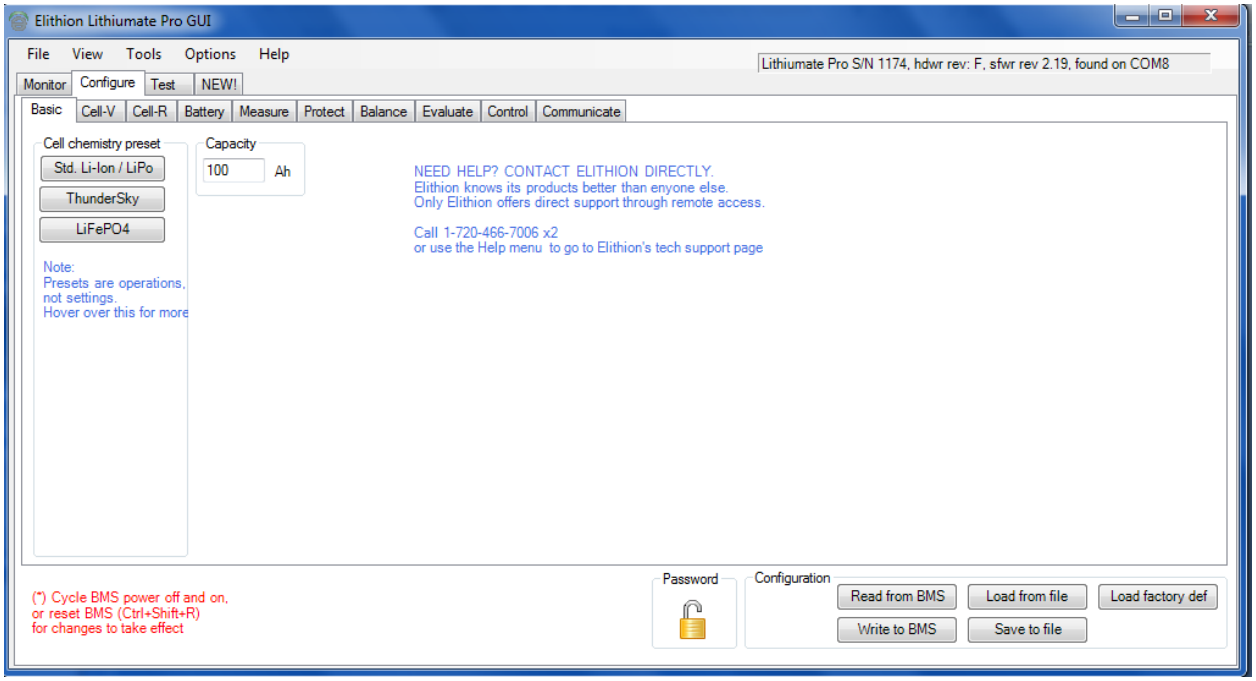

Figure 193: BMS GUI Basic tab configuration settings.

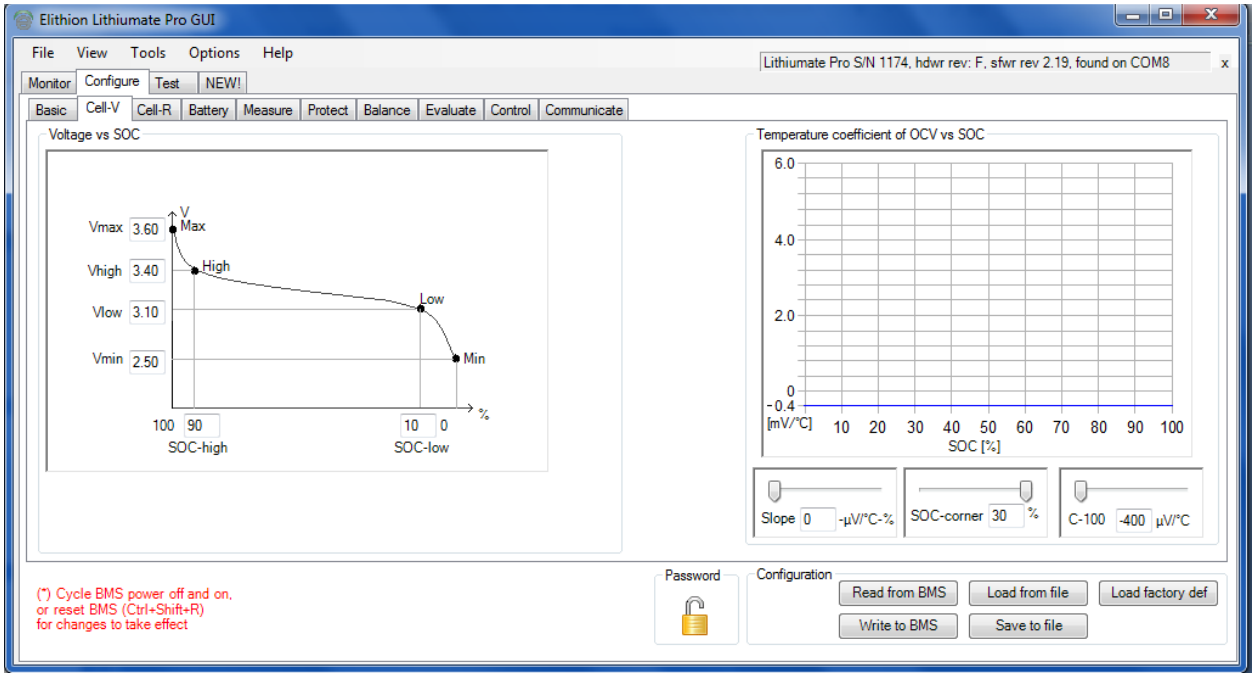

Figure 194: BMS GUI Cell-V tab configuration settings.

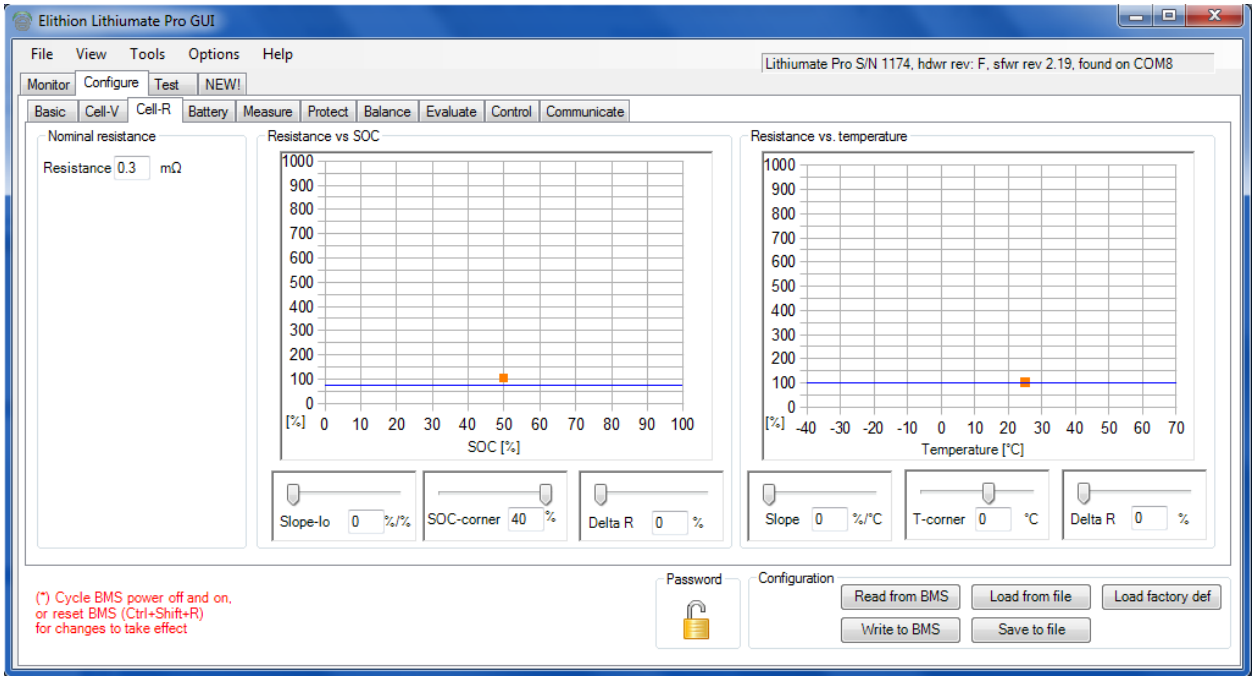

Figure 195: BMS GUI Cell-R tab configuration settings.

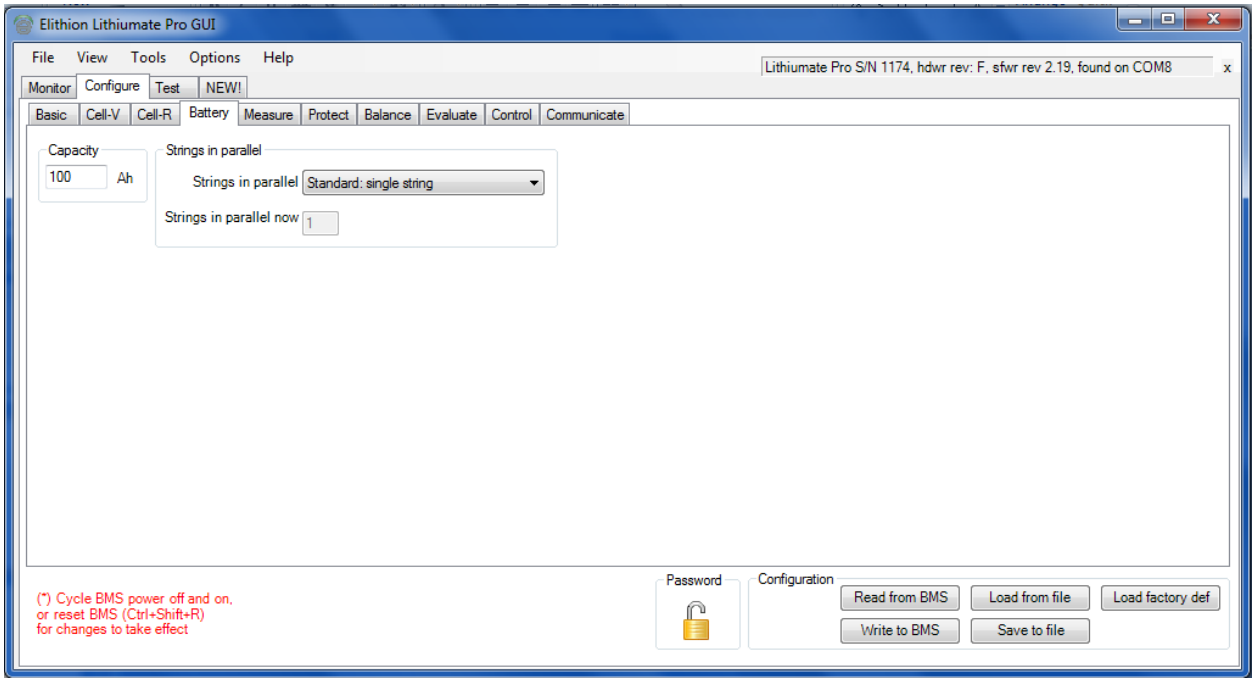

Figure 196: BMS GUI Battery tab configuration settings.

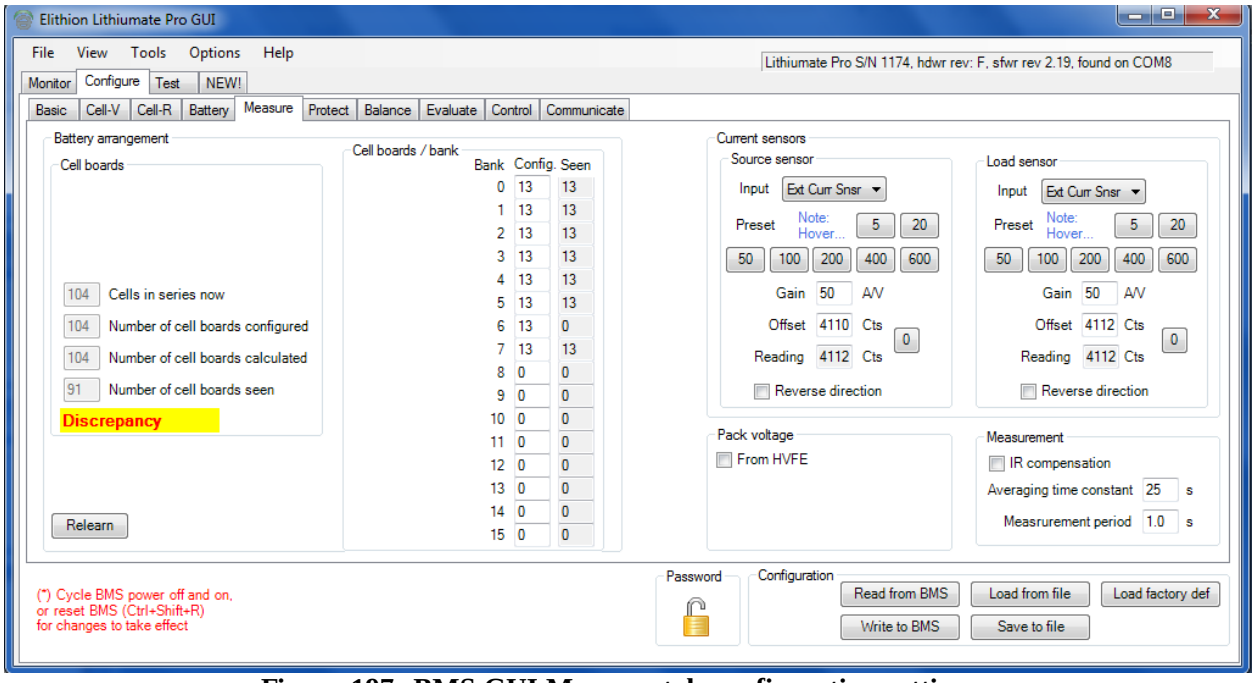

Figure 197: BMS GUI Measure tab configuration settings.

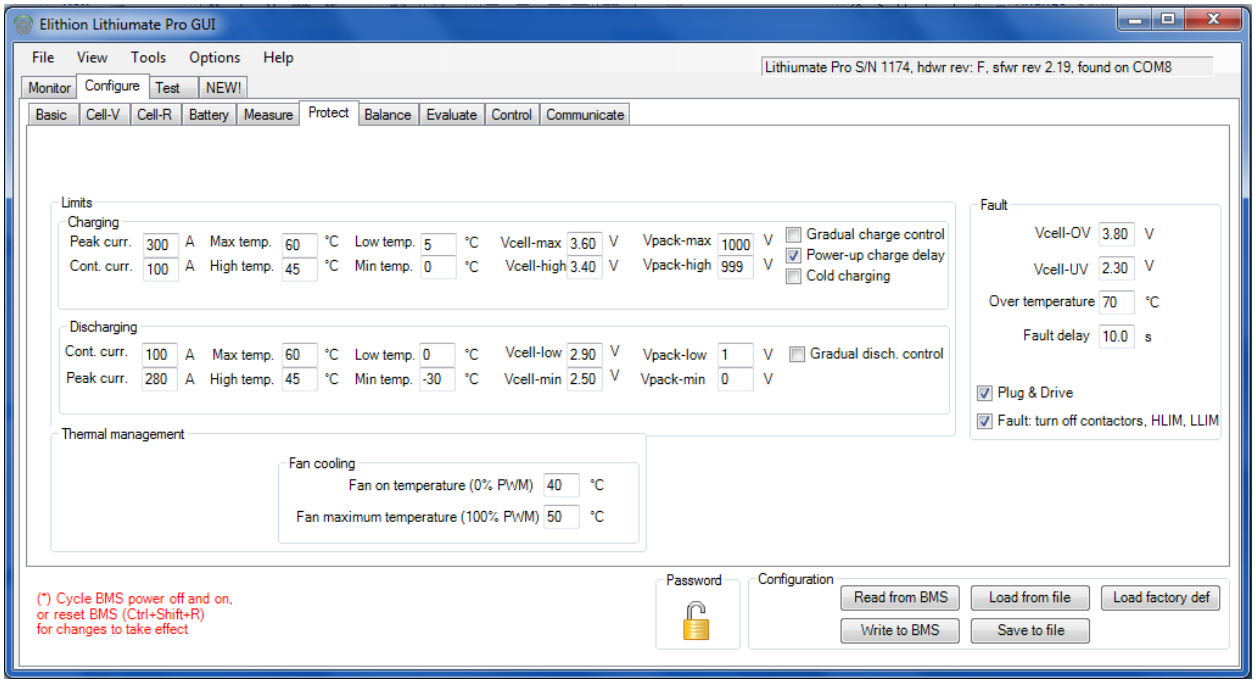

Figure 198: BMS GUI Protect tab configuration settings.

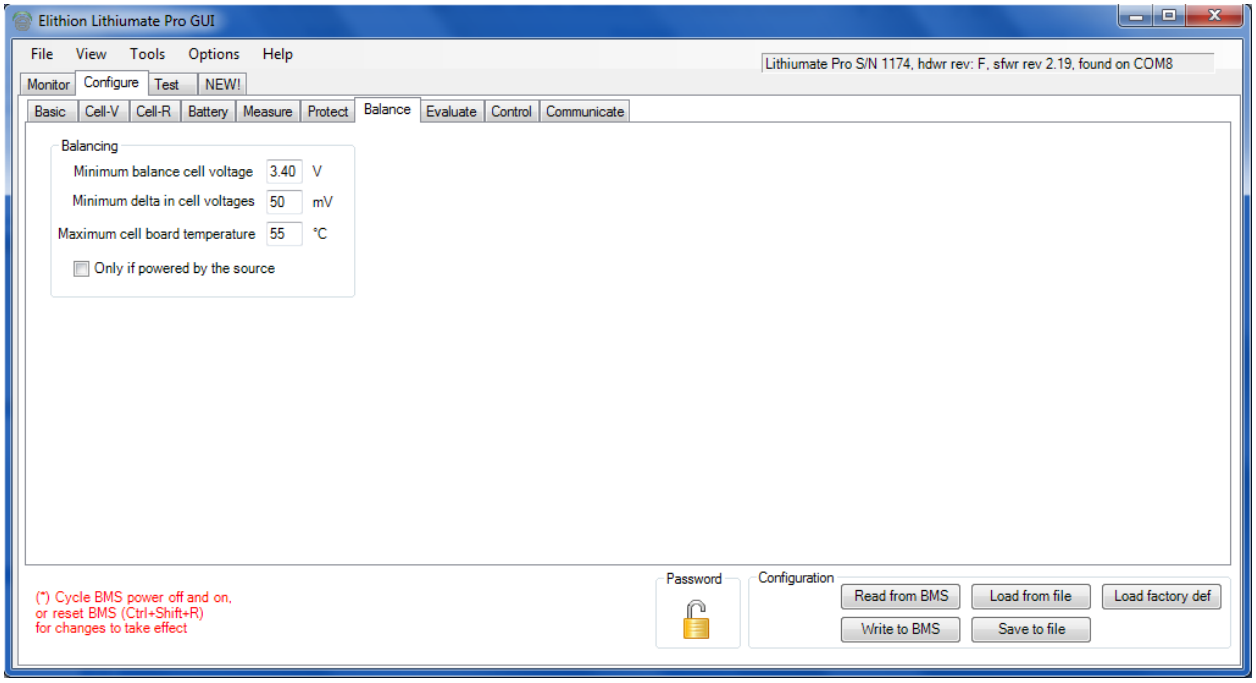

Figure 199: BMS GUI Balance tab configuration settings.

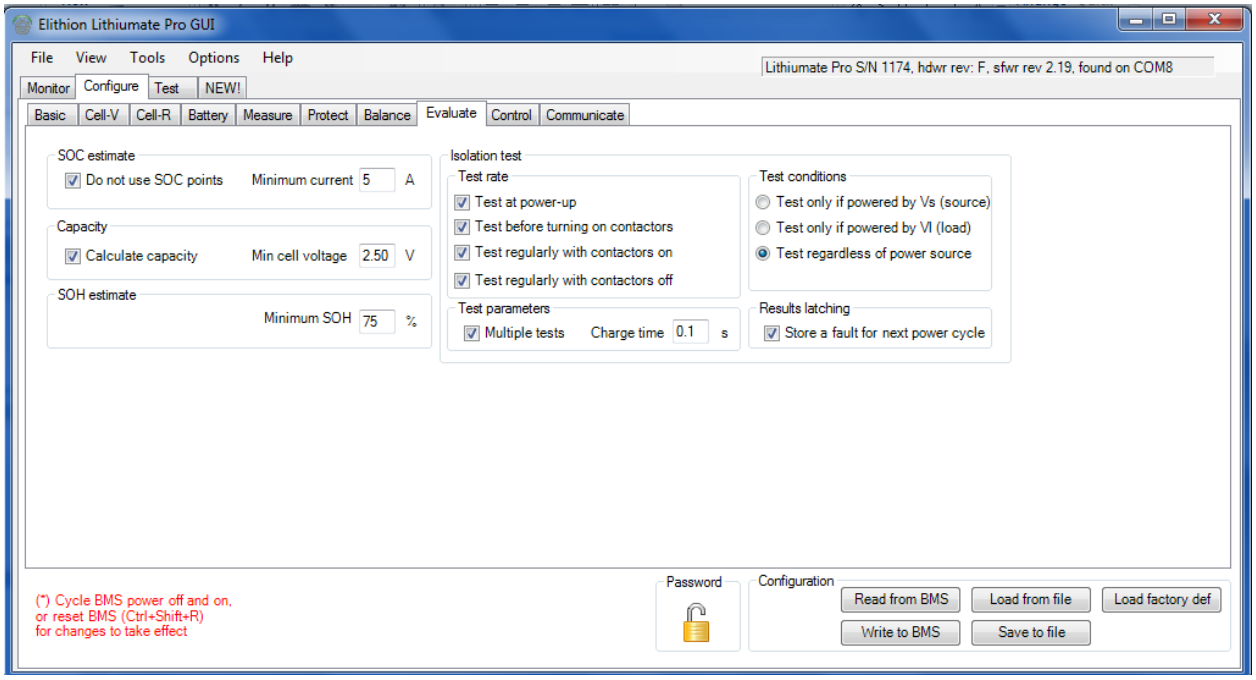

Figure 200: BMS GUI Evaluate tab configuration settings.